Developing Catalytically Active Living Materials for Additive Manufacturing

Trevor G Johnston

A dissertation

submitted in partial fulfillment of the

requirements for the degree of

Doctor of Philosophy

University of Washington

2020

Reading Committee:

Alshakim Nelson, Chair

Champak Chatterjee

Matthew Golder

Program Authorized to Offer Degree:

Chemistry

University of Washington

Abstract

Developing Catalytically Active Living Materials for Additive Manufacturing

Trevor Johnston

Chair of the Supervisory Committee:
Professor Alshakim Nelson
Chemistry

Living materials are created through the embedding of live, whole cells into a matrix that can house and sustain the viability of the encapsulated cells. Through the cell immobilization process, their bioactivity (natural or engineered) can be harnessed for applications such as the production of high-value chemicals or biosensing environmental changes. While the idea of employing whole cell technologies is not new, the materials commonly employed in this space limit their implementation. Naturally derived polymeric materials often lack the robust mechanical properties needed for structural integrity of the materials, while many synthetic alternatives are either difficult to pattern or detrimentally influence cell viability and behavior.

In this work, a novel platform of living materials is created, based on both commercially-available Pluronic F127 and a novel poly(alkyl glycidyl ether)-based triblock copolymer. The

hydrogels that are afforded from these copolymers are stimuli-responsive, allowing for precise additive manufacturing of encapsulated cells into complex geometries. These stimuli responses include (1) a temperature response which allowed for facile processing of the material; (2) the shear response which facilitated the extrusion of the material through a nozzle; and (3) a UV-light induced polymerization which enabled the post-extrusion chemical crosslinking of network chains and the fabrication of robust printed objects. The mechanical properties of the living materials have been extensively characterized through the use of rheology. Additionally, the behavior of encapsulated cells has been explored through extensive microscopy of the living materials.

The living materials developed herein have been demonstrated to effectively encapsulate yeast, bacteria, and algae while maintaining excellent cell viability for each microbial species. Through the use of extrusion 3D printing, precise spatial deposition of one or many cell types is made possible within a single printed construct. The printed living materials are shown to be effective to the on-demand and reusable production of high-value molecules, ranging from small molecules to peptides, through the use of both mono-culture or microbial consortia systems. Through the protection of embedded cells from preservation processes such as lyophilization, these Additively Manufactured Catalytically Active Living Materials (AMCALMs) can provide a platform for the sustainable generation of high-value compounds through repeated production phases.

TABLE OF CONTENTS

LIST OF FIGURES

LIST OF TABLES

ACKNOWLEDGEMENTS

It's tough to get through five years of work in any field without wanting to thank an extensive list of people. I am so thankful for a great number of people who have been an integral part of my time in graduate school and want to specifically highlight a handful of them here. I first want to thank my PI, Alshakim Nelson, for providing me excellent guidance and support throughout my time at UW. As one of Al's first students, I was given the opportunity to build the lab and my projects in directions that excited us both. I can confidently say that Al is the best boss I've ever had. He has an innate ability to simultaneously lead by example, while also empowering his students to leverage their own expertise and experiences in the direction and progress of their research. His trust in me further inspired both my confidence and my research abilities. While working with Al, I feel like the lab has grown into something I am extremely proud to be a part of. I also want to thank Abhijit Saha, who worked as a post-doc in the lab for my first few years of grad school. While we were a small, new lab at the start, Abhi was there for me as a mentor, always willing to help me with my work and answer my many questions.

Many collaborators have also helped me succeed while also expanding the scope of my work, and the breadth of my education. Jesse Zalatan and Chen Dong were instrumental in helping to get our lab ready to handle microbes, and for getting my projects underway. Alberto Carignano and Eric Klavins have been so helpful in expanding my knowledge of yeast and the possibilities (and challenges) of applications that can be developed using our lab's know-how. And most of all, Hal Alper and Shuo-Fu (Joseph) Yuan at UT Austin have provided me with so many resources and knowledge about synthetic biology, while helping grow my projects to heights I wasn't sure we could reach during my time at UW. I am forever grateful for everyone's time, help, and effort.

I also want to thank all of my friends for making my grad school years fun, while also helping me become a better scientist. While I am grateful for all of the members of the Nelson Lab, I specifically want to thank Amrita, Dylan, and Ryan, all of whom also joined the lab in our first year. I am so thankful for their friendship and support, and I couldn't have asked for a better group to work and grow alongside during the past five years.

And of course, I want to thank my family for all their love, and for helping me grow into the man I am today. My mom and dad have always encouraged me to be my best in whatever I pursue. Growing up, I presented them with many potential career options, from sports broadcaster to doctor. No matter my choice, they have always had my back and would do anything to help me achieve my goals. And to my brother, and my best friend, Gabriel, thank you for always believing in me and encouraging me to live my life to the fullest. I love you all.

And lastly, thank you to my girlfriend Camille, for your love, friendship, and encouragement throughout my PhD. Meeting you was not only one of the best moments of the last five years, but also one of the best parts of my life. Thank you for helping me with my quantum mechanics homework, for listening to my practice talks, for all your delicious cooking after long days in lab, and for sharing your life with me. From Huskies football games to happy hours, you've made my life brighter. I couldn't have done this without you.

For my Mom, Tamara.

I can never thank you enough for your endless love and support.

Chapter 1. INTRODUCTION

This chapter has been adapted from the following review paper:

> Sanchez-Rexach, E.; **Johnston, T. G.**; Jehanno, C.; Sardon, H.; Nelson, A. Sustainable Materials and Chemical Processes for Additive Manufacturing. Submitted, **2020**.

1.1 ABSTRACT

Additive manufacturing (AM) technologies are energizing the fields of chemistry and materials science to develop new inks, resins and filaments that meet the emerging needs in many applications that include aerospace, robotics, and healthcare. AM enables the fabrication of innumerable 3D geometries that cannot be easily produced by other means. In spite of the great promise of AM as an advanced form of future manufacturing, there are still fundamental challenges with respect to sustainability that need to be addressed, such as the lack of renewable material feedstocks and the recyclability of the products. The combination of bio-sourced and biodegradable polymers with additive manufacturing would enable the fabrication of objects that can be recycled back into feedstock or degraded into non-toxic products after they have served their function. Herein, we review the recent literature on biodegradable and bio-sourced polymers used in AM, with a focus on the design and chemistry of the polymers to enable the printing process. We also discuss some of the sustainability-related applications that have emerged as a result of AM technologies.

1.2 INTRODUCTION

Additive manufacturing (AM) is an advanced form of manufacturing that holds great promise for the customized, distributed, and on-demand production of parts. Three-dimensional (3D) models are produced in the virtual world, and then a 3D printer deposits a material (via layer-by-

layer or continuous deposition) according to the 3D model provided. AM, also known as 3D printing or rapid prototyping, emerged several decades ago as a method to generate previously unattainable geometric structures and functions.[1, 2] This manufacturing process is also useful across many industries, such as aerospace, where it is used to produce a small number of highly complex aircraft components, or in the medical sector where highly personalized products are required.

AM is a multi-faceted process that requires the convergence of hardware, software/modeling, and materials for its success. While the re-emergence of the field over the last decade has largely been driven by advances in the hardware and software/modeling, there is a growing interest among polymer chemists and materials scientists to design materials specifically for AM processes.[3, 4] Polymeric materials, including thermoplastics, thermosets, elastomers, and composites represent a growing body of suitable materials for AM. However, with increasing concerns of sustainability and the growing volume of plastic waste worldwide, it is imperative to understand how AM can affect global visions of sustainability.[5-8]

In order for AM to reach its full potential, sustainability within the AM ecosystem (hardware, software/modeling, and materials) must be addressed. Some of the material needs for AM include sustainable sources of printing inks, resins, and filaments, as well as pathways for polymer recycling, upcycling, and chemical circularity. With this in mind, there are four contexts by which sustainability in AM can be addressed (Figure 1.1): (i) renewable sources of chemical feedstocks that do not rely on petrochemical sources, (ii) AM hardware and processes that can minimize the production of waste or unwanted byproducts, (iii) end-of-use options for 3D printed products that include options to re-use and recycle, and (iv) applications in sustainability that emerge as a result

of new AM capabilities. This review will address each of these points, with a particular emphasis on the chemical processes and polymeric materials that have been developed recently in the field.

1.3 Additive Manufacturing Techniques

1.3.1 *Material Extrusion*

Material extrusion technologies extrude a material in a layer-by-layer manner from a nozzle that follows a predetermined path over a build plate (Figure 1.2a). This is an attractive technology in additive manufacturing due to the simplicity of operation, as well as the availability of low-cost printers that offer relatively good resolution. This platform accommodates many different printable materials through manipulation of printing temperatures, or shear-thinning behavior of the bulk material, and it offers the possibility of producing a multi-material product with different inks, as well as the combination of polymers with cells and growth factors to create tissue-like structures (bioprinting). Many biologically sourced monomers and polymers either already offer advantageous behaviors for extrusion printing, or such behaviors can be introduced through simple synthetic schemes to change the rheological features of the ink.[9]

Fused Deposition Modeling (FDM) (also referred to as Fused Filament Fabrication or FFF) is the most widely available 3D printing technology. FDM builds parts using a thermoplastic material in a filament form. The filament is pushed through a heated nozzle where it is melted. The printer continuously moves the nozzle to deposit melted material at precise locations following a pre-determined path. In this case, the waste plastic filament from misprints and undesired outputs can be minimal and can be reclaimed and reused. The plastic waste is first ground into granules and then fed into a filament extruder. Polymers, such as poly(lactide) (PLA) can be recycled in this manner with minimal loss in quality.[10]

1.3.2 *Vat Photopolymerization*

Vat photopolymerization utilizes patterned light to initiate the chemical cross-linking of a resin. Typically, UV light is used to activate a catalyst or reactive species for the radical polymerization of acrylates and methacrylates, or ring opening polymerization of epoxides.[11] Vat photopolymerization is particularly attractive for its resolution and the speed at which objects can be printed.

There are different types of vat photopolymerization AM that have been developed.[12] Stereolithographic apparatus (SLA) printing uses a build platform submerged in a resin tank filled with liquid photopolymer resin. A focused laser irradiates through a transparent window and irradiates the resin above the window surface in a patternwise manner (Figure 1.2b). Even though each layer is patterned individually resin components form covalent bonds layer to layer resulting in highly isotropic and smooth parts. Similarly, digital light processing (DLP) uses light to initiate cross-linking of a photopolymerizable resin. In this approach, patterned light is projected toward the resin to initiate polymerization (Figure 1.2c). Consequently, DLP can achieve faster print times compared to SLA, which afford printed objects more rapidly with reduced energy consumption and environmental impact.[13]

1.4 Renewable Feedstocks for Additive Manufacturing

The feedstock chemicals used in an AM process bear a significant role in the sustainability of the process. Bio-sourced small molecules and polymers offer a viable source of precursors that can be modified and formulated into resins and inks for printing. In parallel, alternative solutions are also of interest to reduce the introduction of harmful chemicals and solvents into manufacturing processes. This in turn reduces the amount of waste generated during the synthesis of feedstock materials, while also decreasing residual chemical contaminants that could remain in the part long

after printing is complete. These alternative materials will offer AM users greener manufacturing options.

A central challenge when developing resins and inks for 3D printing is the spatially controlled cross-linking of the material during the AM process. The speed of printing (and rate of parts production) is dependent upon the rate at which physical cross-links (non-covalent interactions such as van der Waals interactions, hydrogen bonding, ionic interactions, and polymer entanglement) or chemical cross-links (typically photo-initiated radical polymerization) can be formed. These cross-links also determine the mechanical properties of the printed object, which is of great concern when used in an application setting.

In general, naturally occurring biopolymers (DNA, proteins, and polysaccharides) possess a high molecular weight, which translates into inherently viscous polymer solutions. As a result, the processing and printing of these biopolymers in AM processes can be a challenge. Some of these biopolymers also require chemical modification to undergo light-initiated cross-linking. Alternatively, synthetic polymers can offer greater control over polymer composition, molecular weight, and the polymer architecture to accommodate the requirements of the printing technique.[14] Examples of biopolymers and synthetic polymers for AM are summarized in Figure 1.3.

1.4.1 *Renewable and Degradable Feedstocks for AM*

1.4.1.1 Polysaccharides, Proteins, and DNA

Naturally occurring biopolymers (polysaccharides, proteins, and DNA) are a source of renewable feedstock materials for AM that can be obtained on large scales from microbes, plants, and other organisms. These biopolymers are biodegradable, biocompatible, and have a life cycle that is the model form of sustainability. In their native roles, these biopolymers serve as signaling elements, infrastructure for energy and energy consumption, information storage, and structural

frameworks that provide living systems with their 3D form. The latter example has attracted significant interest in AM as these biopolymers meet the mechanical requirements to afford 3D objects that can maintain their shape fidelity. Thus, as nature has employed its structural biopolymers, such as cellulose, to create the stiff cell walls found in plants and trees, chemists and materials scientists have sought to co-opt these biopolymers for use with AM tools to pattern 3D objects.

Cellulose is the most abundant organic polymer on the planet, as an important structural polysaccharide of the primary cell wall of plants. Owing to their outstanding mechanical properties, cellulose fibers have been used to strengthen some biomaterial's matrixes in extrusion-based 3D printing.[15] Likewise, nanocellulose in the form of cellulose nanocrystals (CNC) or cellulose nanofibrils (CNF) has been used as a reinforcing agent in inks designed for additive manufacturing. The high orientation capacity of the nanocellulose, allows tailored responses to the applied mechanical load, inspired by the design principles found in wood. In addition, nanocellulose exhibits shear thinning rheology and thixotropic behaviors required for an extrudable material: as the piston of the extruder applies stress, the ink flows out from the nozzle but recovers its high viscosity once deposited, thus preventing its flow once it is deposited on the building platform. Siqueira et al.[16] created viscoelastic CNC-based inks for direct writing by just dispersing CNCs extracted from wood pulp in water. Correspondingly, Magdassi et al.[17] 3D printed objects composed of 100% wood-based materials, using a low value byproduct of the wood industry known as wood flour from grinded eucalyptus, pine or maple, in combination with a binder composed of CNCs that gives the ink shear thinning properties, and xyloglucan hemicellulose. Both materials can be obtained from industrial side streams, and the modulus and strength of the printed woods were within the range of natural woods. Additionally, Wallace et

al.[18] managed to easily print scaffolds made of CNFs with a good fidelity by adding a very low concentration of the UV cross-linkable gelatin methacrylate (Gel-MA), thanks to the strong interaction between the two components. In this study, CNFs were produced by the 2,2,6,6-tetramethylpiperidine-1-oxyl (TEMPO)-mediated oxidation to successfully disintegrate cellulose fibers, and avoid needle clogging while extrusion printing.

Crustacean shells can be used to harvest chitin, which can be deacetylated to form chitosan. While cellulose is comprised entirely of β1-4 linked glucopyranosides, chitosan is comprised of structurally similar β1-4 linked 2-amino-glucopyranosides. Chitosan hydrogels have been successfully 3D printed using extrusion-based processes for engineering bone tissue.[19] Inorganic molecules have also been mixed with chitosan for the purpose of improving its bioactivity to resemble bone. Muller et al.[20] integrated the natural polymer polyphosphate into a N,O-carboxymethyl chitosan matrix using calcium (Ca^{2+}) bridges.

Starch is a polymer blend produced by plants to store energy composed of the linear amylose which consists of D-glucose units joined by the α1-4 glycosidic linkages, and the branched amylopectin which consists of glucose units linked primarily by α1,4-glycosidic bonds but with occasional α1,6-glycosidic bonds, which are responsible for the branching. Similar to cellulose, the structure of starch also has abundant hydroxyl groups, offering the possibility of chemical modification to produce starch-based polymers for 3D printing. Maniglia et al.[21] used ozone oxidation to modify cassava starch for extrusion printing. They used ozonation to cleave the glycosidic bonds of both amylose and amylopectin molecules, and also to replace hydroxyl groups by carbonyl and carboxyl groups. On the one hand, the high inherent viscosity of this natural polymer was lowered thanks to the depolymerization of both amylose and amylopectin, and on the

other, the different interactions created between the oxidized molecules improved the printability of the starch-based inks.

Burdick and co-workers have reported an alternative strategy for physically cross-linking polysaccharides using the host-guest interactions that occur between cyclodextrin (CD) and adamantane (Ad). Hyaluronic acid (HA) was functionalized with either CD or Ad and the two polysaccharides were blended to afford a physically cross-linked hydrogel (Figure 1.4).[22] These shear-thinning hydrogels serve as excellent inks for material extrusion printing. The Cd-Ad pairs disassociated during the extrusion process, and then self-healed after deposition onto a substrate when shear was removed. Alternatively, these modified biopolymers were also developed as jammed microgels that also demonstrated shear-thinning behaviors.[23]

Alginate is a polysaccharide isolated from the cell walls of brown marine algae (seaweed). The viscosity of alginate is tunable with the changes to concentration and degree of oxidation.[24] The rapid ionic cross-linking of sodium alginate in the presence of calcium ions has been utilized for material extrusion printing. Its ease of use without additional modification has led to the widespread use of calcium alginate gels in bio-printing applications.[25-29]

Proteins represent another versatile class of biopolymers that have been adopted for AM. Collagen is a structural protein that is the primary component of connective tissue. This protein is well suited for bio-printing applications due to its ability to promote cell adhesion. Collagen is comprised of elongated fibrils of a triple helix of polypeptide chains, which makes it difficult to process in AM. Alternatively, gelatin is derived from hydrolyzed collagen and has improved processability as a consequence of its lower molecular weight. Gelatin methacrylate (Gel-MA) has seen growing interest in AM for tissue engineering and regenerative medicine.[14, 30-33]

All of the biopolymer examples discussed to this point have been printed via material extrusion, which is the predominant AM technique for 3D printing biopolymers. There are relatively fewer examples of vat photopolymerization approaches for printing biopolymers because the viscosity requirement for resins (up to 10 Pa·s maximum has been suggested) is difficult to achieve with polymers that intrinsically have a high viscosity.[12] One strategy has been to create composites with cellulose nanocrystals, but the biopolymer component is relatively small compared to the matrix material.[34, 35] This is particularly true when structural proteins are employed in these types of processes, as these proteins are designed to associate into larger aggregates or to form fibrous assemblies. However, there are a few recent examples of structural proteins in a vat photopolymerization processes. Silk fibroin is a material that can be harvested from silkworms and chemically processed to afford a water-soluble (and processable) form of the protein. This amorphous form of fibroin has random coil conformations that facilitate its solubility in water, and has been utilized in resins for vat photopolymerization.[36] Methacrylated silk fibroin was developed as a primary resin component, producing printed parts with excellent structural stability and biocompatibility.[37]

Globular proteins have also been shown to be suitable for vat photopolymerization. Methacrylated bovine serum albumin (MABSA) was shown to be highly soluble in water (up to 40 wt% w/v) due to its compact globular shape. The protein was formulated into low viscosity resins for vat photopolymerization using a commercial SLA printer. The 3D printed objects were subjected to a post-print thermal cure, which denatured the proteins and afforded bioplastic with mechanical properties comparable to poly(lactic acid) (PLA).[38] This demonstration opens opportunities for implementing recombinant proteins as sustainable sources.

1.4.1.2 Synthetic (Bio)degradable Polymers for AM

Aliphatic polyesters are a leading alternative to polymers from petrochemical sources because of their range of mechanical properties (as thermoplastics and elastomers) and their chemical and enzymatic degradability.[39] For example, different forms of poly(lactic acid) (PLA) have been synthesized, such as semicrystalline poly-L-lactide (PLLA), or amorphous poly(D,L-lactide) (PDLLA), which can affect their mechanical properties and rates of degradation. The copolymer of PLA and PGA (polyglycolic acid), i.e. PLGA, is commonly used in AM processes to increase the degradation rate of PLA.[40] The rate of degradation of this biodegradable polymer is proportional to the strength of the acidity or alkalinity of the surrounding media. Gassensmith et al.[41] benefited from this degradation behavior to overcome the resolution limitation of FDM. They constructed PLA microneedles with tip sizes as small as 1 μm, via chemical etching of 3D printed needles in an alkaline solution. Poly(L-lactide-co-ε-caprolactone) (PLC) copolymer was also examined for FDM printing which is softer and more elastic than PLA, but degrades faster than poly(ε-caprolactone) (PCL).[42] PLA can also be combined with other dynamic covalent processes, such as thermally reversible Diels-Alder reactions, to improve mechanical properties of the 3D printed objects using self-healing mechanisms.[43]

Polyhydroxyalkanoates (PHAs) are a class of polyesters that can be naturally produced by bacteria with tunable mechanical properties.[44, 45] Among them poly(3-hydroxybutyrate) (PHB) is a natural thermoplastic polyester produced by microorganisms. While PHB possesses many great properties, it is a very brittle substance on its own. However, many studies have investigated various methods to improve its mechanical strength for bone tissue engineering applications. One example involves the formation of composite scaffolds consisting of PHB and hydroxyapatite nanoparticles.[46] Interestingly, it was observed that in the poly(3-hydroxybutyrate-co-3-hydroxyvalerate) (PHBV) microbial polymer, the increase of 3HV content increased the

crystallinity and hydrophobicity of the PHBV.[47, 48] A PHB composite containing biorefinery lignin demonstrated a shear thinning profile which enhanced layer adhesion for extrusion 3D printing. Although not discussed in detail here, lignin has promise as a feedstock for AM.[49-51]

PCL is a well-studied, biocompatible crystalline polymer with a low melting temperature. While in the past was mainly produced from non-natural resources, in the last decades intensive research has been devoted to its production from biomass. Due to its compatibility with many drugs and slow degradation kinetics, PCL is especially suitable for long-term drug-delivery systems.[52] The hydrolysis rate and the mechanical and viscosity properties can be tailored by copolymerizing with other polymers or by incorporating more labile bonds into the PCL backbone. PCL has been widely used as a feedstock material for extrusion-based AM, owing to its excellent processing ability. In fact, high molecular weight PCL lacks printability by methods other than extrusion AM. Hart et al.[53] discussed the modification of PCL diols with a multitude of hydrogen bonding and π-stacking moieties through 2,4-toluene diisocyanate end-capping reactions. The inclusion of these groups at relatively low concentrations led to the formation of supramolecular networks that exhibited shear thinning behavior and successful inkjet printing (Figure 1.5a). To create PCL amenable to other AM techniques, chemical modification is necessary. Elomaa et al.[54] produced three-armed PCL oligomers of various molecular weights, which were end-functionalized with methacrylic anhydride and photocrosslinked to obtain a porous scaffold with a high resolution by SLA (Figure 1.5b). Since macromers were heated above the melting temperature (60 °C) to obtain the suitable viscosity, no solvent was needed. Due this solvent-free SLA approach, no material shrinkage was observed after extraction and drying of the printed scaffolds.

Highly biocompatible hydrogels that degrade in the body for vat photopolymerization can be prepared by tuning the hydrophilicity of PLA with polyethylene glycol (PEG). Seck et al.[55] synthesized PDLLA-PEG-PDLLA-based resins for SLA that allows the generation of designed three-dimensional cross-linked structures. The hydroxyl end groups of the synthesized PDLLA-PEG-PDLLA oligomers were reacted with methacrylic anhydride to obtain MA-DLLA-PEG-DLLA-MA photocrosslinkable macromers (Figure 1.5d).

Polypropylene fumarates (PPF) are another promising class of biocompatible and biodegradable polymeric biomaterials. PPF degrades to propylene glycol and fumaric acid which are biocompatible subunits. PPF is normally processed by vat polymerization method since it has unsaturated sites in its backbone desirable for photopolymerization, and it is usually combined with diethyl fumarate (DEF) to reduce the viscosity of the ink.[40] Even when it is printed by FDM a UV curing head is incorporated to the printing systems, and a photosensitive cross-linker is added to the formulation.[56] The materials made of PPF are generally postcured to obtain a higher cross-linking ratio, and improve the mechanical integrity. Melchiorri et al.[57] printed PPF tubes to help the problems causes by a congenital heart disease from 3D computer models made through medical imaging technologies such as MRI or CT, and Lee et al.[58] used micro-stereolithography to print tridimensional microstructures (Figure 1.5c).[59] Becker et al.[60] 3D printed scaffolds with shape recovery following compression based on PPF star polymers. It should be noted that they used magnesium ethoxide catalyst to avoid the toxicity of cobalt,[61] for the synthess of star-shaped poly(propylene maleate) (PPM) subsequently converted to PPF upon isomerization by using the sugar-based alcohol meso-erythritol as an initiator.[62]

Poly(glycerol sebacate) (PGS) is a widely used biodegradable elastomer synthesized via the thermal condensation of glycerol and sebacic acid. Curing of PGS usually requires high

temperature and high vacuum. Lei et al.[63] 3D printed a PGS/salt composite in an extrusion-based printer, and then it was thermally cured under vacuum to obtain a stable cross-linked 3D structure. Finally, the salt particles were readily removed by dissolution in water to form interconnected micropores throughout the construct. In addition to its excellent biocompatibility and biodegradability, one of the most important advantages of cured PGS is its robust elasticity due to its chemically stable cross-linked structure. Langer et al.[64] 3D printed poly(glycerol sebacate) acrylate (PGSA), a photocurable degradable elastomer compatible with light-based 3D printing. By tailoring the PGS elastomer to the viscoelastic properties of native soft tissues, porous PGS patches were printed to treat myocardial infarction.[63]

Apart of polyesters, other biodegradable polymers have been also investigated for sustainable additive manufacturing such as polyurethanes. One of the key features of most polyurethanes is their ability to phase-separate into soft and hard segments. This phase separation, coming from hydrogen bond-based physical cross-linking of the hard segment, could potentially facilitate the printing process.[65] Unfortunately, polyurethane synthesis usually necessitates the use of isocyanate monomers and organic solvents, all of which have toxicity issues and are environmental pollutants.[66] As an alternative to the traditional solvent-borne PU in response to the environmental concerns, waterborne or water-based polyurethane (PU) have been developed. Waterborne biodegradable PUs can have a range of tunable mechanical and degradation properties, and can even undergo gelation by varying the composition of soft segments in polymer chains.[67] The biodegradable and biocompatible elastomeric PU is used in many biomedical applications, such as scaffolding material for repairing neural and venous defects.[68] Hsie et al.[69] combined a water-based biodegradable PU nanoparticle dispersion with a gelatin solution to prepare a PU-gelatin bioink that could be loaded with cells to print tridimensional constructs with a 3D bioprinter.

Additionally, Hsu et al.[70] developed a water dispersion of PU biodegradable nanoparticles by incorporating ionic hydrophilic groups onto the hydrophobic backbones to form an emulsion without the use of toxic organic solvents. The soft segment was based on PCL diol and polyethylene butylene adipate (PEBA) diol. They designed the soft-segment compositions with the intention of generating mechanical properties and degradation rates appropriate for cartilage tissue engineering. The resulting extrusion printed scaffolds can be seen in Figure 1.6a. In turn, Huang and coworkers[71] synthesized a type of polyurethane acrylate containing disulfide bonds which mixed with the reactive diluent hydroxyethyl acrylate and photoinitiators resulted in a photopolymer resin for DLP with self-healing properties (Figure 1.6b). In spite of the undeniable benefits of polyurethanes in comparison to other polymer families, the starting common isocyanates are synthesized using phosgene, and taking into account the need to guarantee the users' safety, it is important to find alternative and greener routes to PUs, involving non-toxic reagents. In the last decade, alternative and environmentally friendly approaches have been developed to synthesize non-isocyanate biobased polyurethanes (NIPUs) but their use in additive manufacturing processes is still rare.[72, 73]

As an example of the advantages of mixing natural and synthetic sustainable polymers for AM, an L-alanine-derived depsipeptide was used to synthesize a biodegradable, photocrosslinkable poly(ethylene glycol-co-depsipeptide) (PEG-co-PDP) macromer for the SLA-based fabrication of hydrogels. The photocrosslinkable macromer combined both naturally derived and synthetic building blocks. The depsipeptide units introduced biodegradable bonds to the PEG backbone, and by adjusting the light exposure time in the SLA, they could be controlled the swelling capacity, degradation rate, and mechanical stiffness of the resulting hydrogels without the need for changing the intrinsic composition of hydrogel solution (Figure 1.7).[75]

1.4.1.3 Small Molecules as Renewable Sources

While biologically derived materials for vat photopolymerization have not been quite as widely explored as their extrusion counterparts to date, it is an expanding field with promising resin candidates emerging. Voet et al.[76] formulated a number of bioderived resins including isobornyl acrylate, 1,10-decanediol diacrylate, pentaerythritol tetraacrylate, and multifunctional acrylate oligomer. They also developed biobased photopolymer resins based on modified soybean oil methacrylates from commercial epoxidized soybean oil with different stiffness and toughness values depending on the number of functional groups per oligomer (Figure 1.8a).[77]

One such class of resins are based on terpenes, molecules that can be harvested from many plants and even some insects. Weems et al.[78] showed that through the use of various terpene materials and a four-armed thiol linker, 3D mesh structures could be printed through the use of thiol-ene click chemistry. By using these materials in the presence of a radical initiator, the photocrosslinked materials exhibited mechanical properties that ranged from brittle elastomers to engineering grade thermosets. These properties could be easily tailored through simply altering the terpene monomer or prepolymer content of the resin.

Ding et al.[79] utilized natural phenols and thiol-ene click chemistry to develop a resin suitable for SLA printing, aiding in the shift away from dependence on petroleum-derived polymers. They created photoreactive resins from renewable biomass to substitute acrylates combining a structural diacrylate synthesized by a facile dimerization of eugenol (4-allyl-2-methoxyphenol) with a dithiol through the radical thiol–ene click reaction, guaiacol (2-methoxyphenol) methacrylate as diluent, and the photocrosslinker vanillyl alcohol (4-(hydroxymethyl)-2-methoxyphenol) dimethacrylate with a radical photoinitiator (Figure 1.8b).

These interesting inks based on polymers occurring in nature promise alternatives for the development of environmentally friendly processes that can circumvent many of the drawbacks of traditional petroleum-derived polymers for 3D printing.

1.4.2 *Next Generation of Materials to Re-Use and Recycle*

The increase in the volume of plastic waste and its contamination to the environment are global challenges which require innovative solutions. Plastic re-use and recycling are crucial components for a future plastic economy. As 3D printing grows as a viable manufacturing option, it is essential to develop approaches for 3D printed polymeric materials that do not exacerbate the already serious plastic waste issue.

1.4.2.1 Resins from Plastic Wastes

One approach to reduce the impact of 3D printing on plastic waste involves the recovery of consumer-grade plastics and their recycling into a material which could be then 3D printed. Because of the broad commercial use of polymers such as polyolefins, polystyrene or poly(ethylene terephthalate), their associated plastic wastes have been explored for incorporation as feedstock materials for AM.

Studies on polyolefin waste streams have been led to evaluate the possibility of employing such materials as a feedstock for material extrusion printing. Attempts to recycle both high- and low-density polyethylene (PE) have demonstrated that, while high thermal stability and good barrier properties are advantageous, the adhesion and warping issues of the obtained material make it difficult to handle.[80, 81] Similar studies on polypropylene (PP) emphasized the need for obtaining a material that meets the required properties for 3D printing by mixing such PP wastes with natural fibers or different polymers and compatibilizers.[82, 83] Recycled PET (rPET), obtained by grinding and pelleting PET wastes, was also employed as raw material for material extrusion processes.

The resulting bulk material demonstrated similar tensile strength to commercial filaments.[84] It was also determined that polycarbonate (PC) coming from E-wastes could be re-used as filaments for 3D printing up to three times before the properties of the material degraded to a non-printable state.[85, 86] Finally, polylactic acid (PLA) and acetonitrile butadiene styrene (ABS), two polymers regularly employed in 3D printing, have been very recently investigated in their respective recycled forms. Both polymers cannot be re-printed more than twice because of the significant increase in viscosity for PLA,[10] and the increase in both tensile and compressive strengths for ABS.[87]

Although these studies revealed the systematic depletion in the material quality after several cycles of mechanical recycling, some life-cycle assessments suggested that it can be a cost-effective method to reduce plastic waste and increase re-use of these materials – even if for only one additional time of use.[88, 89] While these results are encouraging, more sustainable and durable alternatives are required.

1.4.2.2 Circular-by-Design Materials

A circular-by-design material by definition has been designed and synthesized with consideration to its end-of-life management.[90] By instituting a "switch" into the life cycle of the material (irradiation, temperature, change of catalysts, solvent conditions, etc.), these polymers are synthesized with the intention of post-use recycling and its re-implementation as a material feedstock. This cycle provides the material with a theoretically infinite closed-loop lifecycle, which in turn, drastically reduces waste. The three different methods to recycle a 3D printed polymeric object are categorized as reshape, reprocess, and chemically recycle.

A polymeric material that can be reshaped is one that can be reformed into a new shape upon heating or irradiation with light. This strategy increases the lifetime of the printed object, as it

enables repair if damaged or scratched, (Figure 1.9 – Reshape). A polymeric material can be reprocessed if a 3D printed object can either be grinded or dissolved to obtain pellets or a powder, which can be remolded into resin, ink, or filament for 3D printing (Figure 1.9 – Reprocess). Finally, to be depolymerized, a polymer should undergo a chemical reaction to recover monomers that can be re-polymerized into a fresh resin, ink, or filament which can be 3D printed to obtain a new object with the exact same properties than the initial one (Figure 1.9 – Chemically Recycle). In all three cases, the 3D printed objects must retain the same physical properties. The ideal resin, ink, or filament should comply with these three requirements, but obtaining such a material is a significant challenge. With that being said, the recent literature offers some interesting advances in this pursuit.

In a recent publication, Wei et al.[91] synthesized a polyurethane/carbon foam composite with encouraging reprocessability performance. A commercial thermoplastic polyurethane (TPU) was mixed with carbon black and nanoclay in DMF before its application as a thixotropic fluid for direct ink writing (DIW). After removal of the solvent and freeze drying, a compressible porous and conductive material was obtained for use as a strain and gas sensor. While the ease of reprocessing this material by dissolution in DMF, the notable reduction in mechanical properties after the fourth reprocessing cycle left some room for improvement when considering a truly circular lifecycle.

In addition, Hu et al.[92] developed a fully renewable and 3D-printable material by mixing the biobased elastomer PLBSI with PLA via an in situ dynamic vulcanization process. Morphological studies of the material demonstrated that agglomerates of PLBSI nanoparticles are dispersed in a PLA phase, resulting in good rheological properties. By increasing the PLBSI content to 60-70 wt%, the resulting material exhibited excellent elastic recovery, comparable to that of similar

commercial materials. Cytotoxicity tests also suggested that PLBSI/PLA blends could be used as biocompatible materials. Finally, the material can be reprocessed once with a minimal loss in both tensile strength and elongation at break. However, after 5 reprocessing of the same sample, significant mechanical loss can be observed, from 15.8 MPa for fresh sample to 10.3 MPa in tensile strength and from 255 to 135% in the elongation at break.

1.4.2.3 The Peculiar Case of Thermosets: Reprocessable and Recyclable?

In contrast to thermoplastics, thermosets are inherently non-recyclable because the polymer is permanently cross-linked by covalent bonds. This characteristic makes this family of polymer more resistant to solvent and instills superior thermomechanical properties. Thus, thermosets are typically better candidates for applications such as high-temperature electronic devices or automotive components, which account for 15-20% of current plastic production.[93] Thermosetting polymers actually represent almost 50% of the 3D printing materials market, but they exhibit deficiencies in reshaping. However, the reprocessing and even the chemical recycling of such materials has been recently explored in a very limited number of reports.

Covalent adaptive networks (CANs) are polymer networks that contain exchangeable covalent bonds.[94-96] A sub-category of CANs, known as vitrimers, are particularly attractive as reprocessable and recyclable materials for AM.[97] Vitrimers undergo associative bond exchange reactions upon thermal activation, thus preserving the number of cross-links in the matrix and maintaining the mechanical properties of the thermoset.[98] For example, Shi et al.[99] first presented a fully recyclable thermosetting epoxy ink for 3D printing. This printing method uses solvent-assisted transesterification type bond-exchange reactions of vitrimer epoxy to achieve 3D printing and recycling. The printed epoxy materials were recycled by being dissolved in ethylene glycol in a sealed container at 180 ºC for 6 h to obtain the depolymerized vitrimers. Then, the ethlylene

glycol was evaporated after 8 h at the same conditions, resulting in a partially cured ink with sufficient viscosity for a next round of 3D printing. After four dissolution-3D printing loops, the obtained ink demonstrates equivalent properties than the initial material. However, the fastidious polymerization reaction reduces this material to direct-ink-writing 3D printing techniques, which limits both the geometric complexity and resolution.

Later on, Zhang et al.[100] used an innovative method for the preparation of a reprocessable thermoset for UV curing-based high-resolution 3D printing. Employing a photoinitiator and a cross-linker together with hydroxy-3-phenoxypropylacrylate as monomer, a polymer was produced containing both permanent and dynamic covalent bonds. This allowed the material to be reshaped at elevated temperature, due to the bond-exchange reactions that occurred at temperatures higher than 180 ºC (Figure 1.10). The same material also demonstrated self-healing properties. After being damaged, a structure was polished and additional material was added to re-build the exact same structure with no mechanical performance losses observed in the previously damaged region. Finally, the material was mechanically reprocessed by grinding the printed structure. The resultant powder was subjected to high temperatures to obtain a new ink due to the bond-exchange reactions. The uniaxial tensile tests performed on the reprocessed structures demonstrated minimal stiffness lost through the second cycle, but exhibited decreasing performance in subsequent cycles, from a maximum tensile strength of 15 MPa dropping to less than 12 MPa after the third cycle.

Finally, a recent publication on 4D printing lightweight microlattices reported a UV-curable resin prepared from a molecule otherwise only employed as cross-linker for such applications: bisphenol A glycerolate dimethacrylate (BPAGMA). The shape-memory, self-healing polymer can be reprocessed by means of heating and compressing (9 to 12 MPa) for 2 h at 150 to 200 ºC. The mechanical tests performed on the reprocessed rectangular samples show slight depletion in

the quality of the material. The increase in temperature leads to poor mechanical properties, likely due to the thermal conditions increasing the prevalence of transesterification reactions. The authors claim on behalf of precedent studies that the balanced ratio between hydroxyl and ester groups on the BPAGMA polymer is a key parameter for a good recycled material.[101]

1.5 Additive Manufacturing for Sustainability

When compared with traditional manufacturing methods, there are some potential sustainability benefits to AM: efficient material utilization, reduced waste from the manufacturing process, freedom in the design of printed parts, and most importantly, AM allows the instant fabrication of customized parts in the place of need, reducing the transportation costs and pollution. Below, some significant examples are presented regarding how additive manufacturing can contribute to a more sustainable fabrication.

1.5.1 *Mass Reduction*

While many of the works cited in this review address the implementation of sustainable materials in the future of manufacturing, there are also additional ways in which the implementation of additive manufacturing can have a significant impact on existing manufacturing practices and procedures with commonly employed materials. One such example is through the use of 4D printing.[102, 103] This practice consists of the production of simple 3D printed parts that undergo further shape change as a response to an additional external stimulus, such as osmotic pressure, temperature change, or light exposure.[104, 105] One area in which this can be particularly influential is through the reduction of shipping costs. Through the manufacturing of 2D parts that can be assembled to form furniture,[106] or through shape morphing foods that transform from flat

shapes to their final 3D form during cooking,[107] making shipped goods more compact can make shipping volumetrically efficient, reducing environmental impact (Figure 1.11).

On the other hand, additive manufacturing techniques allow for a reduction of infill density of a printed part. This is a process that involves software analysis of a CAD design prior to printing, allowing for a reduction in material used during fabrication of the final part, while maintaining structural integrity of the part. Through the use of lower infill percentages and commercially available printers and design software, significant energy savings can be made when compared to traditional processing and shipping of plastic products.[88]

Lastly, additive manufacturing could have a significant effect on energy consumption in commercial construction, by moving the entire assembly process to the designated site, reducing the need for transport of pre-assembled goods and parts. Large industrial-scale printers can be deployed on site for the customized manufacturing of individual pieces, or the entirety of buildings of various sizes. By reducing the complexity of shipped goods from pre-assembled and manufactured components down to the raw construction materials of low embodied energy, shipping costs, construction site waste, and their associated environmental impacts could be greatly reduced. Many examples of entirely additively manufactured buildings already exist today, and are being more common, such as seen in Dubai,[108] and Italy.[109] In addition, by introducing more automation and ground-up manufacturing in construction processes, it is even believed that on-site worker injuries and fatalities could be reduced.[110]

1.5.2 *3D-Printed Catalysts and Reactors*

Additive manufacturing has also enabled the production of intelligently designed devices for the fermentation or production of high-value product compounds from a feedstock of less-valuable starting materials. While the idea of reactor technology is not new, the practice of additive

manufacturing of solid-state reactors allows for the precise deposition of catalysts or introduction of reactants at a particular point of space or time during reaction. Cronin has been particularly influential in this space in the production of "Reactionware", in which low cost appliances are additively manufactured from inexpensive starting materials. By printing these reactors, researchers are able to introduce reagents or catalysts in pre-programmed positions in the Reactionware, allowing for reduced manufacturing times and costs, while simplifying operational procedures. Many different types of compounds have already been successfully produced using this technology, including heterocycles, Diels-Alder products, imines, amines, and coordination polymers.[112-115] In one such example, various reaction chambers were printed with connecting channels, allowing for the sealed device to be operated through 90 degree rotations (Figure 1.12).[113] By using this methodology, a multi-step synthesis was possible without the need for any pumps or handling of the liquid reagents during operation. Another strategy for developing fluidic reactors includes the immobilization of enzymes within a printed construct.[116, 117] Precursor material can be flowed into the reactor and exposed to the active enzymes to undergo the designed transformation. Many aspects of the device, such as flow rate and feature sizes, can then be tailored to optimize efficiency of the fermenter for a particular reaction type.

Other materials have also been explored to create reactors via the encapsulation of metabolically active cells (Figure 1.13).[118-121] By entrapping microbes into a porous matrix, the metabolic activity of the cells can be harnessed to act as whole-cell catalysts in designed reactor processes. Many biologically-derived and synthetic materials alike have successfully been 3D-printed to produce these technologies. Naturally occurring polymers such as carrageenan and hyaluronic acid have been combined in blends to produce a printable material that can encapsulate microbes for degrading chemical pollutants, or to produce medically relevant bacterial cellulose.[122]

Similarly, synthetic polymers such as functionalized pluronics, or other novel triblock copolymers have been used to create soft hydrogel materials for the 3D printing of encapsulated yeast cells.[123, 124] The 3D printed lattice constructs have shown to be mechanically robust post-printing curing step, allowing for reusability in many rounds of fermentation, producing small molecules and polypeptides. With so many industries already relying on cellular fermentation for the production of molecules of interest, these materials offer immense promise in the future of sustainable and reusable batch reactor processes.

1.6 Conclusions and Outlook

In the future, AM is projected to enable on-demand and distributed manufacturing of parts and equipment worldwide for medical, aerospace, and other consumer products. Thus, it is imperative to develop sustainability into all aspects of the AM ecosystem (hardware, software/modeling, and materials), but in particular, AM must fit into the future plastics economy. Inks, resins, and filaments for AM will need to rely on renewable sources of chemical feedstocks. Natural biopolymers, (bio)degradable synthetic polymers, and small molecules can be produced using plants, microbes, and other organisms. Chemical modification to alter viscoelastic properties, physical cross-linking, and/or chemical cross-linking of these renewable feedstocks may be required in order to be compatible with AM processes. Currently, materials are largely modified to incorporate functional groups for photo-initiated radical polymerization as it is widely applied in AM. Future research should explore methods to introduce chemical and physical cross-links into a material in a spatially defined manner. For example, new photo-acid and photo-base catalysts can be developed for vat photopolymerization, as well as to provide an expanded set of renewable monomers and polymers for AM.[125]

Plastics have become ubiquitous in our society, and the volume of plastic use and production is expected to increase. The future plastics economy will undoubtedly require methodologies to re-use and recycle (mechanically and chemically) plastics. Recent trends include the use of discarded plastic as a feedstock for the preparation of resins for additive manufacturing or the implementation of new resins that are circular by design in additive manufacturing processes. Recycling the excess and unwanted material primarily into new feedstock, or finding new methods for the material to be easily recyclable is imperative for the evolution of additive manufacturing. Indeed, when the environmental impact of a product is evaluated, both the sustainability of the source and its life-cycle assessment must be performed.

While the ideal scenario is to create circular-by-design materials, few polymers can actually be depolymerized to efficiently close the loop. Thus, the quality of the polymers obtained from chemical recycling (*i.e.* the properties of the material) to date is limited. Future research should extend the range of materials which exhibit quantitative polymer reversal and isolation of pure monomers, especially the ones derived from renewable resources. And while plastic recycling has been implemented for reducing the tremendous volume of plastic waste generated, the use of plastic waste as a "sustainable" and cheap source for producing new 3D printable resins could face the problems of high cost to design cradle-to-cradle processes. Therefore, future chemical recycling processes should not only be focused in minimizing the plastic waste but also in designing new materials able to be manufactured.

Finally, AM will provide the capability to develop new solutions to applications that previously could not be solved. Some examples have already been reported, such as 4D objects that can be shipped globally as sheets that can fold into a 3D object upon the application of a stimulus, or immobilized catalysts and reactor systems that provide more efficient chemical production. AM is

a highly interdisciplinary field that involves chemistry and materials science, in addition to a diverse set of engineering disciplines that include mechanical engineering, chemical engineering, and computer science. Broader collaboration across all of these disciplines is required to provide 21st century solutions to sustainability.

1.7 REFERENCES

1. Hull, C. W. Apparatus for production of three-dimensional objects by stereolithography. U.S. Patent 4,575,330, March 11, 1986.
2. Gross, B. C.; Erkal, J. L.; Lockwood, S. Y.; Chen, C.; Spence, D. M., Evaluation of 3D Printing and Its Potential Impact on Biotechnology. *Anal. Chem.* **2014,** *86*, 3240−3253.
3. Narupai, B.; Nelson, A., 100th Anniversary of Macromolecular Science Viewpoint: Macromolecular Materials for Additive Manufacturing. *ACS Macro Letters* **2020**, 627-638.
4. Ligon, S. C.; Liska, R.; Stampfl, J.; Gurr, M.; Mulhaupt, R., Polymers for 3D Printing and Customized Additive Manufacturing. *Chem. Rev.* **2017,** *117* (15), 10212-10290.
5. Schneiderman, D. K.; Hillmyer, M. A., 50th Anniversary Perspective: There Is a Great Future in Sustainable Polymers. *Macromolecules* **2017,** *50* (10), 3733-3750.
6. Fortman, D. J.; Brutman, J. P.; De Hoe, G. X.; Snyder, R. L.; Dichtel, W. R.; Hillmyer, M. A., Approaches to Sustainable and Continually Recyclable Cross-Linked Polymers. *Acs Sustain Chem Eng* **2018,** *6* (9), 11145-11159.
7. Lange, J. P., Sustainable development: efficiency and recycling in chemicals manufacturing. *Green Chemistry* **2002,** *4* (6), 546-550.
8. Geyer, R.; Jambeck, J. R.; Law, K. L., Production, use, and fate of all plastics ever made. *Sci Adv* **2017,** *3* (7).
9. Hospodiuk, M.; Dey, M.; Sosnoski, D.; Ozbolat, I. T., The bioink: A comprehensive review on bioprintable materials. *Biotechnol. Adv.* **2017,** *35* (2), 217-239.
10. Zhao, P.; Rao, C.; Gu, F.; Sharmin, N.; Fu, J., Close-Looped Recycling of Polylactic Acid Used in 3D Printing: An Experimental Investigation and Life Cycle Assessment. *J. Clean. Prod.* **2018,** *197*, 1046–1055.
11. Bagheri, A.; Jin, J., Photopolymerization in 3D Printing. *ACS Applied Polymer Materials* **2019,** *1* (4), 593-611.
12. Appuhamillage, G. A.; Chartrain, N.; Meenakshisundaram, V.; Feller, K. D.; Williams, C. B.; Long, T. E., 110th Anniversary: Vat Photopolymerization-Based Additive Manufacturing: Current Trends and Future Directions in Materials Design. *Industrial & Engineering Chemistry Research* **2019,** *58* (33), 15109-15118.
13. Malshe, H.; Nagarajan, H.; Pan, Y.; Haapala, K. In *Profile of Sustainability in Additive Manufacturing and Environmental Assessment of a Novel Stereolithography Process*, ASME 2015 International Manufacturing Science and Engineering Conference, Charlotte, North Carolina, USA, Charlotte, North Carolina, USA, 2015.
14. Pekkanen, A. M.; Mondschein, R. J.; Williams, C. B.; Long, T. E., 3D Printing Polymers with Supramolecular Functionality for Biological Applications. *Biomacromolecules* **2017,** *18*, 2669−2687.

15. Duigou, A. L.; Castro, M.; Bevan, R.; N.Martin, 3D printing of wood fibre biocomposites: From mechanical to actuation functionality. *Mater. Des.* **2016,** *96*, 106–114.
16. Siqueira, G.; Kokkinis, D.; Libanori, R.; Hausmann, M. K.; Gladman, A. S.; Neels, A.; Tingaut, P.; Zimmermann, T.; Lewis, J. A.; Studart, A. R., Cellulose Nanocrystal Inks for 3D Printing of Textured Cellular Architectures. *Adv. Funct. Mater.* **2017,** *27*, 1604619.
17. Kam, D.; Layani, M.; Minerbi, S. B.; Orbaum, D.; Harush, S. A. B.; Shoseyov, O.; Magdassi, S., Additive Manufacturing of 3D Structures Composed of Wood Materials. *Adv. Mater. Technol.* **2019,** *4*, 1900158.
18. Xu, W.; Molino, B. Z.; Cheng, F.; Molino, P. J.; Yue, Z.; Su, D.; Wang, X.; Willför, S.; Xu, C.; Wallace, G. G., On Low-Concentration Inks Formulated by Nanocellulose Assisted with Gelatin Methacrylate (GelMA) for 3D Printing toward Wound Healing Application. *Acs Appl Mater Inter* **2019,** *11* (9), 8838-8848.
19. Demirtaş, T. T.; Irmak, G.; Gümüşderelioğlu, M., A bioprintable form of chitosan hydrogel for bone tissue engineering. *Biofabrication* **2017,** *9*, 035003.
20. Muller, W. E. G.; Tolba, E.; Schroder, H. C.; Neufurth, M.; Wang, S.; Link, T.; Al-Nawas, B.; Wang, a. X., A new printable and durable N,O-carboxymethyl chitosan–Ca2+–polyphosphate complex with morphogenetic activity. *J. Mater. Chem. B* **2015,** *3*, 1722.
21. Maniglia, B. C.; Lima, D. C.; Matta Junior, M. D.; Le-Bail, P.; Le-Bail, A.; Augusto, P. E. D., Hydrogels based on ozonated cassava starch: Effect of ozone processing and gelatinization conditions on enhancing 3D-printing applications. *Int. J. Biol. Macromol.* **2019,** *138*, 1087-1097.
22. Ouyang, L.; Highley, C. B.; Rodell, C. B.; Sun, W.; Burdick, J. A., 3D Printing of Shear-Thinning Hyaluronic Acid Hydrogels with Secondary Cross-Linking. *ACS Biomater. Sci. Eng.* **2016,** *2* (10), 1743-1751.
23. Highley, C. B.; Song, K. H.; Daly, A. C.; Burdick, J. A., Jammed Microgel Inks for 3D Printing Applications. *Adv. Sci.* **2019,** *6*, 1801076.
24. Jia, J.; Richards, D. J.; Pollard, S.; Tan, Y.; Rodriguez, J.; P.Visconti, R.; C.Trusk, T.; J.Yost, M.; Yao, H.; R.Markwald, R.; YingMei, Engineering alginate as bioink for bioprinting. *Acta Biomaterialia* **2014,** *10* (10), 4323-4331.
25. Rastogi, P.; Kandasubramanian, B., Review of alginate-based hydrogel bioprinting for application in tissue engineering. *Biofabrication* **2019,** *11*, 042001.
26. Tabriz, A. G.; Hermida, M. A.; Leslie, N. R.; Shu, W., Three-dimensional bioprinting of complex cell laden alginate hydrogel structures. *Biofabrication* **2015,** *7*, 045012.
27. Duan, B.; Hockaday, L. A.; Kang, K. H.; Butcher, J. T., 3D Bioprinting of heterogeneous aortic valve conduits with alginate/gelatin hydrogels. *J Biomed Mater Res Part A* **2013,** *101A* (5), 1255–1264.
28. Axpe, E.; Oyen, M. L., Applications of Alginate-Based Bioinks in 3D Bioprinting. *Int. J. Mol. Sci.* **2016,** *17*, 1976.
29. Bakarich, S. E.; Panhuis, M. i. h.; Beirne, S.; Wallacea, G. G.; Spinks, G. M., Extrusion printing of ionic–covalent entanglement hydrogels with high toughness. *J. Mater. Chem. B* **2013,** *1* (38), 4939-4946.
30. Klotz, B. J.; Gawlitta, D.; Rosenberg, A. J. W. P.; Malda, J.; Melchels, F. P. W., Gelatin-Methacryloy Hydrogels: TowardsBiofabrication-Based Tissue Repair. *Trends Biotechnol.* **2016,** *34* (5), 394-407.

31. Yin, J.; Yan, M.; Wang, Y.; Fu, J.; Suo, H., 3D Bioprinting of Low-Concentration Cell-Laden Gelatin Methacrylate (GelMA) Bioinks with a Two-Step Cross-linking Strategy. *ACS Appl. Mater. Interfaces.* **2018,** *10* (8), 6849-6857.
32. Nichol, J. W.; Koshy, S. T.; Bae, H.; Hwang, C. M.; Yamanlar, S.; Khademhosseini, A., Cell-laden microengineered gelatin methacrylate hydrogels. *Biomaterials* **2010,** *31* (21), 5536-5544.
33. Van Den Bulcke, A. I.; Bogdanov, B.; De Rooze, N.; Schacht, E. H.; Cornelissen, M.; Berghmans, H., Structural and Rheological Properties of Methacrylamide Modified Gelatin Hydrogels. *Biomacromolecules* **2000,** *1* (1), 31-38.
34. Palaganas, N. B.; Mangadlao, J. D.; de Leon, A. C.; Palaganas, J. O.; Pangilinan, K. D.; Lee, Y. J.; Advincula, R. C., 3D Printing of Photocurable Cellulose Nanocrystal Composite for Fabrication of Complex Architectures via Stereolithography. *Acs Appl Mater Inter* **2017,** *9* (39), 34314-34324.
35. Kumar, S.; Hofmann, M.; Steinmann, B.; Foster, E. J.; Weder, C., Reinforcement of Stereolithographic Resins for Rapid Prototyping with Cellulose Nanocrystals. *Acs Appl Mater Inter* **2012,** *4* (10), 5399-5407.
36. Shin, S.; Kwak, H.; Hyun, J., Melanin Nanoparticle-Incorporated Silk Fibroin Hydrogels for the Enhancement of Printing Resolution in 3D-Projection Stereolithography of Poly(ethylene glycol)-Tetraacrylate Bio-ink. *ACS Appl. Mater. Interfaces* **2018,** *10*, 23573−23582.
37. Kim, S. H.; Yeon, Y. K.; Lee, J. M.; Chao, J. R.; Lee, Y. J.; Seo, Y. B.; Sultan, M. T.; Lee, O. J.; Lee, J. S.; Yoon, S.-i.; Hong, I.-S.; Khang, G.; Lee, S. J.; Yoo, J. J.; Park, C. H., Precisely printable and biocompatible silk fibroin bioink for digital light processing 3D printing. *Nat Commun* **2018,** *9*, 1620.
38. Smith, P. T.; Narupai, B.; Tsui, J. H.; Millik, S. C.; Shafranek, R. T.; Kim, D.-H.; Nelson, A., Additive Manufacturing of Bovine Serum Albumin-Based Hydrogels and Bioplastics. *Biomacromolecules* **2020,** *21* (2), 484-492.
39. Vert, M., Aliphatic Polyesters: Great Degradable Polymers That Cannot Do Everything. *Biomacromolecules* **2005,** *6* (2), 538-546.
40. Bose, S.; Ke, D.; Sahasrabudhe, H.; Bandyopadhyay, A., Additive manufacturing of biomaterials. *Prog. Mater Sci.* **2018,** *93*, 45–111.
41. Luzuriaga, M. A.; Berry, D. R.; Reagan, J. C.; Smaldone, R. A.; Gassensmith, J. J., Biodegradable 3D printed polymer microneedles for transdermal drug delivery. *Lab Chip* **2018,** *18*, 1223-1230.
42. Korpela, J.; Kokkari, A.; Korhonen, H.; Malin, M.; Närhi, T.; Seppälä, J., Biodegradable and bioactive porous scaffold structures prepared using fused deposition modeling. *J Biomed Mater Res Part B* **2013,** *101B*, 610–619.
43. Davidson, J. R.; Appuhamillage, G. A.; Thompson, C. M.; Voit, W.; Smaldone, R. A., Design Paradigm Utilizing Reversible Diels–Alder Reactions to Enhance the Mechanical Properties of 3D Printed Materials. *Acs Appl Mater Inter* **2016,** *8* (26), 16961-16966.
44. Li, Z.; Yang, J.; Loh, X. J., Polyhydroxyalkanoates: opening doors for a sustainable future. *NPG Asia Materials* **2016,** *8* (4), e265-e265.
45. Dong, H.; Liffland, S.; Hillmyer, M. A.; Chang, M. C. Y., Engineering in Vivo Production of α-Branched Polyesters. *Journal of the American Chemical Society* **2019,** *141* (42), 16877-16883.
46. Hayati, A. N.; Hosseinalipour, S. M.; Rezaie, H. R.; Shokrgozar, M. A., Characterization of poly(3-hydroxybutyrate)/nano-hydroxyapatite composite scaffolds fabricated without the use

of organic solvents for bone tissue engineering applications. *Materials Science and Engineering C* **2012,** *32*, 416–422.
47. Yu, B. Y.; Chen, P. Y.; Sun, Y. M.; Lee, Y. T.; Young, T. H., Effects of the Surface Characteristics of Polyhydroxyalkanoates on the Metabolic Activities and Morphology of Human Mesenchymal Stem Cells. *Journal of Biomaterials Science, Polymer Edition* **2012,** *21* (1), 17-36.
48. Limb, J.; You, M.; Li, J.; Li, Z., Emerging bone tissue engineering via Polyhydroxyalkanoate (PHA)-based scaffolds. *Mater. Sci. Eng., C* **2017,** *79*, 917–929.
49. Vaidya, A. A.; Collet, C.; Gaugler, M.; Lloyd-Jones, G., Integrating softwood biorefinery lignin into polyhydroxybutyrate composites and application in 3D printing. *Mater. Today Comm.* **2019,** *19*, 286-296.
50. Emerson, J. A.; Garabedian, N. T.; Burris, D. L.; Furst, E. M.; Epps, T. H., Exploiting Feedstock Diversity To Tune the Chemical and Tribological Properties of Lignin-Inspired Polymer Coatings. *Acs Sustain Chem Eng* **2018,** *6* (5), 6856-6866.
51. O'Dea, R. M.; Willie, J. A.; Epps, T. H., 100th Anniversary of Macromolecular Science Viewpoint: Polymers from Lignocellulosic Biomass. Current Challenges and Future Opportunities. *ACS Macro Letters* **2020,** *9* (4), 476-493.
52. Thaore, V.; Chadwick, D.; Shah, N., Sustainable production of chemical intermediatesfor nylon manufacture: A techno-economicanalysis for renewable production of caprolactone. *Chem. Eng. Res. Des.* **2018,** *135*, 140-152.
53. Hart, L. R.; Li, S.; Sturgess, C.; Wildman, R.; Jones, J. R.; Hayes, W., 3D Printing of Biocompatible Supramolecular Polymers and their Composites. *ACS Appl. Mater. Interfaces* **2016,** *8* (5), 3115−3122.
54. Elomaa, L.; Teixeira, S.; Hakala, R.; Korhonen, H.; Grijpma, D. W.; Seppälä, J. V., Preparation of poly(e-caprolactone)-based tissue engineering scaffolds by stereolithography. *Acta Biomaterialia* **2011,** *7*, 3850–3856.
55. Seck, T. M.; Melchels, F. P. W.; Feijen, J.; Grijpma, D. W., Designed biodegradable hydrogel structures prepared by stereolithography using poly(ethylene glycol)/poly(D,L-lactide)-based resins. *Journal of Controlled Release 148 (2010) 34–41* **2010,** *148*, 34-41.
56. Trachtenberg, J. E.; Placone, J. K.; Smith, B. T.; Piard, C. M.; Santoro, M.; Scott, D. W.; Fisher, J. P.; Mikos, A. G., Extrusion-Based 3D Printing of Poly(propylene fumarate) in a Full-Factorial Design. *ACS Biomater. Sci. Eng.* **2016,** *2* (10), 1771–1780.
57. Melchiorri, A. J.; Hibino, N.; Best, C. A.; Yi, T.; Lee, Y. U.; Kraynak, C. A., 3D-Printed Biodegradable Polymeric Vascular Grafts. *Adv. Healthcare Mater.* **2016,** *5*, 319–325.
58. Lee, J. W.; Lan, P. X.; Kim, B.; Lim, G.; Cho, D.-W., 3D scaffold fabrication with PPF/DEF using micro-stereolithography. *Micro. Engn.* **2007,** *84*, 1702–1705.
59. Choi, J.-W.; Wicker, R.; Lee, S.-H.; Choi, K.-H.; Ha, C.-S.; Chung, I., Fabrication of 3D biocompatible/biodegradable micro-scaffolds using dynamic mask projection microstereolithography. *J. Mater. Process. Technol.* **2009,** *209*, 5494–5503.
60. Le Fer, G.; Becker, M. L., 4D Printing of Resorbable Complex Shape-Memory Poly(propylene fumarate) Star Scaffolds. *Acs Appl Mater Inter* **2020**.
61. DiCiccio, A. M.; Coates, G. W., Ring-Opening Copolymerization of Maleic Anhydride with Epoxides: A Chain-Growth Approach to Unsaturated Polyesters. *Journal of the American Chemical Society* **2011,** *133* (28), 10724-10727.
62. Wilson, J. A.; Luong, D.; Kleinfehn, A. P.; Sallam, S.; Wesdemiotis, C.; Becker, M. L., Magnesium Catalyzed Polymerization of End Functionalized Poly(propylene maleate) and

Poly(propylene fumarate) for 3D Printing of Bioactive Scaffolds. *Journal of the American Chemical Society* **2018,** *140* (1), 277-284.
63. Lei, D.; Yang, Y.; Liu, Z.; Chen, S.; Song, B.; Shen, A.; Yang, B.; Li, S.; Yuan, Z.; Qi, Q.; Sun, L.; Guo, Y.; Zuo, H.; Huang, S.; Yang, Q.; Mo, X.; He, C.; Zhu, B.; Jeffries, E. M.; Qing, F. L.; Ye, X.; Zhao, Q.; You, Z., A general strategy of 3D printing thermosets for diverse applications. *Mater. Horiz.* **2019,** *6*, 394-404.
64. Nijst, C. L. E.; Bruggeman, J. P.; Karp, J. M.; Ferreira, L.; Zumbuehl, A.; Bettinger, C. J.; Langer, R., Synthesis and Characterization of Photocurable Elastomers from Poly(glycerol-co-sebacate). *Biomacromolecules* **2007,** *8*, 3067-3073.
65. Sardon, H.; Engler, A. C.; Chan, J. M. W.; Coady, D. J.; O'Brien, J. M.; Mecerreyes, D.; Yang, Y. Y.; Hedrick, J. L., Homogeneous isocyanate-and catalyst-free synthesis of polyurethanes in aqueous media. *Green Chem.* **2013,** *15* (5), 1121-1126.
66. Sardon, H.; Pascual, A.; Mecerreyes, D.; Taton, D.; Cramail, H.; Hedrick, J. L., Synthesis of Polyurethanes Using Organocatalysis: A Perspective. *Macromolecules* **2015,** *48* (10), 3153-3165.
67. Hsieh, C.-T.; Liao, C.-Y.; Dai, N.-T.; Tseng, C.-S.; Yen, B. L.; Hsu, S.-h., 3D printing of tubular scaffolds with elasticity and complex structure frommultiple waterborne polyurethanes for tracheal tissue engineering. *Applied Materials Today* **2018,** *12*, 330–341.
68. Fromstein, J. D.; Woodhouse, K. A., Elastomeric biodegradable polyurethane blends for soft tissue applications. *J. Biomater. Sci., Polym. Ed.* **2002,** *13* (4), 391–406.
69. Hsieh, C.-T.; Hsu, S.-h., Double-Network Polyurethane-Gelatin Hydrogel with Tunable Modulus for High-Resolution 3D Bioprinting. *ACS Appl. Mater. Interfaces* **2019,** *11*, 32746−32757.
70. Hung, K.-C.; Tseng, C.-S.; Hsu, S.-h., Synthesis and 3D Printing of Biodegradable Polyurethane Elastomer by a Water-Based Process for Cartilage Tissue Engineering Applications. *Adv. Healthcare Mater.* **2014,** *3*, 1578–1587.
71. Li, X.; Yu, R.; He, Y.; Zhang, Y.; Yang, X.; Zhao, X.; Huang, W., Self-Healing Polyurethane Elastomers Based on a Disulfide Bond by Digital Light Processing 3D Printing. *ACS Macro Lett.* **2019,** *8*, 1511−1516.
72. Kreye, O.; Mutlu, H.; Meier, M. A. R., Sustainable routes to polyurethane precursors. *Green Chem.* **2013,** *15*, 1431-1455.
73. Bossion, A.; Heifferon, K. V.; Meabe, L.; Zivic, N.; Taton, D.; Hedrick, J. L.; Long, T. E.; Sardon, H., Opportunities for organocatalysis in polymer synthesis via step-growth methods. *Prog. Polym. Sci.* **2019,** *90*, 164-210.
74. Hung, K.-C.; Tseng, C.-S.; Dai, L.-G.; Hsu, S.-h., Water-based polyurethane 3D printed scaffolds with controlled release function for customized cartilage tissue engineering. *Biomaterials* **2016,** *83*, 156-168.
75. Elomaa, L.; Pan, C.-C.; Shanjani, Y.; Malkovskiy, A.; Seppala, J. V.; Yang, Y., Three-dimensional fabrication of cell-laden biodegradable poly(ethylene glycol-co-depsipeptide) hydrogels by visible light stereolithography. *J. Mater. Chem. B* **2015,** *3*, 8348-8358.
76. Voet, V. S. D.; Strating, T.; Schnelting, G. H. M.; Dijkstra, P.; Tietema, M.; Xu, J.; Woortman, A. J. J.; Loos, K.; Jager, J.; Folkersma, R., Biobased Acrylate Photocurable Resin Formulation for Stereolithography 3D Printing. *ACS Omega* **2018,** *3*, 1403−1408.
77. Guit, J.; Tavares, M. B. L.; Hul, J.; Ye, C.; Loos, K.; Jager, J.; Folkersma, R.; Voet, V. S. D., Photopolymer Resins with Biobased Methacrylates Based on Soybean Oil for Stereolithography. *ACS Applied Polymer Materials* **2020,** *2* (2), 949-957

78. Weems, A. C.; Chiaie, K. R. D.; Worch, J. C.; Stubbs, C. J.; Dove, A. P., Terpene- and terpenoid-based polymeric resins for stereolithography 3D printing. *Polym. Chem.* **2019,** *10*, 5959–5966.
79. Ding, R.; Du, Y.; Goncalves, R. B.; Francis, L. F.; Reineke, T. M., Sustainable near UV-curable acrylates based on natural phenolics for stereolithography 3D printing. *Polym. Chem.* **2019,** *10*, 1067.
80. Chong, S.; Pan, G.-T.; Khalid, M.; Yang, T. C.-K.; Hung, S.-T.; Huang, C.-M., Physical Characterization and Pre-Assessment of Recycled High-Density Polyethylene as 3D Printing Material. *J. Polym. Environ.* **2017,** *25* (2), 136–145.
81. Hart, K. R.; Frketic, J. B.; Brown, J. R., Recycling Meal-Ready-to-Eat (MRE) Pouches into Polymer Filament for Material Extrusion Additive Manufacturing. *Addit. Manuf.* **2018,** *21*, 536–543.
82. Zander, N. E., Recycled Polymer Feedstocks for Material Extrusion Additive Manufacturing. In Polymer-Based Additive Manufacturing: Recent Developments. *ACS Symposium Series; American Chemical Society* **2019,** *1315*, 37-51.
83. Pickering, K.; Stoof, D., Sustainable Composite Fused Deposition Modelling Filament Using Post-Consumer Recycled Polypropylene. *J. Compos. Sci.* **2017,** *1* (2), 17.
84. Zander, N. E.; Gillan, M.; Lambeth, R. H., Recycled Polyethylene Terephthalate as a New FFF Feedstock Material. *Addit. Manuf.* **2018,** *21*, 174–182.
85. Gaikwad, V.; Ghose, A.; Cholake, S.; Rawal, A.; Iwato, M.; Sahajwalla, V., Transformation of E-Waste Plastics into Sustainable Filaments for 3D Printing. *ACS Sustain. Chem. Eng.* **2018,** *6* (11), 14432–14440.
86. Reich, M. J.; Woern, A. L.; Tanikella, N. G.; Pearce, J. M., Mechanical Properties and Applications of Recycled Polycarbonate Particle Material Extrusion-Based Additive Manufacturing. *Materials* **2019,** *12* (10), 1642.
87. Mohammed, M. I.; Wilson, D.; Gomez-Kervin, E.; Tang, B.; Wang, J., Investigation of Closed-Loop Manufacturing with Acrylonitrile Butadiene Styrene over Multiple Generations Using Additive Manufacturing. *ACS Sustain. Chem. Eng.* **2019,** *7* (16), 13955–13969.
88. Kreiger, M.; Pearce, J. M., Environmental Life Cycle Analysis of Distributed Three-Dimensional Printing and Conventional Manufacturing of Polymer Products. *ACS Sustainable Chem. Eng.* **2013,** *1*, 1511−1519.
89. Kreiger, M. A.; Mulder, M. L.; Glover, A. G.; Pearce, J. M., Life cycle analysis of distributed recycling of post-consumer high density polyethylene for 3-D printing filament. *Journal of Cleaner Production* **2014,** *70*, 90-96.
90. *Circular by design - Products in the circular economy*; European Environment Agengy: 2017.
91. Wei, P.; Leng, H.; Chen, Q.; Advincula, R. C.; Pentzer, E. B., Reprocessable 3D-Printed Conductive Elastomeric Composite Foams for Strain and Gas Sensing. *ACS Appl. Polym. Mater.* **2019,** *1* (4), 885–892.
92. Hu, X.; Kang, H.; Li, Y.; Geng, Y.; Wang, R.; Zhang, L., Preparation, Morphology and Superior Performances of Biobased Thermoplastic Elastomer by in Situ Dynamical Vulcanization for 3D-Printed Materials. *Polymer* **2017,** *108*, 11-20.
93. Jehanno, C.; Sardon, H., Dynamic Polymer Network Points the Way to Truly Recyclable Plastics. *Nature* **2019,** *568* (7753), 467–468.
94. Kloxin, C. J.; Scott, T. F.; Adzima, B. J.; Bowman, C. N., Covalent Adaptable Networks (CANS): A Unique Paradigm in Cross-Linked Polymers. *Macromolecules* **2010,** *43* (6), 2643-2653.

95. Bowman, C. N.; Kloxin, C. J., Covalent Adaptable Networks: Reversible Bond Structures Incorporated in Polymer Networks. *Angew Chem Int Edit* **2012,** *51* (18), 4272-4274.
96. Kloxin, C. J.; Bowman, C. N., Covalent adaptable networks: smart, reconfigurable and responsive network systems. *Chem. Soc. Rev.* **2013,** *42* (17), 7161-7173.
97. Liu, T.; Zhao, B.; Zhang, J., Recent development of repairable, malleable and recyclable thermosetting polymers through dynamic transesterification. *Polymer* **2020,** *194*, 122392.
98. Montarnal, D.; Capelot, M.; Tournilhac, F.; Leibler, L., Silica-Like Malleable Materials from Permanent Organic Networks. *Science* **2011,** *334* (6058), 965-968.
99. Shi, Q.; Yu, K.; Kuang, X.; Mu, X.; Dunn, C. K.; Dunn, M. L.; Wang, T.; Qi, H. J., Recyclable 3D Printing of Vitrimer Epoxy. *Mater. Horiz.* **2017,** *4* (4), 598–607.
100. Zhang, B.; Kowsari, K.; Serjouei, A.; Dunn, M. L.; Ge, Q., Reprocessable Thermosets for Sustainable Three-Dimensional Printing. *Nat. Commun.* **2018,** *9* (1), 1-7.
101. Li, A.; Challapalli, A.; Li, G., 4D Printing of Recyclable Lightweight Architectures Using High Recovery Stress Shape Memory Polymer. *Sci. Rep.* **2019,** *9* (1), 1–13.
102. Mitchell, A.; Lafont, U.; Hołyńska, M.; Semprimoschnig, C., Additive manufacturing — A review of 4D printing and future applications. *Additive Manufacturing* **2018,** *24*, 606-626.
103. González-Henríquez, C. M.; Sarabia-Vallejos, M. A.; Rodriguez-Hernandez, J., Polymers for additive manufacturing and 4D-printing: Materials, methodologies, and biomedical applications. *Prog. Polym. Sci.* **2019,** *94*, 57-116.
104. Ge, Q.; Dunn, C. K.; Qi, H. J.; Dunn, M. L., Active origami by 4D printing. *Smart Mater. Struct. 23 (2014)* **2014,** *23*, 094007.
105. Tibbits, S.2017.
106. Wang, G.; Yang, H.; Yan, Z.; Gecer Ulu, N.; Tao, Y.; Gu, J.; Kara, L. B.; Yao, L., 4DMesh. In *The 31st Annual ACM Symposium on User Interface Software and Technology - UIST '18*, 2018; pp 623-635.
107. Wang, W.; Yao, L.; Zhang, T.; Cheng, C.-Y.; Levine, D.; Ishii, H. In *Transformative Appetite: Shape-Changing Food Transforms from 2D to 3D by Water Interaction through Cooking*, CHI '17: Proceedings of the 2017 CHI Conference on Human Factors in Computing Systems, Denver, Denver, 2017.
108. Sakin, M.; Kiroglu, Y. C. In *3D Printing of Buildings: Construction of the Sustainable Houses of the Future by BIM*, Energy Procedia 134 , 702–711, Crete, Crete, 2017.
109. 3dwasp.com.
110. Hager, I.; Golonka, A.; Putanowicz, R. In *3D printing of buildings and building components as the future of sustainable construction?*, Procedia Engineering 151, 292 – 299, Cracow, Cracow, 2016.
111. Yuan, C.; Roach, D. J.; Dunn, C. K.; Mu, Q.; Kuang, X.; Yakacki, C. M.; Wang, T. J.; Yu, K.; Qi, H. J., 3D printed reversible shape changing soft actuators assisted by liquid crystal elastomers. *Soft Matter* **2017,** *13*, 5558-5568.
112. Symes, M. D.; Kitson, P. J.; Yan, J.; Richmond, C. J.; Cooper, G. J. T.; Bowman, R. W.; Vilbrandt, T.; Cronin, L., Integrated 3D-printed reactionware for chemical synthesis and analysis. *Nat Chem* **2012,** *4*, 349-354.
113. Kitson, P. J.; Symes, M. D.; Dragone, V.; Cronin, L., Combining 3D printing and liquid handling to produce user-friendly reactionware for chemical synthesis and purification. *Chem. Sci.* **2013,** *4*, 3099.

114. Kitson, P. J.; Marshall, R. J.; Long, D.; Forgan, R. S.; Cronin, L., 3D Printed High-Throughput Hydrothermal Reactionware for Discovery, Optimization, and Scale-Up. *Angew. Chem. Int. Ed.* **2014,** *53*, 12723-12728.
115. Zalesskiy, S. S.; Kitson, P. J.; Frei, P.; Bubliauskas, A.; Cronin, L., 3D designed and printed chemical generators for on demand reagent synthesis. *Nat Commun* **2019,** *10*, 5496.
116. Blanchette, C. D.; Knipe, J. M.; Stolaroff, J. K.; Joshua R. DeOtte, J. S. O.; Maiti, A.; Lenhardt, J. M.; Sirajuddin, S.; Rosenzweig, A. C.; Baker, S. E., Printable enzyme-embedded materials for methane to methanol conversion. *Nat. Commun.* **2016,** *7*, 11900.
117. Peris, E.; Okafor, O.; Kulcinskaja, E.; Goodridge, R.; Luis, S. V.; Garcia-Verdugo, E.; O'Reilly, E.; Sans, V., Tuneable 3D printed bioreactors for transaminations under continuous-flow. *Green Chem.* **2017,** *19*, 5345–5349.
118. Balasubramanian, S.; Aubin-Tam, M.-E.; Meyer, A. S., 3D Printing for the Fabrication of Biofilm-Based Functional Living Materials. *ACS Synthetic Biology* **2019,** *8* (7), 1564-1567.
119. Nguyen, P. Q.; Courchesne, N.-M. D.; Duraj-Thatte, A.; Praveschotinunt, P.; Joshi, N. S., Engineered Living Materials: Prospects and Challenges for Using Biological Systems to Direct the Assembly of Smart Materials. *Adv. Mater.* **2018,** *30* (19), 1704847.
120. Liu, X.; Tang, T.-C.; Tham, E.; Yuk, H.; Lin, S.; Lu, T. K.; Zhao, X., Stretchable living materials and devices with hydrogel–elastomer hybrids hosting programmed cells. *Proceedings of the National Academy of Sciences* **2017,** *114* (9), 2200-2205.
121. Johnston, T. G.; Yuan, S.-F.; Wagner, J. M.; Yi, X.; Saha, A.; Smith, P.; Nelson, A.; Alper, H. S., Compartmentalized microbes and co-cultures in hydrogels for on-demand bioproduction and preservation. *Nat Commun* **2020,** *11*, 563.
122. Schaffner, M.; Rühs, P. A.; Coulter, F.; Kilcher, S.; Studart, A. R., 3D printing of bacteria into functional complex materials. *Science Advances 01 Dec 2017:* **2017,** *3* (12), eaao6804.
123. Saha, A.; Johnston, T. G.; Shafranek, R. T.; Goodman, C. J.; Zalatan, J. G.; Storti, D. W.; Ganter, M. A.; Nelson, A., Additive Manufacturing of Catalytically Active Living Materials. *ACS Appl. Mater. Interfaces* **2018,** *10* (16), 13373-13380.
124. Johnston, T. G.; Fellin, C. R.; Carignano, A.; Nelson, A., Poly(alkyl glycidyl ether) hydrogels for harnessing the bioactivity of engineered microbes. *Faraday Discuss.* **2019,** *219*, 58-72.
125. Zivic, N.; Kuroishi, P. K.; Dumur, F.; Gigmes, D.; Dove, A. P.; Sardon, H., Recent Advances and Challenges in the Design of Organic Photoacid and Photobase Generators for Polymerizations. *Angew. Chem. Int. Ed.* **2019,** *58*, 10410-10422.

1.8 FIGURES

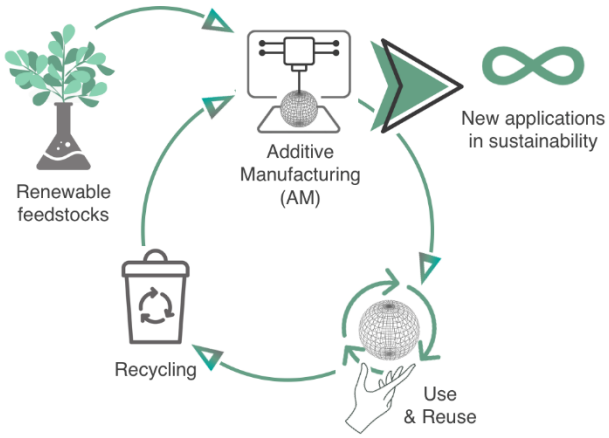

Figure 1.1. Additive manufacturing in a circular plastic economy.

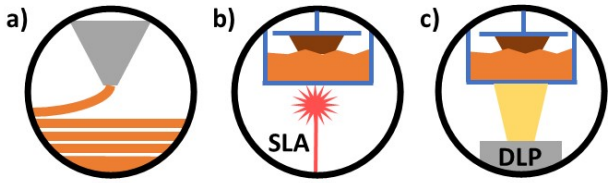

Figure 1.2. Additive manufacturing techniques considered in this review for their potential sustainability.

(a) extrusion, (b) stereolithography (SLA) and (c) direct light processing (DLP).

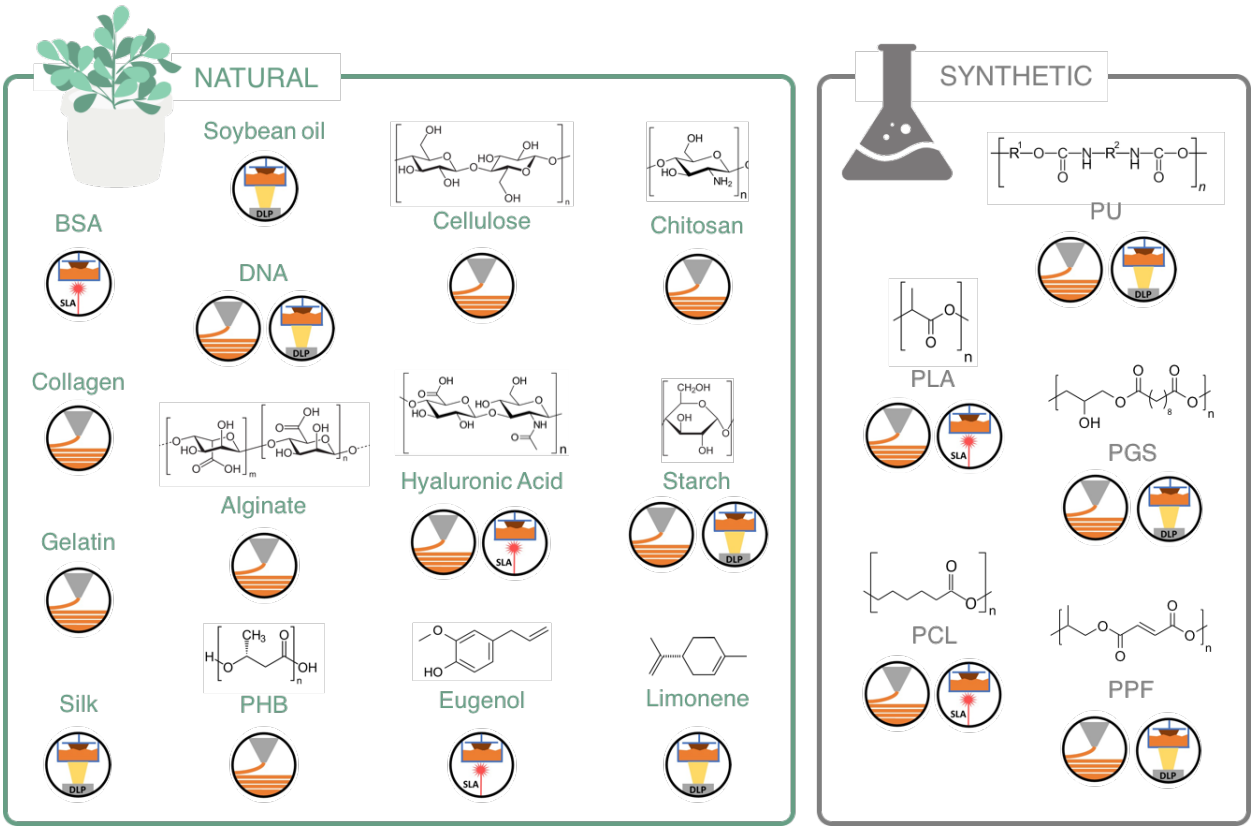

Figure 1.3. Some renewable feedstocks developed for sustainable additive manufacturing.

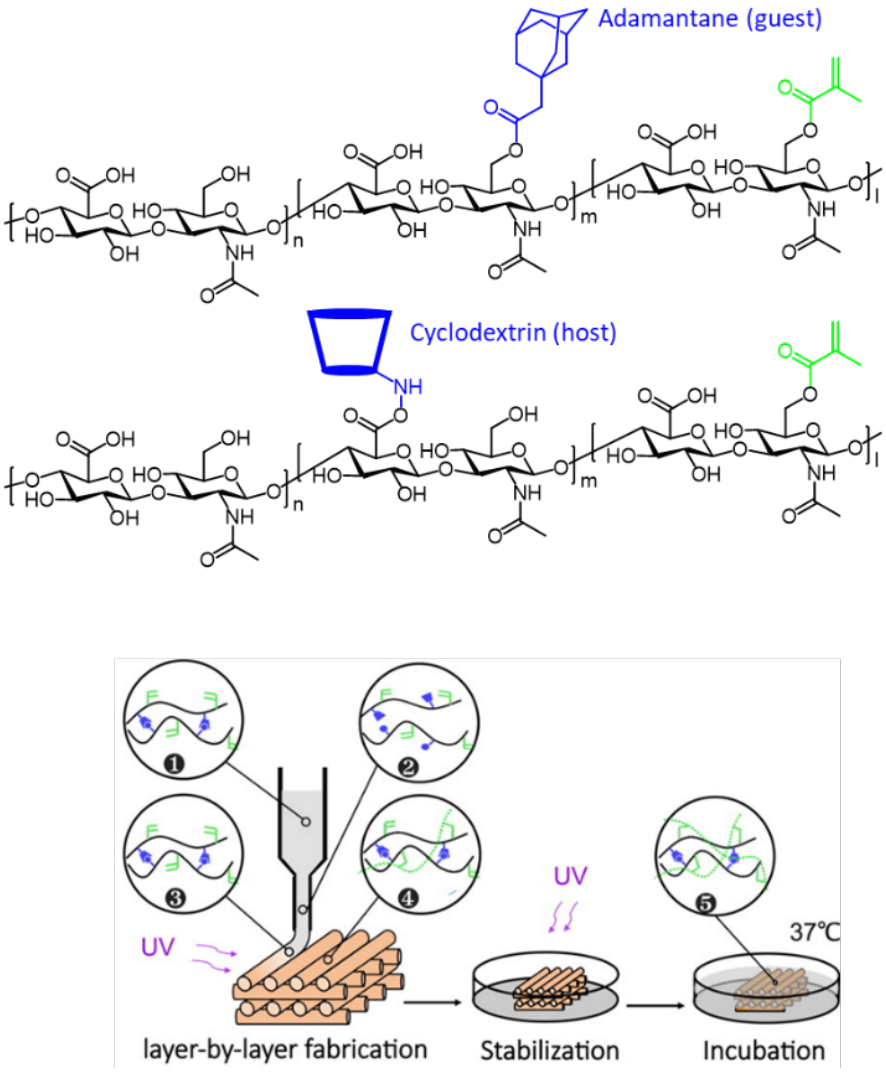

Figure 1.4. General printing scheme for extrusion printing layer-by layer of a chemically modified hyaluronic acid.

Reprinted with permission from ref. [22]. Copyright 2016 American Chemical Society.

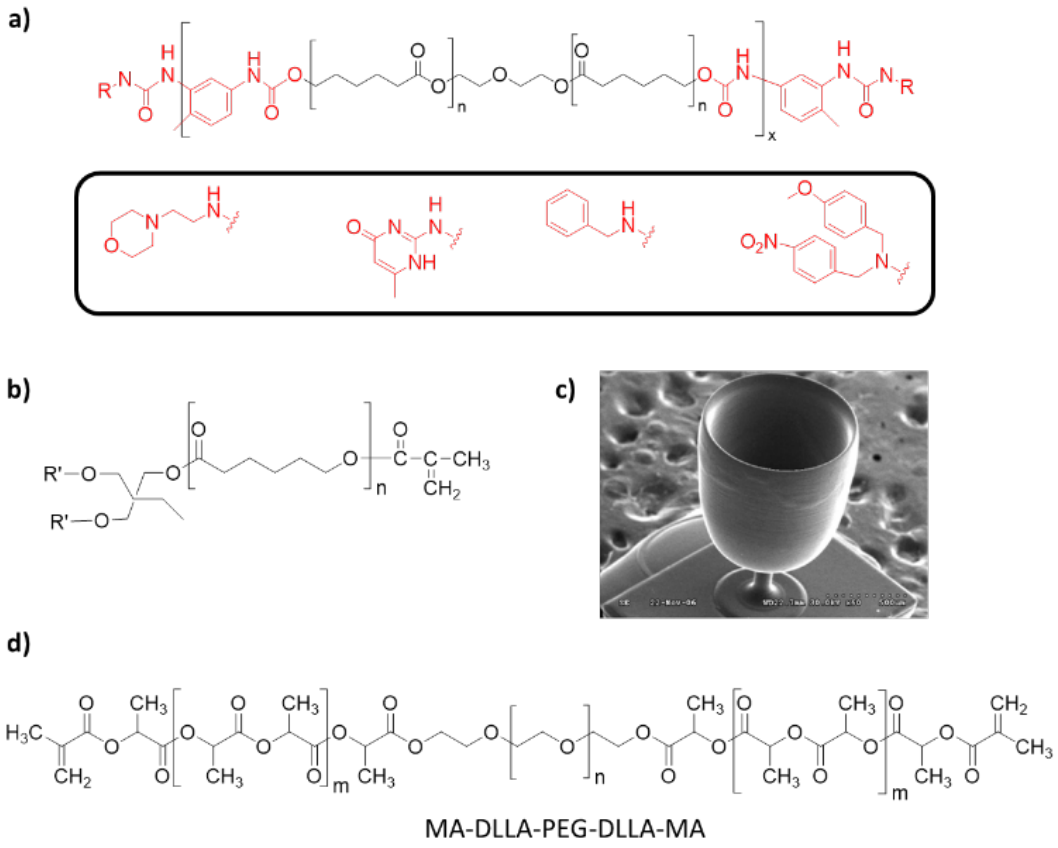

Figure 1.5. Biodegradable polyesters.

(a) Addition of hydrogen bonding moieties to a biodegradable poly(caprolactone)-diol to obtain a tunable ink.[53] Reprinted with permission from ref. [53]. Copyright 2016 American Chemical Society. (b) Synthesis of PCL macromer by methacrylation of hydroxyl-terminated PCL oligomer.[54] Reprinted with permission from ref. [54]. Copyright 2011 Elsevier. (c) Printed microstructures using microstereolithography made of PPF.[58] (d) Synthesis of PDLLA-PEG-PDLLA oligomers and subsequent functionalization with methacrylic anhydride (MAAH) to give MA-PDLLA-PEG-PDLLA-MA macromers.[55] Reprinted with permission from ref. [55]. Copyright 2010 Elsevier.

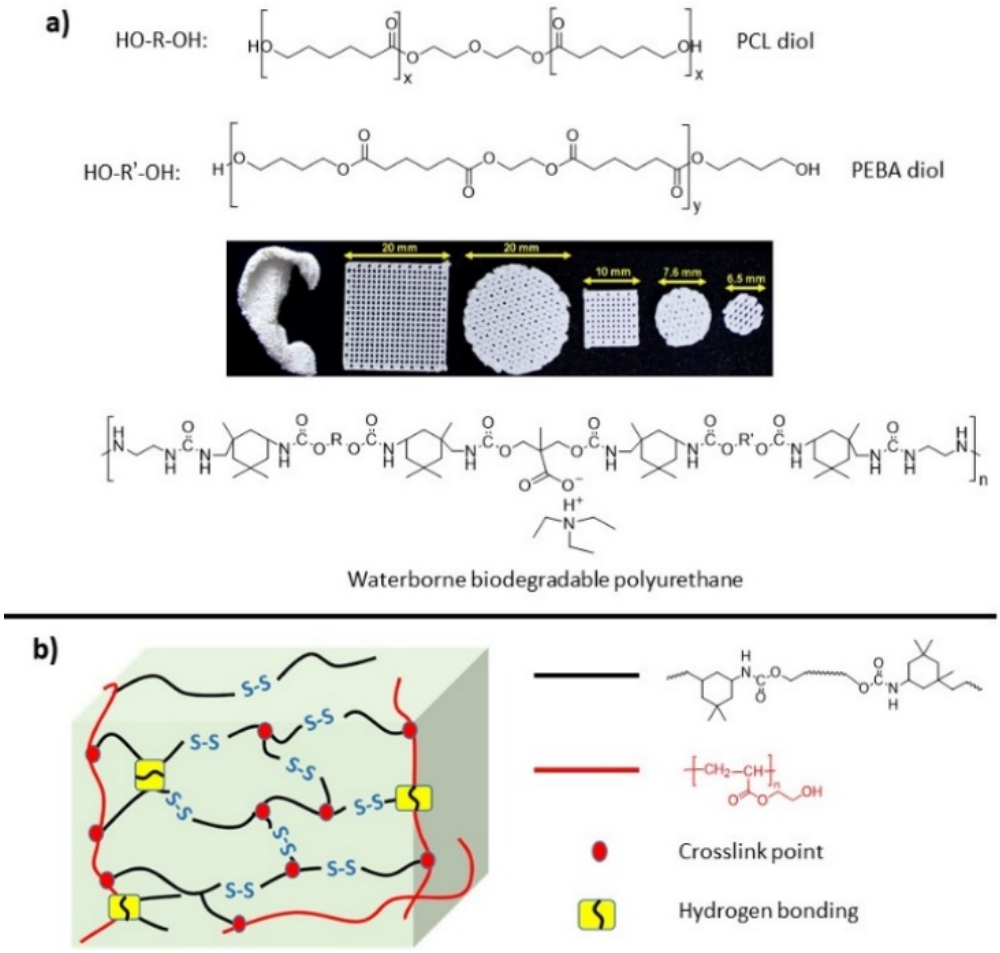

Figure 1.6. Printing of polyurethanes.

(a) Synthesis of the biodegradable PU nanoparticles and 3D printed scaffolds with various shapes and dimensions.[74] Reprinted with permission from ref. [74]. Copyright 2016 Elsevier. (b) Synthesis of a self-healing polyurethane elastomer for DLP 3D printing.[71] Reprinted with permission from ref. [71]. Copyright 2019 American Chemical Society.

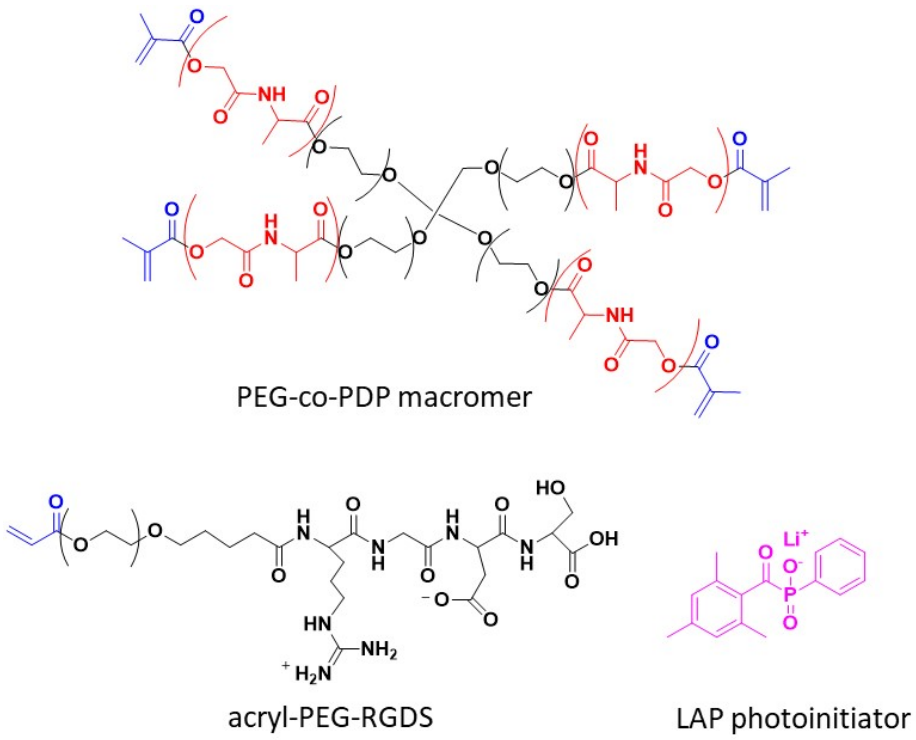

Figure 1.7. SLA Printing of PEG-co-PDP.

Photocrosslinkable poly(ethylene glycol-co-depsipeptide) (PEG-co-PDP) macromer for the SLA-based fabrication hydrogels.[75] Reprinted with permission from ref. [75]. Copyright 2015 Royal Society of Chemistry.

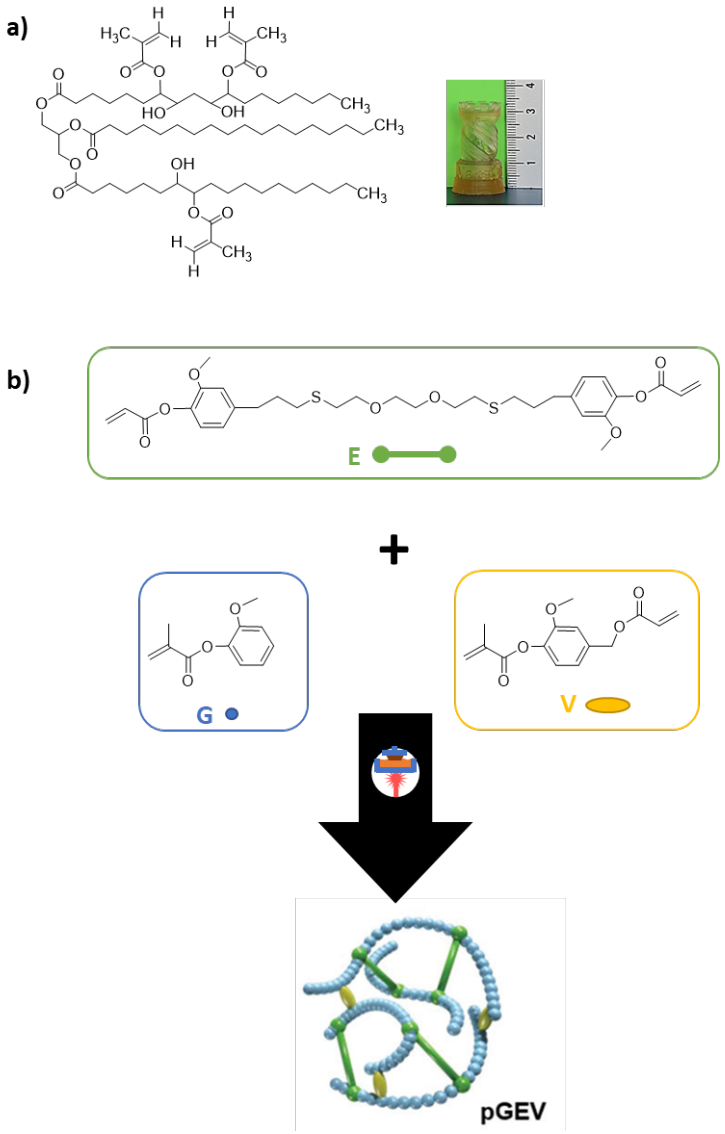

Figure 1.8. Additively manufactured constructs created through vat-photopolymerization of naturally derived polymeric resins.

(a) Soybean oil acrylate.[76] Reprinted with permission from ref. [76]. Copyright 2020 American Chemical Society. (b) Acrylates based on natural phenolics for SLA: E = 3,6-Dioxa-1,8-octanedithiol eugenol, G = guaiacol methacrylate, V = vanillyl alcohol methacrylate.[79] Reprinted with permission from ref. [79]. Copyright 2019 Royal Society of Chemistry.

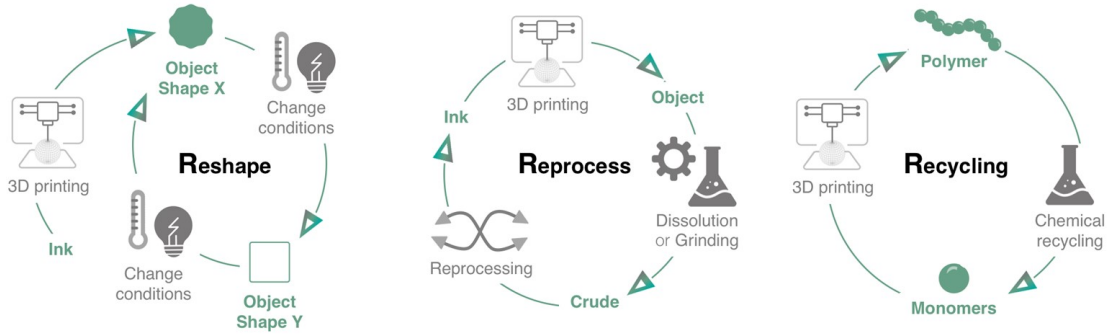

Figure 1.9. The classifications of options for managing the end-of-life of 3D printed objects Reshape, reprocess, and chemically recycle.

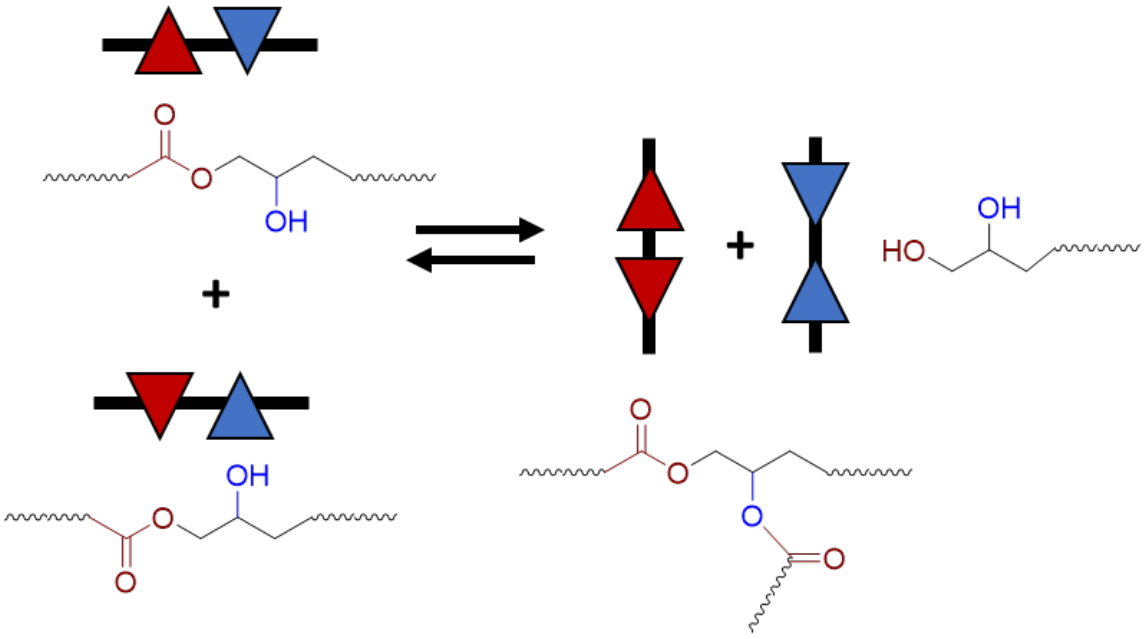

Figure 1.10. Formation of dynamic covalent bonds for the creation of a reprocessable thermoset.

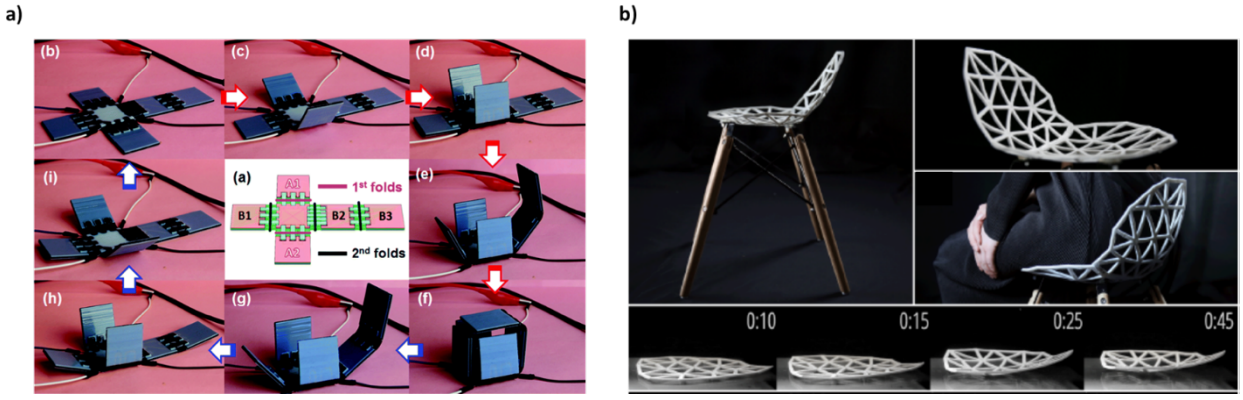

Figure 1.11. 4-dimensionally active additively manufactured parts.

(a) Sequential folding cubic box by printing multiple groups of conductive wires in different layers to heat the liquid crystal elastomer strips with addressability.[111] Reprinted with permission from ref. [111]. Copyright 2017 Royal Society of Chemistry. (b) Combination of the shrinking and bending properties of thermoplastic (PLA) actuators with customized geometric algorithms to 4D print functional non-developable surfaces.[106]

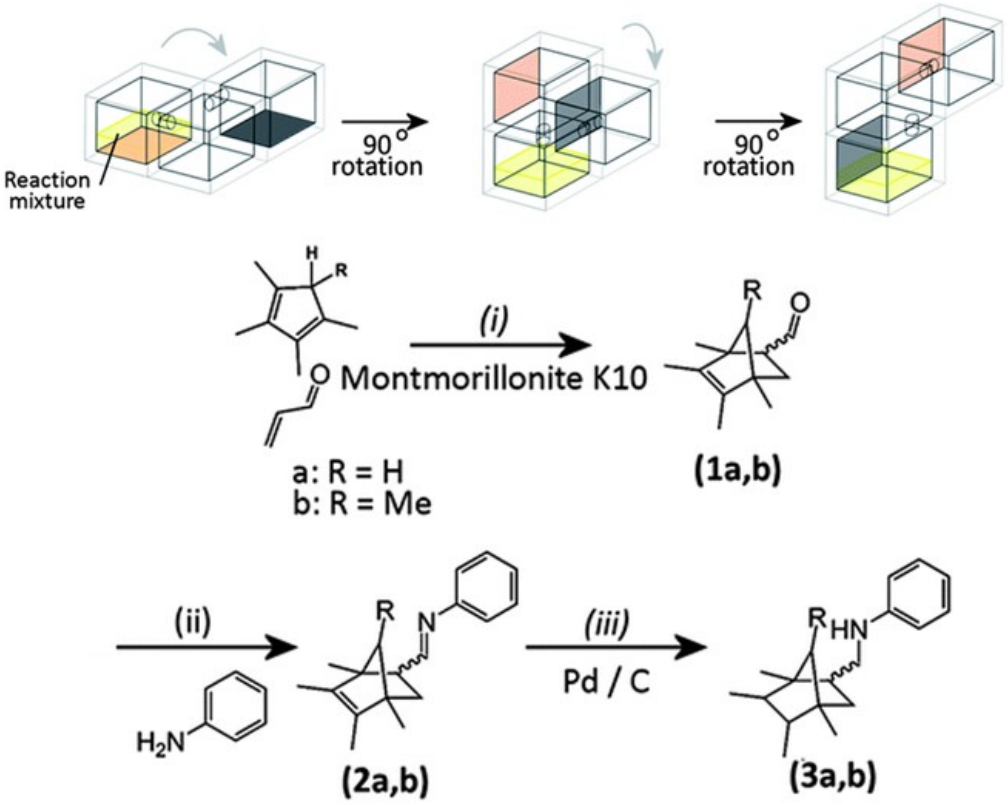

Figure 1.12. Schematic diagram of the multi-step reaction using Cronin's reactionware.

The reaction mixture is transferred from chamber to chamber upon the completion of each reaction step by rotating the device. Three-step organic reaction sequence is performed: (i) Diels–Alder cyclization, (ii) the formation of an imine, and (iii) hydrogenation of the imine to the corresponding secondary amine.113 Reprinted with permission from ref. 113. Copyright 2013 Royal Society of Chemistry.

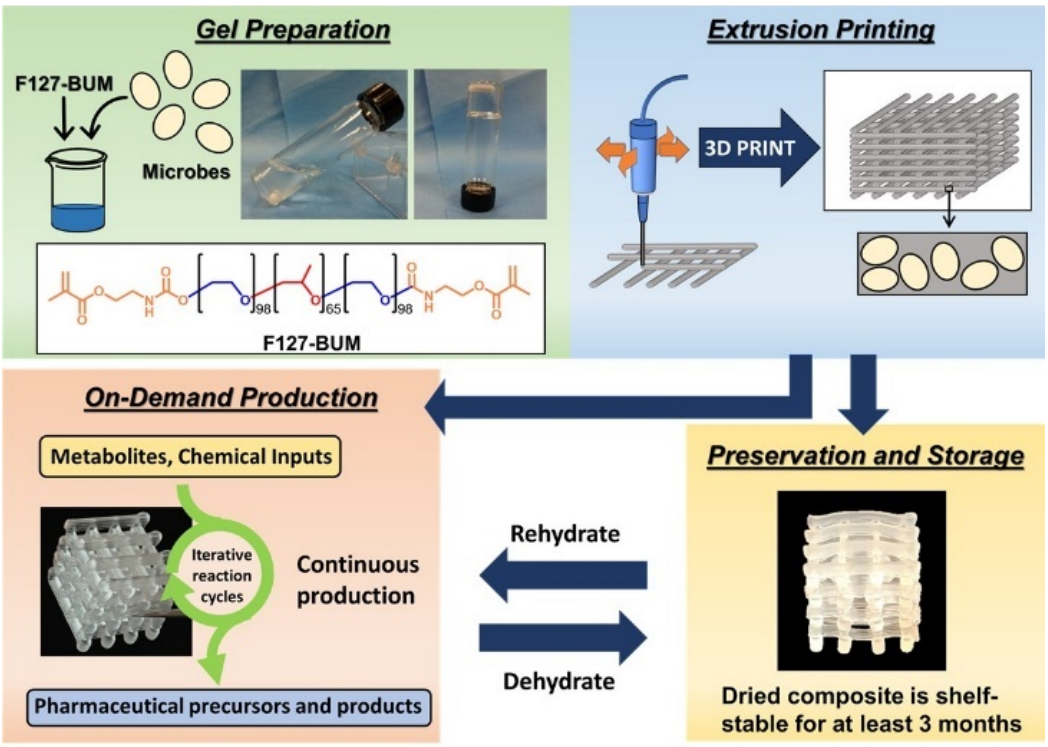

Figure 1.13. F127-based hydrogels used to immobilize yeast and bacteria consortia for the development of a 3D-printable class of living materials.

The materials can either be directly employed in iterative bioprocessing cycles or preserved for on-demand production at a later time. Multiple rounds of reuse are possible without a reduction in efficiency.

Chapter 2. ADDITIVE MANUFACTURING OF CATALYTICALLY ACTIVE LIVING MATERIALS

This chapter has been adapted from the following manuscript:

> Saha, A.; **Johnston, T. G.**; Shafranek, R. T.; Goodman, C. J.; Zalatan, J. G.; Storti, D. W.; Ganter, M. A.; Nelson, A. Additive Manufacturing of Catalytically Active Living Materials. *ACS Applied Materials & Interfaces* **2018**, *10* (16), 13373–13380. https://doi.org/10.1021/acsami.8b02719.

2.1 ABSTRACT

Living materials, which are composites of living cells residing in a polymeric matrix, are designed to utilize the innate functionalities of the cells to address a broad range of applications such as fermentation and biosensing. Herein, we demonstrate the additive manufacturing of catalytically active living materials (AMCALM) for continuous fermentation. A multi-stimuli-responsive yeast-laden hydrogel ink—based on F127-dimethacrylate—was developed and printed using a direct-write 3D printer. The reversible stimuli-responsive behaviors of the polymer hydrogel inks to temperature and pressure are critical, as they enabled the facile incorporation of yeast cells and subsequent fabrication of 3D lattice constructs. Subsequent photo-cross-linking of the printed polymer hydrogel afforded a robust elastic material. These yeast-laden living materials were metabolically active in the fermentation of glucose into ethanol for 2 weeks in a continuous batch process without significant reduction in efficiency (~90% yield of ethanol). This cell immobilization platform may potentially be applicable toward other genetically modified yeast strains to produce other high value chemicals in a continuous bio-fermentation process.

2.2 INTRODUCTION

'Living materials' are composites of living cells that reside within a polymer matrix and have great promise for wearable devices, biosensors, drug-releasing surfaces, and biocatalysis applications.[1-3] An important feature of a living material is that its functionality is derived from the cells residing within the material.[4-7] Polymer hydrogels,[8,9] in particular, offer significant advantages as a scaffold for living materials because they provide a cellular environment that is similar to natural biofilms. Cell-laden hydrogels have been fabricated using yeast, bacteria, and algae to afford metabolically active constructs[1,2,4,10-12] for cell-mediated catalysis[13-24] in the production of food ingredients, biofuels, chemical precursors, and pharmaceuticals. These immobilized-cell bioreactors offer several advantages, such as reduced reactor down-time, ease of product removal, and minimized product inhibition and nutrient depletion. However, the fabrication of these types of composites is challenged by the availability of suitable cell-compatible materials and processes. Calcium alginate hydrogels[11,12,25,26] represent one of the most commonly employed platforms for microbial cell encapsulation. But these ionically cross-linked hydrogels deteriorate over time, unless the concentration of calcium ions in solution is periodically replenished.[26] Alternatively, living material filaments have also been generated by electrospinning microbe-polymer solutions.[27,28] However, electrospinning exposes the biocomposite material to organic solvents, high voltages, and drying steps that potentially compromise the bioactivity and viability of embedded cells. A 3D printed living material could begin to mimic natural systems, but more importantly, provide well-defined lattice frameworks with the ultimate control over feature size, structure, and organization.[29-37] The diffusion of the aqueous medium in/out of the lattice, and the flow of the aqueous medium through the lattice framework can ultimately be maximized by the lattice design.

Herein, we report additive manufactured catalytically active living materials (AMCALMs) using a multi-stimuli-responsive cell-laden hydrogel ink—the materials reversibly respond to temperature and pressure, and become covalently cross-linked upon exposure to light (Figure 2.1). Additive manufacturing enables the fabrication of 3D constructs based on a computer aided design (CAD) model. While several types of 3D printing technologies are available, direct-write 3D printing is attractive for its versatility and cell compatibility.[33,34,38-44] These printers operate by extruding an ink material from a syringe fitted with a nozzle while it traverses across a surface in a pattern that is created by transforming a 3D model into a set of commands that is readable by the printer through the use of additive manufacturing software. An important aspect of our approach is that the hydrogel ink that we employ is multi-stimuli-responsive, which is important to enable the cell-compatible 3D patterning of the living material. The F127-dimethacrylate (F127-DMA) polymer used in this study is derived from Pluronic F127, which is a commercially available triblock copolymer of poly(ethylene glycol)-*b*-poly(propylene glycol)-*b*-poly(ethylene glycol). This polymer (25 wt % in aqueous media) formed a gel at 23 °C that melted when cooled to 5 °C. The temperature-dependent behavior of this hydrogel was ideal for homogeneously incorporating yeast cells (*Saccharomyces cerevisiae*) at low temperature (5 °C) that then afforded a uniform distribution of cells in the gel at room temperature. This material also responds to externally applied pressure—as a shear-thinning hydrogel—which facilitated the 3D printing of the cell-laden hydrogel with a direct-write 3D printer. Finally, the F127-DMA hydrogel underwent covalent cross-linking upon light-initiated polymerization using a photo-initiator. Thus, we utilized the combination of stimuli-responses of the hydrogel to fabricate yeast-laden 3D lattices. Cell viability and metabolic activity (bio-ethanol production) were confirmed over the course of 2 weeks.

2.3 RESULTS AND DISCUSSION

The reversible stimuli-responsive behaviors of F127-DMA hydrogels in synthetic complete (SC) media were rheologically characterized in the presence and absence of yeast cells. A temperature ramp (5-50 °C) experiment was used to determine the gelation temperature (T_{gel}), which is defined as the temperature at which storage modulus (G') intersects with the loss modulus (G") (Figure 2.2a). The 25 wt% F127-DMA hydrogel exhibited a T_{gel} of 16.3 °C, with a G' value of 20.9 kPa and a G" of 1.17 kPa at 23 °C. We further investigated the gel yield stress (Figure 2.2b), which correlates to the force necessary to induce flowing behavior of the physically cross-linked hydrogel network, as well as the maximum stress load that the gel can endure as it supports subsequent stacked layers during fabrication of the cube lattices. The hydrogel was moderately firm at room temperature and afforded a yield stress of 717 Pa (Figure 2.2b). The shear-thinning property of the hydrogel determines the flow behavior of the gel under high shear. As shown in Figure 2.2c, the shear viscosities of the hydrogel decreased as the shear rate increased. This relationship is representative of a non-Newtonian fluid that exhibits shear-thinning behavior. The reversible shear-thinning under stress and rapid recovery of the storage modulus of the hydrogel networks under shear-relaxed conditions manifested itself in the instantaneous response of the gel modulus to changes in the applied strain (Figure 2.2d). The hydrogel exhibited a sharp decrease in the G' at high strains and immediate recovery at low strains for each cycle—each in less than 15 s (Figure 2.2d). This rapid recovery of the G' was necessary to ensure that the extruded hydrogel filament maintains its form after exiting the nozzle. The hydrogel displayed minimal mechanical hysteresis between strain cycles (a desirable property for fabrication of living materials via extrusion) which suggested that the hydrogel can undergo multiple cycles of alternating low and high strain. Rheological experiments also confirmed that the presence of yeast cells had a

negligible effect on material behavior (Figure A.2). Photochemical crosslinking was important for the long-term stability of the printed objects. Photo-rheometry was used to show the G' increased appreciably from 16 kPa to 140 kPa after a 60 s of irradiation with 365 nm light (Figure A.2a), which suggested that the hydrogel rapidly transformed from a physically crosslinked hydrogel, into a chemically cross-linked hydrogel. The rheological experiments can determine the suitability of the hydrogel as ink for direct-write 3D bioprinting.[43,44]

AMCALMs, in the form of cube lattices, were designed using CAD software to render models (.stl files) which were transformed into gcode files using Slic3r software. The 3D printed structures shown in Figures 2.3a and 2.3b are representative designs that allow for easy flow of media through the hydrogel lattice. In general, an AM approach enables the geometry of the lattice to be altered by creating new CAD models that can be printed (see supporting information for other printed designs). The combination of CAD and AM, affords geometries that are challenging or impossible to fabricate by traditional patterning methods. A 3-axis direct-write 3D printer fitted with a pneumatic extrusion system was used to print cubic lattices, which were subsequently UV-cured to chemically cross-link the hydrogel (Figure 2.1, Figure 2.3a,b and Figure A.3). The materials were also suitable for manual casting in the absence of a printer to afford 3D mesh structures (Figure A.4). The filament diameters were largely dictated by the nozzle diameter and pressure, but were approximately 300-450 μM, in the images shown (Figure A.5). The printed structures were highly robust post-cure, and could be stretched, folded, or even rolled without permanent deformation of the structure (Figure A.5b-d).

In order to explore the viability of yeast cells within the AMCALMs, *Saccharomyces cerevisiae* with constitutively expressed mCherry protein was embedded into the gel. The materials were observed visually, as well as under optical, fluorescence, and confocal microscopies for 14

days. The results of the study are presented in Figure 2.3c-f (as well as in Figures A.6 and A.7). Initial results, taken immediately after extrusion and cross-linking of the cell-laden hydrogel, revealed that the hydrogel filaments were transparent, which reflected a low initial cell concentration (Figure A.6a,b). Under optical and fluorescence microscopy, no large cell colonies or aggregates were observed (Figure A.6c,d). Confocal microscopy of the samples using Sytox Green dye revealed a significant population of live cells (red channel), with few dead cells (green channel, Figure A.7), suggesting the cells have a high viability at day zero.[11,46,47] As time progressed, the formation and expansion of yeast colonies were apparent with the increased turbidity of the printed hydrogels. Colonies of yeast cells were clearly visible by eye after 3 days (Figure 2.3c and Figure A.6e,f), which was also confirmed by both optical and fluorescence microscopies (Figure 2.3d and Figure A.6g,h). Live/dead staining with Sytox green again confirmed no significant cell death after 3 days of material incubation in growth media (Figure 2.3e and Figure A.7). The population and size of the colonies increased appreciably over time, and were monitored microscopically at seven, ten and fourteen days (Figure 2.3f and Figures A.6 and A.7). Confocal microscopy after 14 days revealed that the yeast cells were viable in the cross-linked hydrogel for at least two weeks, as indicated by the predominance of the red fluorescent cells. (Figure A.7).

Scanning electron microscopy of the lyophilized hydrogels revealed its porous morphology (Figure A.11), and the yeast cells are expected to reside within these pores. Some of the yeast cells, likely near the surface of the hydrogel filament, were able to escape from the hydrogels into the surrounding media, as evidenced by the presence of turbid growth in the media after a period of a few days. We observed the growth of yeast in the SC media outside of the 3D mesh structure for up to seven days, but this occurrence decreased over time. We speculate that as the immobilized

yeast proliferate within the hydrogel, the porosity of the hydrogel can change, thus affecting the ability of the yeast cells to pass into the surrounding media.

In order to verify the metabolic activity of the immobilized yeast cells, the biocatalytic conversion of glucose into ethanol was selected as a case study.[48] We first investigated the kinetics of ethanol production by the yeast-laden AMCALMs. The glucose concentration in the SC media and the number of yeast cells in the living materials significantly influenced the kinetics of the ethanol production. For example, AMCALMs with 10^8 cells/g and 10^7 cells/g had >90 % conversion efficiency of glucose into ethanol within 12 h (Figure A.8). By contrast, yeast-laden AMCALMs with fewer cells (10^6 cells/g and 10^5 cells/g) catalyzed ~85% of conversion of glucose into ethanol after 24 h (Table S1).

We further investigated the ethanol fermentation at different concentrations of glucose using the printed structures with an initial cell concentration of 10^8 cells/g (Figure 2.4a). This allowed us to examine the efficiency of the living materials under high concentration of the substrate (glucose). After 48 h, the conversion of glucose into ethanol for SC media with 2 wt%, 5 wt%, and 10 wt% glucose was 95.7%, 88.7%, and 86.4%, respectively (Table S2). Thus, the kinetics of ethanol fermentation was influenced by both the number of cells and the quantity of substrate in the media. In comparison, fermentation of glucose into ethanol in the absence of the polymer hydrogel afforded a 90 % conversion in SC media with 2 wt% glucose.

The reusability of the AMCALMs is also an important consideration for the sustainability of the yeast-laden living materials. The yeast-laden printed structures were tested in a continuous batch process, wherein the AMCALM was submerged into a fresh solution of 2% glucose in SC media every 3-4 days (Figure A.9). As shown in Figure 2.4b, the AMCALMs were catalytically active with minimal loss of activity for over two weeks. We observed an 84.3 % conversion of

glucose into ethanol in the first 3 days, and this efficiency was maintained throughout the five-batches of the study with an average conversion of ~90 %. The batch reactor AMCALMs showed a 20% increase in mass over the fourteen days of activity, likely due to the increase in cell concentration within the hydrogel lattice, shown in Figures A.6, A.7, and A.9. Interestingly, the cubes were also found to be active in non-traditional glucose-containing media, such as grape juice. In this case, 6150 ppm of ethanol was produced by the conversion of the natural sugars (Figure A.10).

2.4 CONCLUSIONS

In conclusion, we developed a multi-stimuli-responsive living material ink to fabricate extrudable filaments of yeast-laden hydrogels. The stimuli-responsive characteristics of the hydrogel ink were important for its preparation, as well as its printing via a direct-write 3D printer. The temperature- and shear-responsive properties of F127-DMA hydrogels facilitated the incorporation of yeast cells and extrusion of the living hydrogels into 3D lattice structures under ambient conditions. The Tgel for F127-DMA is 16.3 °C, and thus the hydrogel 'melts' when cooled below this temperature. The temperature-dependent sol-gel phase transition is a consequence of the lower critical solution temperature (LCST) of the polymer,49 in which the solubility of the polymer in water changes with temperature. The shear-thinning behavior is likely caused by the breaking of the physical entanglements and cross-links between micelles, as well as between individual polymer chains within the micelles. The photochemical crosslinking of the terminal methacrylate moieties afforded mechanically robust structures, drastically reducing the effects of temperature and shear on the material. This material exhibited a "living" character, as demonstrated by the excellent viability and metabolic activity of the yeast cells within the polymer hydrogel. In fact, we observed no evidence that the yeast cells were negatively affected by the

temperature, pressure, or 365 nm irradiation used during the process. The AMCALMs were metabolically active in the production of ethanol for over five consecutive cycles without significant loss of biocatalytic activity (~90 % conversion of glucose into ethanol). This work is illustrative of an additive manufacturing-based technology for the future of bio-based sustainable chemical production using a continuous process. By utilizing other microbial species and strains, or by incorporating microbes with engineered genetic modifications, multi-stimuli-responsive living materials may be developed for the production of higher value compounds such as antibiotics, proteins, or other small molecule therapeutics.

2.5 EXPERIMENTAL

2.5.1 *Materials*

Pluronic F-127 (BioReagent, powder, suitable for cell culture), and D-(+)-Glucose (≥99.5%; GC) were purchased from Sigma Life Science. Triethylamine (≥ 99.5%), 2-hydroxy-2-methylpropiophenone (97%), and methacryloyl chloride (97%; 200 ppm monomethyl ether hydroquinone as stabilizer) were purchased from Sigma-Aldrich. Drop-out Mix Complete without Yeast Nitrogen Base D9515) and Yeast Nitrogen Base (Y2025) were purchased from US Biological Life Sciences. Toluene (HPLC Grade, 99.9%) and Diethyl ether (anhydrous) were purchased from Fisher Chemical. Sytox Green nucleic acid strain (5 mM solution in DMSO; Invitrogen) was purchased from Thermo Fisher Scientific. Grape Juice (Organic Pasteurized Concord Grape Juice 100%, 13% of total carbohydrate) was purchased from Trader Joe's.

2.5.2 *Yeast strains*

Saccharomyces cerevisiae strain SO992 was used to perform these experiments. This strain is a derivative of W303 (genotype MATa ura3 leu2 trp1 his3 can1R ade). For microscopy and

Live/Dead viability tests, the strain yJS001 was used (genotype SO992 mfa2::pTEF1_mCherry(kanR)). This strain constitutively expresses mCherry protein, allowing for observation using fluorescence microscopy. Optical density (OD) value of 0.1 at 600 nm of light for yeast cells in solution corresponds to 10^6 cells per mL of solution.[45]

2.5.3 *F127-DMA Synthesis*

The procedure was adapted from a previously reported method.[37] Pluronic F-127 (30 g, 2.4 mmol, 1.0 eq) was dried in a vacuum oven at 50 °C for 24 hours, and then dissolved in 275 mL of anhydrous toluene (dried using activated molecular sieves, Grade 514, 4Å) under N_2 atmosphere at 40 °C. Triethylamine (3.4 mL, 24 mmol, 10 eq) was added to the solution via syringe. Reaction mixture was cooled to 0 °C, then a solution of methacryloyl chloride (2.4 mL, 24 mmol, 10 eq) in 25 mL toluene was added dropwise over 30 minutes with constant stirring. Following complete addition of methacryloyl chloride, the reaction mixture was stirred at 0 °C for 1 h, then warmed to room temperature and stirred for 24 h under N_2 atmosphere. The following day, reaction mixture was warmed to 40 °C and vacuum-filtered through a fritted glass funnel with filter paper. Slightly turbid filtrate was concentrated under reduced pressure, then reconstituted in 300 mL fresh toluene and warmed to 40 °C. This process was repeated for a total of 3 filtrations. Transparent filtrate was concentrated under reduced pressure, then dissolved in 100 mL of toluene and precipitated with large excess (700 mL) of anhydrous diethyl ether (dried over magnesium sulfate). The slurry was centrifuged at 4400 rpm for 15 min, and the supernatant was discarded. Solid residue was rinsed twice with fresh diethyl ether, and then centrifuged. F127-DMA was recovered as a fluffy, white powder and was dried under ambient conditions for 12 h. Finally, powder was dried under reduced pressure at 40 °C for 24 h. Dry F127-DMA (29 g) was transferred to amber glass containers and

stored at 5 °C. ^{1}H NMR spectroscopy indicated 78-83% functionalization of chain ends. ^{1}H NMR sample was prepared in $CDCl_3$ at concentrations of 20 mg / mL (Figure A.1) and ^{1}H NMR spectra was collected on a Brüker Avance 500 MHz spectrometer. Standard ^{1}H NMR spectra of Pluronic F-127 ($CDCl_3$, d1 = 10 s, 298 K) indicated average poly(propylene oxide) block lengths of DP = 59 and poly(ethylene oxide) block lengths of DP = 103 (total M_n = 12,500 g / mol). Based on this estimate, in all F127-DMA spectra, the methyl groups of the poly(propylene oxide) block were calibrated to (59 x 3) = 177. The degree of DMA functionalization (f_n) was estimated by dividing the integrated methacrylate vinyl and methyl protons, as well as the PEO chain-end methylene protons, by their theoretical values. For example, 1.55 (vinyl, actual) / 2 (vinyl, theoretical) x 100 ≈ 78% functionalization of chain ends. The degree of DMA-functionalization is reported as a range of estimates, from lowest to highest. ^{1}H NMR (500 MHz, $CDCl_3$, 298 K): δ = 6.12 (m, 2H, H-CH=C) 5.56 (m, 2H, H-CH=C) 4.29 (t, 3*J* = 4.9 Hz; 4H, $CH_2OC(O)$) 3.79-3.26 (m, 1001H, CH_2O, CH_3CHO) 1.93 (dd, 4*J* = 1.7 Hz, 4*J* = 0.9 Hz; 6H, $CH_3C(CO_2)=CH_2$) 1.12 (dd, 3*J* = 6.1 Hz, 4*J* = 4.4 Hz; 177H, CH_3CO).

2.5.4 *Preparation of synthetic complete media*

To prepare 1 L SC media, 2 g of drop-out mix complete, 6.7 g of yeast nitrogen base and 20 g of Glucose were dissolved in MilliQ water. For 5% and 10% glucose containing SC media (1 L) 50 g and 100 g of Glucose were added respectively, with 2 g of drop-out mix, and 6.7 g of yeast nitrogen base. The SC media were filtered through 0.2 micron Nylon filter for sterilization.

2.5.5 *Preparation of hydrogel*

2.5 g and 3.0 g of F127-DMA was dissolved in 7.5 g and 7.0 g of SC media respectively and cooled at 4 °C overnight to prepare 25 wt% and 30 wt% F127-DMA hydrogels in SC media. To

inoculate the hydrogels, the hydrogel solutions were lowered in temperature to 4 °C in a refrigerator. At this temperature, the hydrogel solutions undergo a gel to sol transition, affording a viscous liquid. Yeast cells are then spun down (10^5, 10^6, 10^7, and 10^8 cells per mL of SC media) and extracted from a liquid culture and pipetted into the hydrogel solution at 4 °C. 10 mL of SC media containing above-mentioned amounts of cells were used for 10 g of 25 wt% F127-DMA hydrogel. Photo radical generator, 2-hydroxymethyl propiophenone (10 μL) was and the solution was vortexed to mix thoroughly to create a homogenous solution. Then the solution was allowed to equilibrate at 4 °C until bubbles were removed. Finally, the solution is then warmed to room temperature to undergo a sol to gel transition, resulting in a shear-responsive gel ready for processing.

2.5.6 *Rheological characterization*

For rheological characterization of the materials, dynamic oscillatory experiments were performed on a TA Instruments Discovery Hybrid Rheometer-2 (DHR-2) equipped with a peltier. The instrument operates by applying a known displacement (stress) and measuring the material's resistance (strain) to the force. Rheology tests were conducted by depositing hydrogel between the rheometer base plate and 20 mm parallel plate geometry at a gap of 1 mm. Samples were equilibrated in an ice bath for at least 30 min and then were carefully loaded onto the Peltier plate at 5 °C and a pre-shear experiment was applied to eliminate the bubbles from the sample. The sample was equilibrated at 25 °C for 8 min before each run. Gel yield stresses were measured under oscillatory stress (frequency 1 Hz, 25 °C) starting with an initial stress of 1 Pa up to 10^4 Pa. Viscosity versus shear rate experiments were performed in the range between 0.01 and 10 of shear rate. Cyclic shear thinning tests (frequency 1 Hz) were performed at 25 °C using alternating strains

of 1% for 5 min and 100% for 3 min per cycle, to investigate the shear-thinning and recovery behavior of the hydrogels. Temperature ramp experiments were performed at 1 Hz from 5−50 °C at 2 °C/min. Photo-curing was performed using a fully integrated smart swap LED photo curing accessory. A 60 s irradiation with 365 nm light at 5 mW/cm^2 intensity was triggered into the experiment, and the sample was monitored for a total of 270 s at 1% of strain and at 1 Hz.

2.5.7 *Fabrication of living materials using hydrogel ink*

The hydrogel ink with desired amount of yeast cells was loaded into a Nordson Optimum 10 cc fluid dispensing barrel syringe at 4 °C equiped with a Metcal 27-gauge conical precision tip nozzle (210 μm of inner diameter), and then the temperature was raised to ambient (above the T_{gel}) to afford a shear-responsive hydrogel material.

2.5.8 *Additive manufacturing (direct-write 3D printing) of a cube-lattice*

Direct-write 3D printing was performed on a Prusa I3 RepRap printer. All CAD models were designed in Solidworks 2016. Printing was controlled through standard 3DP software to generate G-code commands (Slic3r) from CAD-generated (Solidworks). All printing was done using yeast-laden 25 wt% hydrogel ink with extrusion air pressure of 12 psi at 25 mm/s print-speed of the nozzle. The dimension for the 3D printed cubes is 15 cm^3 and each cube weighs about 2.64 g.

2.5.9 *Fabrication of 3D meshes*

The 25 wt% hydrogel with embedded yeast cells was extruded at ambient using a shear-pressure of 15 psi (of N_2) through a conical precision tip nozzle (210 μm of inner diameter).This material was up and down the length of a petri dish in a multilayer structure to produce the final, high surface area 3D meshes (Figure A.3). All 3D printed cube and hand-casted 3D mesh samples

were cured under 365 nm irradiation (at 3.4 mW/cm^2) for 120 seconds to chemically fix the structures. After photo curing, the cube lattices and the meshes were soaked and washed in SC media twice prior to use for cell viability and biocatalysis studies.

2.5.10 *Cell viability*

To test cell viability within the hydrogel, a sample of the yeast-inoculated hydrogel 3D meshes (10^6 cells per g of gel) was incubated in SC media and periodically agitated, while the media was exchanged every 24 hours. In parallel, a thin film of hydrogel was produced by spreading the hydrogel on a glass slide at a thickness of about 100 microns. At the imaging intervals described in this work (Figure 2.3, A.5, and A.6), a small piece (about 1 cm) was cut out from the hydrogel mesh and a small piece of film (5 mm x 5 mm) film for live/dead cell screening. Sytox Green strain was diluted to 5 µM, and 10 µL of the dye solution was exposed to hydrogel sample for 5 minutes. After washing, the sample was imaged using a Leica SP5 confocal microscope. Constitutively expressed mCherry protein fluorescence from the yeast cells was measured to indicate live cells, while the Sytox dye fluorescence indicated the presence of dead cells.

2.5.11 *Microscopy and imaging*

Optical and fluorescent imaging: Images of the fabricated meshes with and without yeast (from day 0 to day 14) were captured by using an i-phone 6. Brightfield and epifluorescence images of day 0 to day 14 samples were captured on a Nikon Ti1 microscope equipped with an Andor Zyla 5.5 sCMOS camera and a 10x lens (CFI Plan DX 10x). A 530 nm LED source was used to excite mCherry expressing cells and the emission was collected in a range of ~550-610 nm. Confocal imaging: Confocal microscopy images were taken using a Leica TCS SP5 II laser scanning confocal microscope. All images were taken with a dry 10x objective. MCherry protein

fluorescence was excited with a 561 nm laser at 5% laser power, and emission was scanned from 569-700 nm. Sytox green viability dye was excited with a 488 nm laser at 5% laser power, and emission was scanned from 500-550 nm. Samples were sequentially scanned, and the output images were processed using ImageJ Java software. Scanning Electron Microscopy (SEM): SEM samples were prepared by crosslinking a sample of the native hydrogel (no embedded cells) under the same preparation conditions previously described. Upon crosslinking, the samples were placed back into SC media for ten minutes to maximize the hydration state of the hydrogel. The hydrogels were then dipped directly into liquid nitrogen for two minutes and freeze-dried overnight under vacuum. After lyophilization, the samples were then sputter-coated with a gold/palladium alloy for 45 seconds and imaged using a Sirion XL30 scanning electron microscope.

2.5.12 *Fermentation of glucose into ethanol*

Kinetic studies of fermentation were performed with the 3D printed Cube structures at an initial cell concentration of 10^5, 10^6, 10^7, and 10^8 cells per g of hydrogel. These Cube lattices were washed twice using SC media, and incubated in 26.5 mL of SCM in glass vessels and degassed by bubbling Argon gas for six minutes. The glass vessels were sealed with septa then placed at 30 °C on a shaker. Similarly, hydrogels containing 10^8 cells per g of gel were used at higher concentrations of glucose (5 wt% and 10 wt%) in SC media for kinetics measurements. To obtain samples for quantification for ethanol production, 0.5 mL of the media was extracted from the reaction tube at the described time points and replaced with 0.5 mL of fresh, degassed media. These measurements proceeded in quadruplets for a period of 48 hours.

To monitor the long-term fermentation of glucose to ethanol, the 3D printed cubes with a cell concentration of 10^8 cells per g of hydrogel were washed twice using SC media, and stored individually in tubes containing 10 mL of synthetic complete media for each gram of living

materials. These tubes were degassed for six minutes by bubbling argon through the solution to ensure anaerobic conditions for the fermentation process. Finally, the tubes were placed into a 30 °C shaker for the fermentation reaction. The media was replaced every 3-4 days and stored for ethanol quantification measurements. This study has taken place over the course of 15 days. Finally, 10 mL of red concord grape juice was used in quadruplet in lieu of SC media using 1 g of yeast-embedded hydrogel mesh and the ethanol was quantified after 48 h.

Samples from kinetics and batch measurements were filtered through 0.2 micron nylon filters and subjected to gas chromatography (GC; Agilent 7890A GC System) equipped with a Restek Rtx-BAC1 column (30m, ID 0.53mm, 3.0um) and oven program was 40 °C for 5 min. A 1 µL sample was injected at 253.07 mL/min of H_2 flow. A peak for ethanol appeared between 1.85-1.95 minutes. Standard samples were prepared by adding known volume of pure ethanol into SC media (e.g., 50 µL of ethanol in 950 µL of SC media corresponds to 50,000 ppm v/v of ethanol) to obtain a calibration curve of concentration vs ethanol peak area in GC.

2.6 ACKNOWLEDGEMENTS

"Reprinted (adapted) with permission from: Saha, A.; Johnston, T. G.; Shafranek, R. T.; Goodman, C. J.; Zalatan, J. G.; Storti, D. W.; Ganter, M. A.; Nelson, A. Additive Manufacturing of Catalytically Active Living Materials. *ACS Applied Materials & Interfaces* **2018**, *10* (16), 13373–13380. https://doi.org/10.1021/acsami.8b02719. Copyright 2018 American Chemical Society.

We acknowledge support from University of Washington, Seattle for start-up funding. We thank Biology Imaging Facility, Dept. of Biology, University of Washington, Seattle for using the confocal microscope. We thank Prof. Joshua C. Vaughan, Dept. of Chemistry, University of Washington, Seattle for using the optical microscope and Environmental Health Laboratory, Dept.

of Environmental and Occupational Health Sciences, University of Washington for GC analysis for the samples.

2.7 REFERENCES

1. Liu, X.; Tang, T.-C.; Tham, E.; Yuk, H.; Lin, S.; Lu, T. K.; Zhao, X. Stretchable Living Materials and Devices with Hydrogel–Elastomer Hybrids Hosting Programmed Cells. *Proc. Natl. Acad. Sci. U. S. A.* **2017**, *114*, 2200–2205.
2. Mora, C. A.; Herzog, A. F.; Raso, R. A.; Stark, W. J. Programmable Living Material Containing Reporter Micro-organisms Permits Quantitative Detection of Oligosaccharides. *Biomaterials* **2015**, *61*, 1–9.
3. Gerber, L. C.; Koehler, F. M.; Grass, R. N.; Stark, W. J. Incorporation of Penicillin-Producing Fungi into Living Materials to Provide Chemically Active and Antibiotic-Releasing Surfaces. *Angew. Chem. Int. Ed.* **2012**, *51*, 11293–11296.
4. Gerber, L. C.; Koehler, F. M.; Grass, R. N.; Stark, W. J. Incorporating Microorganisms into Polymer Layers Provides Bioinspired Functional Living Materials. *Proc. Natl. Acad. Sci. U. S. A.* **2012**, *109*, 90–94.
5. Chen, A. Y.; Deng, Z.; Billings, A. N.; Seker, U. O. S.; Lu, M. Y.; Citorik, R. J.; Zakeri, B.; Lu, T. K. Synthesis and Patterning of Tunable Multiscale Materials with Engineered Cells. *Nat. Mater.* **2014**, *13*, 515–523.
6. Das, A. A. K.; Esfahani, M. M. N.; Velev, O. D.; Pamme, N.; Paunov, V. N. Artificial Leaf Device for Hydrogen Generation from Immobilised C. Reinhardtii Microalgae. *J. Mater. Chem. A* **2015**, *3*, 20698–20707.
7. Chen, A. Y.; Zhong, C.; Lu, T. K. Engineering Living Functional Materials. *ACS Synth. Biol.* **2015**, *4*, 8-11.
8. Lee, K. Y.; Mooney, D. J. Hydrogels for Tissue Engineering. *Chem. Rev.* **2001**, *101*, 1869–1879.
9. Hoffman, A. S. Hydrogels for Biomedical Applications. *Adv. Drug Deliv. Rev.* **2002**, *54*, 3–12.
10. Connell, J. L.; Ritschdorff, E. T.; Whiteley, M.; Shear, J. B. 3D Printing of Microscopic Bacterial Communities. *Proc. Natl. Acad. Sci. U. S. A.* **2013**, *110*, 18380–18385.
11. Lode, A.; Krujatz, F.; Brüggemeier, S.; Quade, M.; Schütz, K.; Knaack, S.; Weber, J.; Bley, T.; Gelinsky, M. Green Bioprinting: Fabrication of Photosynthetic Algae-laden Hydrogel Scaffolds for Biotechnological and Medical Applications. *Eng. Life Sci.* **2015**, *15*, 177–183.
12. Lehner, B. A. E.; Schmieden, D. T.; Meyer, A. S. A Straightforward Approach for 3D Bacterial Printing. *ACS Synth. Biol.* **2017**, *6*, 1124–1130.
13. Peralta-Yahya, P. P.; Zhang, F.; del Cardayre, S. B.; Keasling, J. D. Microbial Engineering for the Production of Advanced Biofuels. *Nature* **2012**, *488*, 320–328.
14. Davy, A. M.; Kildegaard, H. F.; Andersen, M. R. Cell Factory Engineering. *Cell Syst.* **2017**, *4*, 262–275.
15. Zhang, Y.-H. P.; Sun, J.; Ma, Y. Biomanufacturing: History and Perspective. *J. Ind. Microbiol. Biotechnol.* **2017**, *44*, 773–784.

16. Fernandez-Rodriguez, J.; Moser, F.; Song, M.; Voigt, C. A. Engineering RGB Color Vision into Escherichia coli. *Nat. Chem. Biol.* **2017**, *13*, 706–708.
17. Doelle, H. W.; Kirk, L.; Crittenden, R.; Toh, H.; Doelle, M. B. Zymomonas Mobilis—Science and Industrial Application. *Crit. Rev. Biotechnol.* **1993**, *13*, 57–98.
18. DeLoache, W. C.; Russ, Z. N.; Narcross, L.; Gonzales, A. M.; Martin, V. J. J.; Dueber, J. E. An Enzyme-coupled Biosensor Enables (S)-reticuline Production in Yeast from Glucose. *Nat. Chem. Biol.* **2015**, *11*, 465–471.
19. Paddon, C. J.; Westfall, P. J.; Pitera, D. J.; Benjamin, K.; Fisher, K.; McPhee, D.; Leavell, M. D.; Tai, A.; Main, A.; Eng, D.; Polichuk, D. R.; Teoh, K. H.; Reed, D. W.; Treynor, T.; Lenihan, J.; Jiang, H.; Fleck, M.; Bajad, S.; Dang, G.; Dengrove, D.; Diola, D.; Dorin, G.; Ellens, K. W.; Fickes, S.; Galazzo, J.; Gaucher, S. P.; Geistlinger, T.; Henry, R.; Hepp, M.; Horning, T.; Iqbal, T.; Kizer, L.; Lieu, B.; Melis, D.; Moss, N.; Regentin, R.; Secrest, S.; Tsuruta, H.; Vazquez, R.; Westblade, L. F.; Xu, L.; Yu, M.; Zhang, Y.; Zhao, L.; Lievense, J.; Covello, P. S.; Keasling, J. D.; Reiling, K. K.; Renninger, N. S.; Newman, J. D. High-level Semi-synthetic Production of the Potent Antimalarial Artemisinin. *Nature* **2013**, *496*, 528–532.
20. Gerngross, T. U. Advances in the Production of Human Therapeutic Proteins in Yeasts and Filamentous Fungi. *Nat. Biotechnol.* **2004**, *22*, 1409–1414.
21. Awan, A. R.; Blount, B. A.; Bell, D. J.; Shaw, W. M.; Ho, J. C. H.; McKiernan, R. M.; Ellis, T. Biosynthesis of the Antibiotic Nonribosomal Peptide Penicillin in Baker's Yeast. *Nat. Commun.s* **2017**, *8*, ncomms15202.
22. Thodey, K.; Galanie, S.; Smolke, C. D. A Microbial Biomanufacturing Platform for Natural and Semisynthetic Opioids. *Nat. Chem. Biol.* **2014**, *10*, 837–844.
23. Li, Y.; Smolke, C. D. Engineering Biosynthesis of the Anticancer Alkaloid Noscapine in Yeast. *Nat. Commun.* **2016**, *7*, 12137.
24. Galanie, S.; Thodey, K.; Trenchard, I. J.; Interrante, M. F.; Smolke, C. D. Complete Biosynthesis of Opioids in Yeast. *Science* **2015**, *349*, 1095–1100.
25. Nagarajan, S.; Kruckeberg, A. L.; Schmidt, K. H.; Kroll, E.; Hamilton, M.; McInnerney, K.; Summers, R.; Taylor, T.; Rosenzweig, F. Uncoupling Reproduction from Metabolism Extends Chronological Lifespan in Yeast. *Proc. Natl. Acad. Sci. U. S. A.* **2014**, *111*, E1538–E1547.
26. Cheetham, P. S. J.; Blunt, K. W.; Bocke, C. Physical Studies on Cell Immobilization Using Calcium Alginate Gels. *Biotechnol. Bioeng.* **1979**, *21*, 2155–2168.
27. Liu, Y.; Rafailovich, M. H.; Malal, R.; Cohn, D.; Chidambaram, D. Engineering of Bio-hybrid Materials by Electrospinning Polymer-microbe Fibers. *Proc. Natl. Acad. Sci. U. S. A.* **2009**, *106*, 14201–14206.
28. Letnik, I.; Avrahami, R.; Rokem, J. S.; Greiner, A.; Zussman, E.; Greenblatt, C. Living Composites of Electrospun Yeast Cells for Bioremediation and Ethanol Production. *Biomacromolecules* **2015**, *16*, 3322–3328.
29. Schaffner, M.; Rühs, P. A.; Coulter, F.; Kilcher, S.; Studart, A. R. 3D Printing of Bacteria into Functional Complex Materials. *Sci. Adv.* **2017**, *3*, eaao6804.
30. Connell, J. L.; Kim, J.; Shear, J. B.; Bard, A. J.; Whiteley, M. Real-time Monitoring of Quorum Sensing in 3D-printed Bacterial Aggregates Using Scanning Electrochemical Microscopy. *Proc. Natl. Acad. Sci. U. S. A.* **2014**, *111*, 18255–18260.
31. Patra, S.; Young, V. A Review of 3D Printing Techniques and the Future in Biofabrication of Bioprinted Tissue. *Cell Biochem Biophys* **2016**, *74*, 93–98.

32. Bader, C.; Patrick, W. G.; Kolb, D.; Hays, S. G.; Keating, S.; Sharma, S.; Dikovsky, D.; Belocon, B.; Weaver, J. C.; Silver, P. A.; Oxman, N. Grown, Printed, and Biologically Augmented: An Additively Manufactured Microfluidic Wearable, Functionally Templated for Synthetic Microbes. *3D Print. Addit. Manuf.* **2016**, *3*, 79–89.
33. Li, Y.-C.; Zhang, Y. S.; Akpek, A.; Shin, S. R.; Khademhosseini, A. 4D Bioprinting: the Next-generation Technology for Biofabrication Enabled by Stimuli-responsive Materials. *Biofabrication* **2017**, *9*, 012001.
34. Bertassoni, L. E.; Cardoso, J. C.; Manoharan, V.; Cristino, A. L.; Bhise, N. S.; Araujo, W. A.; Zorlutuna, P.; Vrana, N. E.; Ghaemmaghami, A. M.; Dokmeci, M. R.; Khademhosseini, A. Direct-write Bioprinting of Cell-laden Methacrylated Gelatin Hydrogels. *Biofabrication* **2014**, *6*, 024105.
35. Murphy, S. V.; Atala, A. 3D Bioprinting of Tissues and Organs. *Nat. Biotech.* **2014**, *32*, 773–785.
36. Highley, C. B.; Rodell, C. B.; Burdick, J. A. Direct 3D Printing of Shear-Thinning Hydrogels into Self-Healing Hydrogels. *Adv. Mater.* **2015**, *27*, 5075–5079.
37. Müller, M.; Becher, J.; Schnabelrauch, M.; Zenobi-Wong, M. Nanostructured Pluronic Hydrogels as Bioinks for 3D Bioprinting. *Biofabrication* **2015**, *7*, 035006.
38. Gladman, A. S.; Matsumoto, E. A.; Nuzzo, R. G.; Mahadevan, L.; Lewis, J. Biomimetic 4D Printing. *Nat. Materials* **2016**, *15*, 413.
39. Basu, A.; Saha, A.; Goodman, C.; Shafranek, R. T.; Nelson, A. Catalytically Initiated Gel-in-Gel Printing of Composite Hydrogels. *ACS Appl. Mater. Interfaces* **2017**, *9*, 40898–40904.
40. Hospodiuk, M.; Dey, M.; Sosnoski, D.; Ozbolat, I. T. The Bioink: A Comprehensive Review on Bioprintable Materials. *Biotechnol. Adv.* **2017**, *35*, 217–239.
41. Donderwinkel, I.; Hest, J. C. M. van; Cameron, N. R. Bio-inks for 3D Bioprinting: Recent Advances and Future Prospects. *Polym. Chem.* **2017**, *8*, 4451–4471.
42. Lee, J. M.; Yeong, W. Y. Design and Printing Strategies in 3D Bioprinting of Cell-Hydrogels: A Review. *Adv. Healthc. Mater.* **2016**, *5*, 2856–2865.
43. Smith, P. T.; Basu, A.; Saha, A.; Nelson, A. Chemical Modification and Printability of Shear-thinning Hydrogel Inks for Direct-write 3D Printing. *Polymer* **2018**, doi.org/10.1016/j.polymer.2018.01.070.
44. Paxton, N.; Smolan, W.; Böck, T.; Melchels, F.; Groll, J.; Jungst, T. Proposal to Assess Printability of Bioinks for Extrusion-Based Bioprinting and Evaluation of Rheological Properties Governing Bioprintability. *Biofabrication* **2017**, *9*, 044107.
45. Gietz, R. D.; Schiestl, R. H. High-efficiency Yeast Transformation Using the LiAc/SS Carrier DNA/PEG Method. *Nat. Protoc.* **2007**, *2*, 31.
46. Lee, R. E. C.; Puente, L. G.; Kærn, M.; Megeney, L. A. A Non-Death Role of the Yeast Metacaspase: Yca1p Alters Cell Cycle Dynamics. *PLOS ONE* **2008**, *3*, e2956.
47. Haase, S. B. Cell Cycle Analysis of Budding Yeast Using SYTOX Green. *Curr. Protoc. Cytom.* **2004**, *Chapter 7*, Unit 7.23.
48. Krishnan, M. S.; Ho, N. W.; Tsao, G. T. Fermentation Kinetics of Ethanol Production from Glucose and Xylose by Recombinant Saccharomyces 1400(pLNH33). *Appl. Biochem. Biotechnol.* **1999**, *77–79*, 373–388.
49. Yu, G.-E.; Deng, Y.; Dalton, S.; Wang, Q.-G.; Attwood, D.; Price, C.; Booth, C. Micellisation and Gelation of Triblock copoly(oxyethylene/oxypropylene/oxyethylene), F127. *J. Chem. Soc., Faraday Trans.* **1992**, *88*, 2537–2544.

2.8 FIGURES

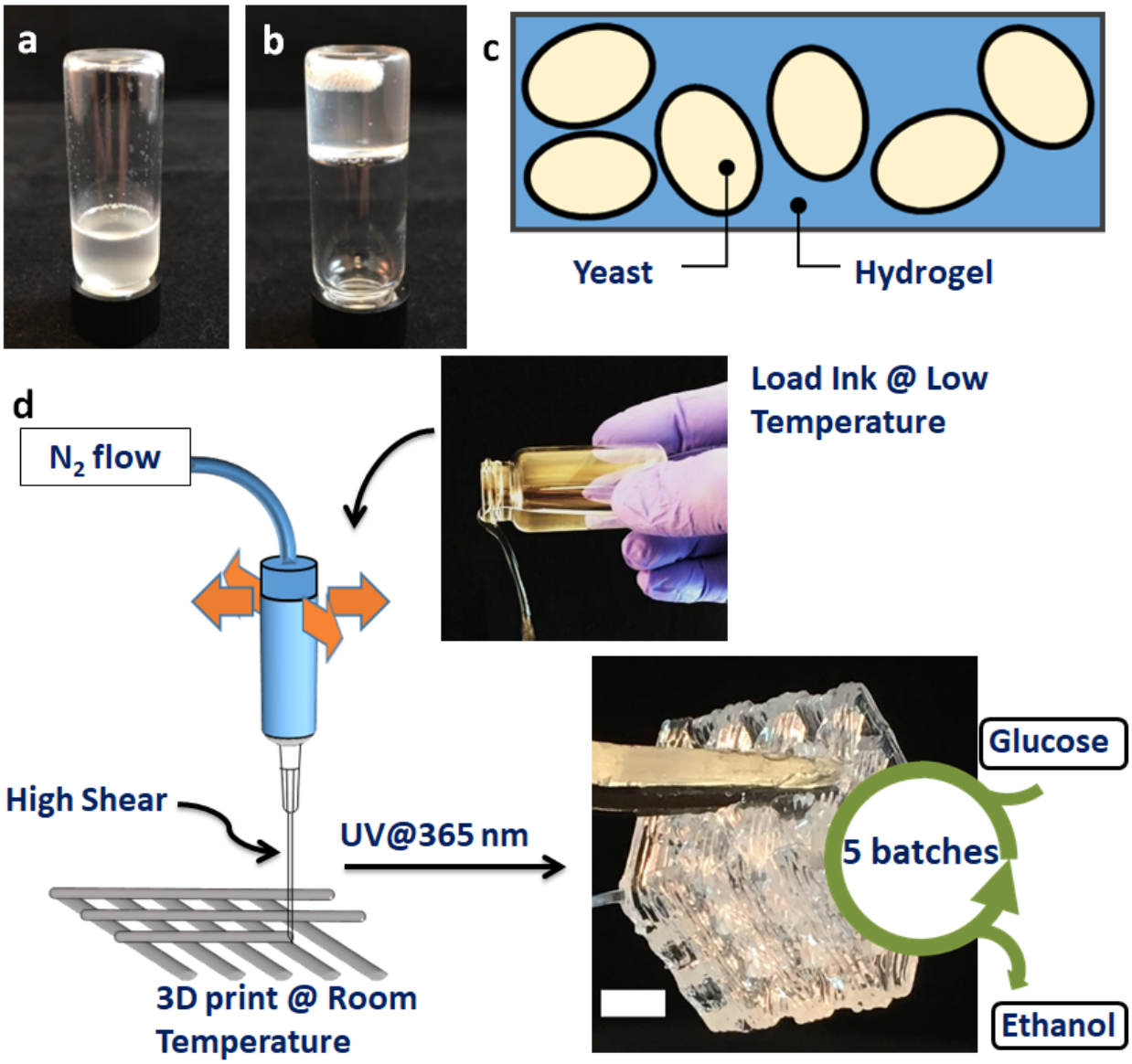

Figure 2.14. Overview of the AMCALM process

The F127-DMA hydrogels (25 wt%) in SC media occupied a 'sol' state at (a) 4 °C and a 'gel' state at (b) 23 °C. Images of 25 wt% F127-DMA hydrogel in SC media a) at and b) at; graphical representation of the c) yeast-laden hydrogel ink for the d) direct-write 3D printing of cube lattice capable of biocatalytic conversion of glucose into ethanol for five batches (Scale bar 5 mm).

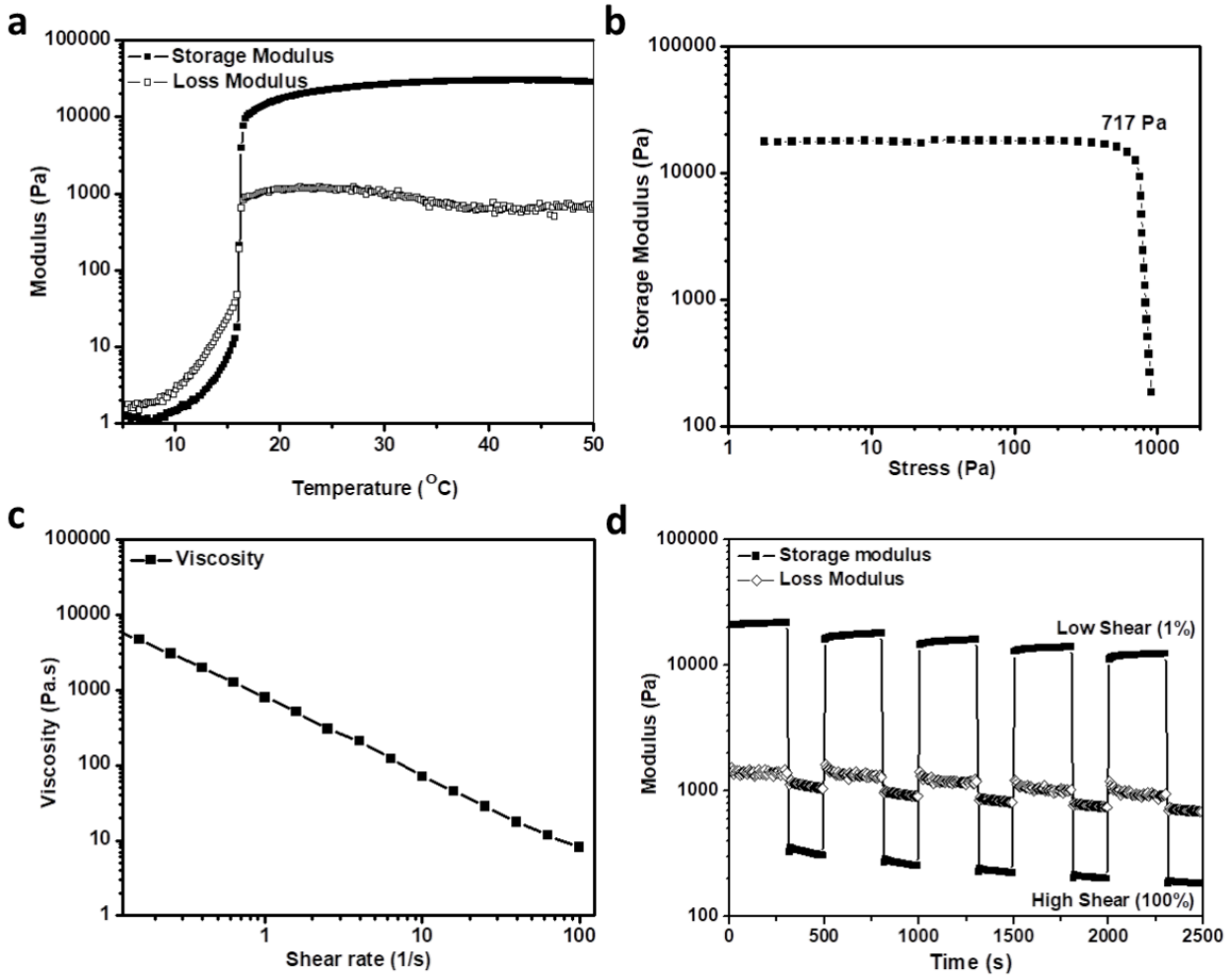

Figure 2.15. Hydrogel rheology

(a) Dynamic oscillatory temperature ramp experiment showing storage and loss moduli for 25 wt% F127-DMA in SC Media. (b) Storage modulus versus shear stress showing a yield stress at 717 Pa for the same hydrogel. (c) Viscosity as a function of shear rate profile of the hydrogel. (d) Cyclic shear experiment for 25 wt% F127-DMA hydrogel in SC media showing storage and loss moduli in response to high (100%) and low (1%) oscillatory strains.

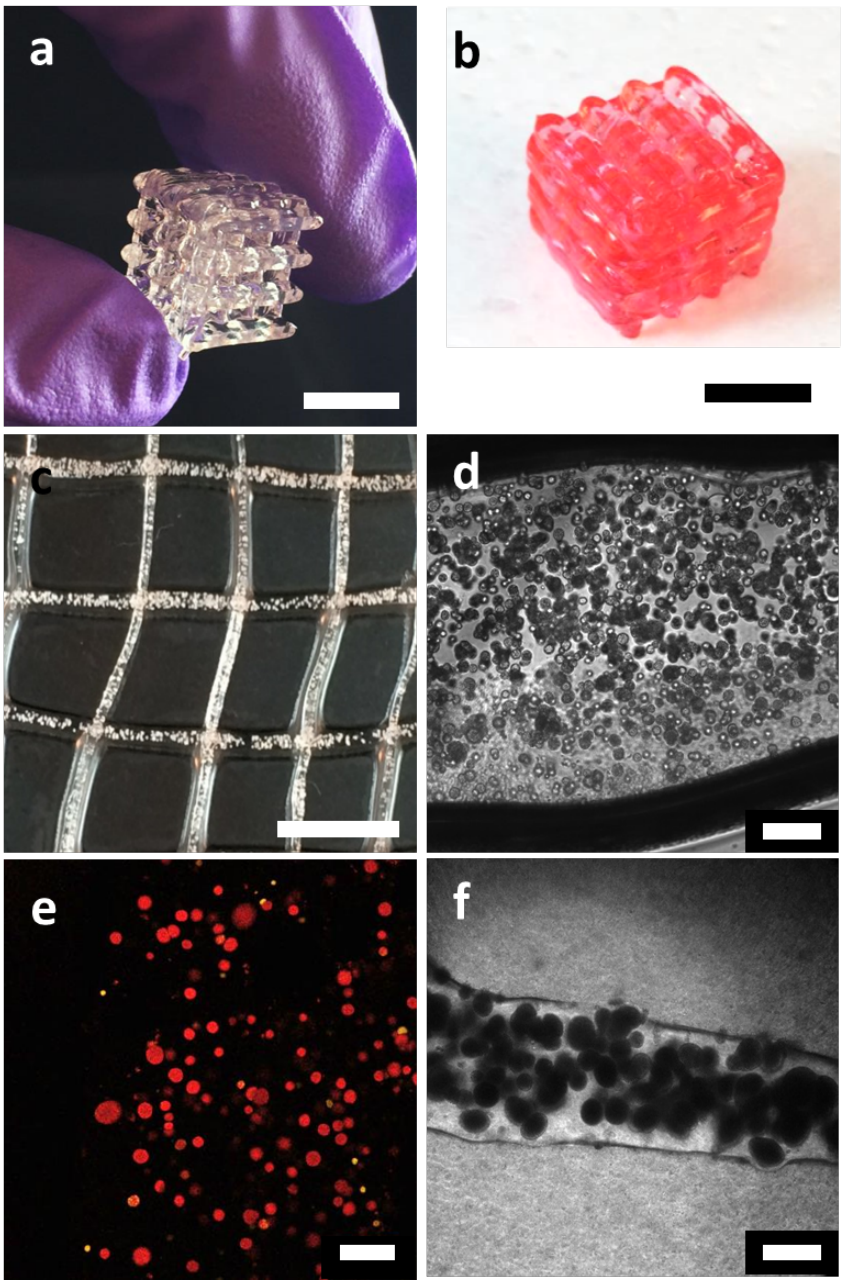

Figure 2.16. Images and microscopy of yeast-laden hydrogels

Images for the yeast cell-laden 3D printed cubes (dimension: 15 mm^3) a) and b). Images of the mCherry expressing cell-laden 3D meshes at day 3: c) visual image, d) optical microscopy image, and e) confocal microscopy image. At day 14: f) optical microscopy image. (The cube in figure b was strained with red dye for better visualization). (Scale bars: a) 15 mm, b-c) 10 mm, d-f) 200 μm)

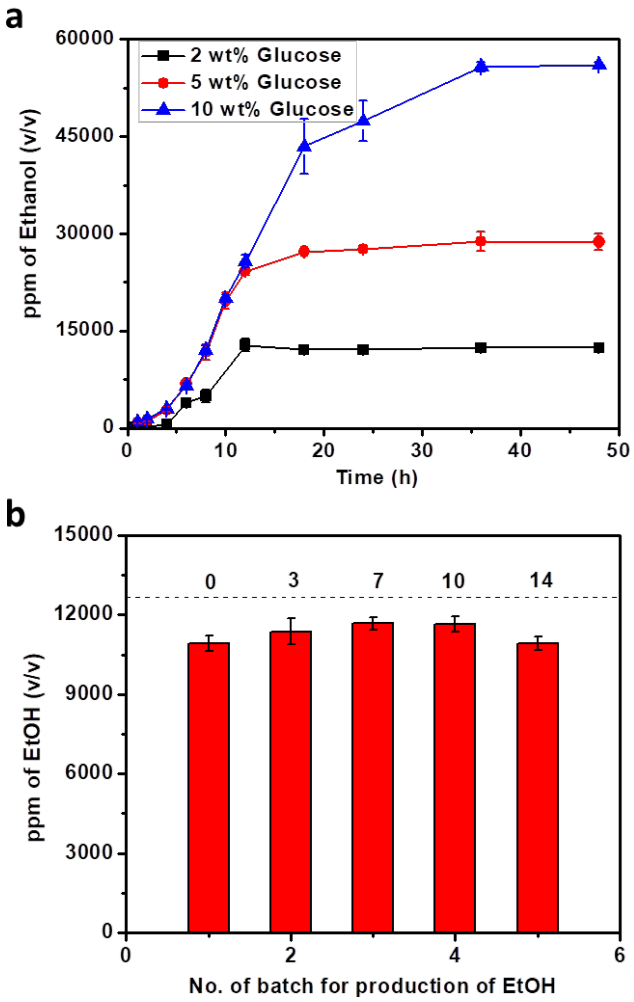

Figure 2.17. Glucose fermentation results

Graphs showing a) the production of ethanol with 108 cells/g of living materials with varying amounts of glucose in SC media, and b) the sustainable production of ethanol using yeast-embedded 3D printed cubes in 5 consecutive batches of 2 wt% of glucose in SC media. The numerical values above the individual bars represent the time (in days) since the start of the experiment (i.e., the last measurement on the chart was taken after 14 consecutive days of bioactivity). The dotted line at 12693 ppm represents 100% theoretical conversion of glucose into ethanol.

Chapter 3. POLY(ALKYL GLYCIDYL ETHER) HYDROGELS FOR HARNESSING THE BIOACTIVITY OF ENGINEERED MICROBES

This chapter has been adapted from the following manuscript:

> **Johnston, T. G.**; Fellin, C. R.; Carignano, A.; Nelson, A. Poly(Alkyl Glycidyl Ether) Hydrogels for Harnessing the Bioactivity of Engineered Microbes. *Faraday Discuss.* **2019**, *219*, 58–72. https://doi.org/10.1039/C9FD00019D.

3.1 ABSTRACT

Herein, we describe a method to produce yeast-laden hydrogel inks for direct-write 3D printing cuboidal lattices for immobilized whole-cell catalysis. A poly(alkyl glycidyl ether)-based triblock copolymer was designed to have three important features for this application: (1) a temperature response which allowed for facile processing of the material; (2) the shear response which facilitated the extrusion of the material through a nozzle; and (3) a UV-light induced polymerization which enabled the post extrusion chemical crosslinking of network chains, and the fabrication of robust printed objects. These three key stimuli responses were confirmed via rheometrical characterization. A genetically-engineered yeast strain with an upregulated α-factor production pathway was incorporated into the hydrogel ink and 3D printed. The immobilized yeast cells exhibited adequate viability of 87.5% within the hydrogel. The production of the up-regulated α-factor was detected using a detecting yeast strain and quantified at 268 nM (s = 34.6 nM) over 72 h. The reusability of these bioreactors was demonstrated by immersion of the yeast-laden hydrogel lattice in fresh SC media and confirmed by the detection of similar amounts of up-regulated α-factor 259 nM (s = 45.1 nM). These yeast-laden materials represent an attractive

opportunity for whole-cell catalysis of other high-value products in a sustainable and continuous manner.

3.2 INTRODUCTION

Whole-cell biocatalysis is a standard practice across a wide range of industries wherein cells are used to transform molecular precursors into a product of interest (antibiotics, drugs, vitamins, insulin, vaccines, etc.). These reactions are generally employed as a batch process wherein the cells and the necessary molecular precursors are combined into a single reaction vessel, stirred for several days, and then the product is isolated from the complex mixture.[1–10] However, batch cell reactors are costly and time consuming because they require sterile conditions, can have low yields, and purification protocols are labor and cost intensive. Immobilized-cell bioreactors, wherein metabolically active cells are trapped within a material such as a hydrogel, offer an alternative method that can simplify the isolation of the product, minimize product inhibition or toxicity, and allow recycling of the cells.[11]

We have previously reported additive manufactured catalytically active living materials (AMCALM) as a platform for immobilized-cell bioreactors.[12] In contrast to previous reports wherein calcium alginate beads[13–16] or electrospun fibers[17–19] were used to encapsulate microbes for fermentation, our approach utilized customized lattices of yeast-laden hydrogels that were printed using a direct-write 3D printer. Additive manufacturing (or 3D printing) is a fabrication process that utilizes layer-by-layer material deposition to construct three-dimensional geometries according to a computer-aided design (CAD) model.[20–27] As such, 3D printing is well-suited for manufacturing living materials[28–33] with spatial and geometrical organization of cells. Hydrogel-based materials are particularly attractive as cell-laden inks for direct-write 3D printing because these materials can recapitulate some of the chemical and physical attributes of the extracellular

matrix that exists in biofilms, living tissue, and other naturally occurring microenvironments.[31,34–36] These features could include the presence of ligands or functional groups,[37–40] or the stiffness of the hydrogel.[41,42]

There were three important features of the yeast-laden hydrogel ink that were developed for AMCALMs: (1) a temperature response, wherein the material exhibited a reversible gel-to-sol transition upon cooling, that enabled homogeneous dispersion of the yeast cells within the gel and facile loading of the hydrogel into a syringe; (2) a shear-thinning response that facilitated the extrusion of the hydrogel ink from a nozzle to enable the layer-by-layer formation of three-dimensional objects; and (3) an irreversible photo-response wherein polymerizable groups chemically cross-linked the hydrogel into a robust structure. Yeast-laden hydrogel lattices were printed and then utilized in a continuous batch process for the fermentation of glucose to produce ethanol.

Herein, we demonstrate a new polymer hydrogel for the encapsulation and direct-write 3D printing of yeast-laden hydrogel lattices that can be used for the production of a polypeptide. The poly(glycidyl ether)-based ABA triblock copolymer (polymer **2**) has similar features (temperature-, shear-, and photo-responses, Figure 3.1) to the Pluronic-based triblock copolymer that was reported previously.[12] Furthermore, a genetically-engineered yeast strain with an upregulated α-factor production pathway was incorporated into the hydrogel to demonstrate the production of an extracellularly excreted polypeptide from the yeast-laden hydrogel. While α-factor is a yeast hormone that does not have any known therapeutic effects, the polypeptide is commonly utilized in the expression and recovery of recombinant proteins.[43,44] When the α-factor leader sequence is appended to the genetic code for an engineered protein, the yeast cell utilizes its native cellular machinery to secrete the protein beyond the cell membrane.[45–50] In our experiments, we not only

demonstrate that the secreted α-factor can be detected in the liquid media surrounding the hydrogel lattice, but also the reusability of the yeast-laden hydrogel lattices.

3.3 Results and Discussion

3.3.1 *Synthesis and Functionalization of the Triblock Copolymer*

ABA triblock copolymers of poly(isopropyl glycidyl ether-*stat*-ethyl glycidyl ether)-*block*-poly(ethylene oxide)-*block*-poly(isopropyl glycidyl ether-*stat*-ethyl glycidyl ether) afford shear-thinning hydrogels that have a tunable sol-gel transition temperature based on the ratio of ethyl and isopropyl glycidyl ether monomers (EGE and iPGE, respectively), 'A' block chain length, and concentration.[51] When these polymers were dissolved in aqueous media, flower-like micelles[52] were expected to form based on the design of this ABA triblock copolymer--hydrophobic 'A' blocks flanking a hydrophilic 'B' block. Hydrogels based on this ABA triblock copolymer platform (20 wt%) were suitable inks for direct-write 3D printing and were able to create self-supporting hydrogel structures.[52] However, the physical cross-links present in this system were insufficient to maintain the integrity of the 3D printed object when subjected to either excess aqueous media or to mechanical loads. Thus, chemically cross-linked hydrogels are necessary to improve the robustness of the 3D printed objects.

Polymer **1** was synthesized (Figure 3.2) via living anionic ring-opening polymerization[53–56] from a poly(ethylene oxide) (PEO) macroinitiator (M_n = 8,000 g mol^{-1}) with an EGE:iPGE ratio of 1.15:1 to afford triblock copolymers with narrow dispersity (Đ = 1.11). Polymerizable methacrylate groups were introduced onto the chain-ends of polymer **1** to afford polymer **2**. We hypothesized that the resulting polymer hydrogel would maintain its thermal- and shear-responses pre-extrusion, and then photochemically cross-link post-extrusion. The degree of chain-end functionalization (f_n) was determined by comparing the integrations of the methacrylate vinyl

(6.12 and 5.55 ppm) and methyl (1.94 ppm) protons, as well as the PEO chain-end methylene protons (5.08-5.15 ppm), to their theoretical values and was found to be quantitative. The polymer was dissolved water (20 wt %) and 2-hydroxy-2-methylpropiophenone was added as the photo-radical initiator (0.1 wt%) for polymerization of the methacrylate groups.

3.3.2 *Rheology of the Functionalized Triblock Copolymer Hydrogel*

The viscoelastic properties of a 20 wt% solution of polymer **2** in water were characterized using a rheometer. The temperature-dependent viscoelastic behavior of the gel was confirmed by the presence of a sol-gel transition as defined by the intersection of the elastic (G') and viscous (G") moduli (15.61 °C, Figure 3.3a). The solution maintained a non-viscous, liquid-like morphology at 5 °C and became a self-supporting hydrogel network by 21 °C. The temperature-dependent sol-gel transition was also confirmed visually as shown in the photographs in Figure B.1.

Hydrogels based on polymer **2** also exhibited shear-thinning behavior. The viscosity of the material decreased with increasing applied shear rate, which is indicative of a shear thinning hydrogel. An oscillatory strain sweep experiment afforded a yield stress value of 1.33 kPa (Figure B.2-3). A dynamic oscillatory strain experiment (Figure 3.3b) demonstrated the strain dependent viscoelastic behavior of the gel upon repeated cycles of high (100%) and low (1%) strain. Initially under low strain, the material exhibited a gel-like morphology as indicated by greater values for G' relative to G". During periods of high strain, G" exceeded G', which indicated that the gel had a higher viscous character consistent with the material in its sol state. The material rapidly recovered to its gel state when the strain was reduced to 1% and exhibited very little mechanical hysteresis.

The post-extrusion UV cure of the gel was simulated under constant strain (1%) and frequency (1 Hz). After 120 s of equilibration time, the hydrogel was subjected to 5 mW cm^{-2} of 365 nm UV light for 420 s. The G' of the hydrogel increased from 21.56 kPa to 94.23 kPa within 75 s of UV exposure, and the G" decreased from 1.88 kPa to 0.47 kPa in the same time frame. These changes to the G' and G" were indicative of a rapid chemical crosslinking of the hydrogel network via photo-induced radical polymerization of the methacrylated chain ends (Figure 3.4a).

3.3.3 *Direct-Write 3D Printing of Triblock Copolymer Dimethacrylate Hydrogels*

Utilizing these three stimuli responses, a proof of concept cuboidal lattice was 3D printed using a pneumatic direct write 3D printer at 5 mm s^{-1} and 20 psi with a 0.41 mm inner diameter conical nozzle. The temperature response allowed for facile processing of the hydrogel into the syringe at 5 °C in its liquid state. The hydrogel was then warmed to ambient temperature and extruded. The shear-response facilitated the extrusion of the hydrogel as rod-like filaments. A cuboidal lattice structure, with dimensions of 1.9 cm by 1.9 cm by 1.2 cm, was cured post-extrusion using a custom-made UV box equipped with two 365 nm A19 UV lamps for 180 s at 3.4 mW cm^{-2} (Figure 3.4b-c).

3.3.4 *Incorporation of Yeast Cells and Cell Viability*

To ensure the viability of encapsulated yeast cells within the polymer 2 hydrogel, Saccharomyces cerevisiae constitutively expressing mCherry fluorescent protein was inoculated into a solution of polymer 2 at 5 °C and mixed to make a homogenous mixture. A film of the resulting yeast-laden solution was cast at the same temperature, subsequently warmed to 21 °C to induce gelation, and cured to create a physically robust hydrogel film. This yeast-laden film appeared transparent after processing due to the relatively low loading concentration of yeast cells.

A small sample of the yeast-laden hydrogel film was extracted, stained, and imaged periodically over seven days. Sytox green staining results showed that cells remained 87.5% viable within the cast hydrogel at the end of the week of imaging, as seen in Figures 3.5a and Figures B.4-B.6. Significant cell colony growth was observed by both confocal microscopy and optical imaging. This growth was also observed visually, as indicated by the opacity of the 3D-printed hydrogel structure in Figure 3.5b-c. These results suggest that the poly(alkyl glycidyl ether)-based hydrogels are comparable in their ability to house and promote yeast cell viability over time to our previously employed[12] F127-based hydrogels.

3.3.5 *α-Factor Production with 3D Printed AMCALMs*

An engineered yeast strain with upregulated α-factor production was used to demonstrate AMCALM lattices that produced a polypeptide. The pGPD promoter present in the secreting yeast strain allowed the constitutive expression of the MFα1 gene, and thus, continuous production of the α-factor polypeptide. After the reaction, the aqueous reaction media was exposed to the detecting strain that fluoresced in the presence of α-factor.

These lattices were incubated in SC media for a period of 72 h (Figure 3.6), producing an average of 268 nM (s = 34.6 nM) of α-factor (Figure 3.7). The induced fluorescence response from the cuboidal lattice with the secreting strain was 4.40 times greater that of the control strain cuboidal lattice (without upregulated α-factor), which indicated that the up-regulation of the α-factor pathway was successful in the secreting strain. These results provide evidence that AMCALMs were suitable for the production of polypeptides, and that the products could readily diffuse out from the hydrogel matrix into the surrounding media.

One advantage of using an immobilized yeast platform for polypeptide synthesis is the potential to reuse the printed cuboidal lattices. We investigated the reusability of the poly(alkyl

glycidyl ether)-based hydrogel living materials for the continued production of α-factor in subsequent batch reactions. When the printed AMCALMs were removed from their first 72 h incubation, and placed into fresh media, they continued to produce an average of 259 nM (s = 45.1 nM) of α-factor after a second 72 h cycle (Figure 3.7). The second batch production was directly comparable to the output achieved during the first batch reaction, which suggests that these immobilized cell bioreactors could be useful for continuous whole-cell catalysis.

3.4 CONCLUSIONS

In conclusion, we developed an ABA triblock copolymer based on a poly(alkyl glycidyl ether) that is suitable for 3D printing yeast-laden hydrogels for whole-cell catalysis. These polymer hydrogels exhibit a temperature, shear, and UV-light responsive behaviors that are integral to the preparation of the hydrogel ink and subsequent printing. The post-extrusion, chemical crosslinking of the polymer micelles induced by UV-light is particularly important to fabricate robust forms that do not degrade or dissolve over time.

The poly(alkyl glycidyl ether) based hydrogels also proved to have a negligible effect on the viability and biological activity of the encapsulated yeast cells. The engineered yeast-laden living materials were shown to be capable of producing an average of 263.5 nM of α-factor during two consecutive batch reactions, exhibiting no significant reduction in efficiency between the two cycles.

In this work, we demonstrated that polypeptides can be produced using the AMCALM platform. This result, combined with the prominence of the α-factor leader sequence in recombinant protein design and production, suggests that that these materials could be employed in the whole-cell catalysis of other higher-value molecules in a sustainable and continuous manner.

3.5 EXPERIMENTAL

3.5.1 *Materials*

All chemicals and solvents were purchased from Sigma-Aldrich or Fisher Scientific and used without further purification unless noted otherwise. Isopropyl glycidyl ether (iPGE, 98%) and ethyl glycidyl ether (EGE, 98%) were dried over CaH_2 for 24 h, distilled into a flask containing butyl magnesium chloride (2 M in tetrahydrofuran, THF), re-distilled, and stored under N_2 atmosphere. Poly(ethylene oxide) (PEO, M_n 8000 g mol^{-1}) was dried under vacuum overnight prior to use. Dry THF was obtained using neutral alumina using a Pure Process Technology solvent purification system. A potassium naphthalenide solution (1M) was prepared by dissolving naphthalene (3.2 g) in THF (25 mL), adding potassium (0.975 g), and storing under N_2 atmosphere. ^{1}H NMR spectra were obtained on a Bruker Advance 300 or 500 MHz spectrometer. Gel permeation chromatography was performed using a Waters chromatograph equipped with two 10 μm Malvern columns (300 mm x 7.8 mm) connected in series with increasing pore size (1,000, 10,000 Å), using chloroform (Optima, 0.1% v/v trimethylamine) as the eluent, and calibrated with poly(ethylene oxide) standards (400 to 40, 000 g mol^{-1}). The relative molecular weights were measured in chloroform using poly(ethylene oxide) standards and a refractive index detector (flow rate: 1 mL min^{-1}). Drop-out Mix Complete without Yeast Nitrogen Base D9515) and Yeast Nitrogen Base (Y2025) were purchased from US Biological Life Sciences. Sytox Green nucleic acid strain (5 mM solution in DMSO; Invitrogen) was purchased from Thermo Fisher Scientific.

3.5.2 *Yeast Strains*

For microscopy and live/dead viability tests, the strain yJS001 was used (genotype SO992 mfa2::pTEF1_mCherry(kanR)). This strain constitutively expressed mCherry protein, which

facilitated characterization using fluorescence microscopy. *Saccharomyces cerevisiae* strain SO992 was used as the control strain in the α-factor production experiments. This strain is a derivative of W303 (genotype MATa ura3 leu2 trp1 his3 can1R ade).

As the α-factor-producing strain, we employed a genetically modified MAT-α yeast strain ('secreting strain') expressing the *S. cerevisiae* gene MFα1 (YPL187W) on a constitutively-expressed promoter pGPD (natively expressing YPL197W). The MFα1 gene expresses 3 copies of the α-factor peptide, a 13-amino acid peptide natively used as mating hormone from the MAT-α to the MAT-A strains.

To quantify the α-factor secreted from the yeast immobilized in the hydrogels, we employed a genetically modified MAT-A yeast strain that expresses the fluorescence protein yeVenus driven by the pFUS1 promoter, which is downstream the MAPK signaling pathway, activated by α-factor detection ('detecting strain'). The MAT-A native strain was engineered by deleting BAR1 (native α-factor protease) and integrating the POG1 gene on a constitutively-expressed pGPD promoter to avoid α-factor-induced growth arrest.

Yeast transformations were carried out using a standard lithium acetate protocol. Yeast cells were made competent by growing 50 mL cultures in rich media to log growth phase, then spinning down the cells and washing with H20. Next, linearized DNA, salmon sperm donor DNA, 50% polyethylene glycol and 1M LiOAc were combined with 50 mL of competent cells and the mixture was heat shocked at 42 °C for 15 min. The cells were then spun down, supernatant was removed, and they were resuspended in H2O and then plated on selective agar media. Transformations were done into MATa W303-1A and MATα W303-1B background strains.

3.5.3 *Synthesis of Polymer 1*

The ABA triblock copolymer was synthesized via anionic ring-opening polymerization. PEO (M_n = 8,000 g mol^{-1}, 20 g, 2.5 mmol) was added to the reaction vessel and dried under vacuum overnight. Dry THF (250 mL) was added under an Ar atmosphere and heated to 50 °C to facilitate dissolution of the macroinitiator. Once sufficiently dissolved, a potassium naphthalenide solution (1M in THF) was titrated into the flask until the solution remained a slight green color, indicating full deprotonation of PEO hydroxyl end groups. Isopropyl glycidyl ether (4.94 g, 42.5 mmol) and ethyl glycidyl ether (4.34 g, 42.5 mmol) were added to begin polymerization. The reaction continued for 24 h at 65 °C and was subsequently quenched with a degassed solution of 1% v/v AcOH in MeOH. The reaction mixture was then precipitated into cold hexane. The polymer was collected via centrifugation (4400 rpm, 10 min) and the supernatant decanted. The product was washed twice with additional hexane and collected again in the same manner. The isolated polymer solution was dried in a vacuum oven for at least 24 h to afford polymer **1** as an off-white solid (27.5 g). ^{1}H NMR (500 MHz, $CDCl_3$): δ = 1.15-1.17 (m, -O-CH-(C$\underline{H}_3$)$_2$), 1.17-1.23 (t, -O-CH$_2$-C$\underline{H}_3$, J = 7.0 Hz), 3.47-3.81 (m -O-C$\underline{H}_2$-C$\underline{H}_2$-O- and -O-C$\underline{H}_2$-C$\underline{H}$(C$\underline{H}_2$-O-C$\underline{H}_2$-CH$_3$)-O- and -O-C$\underline{H}_2$-C$\underline{H}$(C$\underline{H}_2$-O-C$\underline{H}$-(CH$_3$)$_2$)-O-).

3.5.4 *Synthesis of Polymer 2*

Polymer **1** (20g, 1.81 mmol) was dissolved in dry THF (250 mL) under a nitrogen atmosphere until complete dissolution of the polymer. Triethylamine (2.45 mL, 18.1 mmol) was added to increase the reactivity of the polymer hydroxyl chain ends and the mixture was heated at 65 °C for 30 min. Methacrylic anhydride (26.9 mL, 181 mmol) was then added and the reaction mixture was stirred for 16 h at 65 °C. After this time, the reaction was quenched with a degassed solution of 1% v/v AcOH in MeOH. The reaction mixture was then precipitated into cold ether. The polymer

was collected via centrifugation (4400 rpm, 10 min) and the supernatant decanted. The product was washed twice with additional ether, once with hexane, and collected again by centrifugation. The isolated polymer was dried in a vacuum oven for 24 h to afford polymer **2** as an off-white solid (16.7g). The degree of functionalization (f_n) was determined by comparing the integrations of the methacrylate vinyl (6.12 and 5.55 ppm) and methyl (1.94 ppm) protons, as well as the PEO chain-end methylene protons (5.08-5.15 ppm), to their theoretical values. For example, 1.99 (vinyl, actual)/2 (vinyl, theoretical) X 100 ≈ 100% functionalization of chain ends. These integration values were referenced to the total alkyl glycidyl ether protons for each polymer chain (1.12-1.20 ppm, 121 H). ^{1}H NMR (300 MHz, $CDCl_3$): δ = 1.12-1.20 (m, -O-CH-(C$\underline{H}_3$)$_2$) and -O-CH$_2$-C$\underline{H}_3$), 1.94 (s, C$\underline{H}_3$C(CO$_2$)=CH$_2$), 3.39-3.89 (m, -O-C$\underline{H}_2$-C$\underline{H}_2$-O- and -O-C$\underline{H}_2$-C$\underline{H}$(C$\underline{H}_2$-O-C$\underline{H}_2$-CH$_3$)-O-, and -O-C$\underline{H}_2$-C$\underline{H}$(C$\underline{H}_2$-O-C$\underline{H}$-(CH$_3$)$_2$)-O-), 5.08-5.15 (m, -CH$_2$-C$\underline{H}$-O-(C=O)), 5.48 (s, $\underline{H}$-CH=C), 6.18 (s, $\underline{H}$-CH=C).

3.5.5 *Preparation of Synthetic Complete Media*

The SC media (1L) was prepared by dissolving drop-out mix (2 g), yeast nitrogen base (6.7 g), and glucose (20 g) in Milli-Q water. The resulting solution was sterilized by filtration through a 0.2 μm nylon filter.

3.5.6 *Preparation of Hydrogel Solution*

Polymer **2** was dissolved in sterile, deionized water at a concentration of 20 wt % polymer. The resulting polymer solution was cooled overnight at 5 °C to facilitate hydrogel formation via LCST behavior. After homogenization of the solution at low temperature, the solution was warmed to 21 °C to induce the formation of a gel state. Hydrogels used to print the proof-of-

concept models in Figure 3.4 were mixed with the photo-radical initiator 2-hydroxy-2-methylpropiophenone (10 μL) and centrifuged (4400 rpm, 10 min) to remove bubbles.

3.5.7 *Preparation of Yeast-Laden Hydrogel ink*

To prepare yeast-laden hydrogels, the aforementioned hydrogel solution was cooled to 5 °C in a refrigerator. At this temperature, the hydrogel solution underwent gel-to-sol transition, affording a free-flowing liquid. Yeast cells were added from an overnight liquid culture, at a concentration of 10^7 cells per gram of hydrogel while the gel was in its solution state. The resulting solution was mixed thoroughly and allowed to equilibrate at 5 °C until all of the bubbles present in the solution were removed. Finally, the hydrogel was warmed to 21 °C to undergo a sol to gel transition, resulting in a shear-responsive gel.

3.5.8 *Rheometrical Characterization*

For rheometrical characterization of the hydrogels, dynamic oscillatory experiments were performed on a TA Instruments Discovery Hybrid Rheometer-2 (DHR-2) equipped with a Peltier temperature controller. The instrument operates by applying a known displacement (strain) and measuring the material's resistance (stress) to the force. Rheometry experiments were conducted by depositing hydrogel between the rheometer base plate and 20 mm parallel plate geometry with a final gap of 1 mm. Samples were equilibrated in an ice bath for at least 30 min and then were carefully loaded onto the Peltier plate at 5 °C and a preshear experiment was applied to eliminate the bubbles from the sample. The sample was equilibrated at 21 °C for 8 min before each run. The gel yield stress values were measured under oscillatory strain (frequency: 1 Hz, 21 °C) starting with an initial strain of 0.01% and converted to applied oscillatory stress. Viscosity versus shear rate experiments were performed in the range of shear rates between 0.01 and 100 Hz. Cyclic shear

thinning experiments (frequency = 1 Hz) were performed at 21 °C using alternating strains of 1% for 5 min and 100% for 3 min per cycle, to investigate the shear-thinning and recovery behavior of the hydrogels. Temperature ramp experiments were performed at 1 Hz from 5−50 °C at 2 °C min^{-1}. Photocuring was performed using a fully integrated smart swap LED photo curing accessory. A 120 s dwell time (frequency: 1 Hz) elapsed before the UV lamp (365 nm LED with an irradiation intensity of 5 mW cm^{-2}) was turned on for 420 s at a constant oscillatory strain (1%).

3.5.9 *Additive Manufacturing (Direct-Write 3D Printing) of a Cuboidal-Lattice*

A modified pneumatic direct-write 3D printer was assembled based on a Tronxy P802E 3D Printer kit, from Shenzen Tronxy Technology Co. The printer was controlled with an Arduino using the Marlin firmware. All CAD models were designed in OpenSCAD. G-code commands for the printer were generated using Slic3r. The resulting G-code was modified using Python to introduce required commands for the dispensing of the hydrogel via pneumatic pressure. All printing was performed using a 20 wt % hydrogel ink with an extrusion air pressure of 20 psi, a print speed of 5 mm s^{-1}, and a 0.41 mm inner diameter CML Supply conical nozzle attachment.

The dimensions for the 3D printed lattices are 1.9 cm by 1.9 cm by 1.2 cm and each cube weighed between 1.8 and 2.0 g. Upon completion of the 3D printing, the cubes were irradiated under 365 nm light (at 3.4 mW cm^{-2}) for 3 min to cure and chemically fix the structures.

3.5.10 *Microscopy and Imaging*

Optical imaging: Images of the 3D-printed hydrogels were captured using an iPhone XS. Confocal imaging: Confocal microscopy images were taken using a Leica TCS SP5 II laser scanning confocal microscope. All images were taken with a dry 20x objective. MCherry protein fluorescence was excited with a 561 nm laser at 5% laser power, and emission was scanned from

569 to 700 nm. Sytox green viability dye was excited with a 488 nm laser at 5% laser power, and emission was scanned from 500 to 550 nm. Samples were sequentially scanned, and the output images were processed using ImageJ Java software.

3.5.11 *Cell Viability Assay*

The yeast-laden hydrogel was prepared as described above. This gel was cooled to 5 °C to induce a gel-to-sol transition, which was then poured and spread into a sterile petri dish to produce a thin film (~0.5 mm) of the yeast-laden hydrogel. The sample was irradiated with 365 nm UV light for 3 min. This film was then incubated in fresh SC media at 30 °C, and periodically agitated. The media was exchanged every 24 h to ensure fresh nutrient delivery to the embedded cells. At the imaging intervals described in this work, a small square of the film (5 mm × 5 mm) was cut and removed for staining. Sytox Green stain stock solution was diluted to 5 μM, and 20 μL of the dye solution was exposed to hydrogel sample for 5 min. The sample was then washed with SC media and imaged using a Leica SP5 confocal microscope. Constitutively expressed mCherry protein fluorescence from the yeast cells was measured to indicate live cells, while the Sytox dye fluorescence indicated the presence of dead cells.

3.5.12 *α-Factor Production*

α-Factor production from 3D printed yeast-laden cuboidal lattices was quantified as follows. A yeast-laden hydrogel ink containing 10^7 yeast cells per gram of hydrogel was direct-write 3D printed and photo-cured (3 min) with 365 nm irradiation. The lattices were then washed with SC media, and placed into 50 mL falcon tubes. The tubes were then filled with 10 mL of SC media for fermentation and placed in a 30 °C shaker (225 rpm) for incubation. After a period of 72 h, the lattices were removed from the reactors and the media was collected. The fermentation media was

filtered with a 0.2 μm nylon filter. The up-regulated yeast strain experiments were performed in triplicate alongside a wild-type yeast-laden lattice.

To determine the reusability of the lattices in subsequent fermentation cycles, the same lattices from the first round of α-factor were again washed individually in sterile SC media. The lattices were then placed into new falcon tubes containing 10 mL of SC media, and incubated at the same conditions for an additional 72 h. After incubation, the samples were collected and prepared for characterization in the same manner as mentioned above.

3.5.13 *α-Factor Detection and Quantification*

To quantify α-factor synthesis from within the yeast-laden hydrogel, we collected the SC media that was used to submerge the hydrogel sample after 72 h. We collected 9 mL of media for each experimental condition and replicate; each sample was split into six 1.5 mL Eppendorf tube and then dehydrated in a Savant SpeedVac Plus SC110A Concentrator for 12 h at Medium dehydration speed. Subsequently, we added 100 μL of molecular graded water into each dehydrated sample, resuspended, and collected the resulting 600 μL into a single sample. The final sample was run again through the Speed-Vac for 12 h at Medium speed and resuspended into 100 μL of molecular graded water. This process concentrated the initial sample to 90-fold its original concentration.

We experimentally tested for α-factor synthesis using detecting strains with a standard cytometer assay protocol. The detecting strains were grown overnight for 20 h in SC media, then diluted to 30 events/μL again in SC media. After 3 h, we inoculated the concentrated samples from the yeast-laden hydrogels into different vials, plus two extra vials: one kept as control (3 μL of 0.1 M Sodium Acetate) and one was inoculated with 10 μM 98% HPLC-pure α-factor peptide in 0.1 M Sodium Acetate obtained from Zymo Research (Irvine, CA, USA). Samples were collected for

cytometer measurement 8 h after induction, and median fluorescence values were computed from the resulting histogram.

Fluorescence intensity of the detecting strain was measured with a BD Accuri C6 flow cytometer equipped with a CSampler plate adapter using excitation wavelengths of 488 and 640 nm and an emission detection filter at 533 nm (FL1 channel). A total of 10,000 events above a 400,000 FSC-H threshold (to exclude debris) were recorded for each sample with and core size of 22 mm using the Accuri C6 CFlow Sampler software. Cytometry data were exported as FCS 3.0 files and processed using custom Python scripts to obtain the median FL1-A value at each data point.

We used a model fitted to data to estimate the amount of α-factor detected by the detecting strain starting from its median fluorescence value response. The model interpolates a titration curve of an α-factor-detecting strain that is equivalent to the one used in this study, except its synthesis yeGFP fluorescent protein instead of yeVenus. The interpolation follows a standard Hill activation function:

$$y = K\frac{u^n}{\varphi + u^n} + y_0$$

where u represents the α-factor input concentration in nM, and y the median fluorescence output. To account for the different fluorescent protein, we used the control and the 10 μM α-factor median fluorescent outputs from this experiment to re-fit K and y_0.

To estimate the amount of α-factor synthesized by our strains in the hydrogel, we inverted the formula above to get:

$$u = \sqrt[n]{\varphi\frac{y - y_0}{K + y_0 - y}}$$

3.6 ACKNOWLEDGEMENTS

The authors thank Dr. Eric Klavins of the University of Washington for continued consultation and expertise on yeast and biological systems. A.N. gratefully acknowledges support of this research by the National Science Foundation CAREER grant (DMR 1752972). This work was also partially funded by the Army Research Office (W911NF-17-1-0595). The authors thank The Biology Imaging Facility at the University of Washington for the use of the SP5 confocal microscope.

3.7 REFERENCES

1. Zhang, Y.-H. P.; Sun, J.; Ma, Y. Biomanufacturing: History and Perspective. *J. Ind. Microbiol. Biotechnol.* **2017**, *44* (4–5), 773–784.
2. Li, Y.; Smolke, C. D. Engineering Biosynthesis of the Anticancer Alkaloid Noscapine in Yeast. *Nat. Commun.* **2016**, *7* (1), 12137.
3. Thodey, K.; Galanie, S.; Smolke, C. D. A Microbial Biomanufacturing Platform for Natural and Semisynthetic Opioids. *Nat. Chem. Biol.* **2014**, *10* (10), 837–844.
4. Awan, A. R.; Blount, B. A.; Bell, D. J.; Shaw, W. M.; Ho, J. C. H.; McKiernan, R. M.; Ellis, T. Biosynthesis of the Antibiotic Nonribosomal Peptide Penicillin in Baker's Yeast. *Nat. Commun.* **2017**, *8*, 15202.
5. Gerngross, T. U. Advances in the Production of Human Therapeutic Proteins in Yeasts and Filamentous Fungi. *Nat. Biotechnol.* **2004**, *22* (11), 1409–1414.
6. Paddon, C. J.; Westfall, P. J.; Pitera, D. J.; Benjamin, K.; Fisher, K.; McPhee, D.; Leavell, M. D.; Tai, A.; Main, A.; Eng, D.; et al. High-Level Semi-Synthetic Production of the Potent Antimalarial Artemisinin. *Nature* **2013**, *496* (7446), 528–532.
7. DeLoache, W. C.; Russ, Z. N.; Narcross, L.; Gonzales, A. M.; Martin, V. J. J.; Dueber, J. E. An Enzyme-Coupled Biosensor Enables (S)-Reticuline Production in Yeast from Glucose. *Nat. Chem. Biol.* **2015**, *11* (7), 465–471.
8. Yang, S.; Fei, Q.; Zhang, Y.; Contreras, L. M.; Utturkar, S. M.; Brown, S. D.; Himmel, M. E.; Zhang, M. Zymomonas Mobilis as a Model System for Production of Biofuels and Biochemicals. *Microb. Biotechnol.* **2016**, *9* (6), 699–717.
9. Davy, A. M.; Kildegaard, H. F.; Andersen, M. R. Cell Factory Engineering. *Cell Syst.* **2017**, *4* (3), 262–275.
10. Peralta-Yahya, P. P.; Zhang, F.; del Cardayre, S. B.; Keasling, J. D. Microbial Engineering for the Production of Advanced Biofuels. *Nature* **2012**, *488* (7411), 320–328.
11. Verbelen, P. J.; De Schutter, D. P.; Delvaux, F.; Verstrepen, K. J.; Delvaux, F. R. Immobilized Yeast Cell Systems for Continuous Fermentation Applications. *Biotechnology Letters*. Springer Netherlands October 2, 2006, pp 1515–1525.

12. Saha, A.; Johnston, T. G.; Shafranek, R. T.; Goodman, C. J.; Zalatan, J. G.; Storti, D. W.; Ganter, M. A.; Nelson, A. Additive Manufacturing of Catalytically Active Living Materials. *ACS Appl. Mater. Interfaces* **2018**, *10* (16), 13373–13380.
13. Cheetham, P. S. J.; Blunt, K. W.; Bocke, C. Physical Studies on Cell Immobilization Using Calcium Alginate Gels. *Biotechnol. Bioeng.* **1979**, *21* (12), 2155–2168.
14. Nagarajan, S.; Kruckeberg, A. L.; Schmidt, K. H.; Kroll, E.; Hamilton, M.; McInnerney, K.; Summers, R.; Taylor, T.; Rosenzweig, F. Uncoupling Reproduction from Metabolism Extends Chronological Lifespan in Yeast. *Proc. Natl. Acad. Sci.* **2014**, *111* (15), E1538–E1547.
15. Lehner, B. A. E.; Schmieden, D. T.; Meyer, A. S. A Straightforward Approach for 3D Bacterial Printing. *ACS Synth. Biol.* **2017**, *6* (7), 1124–1130.
16. Lode, A.; Krujatz, F.; Brüggemeier, S.; Quade, M.; Schütz, K.; Knaack, S.; Weber, J.; Bley, T.; Gelinsky, M. Green Bioprinting: Fabrication of Photosynthetic Algae-Laden Hydrogel Scaffolds for Biotechnological and Medical Applications. *Eng. Life Sci.* **2015**, *15* (2), 177–183.
17. Townsend-Nicholson, A.; Jayasinghe, S. N. Cell Electrospinning: A Unique Biotechnique for Encapsulating Living Organisms for Generating Active Biological Microthreads/Scaffolds. *Biomacromolecules* **2006**, *7* (12), 3364–3369.
18. Liu, Y.; Rafailovich, M. H.; Malal, R.; Cohn, D.; Chidambaram, D. Engineering of Bio-Hybrid Materials by Electrospinning Polymer-Microbe Fibers. *Proc. Natl. Acad. Sci. U. S. A.* **2009**, *106* (34), 14201–14206.
19. Letnik, I.; Avrahami, R.; Rokem, J. S.; Greiner, A.; Zussman, E.; Greenblatt, C. Living Composites of Electrospun Yeast Cells for Bioremediation and Ethanol Production. *Biomacromolecules* **2015**, *16* (10), 3322–3328.
20. Brimmo, A.; Goyette, P. A.; Alnemari, R.; Gervais, T.; Qasaimeh, M. A. 3D Printed Microfluidic Probes. *Sci. Rep.* **2018**, *8* (1), 10995.
21. Dahlberg, T.; Stangner, T.; Zhang, H.; Wiklund, K.; Lundberg, P.; Edman, L.; Andersson, M. 3D Printed Water-Soluble Scaffolds for Rapid Production of PDMS Micro-Fluidic Flow Chambers. *Sci. Rep.* **2018**, *8* (1), 3372.
22. Mamatha, S.; Biswas, P.; Ramavath, P.; Das, D.; Johnson, R. 3D Printing of Complex Shaped Alumina Parts. *Ceram. Int.* **2018**, *44* (16), 19278–19281.
23. Melnikova, R.; Ehrmann, A.; Finsterbusch, K. 3D Printing of Textile-Based Structures by Fused Deposition Modelling (FDM) with Different Polymer Materials. *IOP Conf. Ser. Mater. Sci. Eng.* **2014**, *62*, 012018.
24. Sa, M.-W.; Nguyen, B.-N. B.; Moriarty, R. A.; Kamalitdinov, T.; Fisher, J. P.; Kim, J. Y. Fabrication and Evaluation of 3D Printed BCP Scaffolds Reinforced with ZrO 2 for Bone Tissue Applications. *Biotechnol. Bioeng.* **2018**, *115* (4), 989–999.
25. Kiran, R. U.; Malferrari, S.; Van Haver, A.; Verstreken, F.; Rath, S. N.; Kalaskar, D. M. Optimization of Extrusion Based Ceramic 3D Printing Process for Complex Bony Designs. *Mater. Des.* **2018**, *162*, 263–270.
26. Ligon, S. C.; Liska, R.; Stampfl, J.; Gurr, M.; Mülhaupt, R. Polymers for 3D Printing and Customized Additive Manufacturing. *Chem. Rev.* **2017**, *117* (15), 10212–10290.
27. Kimlinger, M. J.; Martin, R. S. The Use of a 3D-Printed Microfluidic Device and Pressure Mobilization for Integrating Capillary Electrophoresis with Electrochemical Detection. *Electroanalysis* **2018**, *30* (10), 2241–2249.

28. Müller, M.; Becher, J.; Schnabelrauch, M.; Zenobi-Wong, M. Nanostructured Pluronic Hydrogels as Bioinks for 3D Bioprinting. *Biofabrication* **2015**, *7* (3), 035006.
29. Bertassoni, L. E.; Cardoso, J. C.; Manoharan, V.; Cristino, A. L.; Bhise, N. S.; Araujo, W. A.; Zorlutuna, P.; Vrana, N. E.; Ghaemmaghami, A. M.; Dokmeci, M. R.; et al. Direct-Write Bioprinting of Cell-Laden Methacrylated Gelatin Hydrogels. *Biofabrication* **2014**, *6* (2), 024105.
30. Li, Y.-C.; Zhang, Y. S.; Akpek, A.; Shin, S. R.; Khademhosseini, A. 4D Bioprinting: The next-Generation Technology for Biofabrication Enabled by Stimuli-Responsive Materials. *Biofabrication* **2016**, *9* (1), 012001.
31. Patra, S.; Young, V. A Review of 3D Printing Techniques and the Future in Biofabrication of Bioprinted Tissue. *Cell Biochem. Biophys.* **2016**, *74* (2), 93–98.
32. Schaffner, M.; Rühs, P. A.; Coulter, F.; Kilcher, S.; Studart, A. R. 3D Printing of Bacteria into Functional Complex Materials. *Sci. Adv.* **2017**, *3* (12), eaao6804.
33. Bader, C.; Patrick, W. G.; Kolb, D.; Hays, S. G.; Keating, S.; Sharma, S.; Dikovsky, D.; Belocon, B.; Weaver, J. C.; Silver, P. A.; et al. Grown, Printed, and Biologically Augmented: An Additively Manufactured Microfluidic Wearable, Functionally Templated for Synthetic Microbes. *3D Print. Addit. Manuf.* **2016**, *3* (2), 79–89.
34. Lee, J. M.; Yeong, W. Y. Design and Printing Strategies in 3D Bioprinting of Cell-Hydrogels: A Review. *Adv. Healthc. Mater.* **2016**, *5* (22), 2856–2865.
35. Hoffman, A. S. Hydrogels for Biomedical Applications. *Adv. Drug Deliv. Rev.* **2002**, *54* (1), 3–12.
36. Lee, K. Y.; Mooney, D. J. Hydrogels for Tissue Engineering. *Chem. Rev.* **2001**, *101* (7), 1869–1880.
37. Smetana, K. Cell Biology of Hydrogels. *Biomaterials* **1993**, *14* (14), 1046–1050.
38. Smetana, K.; Vacík, J.; Součková, D.; Krčová, Z.; Šulc, J. The Influence of Hydrogel Functional Groups on Cell Behavior. *J. Biomed. Mater. Res.* **1990**, *24* (4), 463–470.
39. Benoit, D. S. W.; Schwartz, M. P.; Durney, A. R.; Anseth, K. S. Small Functional Groups for Controlled Differentiation of Hydrogel-Encapsulated Human Mesenchymal Stem Cells. *Nat. Mater.* **2008**, *7* (10), 816–823.
40. Lee, J. H.; Jung, H. W.; Kang, I.-K.; Lee, H. B. Cell Behaviour on Polymer Surfaces with Different Functional Groups. *Biomaterials* **1994**, *15* (9), 705–711.
41. Discher, D. E.; Janmey, P.; Wang, Y. L. Tissue Cells Feel and Respond to the Stiffness of Their Substrate. *Science*. American Association for the Advancement of Science November 18, 2005, pp 1139–1143.
42. Buxboim, A.; Rajagopal, K.; Brown, A. E. X.; Discher, D. E. How Deeply Cells Feel: Methods for Thin Gels. *J. Phys. Condens. Matter* **2010**, *22* (19), 194116.
43. Liu, Z.; Tyo, K. E. J.; Martínez, J. L.; Petranovic, D.; Nielsen, J. Different Expression Systems for Production of Recombinant Proteins in Saccharomyces Cerevisiae. *Biotechnol. Bioeng.* **2012**, *109* (5), 1259–1268.
44. Achstetter, T. Regulation of Alpha-Factor Production in Saccharomyces Cerevisiae: A-Factor Pheromone-Induced Expression of the MF Alpha 1 and STE13 Genes. *Mol. Cell. Biol.* **1989**, *9* (10), 4507–4514.
45. Baba, E. H.; Berkower, I. Production of a Soluble and Secreted Antigenic Fragment of HBsAg in Yeast. *Biochem. Biophys. Res. Commun.* **1992**, *184* (1), 50–59.

46. Rakestraw, J. A.; Sazinsky, S. L.; Piatesi, A.; Antipov, E.; Wittrup, K. D. Directed Evolution of a Secretory Leader for the Improved Expression of Heterologous Proteins and Full-Length Antibodies in *Saccharomyces Cerevisiae*. *Biotechnol. Bioeng.* **2009**, *103* (6), 1192–1201.
47. Robinson, A. S.; Hines, V.; Wittrup, K. D. Protein Disulfide Isomerase Overexpression Increases Secretion of Foreign Proteins in Saccharomyces Cerevisiae. *Nat. Biotechnol.* **1994**, *12* (4), 381–384.
48. Staniulis, J. Synthesis of Hepatitis B Virus Surface Protein Derivates in Yeast S . Cerevisiae. *Biologija* **2006**, *3* (4), 49–53.
49. Chigira, Y.; Oka, T.; Okajima, T.; Jigami, Y. Engineering of a Mammalian O-Glycosylation Pathway in the Yeast Saccharomyces Cerevisiae: Production of O-Fucosylated Epidermal Growth Factor Domains. *Glycobiology* **2008**, *18* (4), 303–314.
50. Kjeldsen, T.; Frost Pettersson, A.; Hach, M. The Role of Leaders in Intracellular Transport and Secretion of the Insulin Precursor in the Yeast Saccharomyces Cerevisiae. *J. Biotechnol.* **1999**, *75* (2–3), 195–208.
51. Fellin, C. R.; Adelmund, S. M.; Karis, D. G.; Shafranek, R. T.; Ono, R. J.; Martin, C. G.; Johnston, T. G.; DeForest, C. A.; Nelson, A. Tunable Temperature- and Shear-Responsive Hydrogels Based on Poly(Alkyl Glycidyl Ether)S. *Polymer International*. John Wiley & Sons, Ltd October 30, 2018.
52. Winnik, M. A.; Yekta, A. Associative Polymers in Aqueous Solution. *Curr. Opin. Colloid Interface Sci.* **1997**, *2* (4), 424–436.
53. Lee, B. F.; Kade, M. J.; Chute, J. A.; Gupta, N.; Campos, L. M.; Fredrickson, G. H.; Kramer, E. J.; Lynd, N. A.; Hawker, C. J. Poly(Allyl Glycidyl Ether)-A Versatile and Functional Polyether Platform. *J. Polym. Sci. Part A Polym. Chem.* **2011**, *49* (20), 4498–4504.
54. Heinen, S.; Rackow, S.; Schäfer, A.; Weinhart, M. A Perfect Match: Fast and Truly Random Copolymerization of Glycidyl Ether Monomers to Thermoresponsive Copolymers. *Macromolecules* **2017**, *50* (1), 44–53.
55. Satoh, Y.; Miyachi, K.; Matsuno, H.; Isono, T.; Tajima, K.; Kakuchi, T.; Satoh, T. Synthesis of Well-Defined Amphiphilic Star-Block and Miktoarm Star Copolyethers via t-Bu-P4-Catalyzed Ring-Opening Polymerization of Glycidyl Ethers. *Macromolecules* **2016**, *49* (2), 499–509.
56. Barteau, K. P.; Wolffs, M.; Lynd, N. A.; Fredrickson, G. H.; Kramer, E. J.; Hawker, C. J. Allyl Glycidyl Ether-Based Polymer Electrolytes for Room Temperature Lithium Batteries. *Macromolecules* **2013**, *46* (22), 8988–8994.

3.8 FIGURES

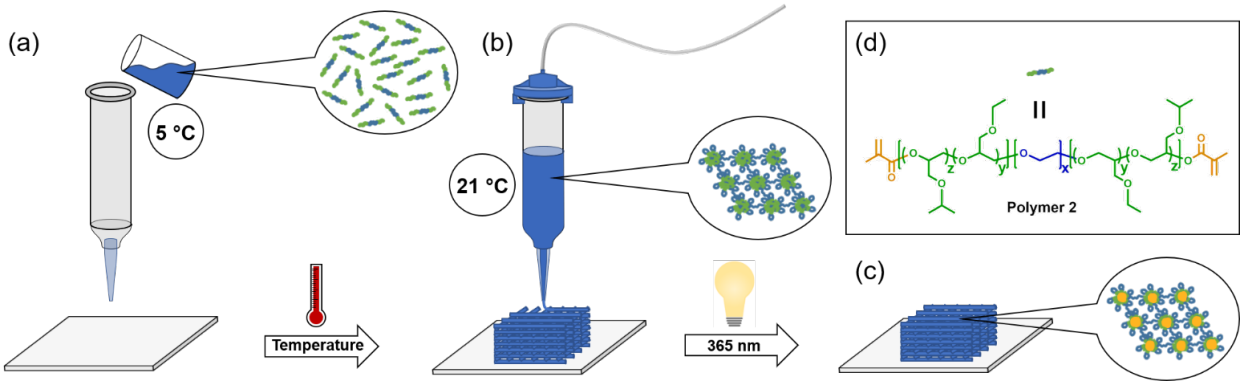

Figure 3.18. Stimuli responses of the hydrogels for AMCALM applications

A graphical overview of the three key stimuli responses of polymer **2** hydrogels necessary for AMCALM applications. a) The temperature responsive feature of the hydrogels enabled facile loading of the hydrogel material at 5 °C. b) The shear-stress response facilitated the formation of complex three-dimensional objects at 21 °C. c) UV-light (365 nm) initiated the polymerization of the methacrylate end-groups and chemical crosslinking of the polymer **2** hydrogel. d) The chemical structure of polymer 2. The letter designations (z = 6.4, y = 7.4, x = 182) refer to the average number of isopropyl glycidyl ether, ethyl glycidyl ether, and ethylene oxide repeat units, respectively.

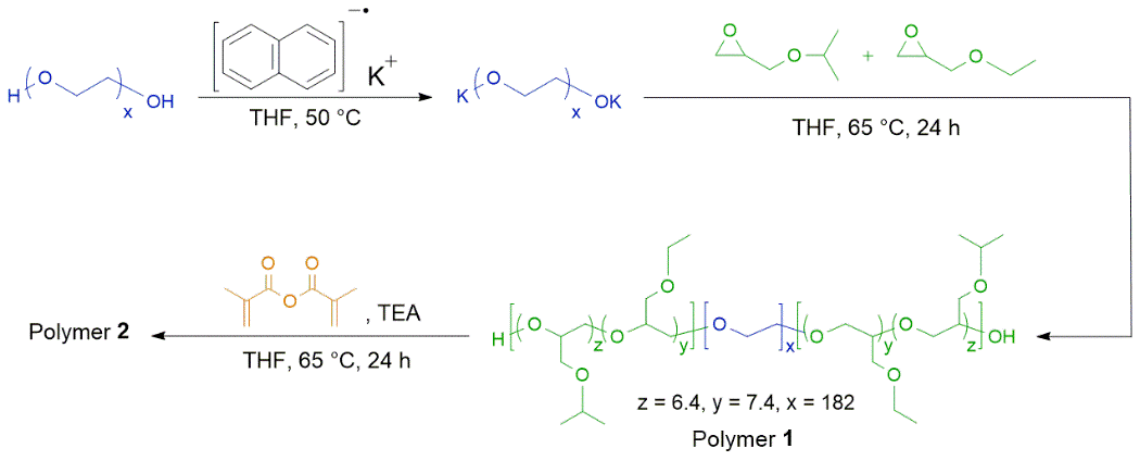

Figure 3.19. Synthesis of the ABA triblock copolymer

Synthesis of the ABA triblock copolymer (polymer **1**) and functionalization with methacrylic anhydride (polymer **2**). The letter designations (z = 6.4, y = 7.4, x = 182) refer to degree of polymerization for isopropyl glycidyl ether, ethyl glycidyl ether, and ethylene oxide, respectively.

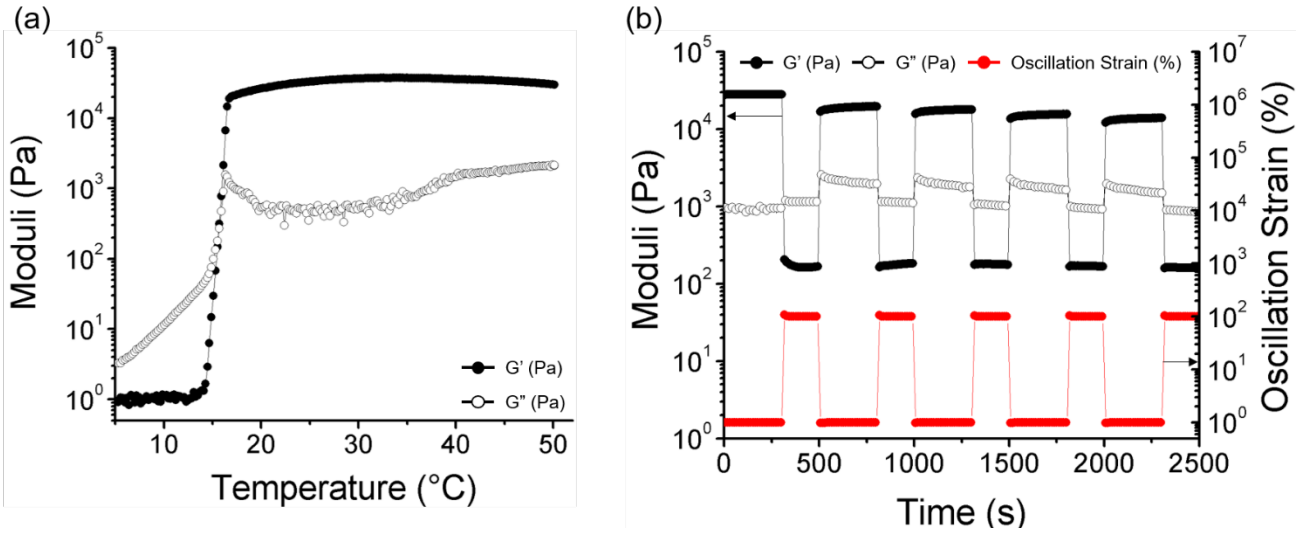

Figure 3.20. Rheology of the ABA Triblock hydrogels

Rheometrical experiments for a 20 wt% formulation of polymer **2**. a) Dynamic oscillatory temperature ramp displaying elastic (G', filled) and viscous (G'', open) moduli. T_{gel} = 15.61 °C. b) Cyclic strain experiment demonstrating rapid recovery of hydrogel elastic modulus (black circles) from periods of high (100%) to low (1%) oscillatory strain (red circles). Arrows indicate reference axis; elastic/viscous moduli (left axis) and oscillatory strain (right axis).

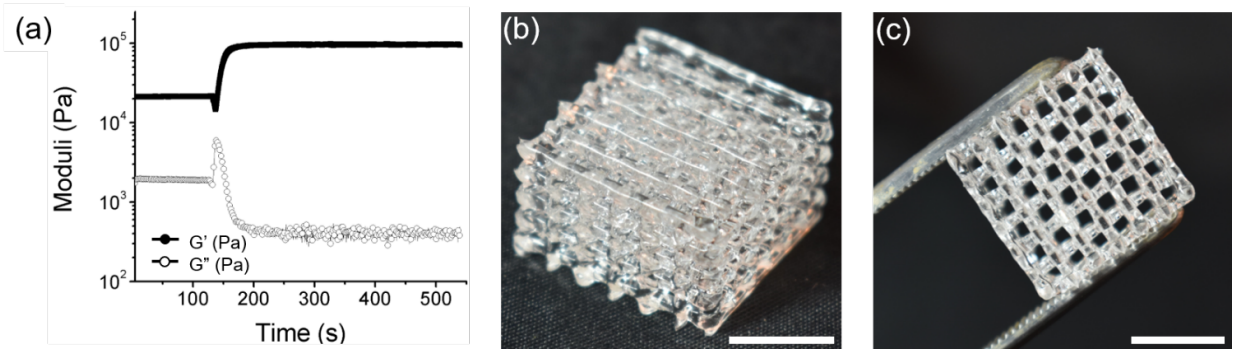

Figure 3.21. UV-curing rheology experimental results

a) A rheological UV-cure experiment using a 20 mm parallel plate geometry. The hydrogel was equilibrated for 120 s before being subjected to 5 mW cm-2 of 365 nm UV light for 420 s at a constant strain (1%) and frequency (1 Hz). b-c) A 3D printed, proof of concept cuboid structure (1.9 cm by 1.9 cm by 1.2 cm). This structure was printed from a pneumatic direct write 3D printer at 5 mm s-1 and 20 psi using a 0.41 mm inner diameter nozzle (scale bar: 1 cm).

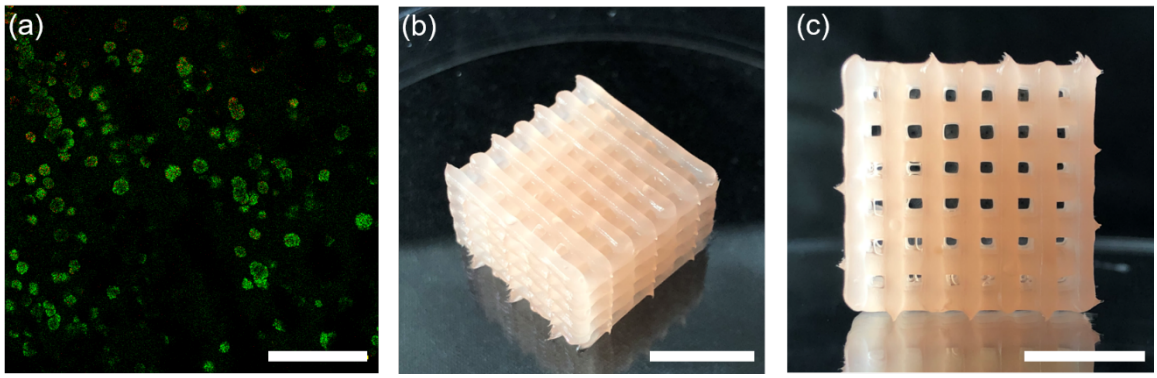

Figure 3.22. Imaging of yeast cells within hydrogels

a) A sample composite image of live cells (green channel) and dead cells (red channel) after 7 days of incubation (scale bar: 200 µm). b) Side and c) top-down view of the 3D-printed, yeast-laden hydrogel after two rounds of α-factor synthesis in SC media (scale bar 1 cm).

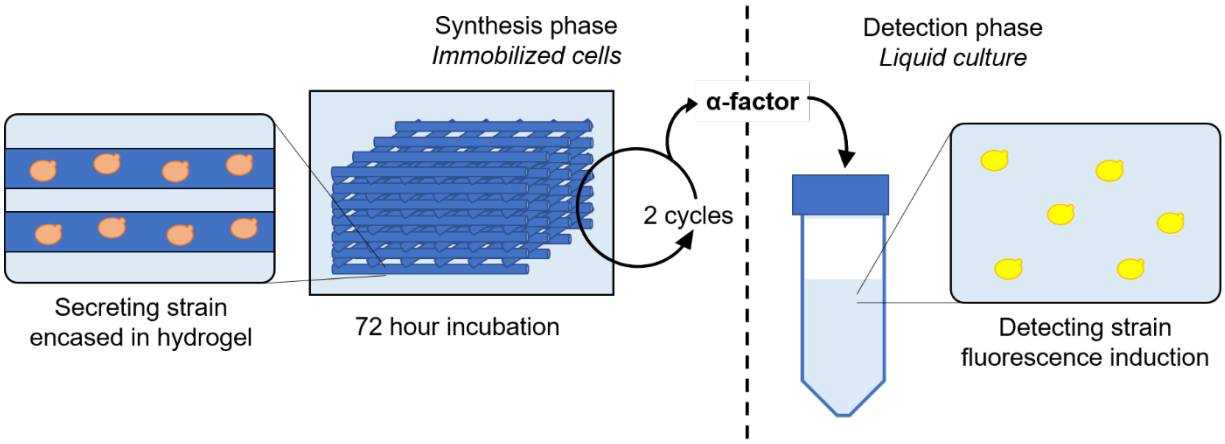

Figure 3.23. α-factor production and detection scheme

Immobilized yeast within the hydrogel matrix were incubated in SC media for 72 h at 30 °C with automated shaker agitation. The media was collected at the end of the incubation period and exposed to the receiver strain in a separate tube, and the resulting fluorescence was measured. The cuboidal lattice was reused in a subsequent incubation with fresh media to produce an additional batch of α-factor.

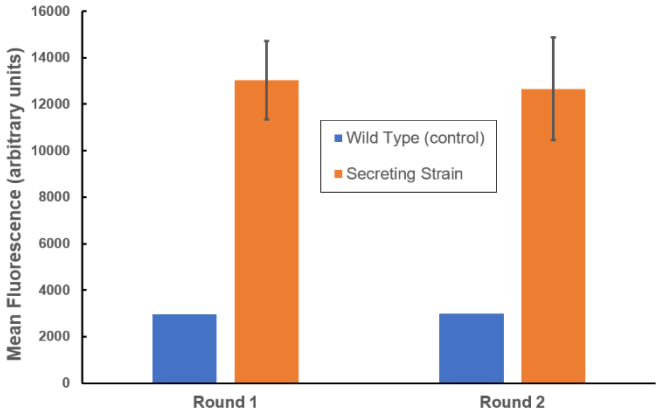

Figure 3.24. α-factor production results

Fluorescence values obtained from the quantification of α-factor produced from the wild type (control) AMCALMs and the secreting strain AMCALMs. Round 1 indicates the first incubation period of 72 h, while Round 2 indicates the reemployment of the same printed materials in a second, subsequent 72 h batch reaction in fresh SC media.

Chapter 4. COMPARTMENTALIZED MICROBES AND CO-CULTURES IN HYDROGELS FOR ON-DEMAND BIOPRODUCTION AND PRESERVATION

This chapter has been adapted from the following manuscript:

> **Johnston, T. G.**; Yuan, S.-F.; Wagner, J. M.; Yi, X.; Saha, A.; Smith, P.; Nelson, A.; Alper, H. S. Compartmentalized Microbes and Co-Cultures in Hydrogels for on-Demand Bioproduction and Preservation. *Nat Commun* **2020**, *11* (1), 563. https://doi.org/10.1038/s41467-020-14371-4.

4.1 ABSTRACT

Most mono- and co-culture bioprocess applications rely on large-scale suspension fermentation technologies that are not easily portable, reusable, or suitable for on-demand production. Here, we describe a hydrogel system for harnessing the bioactivity of embedded microbes for on-demand small molecule and peptide production in microbial mono-culture and consortia. This platform bypasses the challenges of engineering a multi-organism consortia by utilizing a temperature-responsive, shear-thinning hydrogel to compartmentalize organisms into polymeric hydrogels that control the final consortium composition and dynamics without the need for synthetic control of mutualism. We demonstrated that these hydrogels provide protection from preservation techniques (including lyophilization) and can sustain metabolic function for over 1 year of repeated use. This approach was utilized for the production of four chemical compounds, a peptide antibiotic, and carbohydrate catabolism by using either mono-cultures or co-cultures. The printed microbe-laden hydrogel constructs' efficiency in repeated production phases, both pre- and post-preservation, outperformed liquid culture.

4.2 INTRODUCTION

Microbial production of value-added products ranging from small molecules to complex proteins is becoming increasingly attractive and effective across industry and academia [1-4]. Recent advances in synthetic biology have further enabled microbial production to be modular and distributed across multiple organisms, thus creating synthetic consortia that can reduce metabolic loads and afford more robust cell populations [5-7]. Though commonly employed in bioreactor and cellular interaction studies, the limitations of liquid culture systems are especially poignant when attempting to control the dynamics of a multi-organism consortium. Specifically, repeated (and sometimes even single) batch liquid co-cultures typically fail over time without sophisticated genetic control systems or particular nutrient conditions that seek to minimize the competitive growth bias that often occurs when utilizing disparate microorganisms [8-11].

Immobilized cell technologies, wherein microbes are encapsulated within a polymeric matrix, have been developed as an alternative to suspension cell culture [12-16]. These microbe-laden matrices have been used to investigate quorum sensing between microbial species [14], and as 3D architected 'living materials' [15-17]. Calcium alginate and other polysaccharides are the most common matrices used for immobilizing cells, despite the sensitivity of the ionic cross-links to the presence of charge-bearing molecules and the pH of the medium [18]. Various other hydrogel materials, comprised of synthetic or modified naturally occurring polymers, have been explored but fail to produce a material that is simultaneously readily processable, mechanically robust, and inert to the chemicals and biochemicals present in the media [19-29].

Herein, we demonstrate a platform that utilizes a hydrogel system to compartmentalize microbes to build spatially segregated microbial consortia. To this end, Nelson and co-workers previously reported shear-thinning hydrogels based on F127-dimethacrylate (F127-DMA)

polymer[16]. The F127-bisurethane methacrylate (F127-BUM) hydrogels employed in this study also exhibit a temperature-dependent sol-gel transition (~17 °C), which was used to immobilize yeast cells. The temperature response of the material facilitated the facile incorporation of the cells homogeneously throughout the hydrogel, while the shear-thinning behavior facilitated the extrusion of the cell-laden hydrogel from a nozzle.

In this work, we show that this F127-BUM hydrogel can be used to compartmentalize the various constituent organisms of an engineered microbial consortium that would otherwise be incompatible in a traditional liquid suspension culture. In doing so, we show that mono- and co-culture systems immobilized within hydrogels can be extrusion printed to form solid-state bioreactors capable of producing small molecules and antimicrobial peptides for multiple, repeated cycles of use. Interestingly, the microbe-laden hydrogels can also be preserved via lyophilization, stored in a dried state, and then re-hydrated at a later time for on-demand chemical and pharmaceutical production (Figure 4.1) in a manner that outperforms a traditional liquid-based culture format. Moreover, for co-culture systems, the spatial compartmentalization of the microbes enabled precise control of the consortium composition and dynamics without the need for genetically encoded mutualism.

4.3 Results and Discussion

4.3.1 *Encapsulation of microbes within F127-BUM Hydrogels*

To test the repeated use and preservation capacity of these microbe-laden hydrogels, we conducted a series of demonstration tests using mono-cultures or co-cultures to produce a variety of important biochemical compounds and an antimicrobial agent. In each case, the microbe-laden hydrogel was based on 30 wt% F127-BUM, a polymer that forms a temperature responsive and shear-thinning hydrogel capable of encapsulating yeast (e.g., *Saccharomyces cerevisiae*) and/or

bacteria (e.g., *Escherichia coli*) cells. While this material was not optimized based on the motility of encapsulated cells (such as cell leakage seen in Figure C.8b), the polymer concentration 30 wt% of F127-BUM hydrogel was optimized for their stimuli-responsive behaviors that facilitated their processability.[16] The shear-thinning behavior of this hydrogel allowed the material to be cast into films or extruded as filaments from a nozzle. A photo-initiator was included in the hydrogel formulation to facilitate polymerization of the methacrylate functionalities of the polymer upon brief UV curing. The resulting microbe-laden hydrogels were mechanically robust and were suitable for multiple rounds of reuse without any visual signs of degradation. For these studies, mono- or co-culture hydrogels were evaluated for continuous production over multiple fermentation cycles, where we define the initial cell outgrowth stage as round 0 of gel use and the repeated, on-demand production phase (either immediately after outgrowth or post-preservation) as round 1 and onward (Figure 4.1).

4.3.2 *On-demand productions using mono-culture laden hydrogels*

As test cases, we selected the production of value-added biochemicals, 2,3-butanediol (2,3-BDO) and 3,4-dihydroxy-L-phenylalanine (L-DOPA) as examples, due to their market potential and their ability to evaluate two distinct metabolically engineered microbial hosts in these printed constructs [30-31]. First, a yeast-strain overproducing 2,3-BDO [32] was encapsulated in the gel matrix and production (titer at 48 h in a test tube) was assessed both pre- and post-preservation (Figure 4.2a). It should be noted that the lyophilization procedure also included a 10-minute freezing step and vacuum drying without the use of any cryoprotectants. Nevertheless, after lyophilization, the preserved yeast-laden hydrogel retained nearly 90% of its BDO production capacity (1.5±0.09 g L^{-1}) compared to a paired sample prior to preservation (1.7±0.04 g L^{-1}). While these initial results

were obtained for an *S. cerevisiae* BY4741-based strain, a similar phenomenon was also observed with an alternative strain constructed in the CEN.PK2 background (Figure C.1).

Second, we evaluated the performance of the hydrogel using a metabolically engineered strain of *E. coli* designed to overproduce L-DOPA (Figure 4.2b, Figure C.2). In similar fashion to the 2,3-BDO yeast example, L-DOPA production from printed hydrogels did not differ significantly ($p>0.05$, paired t tests) pre- and post-lyophilization (both producing >150 mg L^{-1} after 22 hours). Collectively, these results demonstrate that yeast and bacteria-laden gels were both metabolically active, and that entrapment of cells in the F127-BUM hydrogel resulted in minimal loss of biocatalytic activity during lyophilization.

Third, we sought to evaluate the long-term stability and re-use potential of the cell-laden gels for continued, repeated production. To do so, we utilized a direct-write extrusion printer to create a yeast-laden hydrogel lattice (containing *S. cerevisiae* SO992) and evaluated its ethanol production capacity over the course of one year of repeated batch culturing (Figure 4.2c). Through this one-year period, the average titer achieved in these batches (8.74±0.53 g L^{-1}) exhibited no noticeable decrease in performance and, if anything, slightly increased throughout the process (Figure C.3). It should be noted that all four replicate samples were still operational at the end of the year-long process, which demonstrated the robustness and potential longevity-enhancing capacity of these hydrogel materials.

Finally, we evaluated one additional mono-culture within our microbe-laden hydrogel constructs that demonstrated the ability of larger molecules (in this case, the peptide antibiotic, colicin V) to be produced and effectively diffuse out of the gel and into the surrounding culture media. To do so, we printed gels containing *E. coli* capable of secreting the pore-forming antibiotic colicin V (ColV) [33] (Figure 4.2d). For both the round 0 gel use and for four consecutive uses after

lyophilization, the *E. coli*-laden hydrogel was able to produce colicin V at relatively constant levels as measured by a zone-of-inhibition assay. Furthermore, we sought to compare this gel-based performance to that of a traditional free-cell system culture process (Figure C.4b). During this comparison, the level of ColV antimicrobial peptide produced by a free cell system was inconsistent across iterative subculture cycles, unlike the microbe-laden hydrogel that retained more consistent production across repeated uses (Supplementary Note). Specifically, no zone-of-inhibition was observed for the free cell system by the third round of re-use, and the bactericidal activity of the corresponding supernatant was dramatically reduced to 6.5% of its prior value. Collectively, these mono-culture results demonstrate that this hydrogel ink formulation can enable reusable and stable, on-demand production of both small molecules and peptide antibiotics using yeast or bacteria.

4.3.3 *Using spatially compartmentalized microbial consortia to establish stable co-cultures*

The experiments outlined thus far illustrate the use of mono-culture based microbe-laden hydrogels. However, compartmentalizing a consortium through simple spatial separation within printed hydrogel constructs may provide a facile manner to control dynamics, especially for the endpoint balance within a co-culture. Natural microbial consortia rely upon spatial organization, as demonstrated by insect hindguts and biofilms [34]. In this regard, a synthetic microbial consortium that mimics these natural systems should provide both spatial organization as well as a protective environment for the microbes to thrive non-competitively. Moreover, achieving stable liquid co-cultures is challenging due to different competitive growth rates exhibited by many organisms, especially at different temperatures. This behavior is evident in a simple *S. cerevisiae* / *E. coli* co-culture expressing RFP and GFP, respectively, where one organism quickly dominates the other in a temperature dependent manner (Figure C.5). As an alternative, the printing of microbe-laden

hydrogels that spatially compartmentalize each organism can minimize or remove this competition. For example, when an alternating striped pattern of RFP-producing *S. cerevisiae* and GFP-producing *E. coli* laden hydrogels was printed, confocal imaging and fluorescent macroscopy (i.e. macroscopic fluorescence imaging of the gel) showed that cell colony expansion was localized to the respective yeast and bacterial regions (Figure 4.3a and Figure C.6). Moreover, these gels did not impede cell growth when co-cultured, as the yeast samples achieved a maximum confluence of 93.5% and the bacterial samples achieved a maximum confluence of 88.6% in their respective hydrogel compartments relative to similar mono-culture gels (Figure C.6a). Importantly, the physical segregation and hydrogel-based immobilization of the distinct microbial species offers advantages in controlling consortium population dynamics when compared to a mixed liquid culture system. The microbe-laden hydrogels can be deposited via deposition from a nozzle, which allows the final consortium composition to be specified over a broad range by simply changing the amount of each respective gel extruded, thus enabling a plug-and-play approach to consortium bioprocessing. Furthermore, the volume of gel and its spatial pattern can be digitally controlled using a direct-write extrusion printer. To test the efficacy of our hydrogel inks to spatially organize stable consortia, we explored two different types of consortia: (i) a commensal consortium for betaxanthins production and (ii) a parallel consortium for more efficient glucose and xylose utilization in fermentation.

For a commensal consortium, we demonstrated the production of betaxanthins, a natural food colorant [35], through simple combination of an engineered *E. coli* and *S. cerevisiae* strain together to form a gel-based consortium (Figure 4.3b). To do so, a L-DOPA producing bacteria-laden hydrogel was printed alongside a yeast-laden hydrogel that contain engineered yeast capable of converting L-DOPA into betaxanthins. No further synthetic engineering was conducted on these

strains to enable mutualism or matched growth rates. To provide a qualitative comparison with liquid culture, we analyzed the performance of this consortium by assessing production of betaxanthins across a range of temperatures and cell ratios (enabled by altered inoculum ratios for the liquid culture and respective gel masses for the hydrogel system). Even in the round 0 condition (when both species were grown to confluence), production by the hydrogel consortium surpassed the liquid suspension culture for most conditions and had a more consistent production response curve, especially across a range of temperatures (25.0-30 °C) (Figure 4.3c and Figure C.7). A difference in the optimal temperature is seen between the free-cell liquid suspension culture and hydrogel systems and is likely the result of cell growth competition that exists in the free-cell system—a constraint that is relieved when using this hydrogel system. Although the use of the hydrogel provides spatial segregation of the co-culture members, total nutrients fed to the system can ultimately be limiting. Nevertheless, one of the advantages of this system is the ability to specify the final desired consortia composition by altering the ratio of cell-laden gels. In this regard, the nutrient limitation issue can be solved by establishing a consortia ratio that favors either *E. coli* or *S. cerevisiae* for a given condition as demonstrated above. Therefore, the issues of imbalanced biosynthesis capacities can be addressed by changing this cell-laden gel volume.

To further demonstrate the importance of spatial segregation of the consortium members for a stable co-culture system, we evaluated the metabolic activity of a spatially separated consortia hydrogel as described above with that of a mixed gel (i.e. both organisms were mixed and combined together into a single hydrogel) (Figure 4.4). The spatial organization of consortia members within separate hydrogels significantly improved the betaxanthins production compared with mixed gels ($p=0.0054$, unpaired t test with Welch's correction) and had a substantially lower variance between samples ($p=0.024$, Levene's test), suggestive of the fact that competitive cell

growth still occurs even within the structure of a hydrogel and this can only be bypassed with spatial separation afforded by distinct gels for each organism, as explored here.

Next, this consortium-based gel approach was also evaluated on the basis of reusability and on-demand production (Figure 4.3d). Whereas the liquid culture quickly lost its ability to produce betaxanthins due to unstable co-culturing (Figure C.8), the metabolic activity of the immobilized consortium retained over 100% of the production compared to the round 0 hydrogel across five continuous re-use cycles at 33.5 °C (Figure C.9b). In fact, higher production was seen after round 0, possibly because the consortium was already mature and established, and thus the gels could more readily achieve a faster biocatalytic rate and economize sugar conversion (Figure C.8e and C.9b). These promising results for reusability prompted us to further investigate preservation of microbial consortium-laden hydrogels for on-demand production of betaxanthins. In this case, lyophilization and re-use (similar to the scheme previously describe for mono-cultures) resulted in essentially the same production level over five subsequent fermentations (Figure 4.3d), demonstrating that microbe-laden hydrogels containing co-cultures could function for a culturing period of at least 2 months. As with the ethanol mono-culture example above, all hydrogel samples were still operational at the end of this time period.

To complement these preservation results, we additionally evaluated the impact of both refrigerated storage and liquid nitrogen freezing on these consortium-containing gels (Figure 4.3d and Figure C.9b). The refrigerated storage treatment exhibited no loss in productivity for an additional five rounds of re-use, whereas cryopreservation samples showed a mild reduction in metabolic activity, to 85% of the original productivity (Figure C.9b). On the contrary, the liquid culture provided an inconsistent production across all preservation methods used in this study (Figure C.9c-d).

Next, we sought to evaluate the impact of storage on production and gel integrity. Specifically, we observed that the lyophilized consortia hydrogel maintained 100% efficiency of betaxanthins upon rehydration even after long-term storage of the lyophilized at room temperature for three months (Figure C.9e). Furthermore, the lyophilization process had minimal impact on the mechanical integrity of the samples. The Young's moduli before and after preservation were identical for the material (Figure C.9f top), and SEM images indicated that there was little change in the microstructure (Figure C.9f bottom). The cell distribution within the material after rehydration was also unchanged (Figure C.9g). We observed that the overall cell leakage rate from the gel actually decreased after lyophilization and rehydration compared to the pre-lyophilized condition (Figure C.9h). In sum, this F127-BUM hydrogel system provides for a strong preservation capacity of consortia.

As a final benchmarking, we sought to provide a comparison of our F127-BUM hydrogel with standard calcium alginate encapsulation using the same consortium. Calcium alginate hydrogels require constant replenishing of calcium ions in the reactor media in order to retain the charged crosslinks between the individual polymer strands. Additionally, the charged nature of the polymer itself may lead to unwanted interactions between the hydrogel and fermentation products, possibly interfering with diffusion out of the hydrogel [18]. In this comparison, we found a greater than 2.5-fold improvement in betaxanthins production for microbe-laden F127-BUM-based hydrogel when compared to microbe-laden calcium alginate (Figure C.10). Moreover, we observed that the microbe-laden calcium alginate gels softened and degraded slightly over a 72-hour incubation period, whereas the microbe-laden F127-BUM hydrogels retained structural integrity. These results demonstrate the re-use and stability of this platform compared with commonly used calcium alginate gels.

As a final demonstration, we assembled a parallel yeast-yeast strain consortium to enable glucose and xylose fermentation. In this case, we established a parallel consortium hydrogel comprised of a glucose-consuming wild-type *S. cerevisiae* S288C and a xylose-utilizing yeast YSX3 [36] and compared net sugar utilization to that of a free-cell, liquid culture consortia (Figure 4.3e and Figure C.11). As in the betaxanthins example above, there is an implicit selection pressure in this system wherein the faster growing S288C wild-type strain will be enriched in glucose-rich conditions. The free-cell system at this condition exhibited a lower average xylose consumption rate (around 0.07 g L^{-1} h^{-1}) (Figure C.11c; left) compared with the liquid culture conducted in YPDX for round 0 (about 0.16 g L^{-1} h^{-1}) (Figure C.11c; right), suggesting that suspension yeast cultures grown in YPD after round 0 probably were already self-selected to possess a higher proportion of wild-type, non-xylose consuming yeast (as this strain exhibits faster, more robustly growth). In contrast, the gel-based consortium mitigated this selection pressure and maintained a consistent xylose consumption rate of nearly 3.5-fold over the liquid culture condition when cells were initially cultured on glucose (Figure C.11a). Even when initial growth was conducted in a more xylose-strain permissive condition (such as YPDX in Figure 4.3e), the gel-based consortium still outperforms the liquid culture format and remains stable, whereas the liquid consortium fails rather rapidly after only three subculture cycles (Supplementary Note).

While all experiments were conducted at laboratory scale, we envision its utilization in a perfusion style reactor in which media is constantly flowed through the immobilized lattice, allowing constant flow and production of target molecules without the need for reactor downtime. Alternatively, these materials can also be employed on a smaller scale, in a modular production scheme. This approach would allow for easy, mobile deployment of the hydrogel constructs for production of smaller volumes of the target compounds. When aligned with the ability to preserve

and rehydrate the materials for continued bioprocessing, we believe that these hydrogels could one day allow for the implementation of immobilized bioreactors in more extreme or remote settings, where access to bioreactor technology and bulk resources is otherwise difficult or impossible.

4.4 CONCLUSIONS

We have developed a microbe-laden hydrogel platform that can compartmentalize and spatially organize individual microbial populations and consortium members into hydrogel constructs for the production of both small molecules and active peptides. The approach enables repeated re-use and preservation through refrigeration or lyophilization, thus enabling on-demand production of these molecules in a manner that is unmatched by traditional liquid-based culturing. The ability to enable long-term stability of cells and consortia (up to 1 year in the continuous fermentation of yeast to produce ethanol and at least 3 months in the case lyophilized gel storage and subsequent use for betaxanthins) provides a niche for preserving catalytic function in industrial bioprocesses. Moreover, the ability to control consortium dynamics simply by changing the amount of hydrogel ink printed provides a newfound capacity for plug-and-play synthetic consortia. Looking forward, this strategy enables a portable, reusable, and on demand capacity for small molecule and pharmaceutical production from a variety of microorganisms.

4.5 EXPERIMENTAL

4.5.1 *Strains, media and plasmid construction*

All strains, plasmids and primers used in this study are listed in Supplementary Table 1 and Table 2. NEB10β was used for gene cloning or propagation of all expression vectors. It was cultivated in LB medium supplemented with appropriate antibiotics (100 μg mL^{-1} ampicillin, 50 μg mL^{-1} kanamycin or 50 μg mL^{-1} spectinomycin (Sigma)) with 225 rpm orbital shaking at 37 °C.

Starter cultures of yeast strains were routinely grown in yeast synthetic complete (YSC) media with the appropriate dropouts for auxotrophic selection. YPD (10 g L^{-1} yeast extract, 20 g L^{-1} peptone and 20 g L^{-1} glucose) and YPDX (10 g L^{-1} yeast extract, 20 g L^{-1} peptone, 15 g L^{-1} glucose and 15 g L^{-1} xylose) media were used in glucose/xylose utilization studies. LBYSD (1X LB, 1X YSC+CSM-URA, 10 mM vitamin C, 50 µg mL^{-1} kanamycin and 50 µg mL^{-1} spectinomycin) and M9YSD (1X M9, 2 mM $MgSO_4$, 0.1 mM $CaCl_2$, 1X YSC+CSM-URA, 10 mM vitamin C, 50 µg mL^{-1} kanamycin and 50 µg mL^{-1} spectinomycin) were used for medium optimization studies.

Oligonucleotide primers used for PCR amplification were purchased from Integrated DNA Technologies (Coralville, IA). All ligated or Gibson-assembled DNA [37] were electroporated (2mm Electroporation Cuvettes, Bioexpress) into *E. coli* competent cells with a BioRad Genepulser Xcell at 2.5 kV. The Frozen EZ Yeast Transformation II Kit (Zymo Research) was used to transform an integrative cassette into the yeast. For tyrosine production, Gibson assembly method was employed to combine an amplicon containing two T7 promoters amplified from pRSFDuet-1 (Addgene) with primers 11 as well as 12 and the PCR product amplified from pET28b empty vector (Addgene) with primers 13 and 14 to construct pET28b-Duet-1. To construct pCDF-pT7-*tyrA*$^{(fbr)}$-pT7-*aroG*$^{(fbr)}$, the FRT-flanked kanamycin resistance gene on the plasmid pCDF-Kan^{FRT}-*tyrA*$^{(fbr)}$-*aroG*$^{(fbr)}$ was removed using primers P7-P10 via Gibson assembly. To construct pCDFDuet-1, two T7 promoters amplified from pRSFDuet-1 with primers 11 and 12 was Gibson assembled with the PCR product amplified from pCDF-pT7-*tyrA*$^{(fbr)}$-pT7-*aroG*$^{(fbr)}$ with primers 13 and 14. To construct pET28-pT7-*aroG*$^{(fbr)}$-tT7, the DNA fragment PCR-amplified from pCDF-pT7-*tyrA*$^{(fbr)}$-pT7-*aroG*$^{(fbr)}$ with primers P25 and P26 was cloned into the amplicon amplified from pET28b empty vector with primers P27 and P28. For pET28-pYIBN-*aroG*$^{(fbr)}$ construction, native promoter *yibN* and DNA fragment containing *aroG*$^{(fbr)}$ gene was PCR-amplified from *E. coli*

MG1655 genomic DNA with primers P33 as well as P34 and from pET28-pT7-*aroG*$^{(fbr)}$-tT7 with primers P35 as well as 36, respectively. The resulting two amplicons were then cloned into the PCR product amplified from pET28b-Duet-1 with primers P37 and 38 using Gibson assembly. To construct pET28-pYIBN-*aroG*$^{(fbr)}$-B30rbs-*tyrA*$^{(fbr)}$-tRRNC, DNA fragment containing *tyrA*$^{(fbr)}$ PCR-amplified from pCDF-pT7-*tyrA*$^{(fbr)}$-pT7-*aroG*$^{(fbr)}$with primers P41 as well as P42 was combined with primer 43 and cloned into the amplicon obtained from pET28-pYIBN-*aroG*$^{(fbr)}$ with primers P39 as well as P40. For L-DOPA production, primer set P69 and P70 were used for amplifying *HpaB-HpaC* from BL21 (DE3) genomic DNA, and the resulting amplicon as well as primer 67 were Gibson assembled with the PCR product amplified by using primers P72 and P73 from the template pCDFDuet-1 to construct pCDF-pLPP-B30rbs-*hpaB-hpaC*-T7t. For the construction of pCDF-pLPP-B32rbs-*hpaB-hpaC*-T7t, primer set P70 and P71 were used for amplifying *HpaB-HpaC* from BL21 (DE3) genomic DNA, and the resulting amplicon as well as primer 68 were Gibson assembled with the PCR product amplified by using primers P72 and P73 from the empty vector pCDFDuet-1. For betaxanthins production, primer set P74 and P75 were first used for amplifying *MjDOD* gene from pCMC0759. The resulting amplicon was then linearized with restriction enzymes SpeI as well EcoRI and ligated with SpeI/EcoRI digested mumberg plasmid p416-pGPD-tPRM9 to yield p416-pGPD-*MjDOD*-tPRM9. To generate an URA3 integrative cassette, primers P78 and P79 were used for amplifying a linear DNA fragment with 65 bp-long *Leu2* homology arms from p416-pGPD-*MjDOD*-tPRM9.

4.5.2 *Polymer synthesis/functionalization*

Glassware was oven-dried at 125 °C for at least 16 h. F127 (60 g, 4.8 mmol) was dried under vacuum (~ 2 Pa) for at least 16 h at room temperature in a round-bottom flask. Anhydrous CH_2Cl_2 (550 mL) was charged to the flask under an N_2 atmosphere. The mixture was stirred at 30 °C, and

following complete dissolution of the F127, dibutyltin dilaurate (12 drops) was added using a glass Pasteur pipette. The 2-isocyanatoethyl methacrylate (3.5 mL, 24.8 mmol) was diluted in anhydrous CH_2Cl_2 (50 mL) and was added to the reaction mixture at a rate of approximately 1 drop/s. The reaction was allowed to proceed while stirring under dry N_2 at 30 °C. After 2 days, the reaction was quenched by the addition of MeOH (60 mL), and the mixture was concentrated at 30 °C using a rotary evaporator. The F127-BUM was precipitated in Et_2O (2000 mL). During the precipitation, Et_2O was stirred in a large conical flask, and the concentrate was poured in slowly. The precipitate mixture was stirred for an additional 15 min before separation via centrifugation. Eight 50 mL centrifuge tubes were filled with precipitate mixture and centrifuged (3000 g) for approximately 10 min. The transparent supernatant in each tube was decanted from the F127-BUM pellet, and more of the precipitate mixture was added on top of each pellet. This process was repeated until all of the precipitate had been collected in the eight centrifuge tubes, and all of the solvent had been discarded. The F127-BUM precipitate was then washed twice. Each wash was performed by adding Et_2O (approximately 30 mL) to each pellet and vortex-mixing until redispersion of the precipitate was observed; redispersion was followed by centrifugation (3000 g) for re-separation of the F127-BUM precipitate, and supernatants were again discarded. After washing, the F127-BUM from each tube was pooled and transferred to a large beaker. Excess ether was allowed to evaporate while agitating the F127-BUM with a spatula under an N_2 atmosphere. The resultant F127-BUM powder was dried fully overnight at room temperature under vacuum (~ 2 Pa) and stored in the dark at 4 °C until further use.

4.5.3 *Materials Generation and Processing*

F127-BUM (3 g) was dissolved in sterile, deionized water (7 g) and the resulting mixture was cooled overnight at 5 °C to facilitate complete dissolution of the polymer. Then, the solution was

warmed to room temperature (21 °C) to induce the sol-to-gel transition. The hydrogels used for extrusion printing were mixed with the photo-radical initiator 2-hydroxy-2-methylpropiophenone (10 μL for every 10 grams of hydrogel solution). For the preparation of microbe-laden hydrogels, the aforementioned 30 wt% hydrogel was cooled to 5 °C in a refrigerator. At this temperature, the hydrogel underwent a gel-to-sol transition, affording a free-flowing liquid. Yeast or bacteria cells were added from liquid culture, at the desired concentration, as determined by OD600 measurements. The resulting solution was mixed thoroughly and allowed to equilibrate at 5 °C until all of the bubbles present in the solution were removed. Finally, the hydrogel was warmed to 21 °C to undergo a sol-to-gel transition, to afford a shear-responsive gel. These cell-laden materials were then extruded through the end of a syringe in cylindrical samples of the appropriate microbial hydrogel. The hydrogels could then be photocured with an exposure to 365 nm light (at 3.4 mW cm^{-2}) for 90 s.

4.5.4 *Extrusion of microbial hydrogels*

For hand-extruded hydrogel samples, the microbial hydrogels were transferred while cold (~5 °C) into 5 mL syringes. Once the hydrogel was inside the syringe, the samples were warmed to 21 °C to afford a shear-responsive hydrogel. These hydrogels could then be extruded through the end of the syringe by applying back pressure to the hydrogel sample with the syringe plunger. Samples were deposited in increments of 250 μL. For co-culture gels, we deposited the samples side-by-side prior to UV curing. Due to the self-healing nature of the pre-cure hydrogels, this approach allows the final construct (after UV curing) to be comprised of a single continuous hydrogel, but with spatially distinct regions, each containing a particular microbial strain. For CAD model extrusion printing, a modified pneumatic direct-write extrusion printer was assembled based on a Tronxy P802E 3D Printer kit, from Shenzen Tronxy Technology Co. The printer was controlled

with an Arduino using the Marlin firmware. All CAD models were designed in OpenSCAD. G-code commands for the printer were generated using Slic3r. The resulting G-code was modified using Python to introduce required commands for the dispensing of the hydrogel via pneumatic pressure. All printing was performed using a 30 wt % hydrogel ink with an extrusion air pressure of 20 psi, a print speed of 15 mm s^{-1}, and a 0.21 mm inner diameter CML Supply conical nozzle attachment. Upon completion of the extrusion printing, the structures were irradiated under 365 nm light (at 3.4 mW cm^{-2}) for 90 s to cure and chemically fix the structures.

4.5.5 *Imaging and co-culture flow cytometry*

For optical imaging, images of the extrusion printed hydrogels were captured using an iPhone X. For confocal imaging, the microscopy images were taken using a Leica TCS SP5 II laser scanning confocal microscope. Confocal microscopy output images were processed using ImageJ Java software.

Cell segregation studies were conducted by printing strands of yeast (*S. cerevisiae* yJS001)- and bacteria (*E. coli* CD02)-laden hydrogel in contact with one another, by utilizing the two-material printing capabilities of the pneumatic-driven extrusion printer. Bacteria and yeast were both seeded at concentrations of 10^7 cells/gram of hydrogel. Strands of the two hydrogel samples were printed in contact with one another and cured. The resulting structures were submerged incubated at 30 °C in 1:1 SC:LB media and imaged under confocal microscopy at 1, 3, and 7 days. The interface between the strands was imaged across 100 microns, with images taken at steps of approximately 3 microns. The resulting z-stacks were merged into one image to ensure the integrity of the interface through the thickness of the printed structure. E. coli used in this study are shown in the green channel, and yeast are shown in the red channel. All images were taken with a dry 10x objective. RFP fluorescence was excited with a 561 nm laser at 5% laser power,

and emission was scanned from 569 to 700 nm. GFP fluorescence was excited with a 488 nm laser at 5% laser power, and emission was scanned from 500 to 550 nm.

For confluence imaging, standard samples of bacteria (*E. coli* CD02)-laden and yeast (*S. cerevisiae* yJS001)-laden hydrogels were prepared in the same manner as previously discussed. Individual samples of each type of hydrogel were printed and cured. The yeast samples were incubated in SC media at 30 °C, while the bacteria samples were incubated in LB media at 37 °C. These samples were incubated in their respective shakers for 7 days. At the end of the incubation, the samples were imaged under confocal microscopy, and the imaging settings were standardized and saved. For the co-culture samples, bacteria- and yeast-laden hydrogels were printed in the same fashion as the cell segregation study. These samples were then incubated in 1:1 LB:SC media, and placed into shakers at the five temperatures explored in our fermentation studies (25, 30, 33.5, 37, 40 °C). These samples were extracted and imaged at 1, 3, and 7 days, using the same settings that were established in the standard sample imaging. Lastly, the percent area of fluorescence in all the images was quantified using ImageJ, and the percent confluence of the various conditions of co-culture were calculated against the standard samples. All images were taken with a dry 10x objective. RFP fluorescence was excited with a 561 nm laser at 5% laser power (850 gain), and emission was scanned from 569 to 700 nm. GFP fluorescence was excited with a 488 nm laser at 10% laser power (850 gain), and emission was scanned from 500 to 550 nm.

E. coli CD02 and *S. cerevisiae* JMW001 were used for co-culture experiments analyzed using flow cytometry. Flask cultures containing GFP-expressing *E. coli* and RFP-expressing *S. cerevisiae* (initially seeded at 1.5E6 cells/mL each) were grown for 20 hours at various temperatures in identical shaking incubators with agitation set to 225 RPM. Culture samples were

then diluted in DPBS and held on ice to minimize further growth during analysis. Flow cytometry was performed using a BD LSRII Fortessa instrument and BD FACSDiva software with GFP and mCherry (RFP) acquisition settings. Gates were initially drawn based on FSC and SSC signals, and the percentages of each cell type in the resulting scatter-based gates were confirmed based on fluorescence (i.e. GFP for *E. coli*, RFP for *S. cerevisiae*). This analysis was completed for triplicate cultures started from the same frozen vial of *E. coli* and *S. cerevisiae*.

4.5.6 *Ethanol production*

S. cerevisiae SO992 was used for ethanol production. To monitor the long-term fermentation of glucose to ethanol, we utilized extrusion printed hydrogel cubes with a yeast cell concentration of 10^8 cells per gram of hydrogel. The printed cubes were washed twice using SC media, and stored individually in tubes containing 10 mL of synthetic complete media for each gram of living material. These tubes were degassed for 6 min by bubbling argon through the solution to ensure anaerobic conditions for the fermentation process. Finally, the tubes were placed into a 30 °C shaker for the fermentation incubation. The media was replaced every 3−4 days and stored for ethanol quantification measurements by gas chromatography. This study was performed over the course of 365 days.

4.5.7 *Tyrosine production*

A lambda-red recombination-based method was employed to delete chromosomal transcriptional regulator *tyrR* in *E. coli* BL21 (DE3) strain [38]. Primers P1 and P2 were used to PCR-amplify an FRT-flanked kanamycin resistance gene (FRT-KanR) from the plasmid pKD13. The resulting PCR product was then be used as a template and primers P3 as well as P4 were utilized for PCR-amplification. The amplified FRT-KanR cassette carried 100 bp of homology with the

ends of chromosomal *tyrR* to facilitate knockout efficiency. Following transformation of the knockout cassette into *E. coli*, colonies were verified by colony PCR and sequencing with primers P5 and P6. Excision of FRT-KanR from the resulting strain *E. coli* Δ*tyrR* was mediated by transformation with pCP20 expressing FLP recombinase as described in the literature [38]. Colonies were verified by colony PCR and elimination of temperature-sensitive pCP20 was carried out via nonselective incubation at 43°C. To ensure FRT-KanR excision and knockout of *tyrR*, the gene fragment PCR-amplified from *E. coli* Δ*tyrR* genomic DNA prepared using the Wizard Genomic DNA Purification Kit (Promega, Madison, WI) was then sequence verified via Sanger sequencing. The resulting *E. coli* BL21 (DE3) Δ*tyrR* strain was designated as eBL01. The tyrosine producing plasmid pET28-pYIBN-*aroG*$^{(fbr)}$-B30rbs-*tyrA*$^{(fbr)}$-tRRNC was transformed into eBL01 leading to an eBL04 strain. For tyrosine production, starter culture of *E. coli* was grown in 2 mL LB medium containing 50 μg mL^{-1} kanamycin with 225 rpm orbital shaking at 37 °C overnight. Then seed culture was inoculated into 2 mL M9 medium supplemented with 2% glucose as well as 50 μg mL^{-1} kanamycin with an initial OD_{600} of 0.05 and incubated at 37 °C. After 18 hr fermentation, suspension culture was centrifuged at 16000 g for 2 minutes and supernatant fraction was collected for measurement of tyrosine production using HPLC. The cell growth was measured by Ultrospec 2100 Pro UV/Visible Spectrophotometer observing optical density at 600 nm. The recombinant strain produced 0.44 mM of tyrosine. The results represented the mean ± S.D. of three biological replicates.

4.5.8 *L-DOPA production*

The L-DOPA producing plasmids listed in Supplementary Table 1 were individually transformed into tyrosine producer *E. coli* eBL04. The eBL04 transformed with empty vectors pET28b-Duet-1 and pCDF-Duet-1 resulting in a control strain was used in this experiment. For L-

DOPA production, cells were precultured in 2 mL LB medium containing 50 μg mL^{-1} kanamycin as well as 50 μg mL^{-1} spectinomycin with 225 rpm orbital shaking at 37 °C overnight. Seeding cultures were then transferred to 3 mL LB medium supplemented with antibiotics with an initial OD_{600} of 0.05 and incubated at 30 °C for 15 hours. After fermentation, cultures were pelleted at 16,000 g for 2 minutes and media supernatant were collected for measurement of L-DOPA production using HPLC. For L-DOPA production in *E. coli* with lyophilization and re-use, the starter culture of highest producer *E. coli* eBL0430D was inoculated from glycerol stocks into 3 mL LB medium containing 50 μg mL^{-1} kanamycin and 50 μg mL^{-1} spectinomycin and incubated at 37 °C overnight. The details of preparation of hand-extruded hydrogel samples were described above. Briefly, 4.5 x 10^7 overnight cells were encapsulated in 0.3 gram of polymer. The printed and cured cell-laden gels were then incubated in 3 mL LB medium containing 50 μg mL^{-1} kanamycin and 50 μg mL^{-1} spectinomycin with 225 rpm orbital shaking at 37 °C for 22 hours. Subsequently, the gel samples were treated with lyophilization process as described below. The preserved gels were next transferred to 3 mL LB medium with appropriate antibiotics and incubated at 37 °C for 22 hours. Cultures were collected at the end of each batch and supernatant fractions from pelleted samples were filtered and analyzed by HPLC for L-DOPA quantification. The results represented the mean ± S.D. of three biological replicates.

4.5.9 *2,3-Butanediol production*

For 2,3-BDO production in yeast with lyophilization and re-use, the starter cultures of 2,3 BDO-producing BY4741 and CEN.PK2-a yeasts were inoculated from glycerol stocks [32] into 3 mL YSC dropout media (CSM-URA-LEU) and incubated at 30 °C for 60 hours. 4.5 x 10^7 overnight yeast cells were afterwards encapsulated in 0.3 gram of polymer. The details of preparation of hand-extruded hydrogel samples were described above. The printed and cured cell-

laden gels were then incubated in 3 mL YSC+CSM-URA-LEU at 30 °C for 72 hours. Subsequently, the gel samples were treated with lyophilization process as described below. The lyophilized gels were then transferred to 3 mL YSC+CSM-URA-LEU and incubated at 30 °C for 72 hours. In each batch, 200 uL culture samples were taken for every 24 hours and the concentrations of 2,3-BDO and acetoin in supernatant part from pelleted cells were analyzed by HPLC. The results represented the mean ± S.D. of three biological replicates.

4.5.10 *Antimicrobial peptide production*

E. coli MC4100_pHK11 [33] and the sensitive strain DH5α_pET28b were used in this study. For antimicrobial peptide colicin V production, toxin-producing cells were precultured in 3 mL LB medium supplemented with 100 μg mL^{-1} ampicillin at 37 °C for 15 hours with 225 rpm orbital shaking. The control strain was routinely cultivated in 3 mL LB medium with 50 μg mL^{-1} kanamycin at 37 °C for 15 hours to maintain cell growth. 4.5 x 10^7 toxin-producing cells were afterwards immobilized in 0.3 gram of hydrogel. The printed and cured cell-laden living materials were then incubated in 3 mL LB medium containing 100 μg mL^{-1} ampicillin at 37 °C. Subsequently, the gel samples were proceeded to lyophilization treatment as described in the preservation section below. The preserved gels were next transferred to 3 mL LB medium with 100 μg mL^{-1} ampicillin and incubated at 37 °C. Four consecutive uses after lyophilization were performed. For round 0 in free cell system, 4.5 x 10^6 toxin-producing cells were transferred from overnight culture to 3 mL LB medium containing 100 μg mL^{-1} ampicillin and incubated at 37 °C. Four repetitive uses were subsequently carried out through transferring 50 uL of bacterial suspension from previous batch to the next batch. In each batch, samples at the 21-hr time point were taken for zone of inhibition or broth test to determine the bactericidal activity of Col V. For zone of inhibition test, 3 x 10^8 sensitive *E. coli* cells were first spread onto the LB agar plate

supplemented with 50 μg mL^{-1} kanamycin. After centrifuging Col V-producing cultures at 16,000 g for 25 minutes, 10 uL of supernatants containing antimicrobial peptides were spotted on the same plate and incubated the plate at 37 °C for 16 hours. The diameter of each inhibition zone was then measured to assess bactericidal activity of Col V. For broth test, 50 uL of supernatant from the 21-hr timepoint pelleted culture (centrifuged at 16,000 g for 25 minutes) was added to the tube containing 2.25 x 10^6 sensitive *E. coli* cells as well as 1.5 mL LB medium supplemented with 50 μg mL^{-1} kanamycin and then the tube was incubated at 37 °C for 16 hrs. The value of OD_{600} for each tube was measured after incubation to evaluate antimicrobial efficiency in each batch. The results represented the mean ± S.D. of three biological replicates.

4.5.11 *Betaxanthins production*

The yeast integration cassette listed in Supplementary Table 1 was transformed into wild-type *S. cerevisiae* BY4741 resulting in a DOD enzyme-overexpressing sBY08 strain. To investigate the effect of medium composition and fermentation temperature on betaxanthins production with the use of a synthetic consortium, L-DOPA producer *E. coli* eBL0430D and DOD-expressing *S. cerevisiae* sBY08 were used in this study. The starter cultures of *E. coli* eBL0430D and *S. cerevisiae* sBY08 were cultivated into LB medium supplemented with 50 μg mL^{-1} kanamycin as well as 50 μg mL^{-1} spectinomycin and YSC+CSM-URA, respectively. The seeding *E. coli* and yeast cultures were then transferred to LBYSD or M9YSD medium (with initial OD_{600} of 0.05 for yeast and 0.0015 for *E. coli*) and incubated at various temperatures (25, 30, 33.5, 37 and 40 °C). For each time point, 100 uL of supernatant parts taken from 250 uL of pellet samples (with centrifugation at 2,750 g for 10 minutes) were transferred to a microtiter plate. Betaxanthins fluorescence was measured by the plate reader (BioTek) with reading gain 100, excitation at 482nm and emission at 510nm. The results represented the mean ± S.D. of three biological

replicates. To evaluate if the reactor scale will affect the betaxanthin production, fermentations were conducted in 3 mL culture tube or 25 mL shaking flask containing M9YSD medium and incubated at 30 °C with initial OD_{600} of 0.05 for yeast and 0.015 for *E. coli*. 200 mg/L DOPA was also added to the medium to act as a positive control. Betaxanthins fluorescence was measured by the plate reader with reading gain 75, excitation at 482nm and emission at 510nm. To investigate the effects of aeration in culture tube and initial yeast cell number on betaxanthins production for the gel system, conditions including medium working volume 3 mL or 5 mL with 4.5 x 10^7 or 4.5 x 10^6 seeding yeast cells embedded in 0.3 gram of hydrogels were examined in this study. 100 or 200 mg L^{-1} L-DOPA was added into the M9YSD medium for production testing. Samples were taken at 24-hour intervals. Fluorescence was measured by the plate reader with reading gain 75, excitation at 482nm and emission at 510nm. To study the impact of fermentation temperature and initial cell density on betaxanthins production with the use of gel or free cell system, various temperatures (25, 30, 33.5, 37 and 40 °C) as well as yeast : *E. coli* cell/gel ratios (100:1, 10:1, 1:1, 1:10 and 1:100 for liquid cultures system; 6:1, 3:1, 1:1, 1:3 and 1:6 for hydrogels) were adopted for production testing. For hydrogel system, each printed gel carried the same initial yeast or *E. coli* cell concentration 1.5 x 10^8 cells $gram^{-1}$ of polymer. For free cell system, all conditions included the same initial net yeast and *E. coli* cells concentration (3 x 10^6 cells mL^{-1}). An addition condition (1:1, 10X) mimicking the same number of initial cells used in the 1:1 gel ratio condition was employed in liquid culture system. 100 uL of supernatant taken from 120 uL of samples after centrifugation at 2,750 g for 10 minutes was transferred to a microtiter plate. Fluorescence was measured by the plate reader with reading gain 60, excitation at 482nm and emission at 510nm. To investigate the reusability of cell-laden living materials, five consecutive uses after round 0 were performed. The gels (6:1) and liquid culture samples (100:1 and 1:1 (10X)) with the highest

betaxanthins titer at 30 and 33.5 °C were selected from the round 0 experiment and transferred to 3 mL M9YSD media for production testing. For liquid culture, repetitive uses were carried out through transferring 50 μL of consortia suspension from previous batch to the next batch. Samples were taken at 24-hour intervals and each batch of reuse was performed for 3 days. Fluorescence was recorded by the plate reader with reading gain 60, excitation at 482nm and emission at 510nm. To evaluate the impact of preservation process on consortia activity in gel system, three different preservation methods including lyophilization, 4 °C storage and liquid nitrogen freezing were applied to preservation of consortia-laden polymers as described below. Additional five consecutive uses after preservation process were performed. Samples were taken at 24-hour intervals and each batch of reuse was performed for 3 days. Betaxanthins fluorescence was recorded by the plate reader with gain setting of 60, excitation at 482nm and emission at 510nm. To evaluate the impact of three preservation processes on betaxanthins production between liquid culture and hydrogel system, 100 or 500 μL of pre-preserved consortia suspension was taken and individually proceeded to lyophilization, 4 °C storage and liquid nitrogen freezing. The spatially separated consortia hydrogels with 6:1 (yeast:*E.coli*) gel ratio were used in this study. The details of inoculum ratio of yeast to *E. coli* were described above. The preserved samples were then transferred to fresh media for the production and supernatants were taken at day 3. Fluorescence was recorded by the plate reader with reading gain 60, excitation at 482nm and emission at 510nm. For the long-term storage measurement, betaxanthins production was measured after 96 hours of initial incubation to establish baseline production. After the hydrogels were then lyophilized. After one month of storage at room temperature, the hydrogels were resuspended in medium, and betaxanthin production was again measured after 96 hours of incubation. To investigate the importance of spatial organization of consortia member in betaxanthins production, supernatants

from 72-h fermentation cultures of separate hydrogel (L-DOPA producing bacteria-laden hydrogel was printed alongside a yeast-laden hydrogel) and mixed gel (two species were embedded in the same gel) were collected for betaxanthins measurement. Both separate and mixed gels (n=9) carried the same initially inoculated cell numbers with 6:1 yeast-*E. coli* ratio. Fluorescence was recorded by the plate reader with reading gain 60, excitation at 482nm and emission at 510nm. To compare the F127-BUM hydrogel to caclium alginate hydrogels, a solution of 8 weight percent sodium alginate was prepared in water. This solution was then inoculated with 4.5 x 10^7 cells for every 300 μL of alginate solution. This solution was then extruded into a bath of 3 weight percent calcium chloride to induce physical crosslinking and to produce self-supporting calcium alginate hydrogels. 300 μL of bacteria and yeast calcium alginate hydrogels were then incubated in the fermentation media for 72 hours at 30 °C. The resulting betaxanthins production was then compared to the 1:1 ratio of F127-BUM hydrogel.

4.5.12 *Determination of the percentage of leaked cells*

To determine the degree of leaked *E. coli* and yeast cells in the hydrogel system, serial dilutions of the cultures incubated for 0.5 hours from immobilized betaxanthins-producing consortia samples (with 6:1 yeast-*E.coli* gel ratio) were plated on YPD agar plate supplemented with 100 μg mL^{-1} of ampicillin to measure colony forming units (CFUs) of *S. cerevisiae* and solid LB supplemented with 10 μg mL^{-1} of nystatin (VWR Catalog No.: AAJ62486-06), an antifungal antibiotic, to measure CFUs of *E. coli*. To investigate the impact of washing process for consortia-laden hydrogels on the percentage of leaked cells between pre- and post-preservation, the CFUs of each specie for preserved gels with 0, 1 or 2 wash were normalized to that of pre-preserved samples with 0 wash. Gel samples for each treatment (n=1) were incubated at 30 °C.

4.5.13 *Glucose/Xylose utilization with repeated uses*

To investigate the consortia activity on glucose/xylose utilization with repeated uses for gel and liquid culture systems, a parallel consortium *S. cerevisiae* wild-type S288C and xylose-utilizing YSX3 strains [36] were used in this study. The yeast strains were precultured in YPD medium at 30 °C for 37 hours. For hydrogel system, 4.5 x 10^7 seeding cells for each yeast strain were individually immobilized in 0.3 gram of hydrogel. For liquid culture system, 4.5 x 10^6 seeding yeast cells for each strain were mixed and transferred to 3 mL medium. For round 0, two separate trials were carried out in parallel: one condition consisted of growing the yeast-yeast consortia in YPD media and the other grew the yeasts in YPDX media at 30 °C for 5 days to outgrow the population. Subsequently, three consecutive rounds of use were performed with all samples cultivated in YPDX media to test glucose and xylose consumption. Each re-use batch was carried out with 30 °C incubation for 96 hours. For liquid cultures, repetitive uses were carried out through transferring 50 uL of consortia suspension from previous batch to the next batch. Samples were taken at 24-hour intervals and the concentrations of residual glucose and xylose were analyzed by HPLC. The initial xylose consumption rate was determined at 24-hour time point. The results represented the mean ± S.D. of three biological replicates.

4.5.14 *GC and HPLC analysis*

For ethanol fermentation, samples from batch reactions were filtered through 0.2 μm nylon filters and subjected to gas chromatography (GC; Agilent 7890A GC System) equipped with a Restek Rtx-BAC1 column (30 m, ID 0.53 mm, 3.0 μm) and oven program was 40 °C for 5 min. A 1 μL sample was injected at 253.07 mL min^{-1} of H2 flow. A peak for ethanol appeared between 1.85 and 1.95 min. Standard samples were prepared by adding known volume of pure ethanol into SC media (e.g., 50 μL of ethanol in 950 μL of SC media corresponds to 50000 ppm v/v of ethanol)

to obtain a calibration curve of concentration versus ethanol peak area in GC. For the rest of experiments, samples were filtered with 0.2-μm nylon syringe filters (Wheaton Science) prior to running HPLC. HPLC confirmation of tyrosine or L-DOPA production was performed using a Dionex UltiMate 3000 (Thermo Fisher Scientific) equipped with an Agilent Eclipse Plus C18 column (3.0 × 150 mm, 3.5 μm) with detection wavelength set to 280 nm. Column oven was held at 25 °C with 1% acetic acid in water or acetonitrile as the mobile phase over the course of the 20-minute sequence under the following conditions: 5% to 15% organic (vol/vol) for 5 minutes, 15% to 100% organic (vol/vol) for 8 minutes, 100% organic (vol/vol) for 2 min, 100% to 5% organic for 2 minutes followed by 5% organic for 3 minutes. The constant flow rate was set at 0.8 mL min^{-1}. A standard curve was prepared using 98.0% purity L-DOPA (3,4-Dihydroxy-L-phenylalanine) from Sigma or 99% purity tyrosine (Acros Organics). For quantification of 2,3-BDO, an Aminex HPX-87H ion exclusion column (BioRad) was used. The flow rate using an isocratic mobile phase of 5 mM H_2SO_4 was set at 0.6 mL min^{-1} over 25 minutes. The column temperature was held at 60 °C and a refractive index detector (RID) (Kawaguchi) was used at 25 °C. A standard curve was prepared from 98% purity 2,3-butanediol (Sigma). For quantification of glucose and xylose concentration, an Aminex HPX-87P Column (BioRad) was used to measure samples. Filtered and degassed H2O was used as mobile phase with a flow rate of 0.6 mL min^{-1} over 38 minutes. The column was kept at 85 °C and a refractive index detector (RID) (Kawaguchi) was used at 25 °C. A standard curve was prepared using 99% purity glucose (MP Biomedicals) and xylose (Sigma). Data was analyzed using the Chromeleon 7.2 Chromatography Data System (Dionex).

4.5.15 *Preparation of tensile specimens*

The 30 wt% F127-BUM hydrogels were brought below their T_{gel} and poured into ASTM D638 type V specimen molds. Each specimen was then brought back to 21 ºC to induce gelation. Upon

complete gelation, the specimens were cured for 30 minutes in a custom-fabricated curing chamber with sunlite 365 nm A19 UV Lamps. After photo curing, half of the samples were lyophilized. Prior to testing, all samples were stored in an excess of DI water for at least 24 hours to reach equilibrium swelling.

4.5.16 *Mechanical tests*

Tensile mechanical measurements were performed on as-prepared tensile specimens using an Instron 5585H load frame with a 50 N load cell and flat pneumatic grips. All tests were conducted at room temperature (22 ˚C) using a crosshead rate of 10mm/min, until specimen failure. The dimensions of each specimen were measured with calipers prior to testing to ensure accurate calculation of stress and strain. At least five specimens of each formulation were tested. The Young's moduli were calculated from the linear region of stress vs strain curve.

4.5.17 *SEM analysis of material structure*

Prior to imaging, the hydrogel samples were dipped into liquid nitrogen and lyophilized overnight. One sample was imaged before on-demand production of betaxanthins, while the second sample was subjected to two consecutive, on-demand fermentation cycles before imaging. All SEM images were captured using a ThermoScientific Apreo-S scanning electron microscope.

4.5.18 *General scheme for preservation and re-use cycles*

Prior to preservation process, all gel samples were taken from the gel cultures at the end of fermentation and washed 1-2 times with 400-800 μL of fresh medium. The cell-laden materials were then transferred to a new sterile culture tube. For the lyophilization process, the culture tubes carrying hydrogels were first placed into a liquid nitrogen tank for 10-15 mins. After the freezing step, the tubes containing frozen gels were placed into a dryer chamber Figure C.9a; right). During

the drying process, the moisture was withdrawn from the polymers through sublimation under vacuum. Vacuum was applied to the dryer chamber overnight to ensure the water was completely removed from the gels. For refrigerated storage treatment, the culture tube carrying *E. coli*-yeast gels was stored in the refrigerator (set to 4°C) for a week. For liquid nitrogen freezing process, the culture tubes containing hydrogels were first placed into a liquid nitrogen tank for 10-15 mins. Subsequently, the frozen tubes were stored at -80 °C for 16 hours. After preservation process, the preserved gels were then transferred to fresh medium to proceed with continuous re-use.

4.5.19 *Statistical analysis*

For comparing pre- and post-lyophilized samples for 2,3-BDO and L-DOPA production, statistical analysis was performed using Wilcoxon matched-pairs signed-rank test in GraphPad Prism 6 software. Data were considered statistically significant when $p < 0.05$ by paired t tests. For comparing betaxanthins production between separate and mixed hydrogel samples, statistical analysis for the means of two groups was performed using unpaired t test with Welch's correction in GraphPad Prism 6. Statistical analysis for the standard deviations of two groups was performed using the Levene's test in Excel. Data are presented as the mean ± S.D. from at least 3 biological replicates, unless stated otherwise in Figure legends and experimental methods.

4.6 ACKNOWLEDGEMENTS

This work was supported by the Camille and Henry Dreyfus Foundation (H.A.). A.N. acknowledges both UW CoMotion and Royalty Research Fund for supporting this work. We thank Hung-wen (Ben) Liu for access to the lyophilizer and Bryan Davies for providing the MC4100_pHK11 strain. We also thank Dylan Karis for the polymer synthesis.

4.7 REFERENCES

1. Lee, S. Y.; Kim, H. U.; Chae, T. U.; Cho, J. S.; Kim, J. W.; Shin, J. H.; Kim, D. I.; Ko, Y.-S.; Jang, W. D.; Jang, Y.-S., A comprehensive metabolic map for production of bio-based chemicals. *Nature Catalysis* **2019,** *2* (1), 18-33.
2. Clomburg, J. M.; Crumbley, A. M.; Gonzalez, R., Industrial biomanufacturing: The future of chemical production. *Science* **2017,** *355* (6320), aag0804.
3. Cordova, L. T.; Alper, H. S., Central metabolic nodes for diverse biochemical production. *Curr. Opin. Chem. Biol.* **2016,** *35*, 37-42.
4. Yuan, S.-F.; Alper, H. S., Metabolic engineering of microbial cell factories for production of nutraceuticals. *Microbial Cell Factories* **2019,** *18* (1), 46.
5. McCarty, N. S.; Ledesma-Amaro, R., Synthetic Biology Tools to Engineer Microbial Communities for Biotechnology. *Trends Biotechnol.* **2019,** *37* (2), 181-197.
6. Zhang, H.; Wang, X., Modular co-culture engineering, a new approach for metabolic engineering. *Metab. Eng.* **2016,** *37*, 114-121.
7. Roell, G. W.; Zha, J.; Carr, R. R.; Koffas, M. A.; Fong, S. S.; Tang, Y. J., Engineering microbial consortia by division of labor. *Microbial Cell Factories* **2019,** *18* (1), 35.
8. Bittihn, P.; Din, M. O.; Tsimring, L. S.; Hasty, J., Rational engineering of synthetic microbial systems: from single cells to consortia. *Curr. Opin. Microbiol.* **2018,** *45*, 92-99.
9. Jones, J. A.; Wang, X., Use of bacterial co-cultures for the efficient production of chemicals. *Curr. Opin. Biotechnol.* **2018,** *53*, 33-38.
10. Zhou, K.; Qiao, K.; Edgar, S.; Stephanopoulos, G., Distributing a metabolic pathway among a microbial consortium enhances production of natural products. *Nature Biotechnology* **2015,** *33*, 377.
11. Zhang, H.; Pereira, B.; Li, Z.; Stephanopoulos, G., Engineering Escherichia coli coculture systems for the production of biochemical products. *Proceedings of the National Academy of Sciences* **2015,** *112* (27), 8266.
12. Niwas, R.; Singh, V.; Singh, R.; Pant, G.; Mitra, K.; Tripathi, C. K. M., Cholesterol oxidase production from entrapped cells of Streptomyces sp. *J. Basic Microbiol.* **2014,** *54* (11), 1233-1239.
13. Kumaravel, V.; Gopal, S. R., Immobilization of Bacillus amyloliquefaciens MBL27 cells for enhanced antimicrobial protein production using calcium alginate beads. *Biotechnol. Appl. Biochem.* **2010,** *57* (3), 97-103.
14. Connell, J. L.; Ritschdorff, E. T.; Whiteley, M.; Shear, J. B., 3D printing of microscopic bacterial communities. *Proceedings of the National Academy of Sciences* **2013,** *110* (46), 18380.
15. Schaffner, M.; Rühs, P. A.; Coulter, F.; Kilcher, S.; Studart, A. R., 3D printing of bacteria into functional complex materials. *Science Advances* **2017,** *3* (12), eaao6804.
16. Saha, A.; Johnston, T. G.; Shafranek, R. T.; Goodman, C. J.; Zalatan, J. G.; Storti, D. W.; Ganter, M. A.; Nelson, A., Additive Manufacturing of Catalytically Active Living Materials. *ACS Applied Materials & Interfaces* **2018,** *10* (16), 13373-13380.
17. Liu, X.; Tang, T.-C.; Tham, E.; Yuk, H.; Lin, S.; Lu, T. K.; Zhao, X., Stretchable living materials and devices with hydrogel–elastomer hybrids hosting programmed cells. *Proceedings of the National Academy of Sciences* **2017**, 201618307.
18. Cheetham, P. S. J.; Blunt, K. W.; Bocke, C., Physical Studies on Cell Immobilization Using Calcium Alginate Gels. *Biotechnol. Bioeng.* **1979,** *21* (12), 2155-2168.

19. Higashi, K.; Ogawa, M.; Fujimoto, K.; Onoe, H.; Miki, N., Hollow Hydrogel Microfiber Encapsulating Microorganisms for Mass-Cultivation in Open Systems. *Micromachines (Basel)* **2017,** *8* (6), 176.
20. Lehner, B. A. E.; Schmieden, D. T.; Meyer, A. S., A Straightforward Approach for 3D Bacterial Printing. *ACS Synth Biol* **2017,** *6* (7), 1124-1130.
21. Qian, F.; Zhu, C.; Knipe, J. M.; Ruelas, S.; Stolaroff, J. K.; DeOtte, J. R.; Duoss, E. B.; Spadaccini, C. M.; Henard, C. A.; Guarnieri, M. T.; Baker, S. E., Direct Writing of Tunable Living Inks for Bioprocess Intensification. *Nano Lett.* **2019**.
22. Schmieden, D. T.; Basalo Vázquez, S. J.; Sangüesa, H.; van der Does, M.; Idema, T.; Meyer, A. S., Printing of Patterned, Engineered E. coli Biofilms with a Low-Cost 3D Printer. *ACS Synth Biol* **2018,** *7* (5), 1328-1337.
23. Kadilak, A. L.; Rehaag, J. C.; Harrington, C. A.; Shor, L. M., A 3D-printed microbial cell culture platform with in situ PEGDA hydrogel barriers for differential substrate delivery. *Biomicrofluidics* **2017,** *11* (5), 054109-054109.
24. Au - Spiesz, E. M.; Au - Yu, K.; Au - Lehner, B. A. E.; Au - Schmieden, D. T.; Au - Aubin-Tam, M.-E.; Au - Meyer, A. S., Three-dimensional Patterning of Engineered Biofilms with a Do-it-yourself Bioprinter. *JoVE* **2019,** (147), e59477.
25. Desai, R. M.; Koshy, S. T.; Hilderbrand, S. A.; Mooney, D. J.; Joshi, N. S., Versatile click alginate hydrogels crosslinked via tetrazine–norbornene chemistry. *Biomaterials* **2015,** *50*, 30-37.
26. Li, P.; Müller, M.; Chang, M. W.; Frettlöh, M.; Schönherr, H., Encapsulation of Autoinducer Sensing Reporter Bacteria in Reinforced Alginate-Based Microbeads. *ACS Applied Materials & Interfaces* **2017,** *9* (27), 22321-22331.
27. Smith, M. J.; Francis, M. B., Improving metabolite production in microbial co-cultures using a spatially constrained hydrogel. *Biotechnol. Bioeng.* **2017,** *114* (6), 1195-1200.
28. Huang, J.; Liu, S.; Zhang, C.; Wang, X.; Pu, J.; Ba, F.; Xue, S.; Ye, H.; Zhao, T.; Li, K.; Wang, Y.; Zhang, J.; Wang, L.; Fan, C.; Lu, T. K.; Zhong, C., Programmable and printable Bacillus subtilis biofilms as engineered living materials. *Nat. Chem. Biol.* **2019,** *15* (1), 34-41.
29. Kandemir, N.; Vollmer, W.; Jakubovics, N. S.; Chen, J., Mechanical interactions between bacteria and hydrogels. *Sci. Rep.* **2018,** *8* (1), 10893.
30. Köpke, M.; Mihalcea, C.; Liew, F.; Tizard, J. H.; Ali, M. S.; Conolly, J. J.; Al-Sinawi, B.; Simpson, S. D., 2,3-Butanediol Production by Acetogenic Bacteria, an Alternative Route to Chemical Synthesis, Using Industrial Waste Gas. *Appl. Environ. Microbiol.* **2011,** *77* (15), 5467.
31. Miguelez, C.; Benazzouz, A.; Ugedo, L.; De Deurwaerdère, P., Impairment of Serotonergic Transmission by the Antiparkinsonian Drug L-DOPA: Mechanisms and Clinical Implications. *Front. Cell. Neurosci.* **2017,** *11* (274).
32. Deaner, M.; Holzman, A.; Alper, H. S., Modular Ligation Extension of Guide RNA Operons (LEGO) for Multiplexed dCas9 Regulation of Metabolic Pathways in Saccharomyces cerevisiae. *Biotechnology Journal* **2018,** *13* (9), 1700582.
33. Gilson, L.; Mahanty, H. K.; Kolter, R., Four plasmid genes are required for colicin V synthesis, export, and immunity. *J. Bacteriol.* **1987,** *169* (6), 2466.
34. Agapakis, C. M.; Boyle, P. M.; Silver, P. A., Natural strategies for the spatial optimization of metabolism in synthetic biology. *Nature Chemical Biology* **2012,** *8*, 527.

35. Grewal, P. S.; Modavi, C.; Russ, Z. N.; Harris, N. C.; Dueber, J. E., Bioproduction of a betalain color palette in Saccharomyces cerevisiae. *Metab. Eng.* **2018,** *45*, 180-188.
36. Jin, Y.-S.; Ni, H.; Laplaza, J. M.; Jeffries, T. W., Optimal Growth and Ethanol Production from Xylose by Recombinant Saccharomyces cerevisiae Require Moderate D-Xylulokinase Activity. *Appl. Environ. Microbiol.* **2003,** *69* (1), 495.
37. Gibson, D. G.; Young, L.; Chuang, R.-Y.; Venter, J. C.; Hutchison Iii, C. A.; Smith, H. O., Enzymatic assembly of DNA molecules up to several hundred kilobases. *Nature Methods* **2009,** *6*, 343.
38. Datsenko, K. A.; Wanner, B. L., One-step inactivation of chromosomal genes in Escherichia coli K-12 using PCR products. *Proceedings of the National Academy of Sciences* **2000,** *97* (12), 6640.

4.8 FIGURES

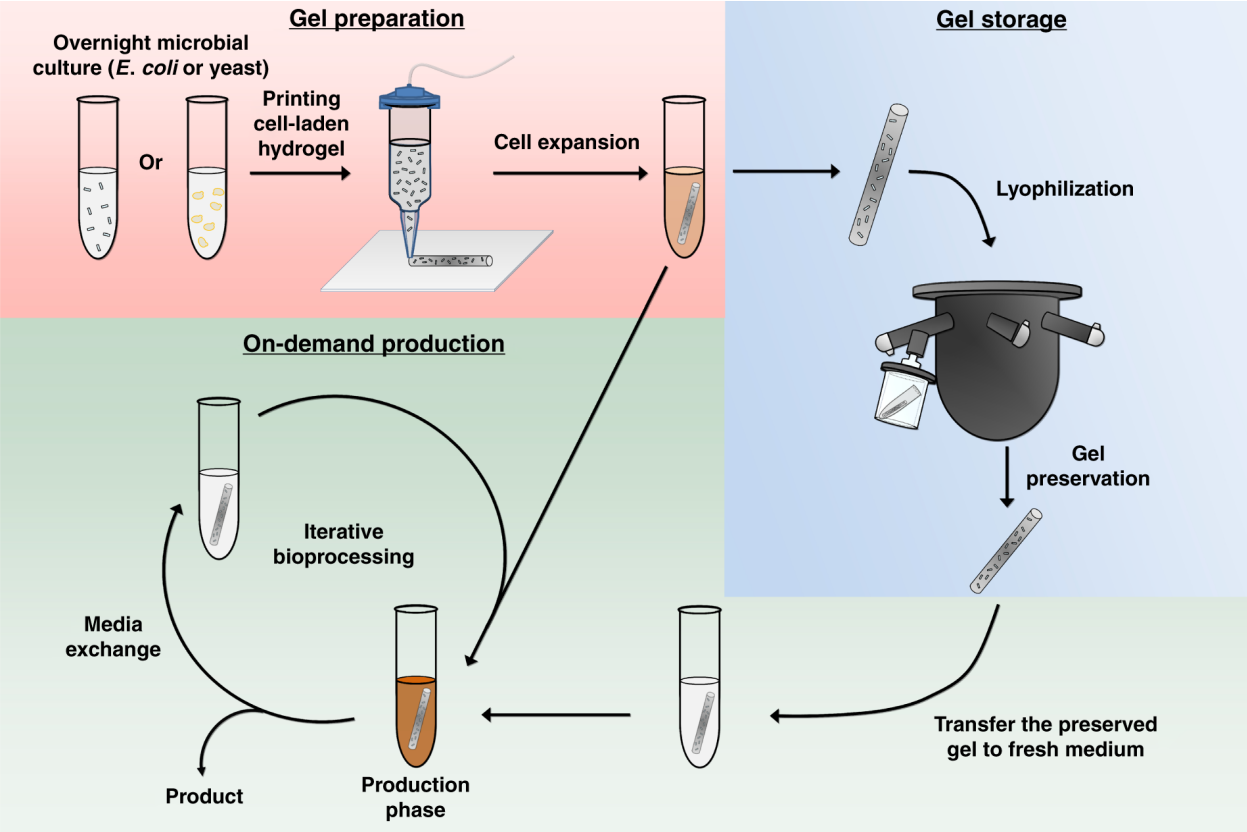

Figure 4.25. Overview of microbe-laden, extrusion-printed hydrogels for on-demand production

The hydrogel encapsulation and on-demand production process is divided into three parts. In the Gel Preparation stage, the printed and UV-cured microbial hydrogels are transferred to culture medium for cell outgrowth. While this initial outgrowth can also be used for production, the resulting cell-laden living materials can proceed to either the Gel Storage or On-Demand Production phase depending on user needs. In the Gel Storage stage, the microbial gels are treated with different types of preservation methods for storage and future use. The preserved gels are subsequently rehydrated and incubated in fresh medium to perform on-demand production, with iterative re-uses as desired.

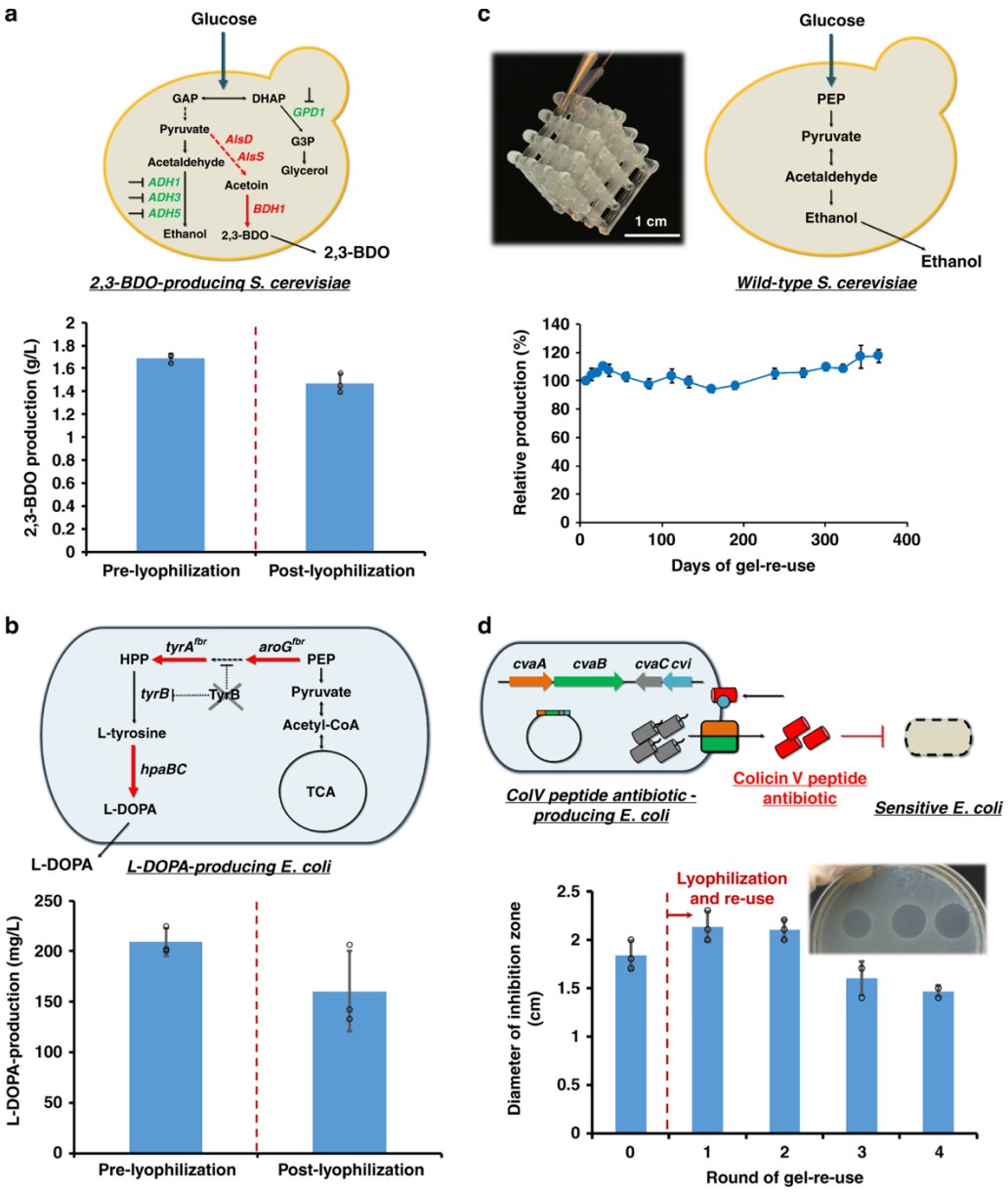

Figure 4.26. Re-use and preservation of mono-culture microbe-laden hydrogels

The fermentation performance of the printed hydrogel inks was tested for both bacterial (E. coli) and yeast (S. cerevisiae)-laden gels testing the production of 2,3-butanediol (a), L-DOPA (b), ethanol (c) and a peptide antibiotic (d). The production (pre- and post-preservation) is demonstrated in (a), (b), and (d). The production of ethanol from a year-long fermentation re-use process was evaluated using cell-laden hydrogel lattices (pictured top left in c. Scale bar: 1 cm). Data are mean ± s.d.; n = 3 biological replicates for (a), (b) and (d); n = 4 biological replicates for (c).

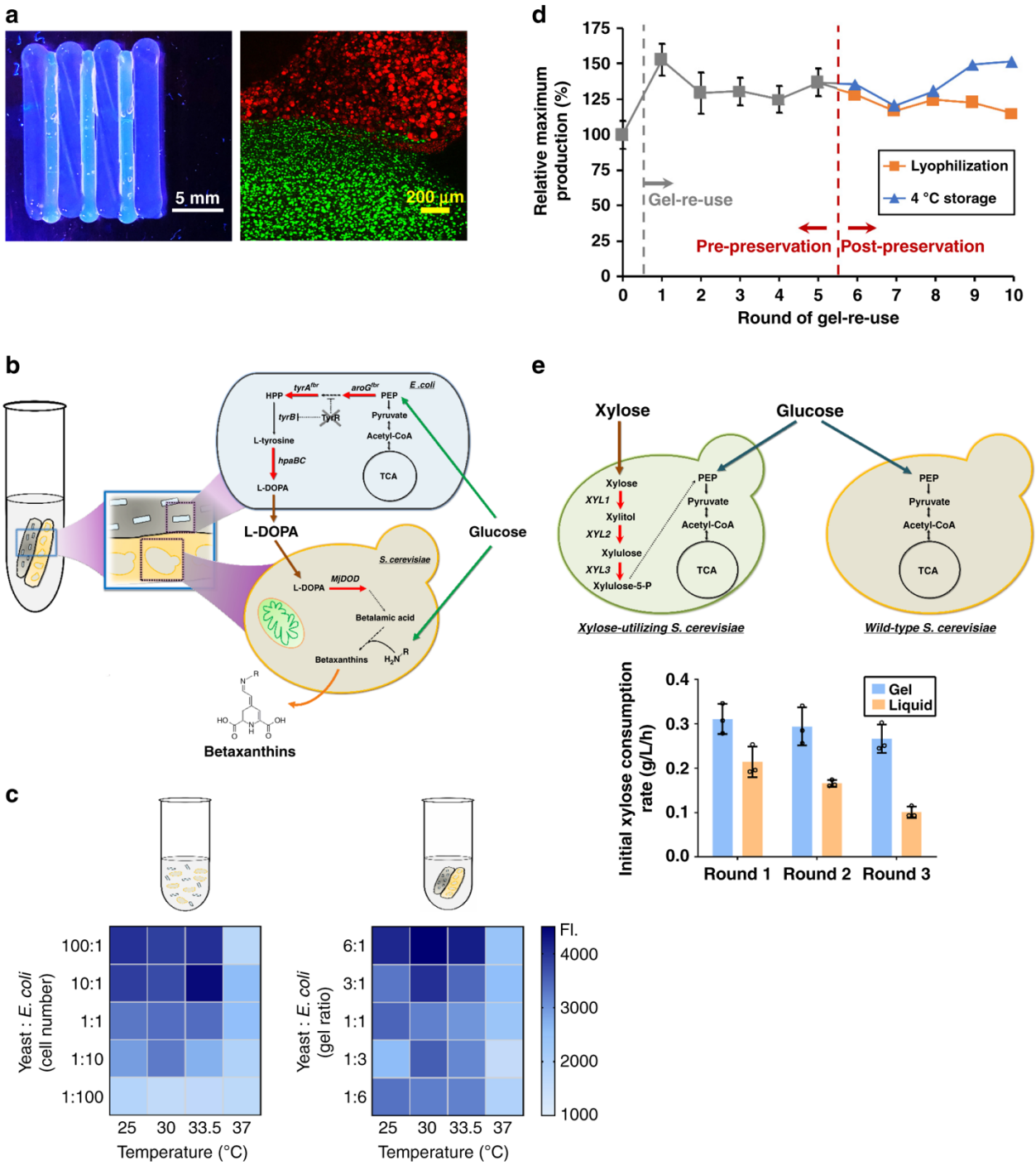

Figure 4.27. Spatially organized consortia in hydrogels outperforms tradition liquid co-culture systems

a Images of printed cell-containing hydrogel. Left: a UV-illuminated camera image of alternating stripes containing RFP yeast and GFP bacteria (scale bar: 5 mm). Right: confocal microscopy of 100 microns z-stack at the interface of these stripes. Little to no movement of cells out of their designed boundaries is observed at the interface (scale bar: 200 micron). b Schematic metabolic pathway of a commensal consortium E. coli–yeast for betaxanthins production. c Heat maps for betaxanthins consortia performance in the hydrogel and liquid-based culturing across altered cell number/gel ratios and fermentation temperatures. The color sale represents the intensity of betaxanthins fluorescence. d The reusability of 30 °C hydrogels with 6:1 (yeast:E.coli) gel ratio for betaxanthins production is compared pre- and post-lyophilization. e Glucose/xylose utilization via a parallel consortium with repeated use compared to liquid culture performance. Data are mean; n = 3 biological replicates for (c); data are mean ± s.d.; n = 3 biological replicates for (e); n = 2 biological replicates for (d) and gels after round 5 were split (n=1) for examining the impact of lyophilization and refrigerated storage on betaxanthins production.

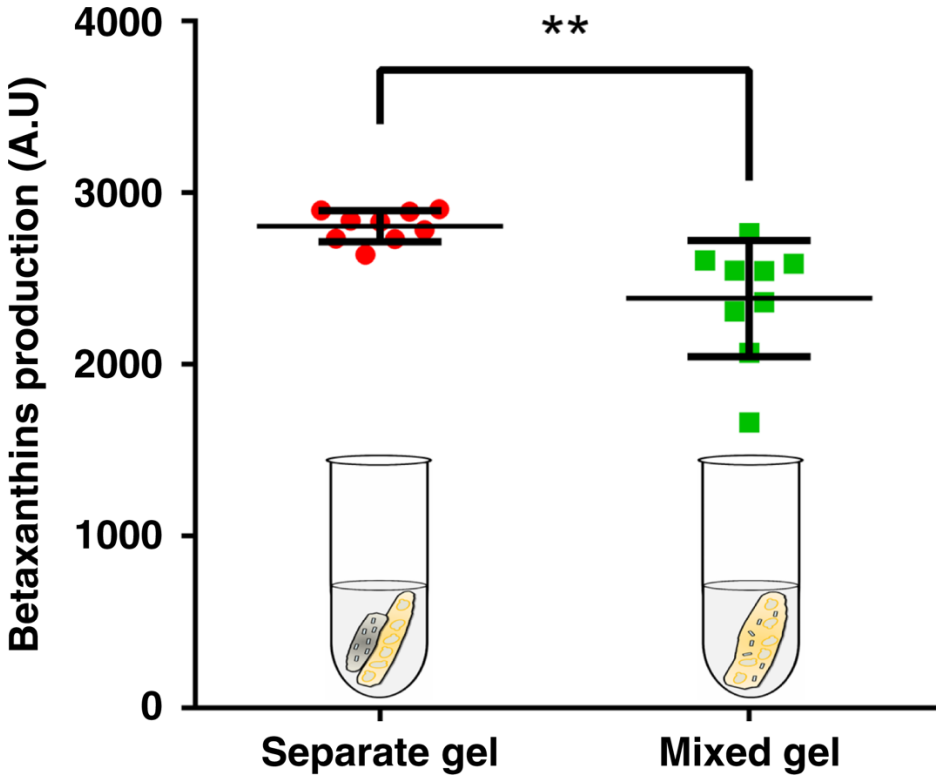

Figure 4.28. Spatial organization of microbial consortia improves on-demand production over a mixed gel

Betaxanthins production was compared between separate (printing E. coli and yeast gel separately) and mixed (mixing two species in the same gel) hydrogels. Both separate and mixed gels encapsulated the same initial number of consortia cells. Data are mean ± s.d.; n = 9 biological replicates. **p-value (0.0054) for the means of two groups was calculated using unpaired t test with Welch's correction. p-value (0.024) for the standard deviations of two groups was calculated using the Levene's test.

Chapter 5. CELL-LADEN HYDROGELS FOR MULTI-KINGDOM 3D PRINTING

This chapter has been adapted from the following manuscript:

> **Johnston, T. G.**; Fillman, J. P.; Priks, H.; Butelmann, T.; Tamm, T.; Kumar, R.; Lahtvee, P.-J.; Nelson, A. Cell-Laden Hydrogels for Multi-Kingdom 3D Printing. Accepted, *Macromol. Biosci.* **2020**.

5.1 ABSTRACT

Living materials are created through the embedding of live, whole cells into a matrix that can house and sustain the viability of the encapsulated cells. Through the immobilization of these cells, their bioactivity can be harnessed for applications such as bioreactors for the production of high-value chemicals. While the interest in living materials is growing, many existing materials lack robust structure and are difficult to pattern. Furthermore, many living materials employ only one type of microorganism, or microbial consortia with little control over the arrangement of the various cell types. In this work, a Pluronic F127-based hydrogel system was characterized for the encapsulation of algae, yeast, and bacteria to create living materials. This hydrogel system was also demonstrated to be an excellent material for additive manufacturing in the form of direct write 3D-printing to spatially arrange the cells within a single printed construct. These living materials allow for the development of incredibly complex, immobilized consortia, and the results detailed herein further the understanding of how cells behave within living material matrices. The utilization of these materials allows for interesting applications of multi-kingdom microbial cultures in immobilized bioreactor or biosensing technologies.

5.2 INTRODUCTION

Living materials are a class of materials that feature an interface of active, living cells within a polymeric network serving as an enclosure or matrix in which the cells reside.[1–7] Such materials offer a diverse series of possible applications, ranging from sensors and wearable devices to fermentation bioreactors.[1,2,6,7] Ideally, these materials should be easy to handle and process, promote viability and longevity of the enclosed cells, and produce physically robust structures for extended use. While there has been extensive work to encapsulate cells in polymeric matrices to produce living materials, many of commonly employed networks suffer from drawbacks such as low mechanical strength, or sensitivities to pH or ionic composition of the media.[8–17]

Pluronic F127 is a triblock copolymer comprised of poly(ethylene glycol)-b-poly(propylene glycol)-b-poly(ethylene glycol), which has been used as a material that offers a number of advantages for application in additive manufacturing. This polymer self-assembles into micelles in aqueous environments, and forms hydrogels at concentrations that range from 25-40 wt%. These hydrogels exhibit a reversible gelation temperature (T_{gel}) at approximately 17 °C, below which the gel transforms into its sol state. This feature of these hydrogels allows for easy loading of cells into the material at temperatures below the T_{gel}, and allows the mixture to re-gel at ambient temperature (21° C). Additionally, the resulting hydrogels are shear-thinning, and when this shear force is removed, the hydrogels are self-supporting. Thus, these hydrogels can be extruded via a syringe and nozzle in a patternwise manner using a direct-write 3D printer to form multi-layered 3D objects. In our previous work, we fabricated immobilized-cell bioreactors using cell-laden Pluronic F127 derivative (F127-dimethacrylate (F127-DMA)[1] and F127-bisurethane methacrylate (F127-BUM))[18,19] hydrogels (Figure 5.1) for the production of small molecules and peptides.[2] The conserved biological activity of these microbial species suggested that the viability and

fermentative capability of the encapsulated cells is comparable to, or even greater than that of the free-cell system in liquid culture.

Naturally occurring biofilms are microenvironments in which cells adhere to one another and quite often to a surface.[20,21] The production of an extracellular matrix, comprised of a variety of polymeric substances such as polysaccharides, DNA, and proteins, provides a three-dimensional architecture in which one or more microbial species can organize and coexist. These hydrogel matrices are also capable of changing the phenotype of encapsulated cells, while providing other benefits such as protection from environment and resistance to antibiotics.[22–25] With the advent of multi-material 3D printing,[26–31] new capabilities are emerging that will enable the creation of synthetic hydrogel structures that can approximate the microenvironment of biofilms.[32–34]

While there is growing research that details the development of materials for cellular encapsulation for the production of living material bioreactors,[35–42] there are few reports of multi-material printed objects with more than one microorganism, and our understanding of the mobility of the immobilized cells (particularly through F127-based hydrogel matrices) is still lacking. In this study, we present an investigation of F127-BUM hydrogel inks for multi-material printing objects that are comprised of up to three microorganisms from different taxonomic kingdoms. We show that yeast, bacteria, and algae are all capable of being encapsulated within the hydrogel matrix and 3D-printed into complex structures through the use of Computer Aided Design (CAD), and our multi-material direct write extrusion printer (Figure 5.2). Furthermore, we show that the encapsulated cells exhibit excellent viability over an incubation of one week in a consortium print. We also show through microscopy that the cells remain confined to their designed architecture, resisting cross contamination from microbes housed elsewhere in the overall hydrogel construct, or in the surrounding media during incubation. These results suggest that F127-BUM living

materials continue to offer exciting possibilities for the study of microbial consortium, or the utilization of the bioactivity of the printed cells.

5.3 Results and Discussion

We employed hydrogel formulations of 30 w/w% F127-bisurethane methacrylate (F127-BUM) in this study, as we have previously determined that the viscoelastic properties of the hydrogel at this concentration is ideal for extrusion-based printing.18,19 In addition to exhibiting a yield-stress of 946.8 Pa, the hydrogels were shear-thinning and rapidly recovered their storage modulus after extrusion. As a result, these hydrogels can be extrusion printed to form multi-layered hydrogel constructs. One such print is shown in Figure 5.2. Each ink segment is 15 mm long and 15 mm wide, with a height of 2 mm, with two strands of ink spanning the interior of the structure. Three total ink segments are stacked atop on another during the printing process, giving the complete structure a height of 6 mm. After the entire object was printed, the methacrylate end groups of F127-BUM were polymerized during a UV-cure step to afford cross-linked, elastomeric hydrogels. Without chemical fixation, the printed structures dissolved over time when placed in aqueous media. The chemical cross-linking step instead affords a robust structure that does not degrade in media, even over an incubation period of one year.[19]

Three different hydrogel inks based on 30 w/w% F127-BUM were investigated, each embedded with a different strain of microorganism: bacteria, algae, and yeast, which will be referred to as B-ink, A-ink, and Y-ink. These inks were identical in composition aside from the cells contained within. The hydrogel inks were inoculated by first cooling the hydrogel below its gelation temperature (~17 °C) to induce its reversible gel-sol transition. After seeding cells into the sol, the mixture was briefly stirred then warmed to ambient temperature (21 °C) to afford the respective cell-laden hydrogels.

Each of the microbe-laden hydrogel inks was transferred to a syringe fitted with a 27-gauge nozzle for direct-write 3D printing. As a first demonstration of multi-material printing, we created objects with two different inks printed in a spatially controlled manner based on a CAD model. This model consisted of one strand of each ink printed in contact with one another. The total length of the print was 20 mm, and the width was 2 mm. We observed that for all of the ink combinations (B-ink/A-ink, B-ink/Y-ink, and A-ink, Y-ink), the F127-BUM hydrogel afforded discrete deposition of the cell-laden material without visible indication of the deposited inks blending together.

To ensure the viability of the encapsulated yeast, bacteria, and algae cells within the F127-BUM hydrogel formulations, we incorporated microbes that were capable of constitutively expressing red fluorescence for analysis with fluorescence confocal microscopy. At time intervals of 1, 3, and 7 d, the hydrogels were stained to probe viability. Over the week of testing, all three cell types showed viability of >90%. Thus, F127-BUM hydrogels can maintain the viability of these different microbial strain combinations, and are suitable for consortia studies (Figure 5.3).

The printed and cross-linked F127-BUM hydrogels also successfully maintained isolated populations of microbes within their respective inks. Microbial cells embedded within hydrogel matrices are known to escape into the surrounding media over time.[1] Interestingly, the cells did not infiltrate into printed regions of hydrogel, which included independently printed adjacent hydrogel regions that were in physical contact with each other, as well as cells in the surrounding aqueous media penetrating into the hydrogel. The migration of cells across a multi-material hydrogel interface was investigated using linear filaments of B-ink and Y-ink that were printed side-by-side in physical contact with one another. Irradiation with UV light after printing afforded the cross-linked multi-material construct. Because the photo-curing was performed after the entire

construct was printed, the cross-linking occurs across the boundary of the hydrogels to afford a continuous hydrogel network. The printed construct was then incubated in a 1:1 SC:LB media mixture for 7 d. At periods of 1, 3, and 7 d, the samples were imaged with confocal microscopy. Across a depth of 100 μm at the interface of the two hydrogels, there was little to no migration of cells from one printed filament into the neighboring hydrogel (Figure 5.4).

To explore possible contamination from the surrounding growth media, samples of red fluorescing yeast hydrogel and green fluorescing bacterial hydrogel were printed separately. These samples were cured and then submersed into liquid culture samples of the alternate microbial species in a 1:1 SC:LB media mixture for 7 d (i.e., printed and cured Y-ink incubated in media with E. coli, and printed and cured B-ink incubated in media with S. cerevisiae). At the end of the incubation period, the hydrogels were removed from the growth media, and the exterior of the hydrogels were imaged with confocal microscopy to look for cell invasion into the cured hydrogels. For the printed bacterial hydrogels, the yeast cells were not observed to have migrated into the hydrogel. The results for the printed yeast hydrogels were similar, although bacterial cells appeared to adhere to the hydrogel surface. Thus, the cross-linked F127-BUM hydrogel is effective as a protective medium for the immobilized cell culture that can prevent contamination by other potentially invasive cells.

Optical microscopy and scanning electron microscopy were utilized to further explore cell distribution within the hydrogels when incubated in aqueous media. Samples of yeast-laden hydrogel were incubated in minimal media and imaged at the end of a 7 d incubation period. The optical microscope images of the hydrogel cross-section show that yeast colonies form within the hydrogel matrix, and the colonies closer to the periphery of the hydrogel were larger than the colonies toward the center. This phenomenon was likely a consequence of a gradient of nutrients

that forms within the hydrogel. The cells present closer to the hydrogel surface can consume nutrients that diffuse into the hydrogel, which leads to a lower concentration of these nutrients toward the hydrogel core. These results were confirmed with scanning electron microscopy imaging of the cell-laden hydrogels, as seen in Figure 5.5. Printing structures with features thicker than 500 μm provides a more durable structure, but likely does not provide adequate diffusion of nutrients to the cells at the core of the hydrogel.

5.4 CONCLUSIONS

In conclusion, we have shown that the F127-BUM hydrogel living materials were capable of promoting excellent cell viability for multiple kingdoms of microbes and can serve as a protective matrix for the immobilized cells. The use of a multi-material 3D printer enabled the deposition of hydrogel inks embedded with a microbial species (*S. cerevisiae*, *E. coli*, or algae) into a single printed part, while microscopy confirms that the cells remain confined to their respective printed regions. While cells were observed to escape into the surrounding aqueous medium after several days of incubation, we observed no evidence of the infiltration of cells in liquid suspension into the hydrogel. Moreover, cells did not migrate across boundaries of adjacent printed regions of cell-laden hydrogels. This 3D printing compatibility of the F127-BUM hydrogels, coupled with the precise seclusion of the various microbial species will allow for future investigations into cell-cell interactions and behavior of microbial consortia, or the utilization of these consortia for distributed metabolic processes in biomanufacturing. The ease of patterning with F127-BUM hydrogels, coupled with its cell-friendly characteristics detailed here and in our previous work offers a flexibility of consortium studies and applications that have not yet been possible with other existing materials or liquid culture schemes.

5.5 EXPERIMENTAL

5.5.1 *Materials*

Pluronic® F-127 (P2443-1KG; referred to as F127) and 2-hydroxy-4′-(2-hydroxyethoxy)-2-methylpropiophenone (410896-10 G; 98%), and 2-acrylamido-2-methyl-1-propanesulfonic acid sodium salt solution (655821-250 ML; 50 wt%; referred to as AMPS) were all purchased from Sigma Aldrich. Dibutyltin dilaurate (D0303; >95.0%) was purchased from TCI America. 2-Isocyanatoethyl methacrylate (ACT34296) was purchased from Arctom Chemicals. CDCl3 (DLM-7-PK; 99.8%) was purchased from Cambridge Isotope Laboratories. Common solvents (Certified ACS) were purchased from Fisher Scientific. Media components were purchased from US Biological Life Sciences. Sytox Green nucleic acid strain (5 mM solution in DMSO; Invitrogen) was purchased from Thermo Fisher Scientific.

5.5.2 *Microbial strains/information*

Microbes employed in this study include *Saccharomyces cerevisiae*, *Escherichia coli*, and *Chlamydomonas reinhardtii*. For microscopy and Live/Dead viability tests, the yeast strain yJS001 was used (genotype SO992 mfa2::pTEF1_mCherry(kanR)). The bacteria strain CD02 was used (genotype [MG1655] nfsA::BBa J23119-sfGFP; KanR). For scanning electron microscopy and optical microscopy, the *S. cerevisiae* strain CEN.PK113-7D (*MATa, MAL2-8^c, SUC2*) was used.

5.5.3 *Polymer synthesis/functionalization*

This procedure was adapted from previous works.[18] Glassware was oven-dried at 125 °C for at least 16 h. F127 (60 g, 4.8 mmol) was dried under vacuum (~ 2 Pa) for at least 16 h at room temperature in a round-bottom flask. Anhydrous CH_2Cl_2 (550 mL) was charged to the flask under an N_2 atmosphere. The mixture was stirred at 30 °C, and following complete dissolution of the

F127, dibutyltin dilaurate (12 drops) was added using a glass Pasteur pipette. The 2-isocyanatoethyl methacrylate (3.5 mL, 24.8 mmol) was diluted in anhydrous CH_2Cl_2 (50 mL) and was added to the reaction mixture at a rate of approximately 1 drop/s. The reaction was allowed to proceed while stirring under dry N_2 at 30 °C. After 2 d, the reaction was quenched by the addition of MeOH (60 mL), and the mixture was concentrated at 30 °C using a rotary evaporator. The F127-BUM was precipitated in Et_2O (2000 mL). During the precipitation, Et_2O was stirred in a large conical flask, and the concentrate was poured in slowly. The precipitate mixture was stirred for an additional 15 min before separation via centrifugation. Eight 50 mL centrifuge tubes were filled with precipitate mixture and centrifuged (3000 g) for approximately 10 min. The transparent supernatant in each tube was decanted from the F127-BUM pellet, and more of the precipitate mixture was added on top of each pellet. This process was repeated until all of the precipitate had been collected in the eight centrifuge tubes, and all of the solvent had been discarded. The F127-BUM precipitate was then washed twice. Each wash was performed by adding Et_2O (approximately 30 mL) to each pellet and vortex-mixing until redispersion of the precipitate was observed; redispersion was followed by centrifugation (3000 g) for re-separation of the F127-BUM precipitate, and supernatants were again discarded. After washing, the F127-BUM from each tube was pooled and transferred to a large beaker. Excess ether was allowed to evaporate while agitating the F127-BUM with a spatula under an N_2 atmosphere. The resultant F127-BUM powder was dried fully overnight at room temperature under vacuum (~ 2 Pa) and stored in the dark at 4 °C until further use.

5.5.4 *Preparation of media*

To prepare COREs media, $MgSO_4 \cdot 7H_2O$ (50 g/L), KCl (3g/L), NH_4Cl (2.68 g/L), $NaNO_3$ (20 g/L), Beta-glycerophosphate (2.16 g/L), H_3BO_3 (0.8 g/L), $Na_2EDTA \cdot 2H_2O$ (8 g/L), $FeCl_3 \cdot$

$6H_2O$ (1 g/L), $CaCl_2 \cdot 2H_2O$ (75 g/L), 3.86M NaCl (225.6 g/L), 3M Tris base (363.42 g/L), $MnCl_2 \cdot 4H_2O$ (0.2 mg/L), $ZnSO_4 \cdot 7H_2O$ (40 μg/L), $CoCl_2 \cdot 6H_2O$ (8 μg/L), $Na_2MoO_4 \cdot 6H_2O$ (20 μg/L), $Na_3VO_4 \cdot H_2O$ (2 μg/L), H_2SeO_3 (2 μg/L), Vitamin B12 (0.5 mg/L dH2O), Biotin (50 μg/L dH2O), Thiamine • HCl (100 μg/L), and 2 mL of soil extract were dissolved in Milli-Q water. The media was autoclaved for 30 minutes for sterilization. To prepare LB media (1L), lysogeny broth mix (25 g) was dissolved in Milli-Q water and autoclaved for 60 minutes for sterilization. To prepare SC media (1L), drop-out mix (2 g), yeast nitrogen base (6.7 g), and glucose (20 g) were dissolved in Milli-Q water. The resulting solution was sterilized by filtration through a 0.2 μm nylon filter.

5.5.5 *Preparation of hydrogels*

F127-BUM was dissolved in sterile, deionized water at a concentration of 30 wt % polymer. The resulting polymer solution was cooled overnight at 5 °C to facilitate homogenous hydrogel formation via lower critical solution behavior. For chemical curing of patterned structures, the photo-radical initiator 2-hydroxy-2-methylpropiophenone (10 μL for every 10 g of hydrogel solution) was added. After homogenization, the solution was warmed to room temperature to induce the formation of a gel state.

5.5.6 *Preparation of microbial hydrogels*

To prepare microbe-laden hydrogels, the aforementioned hydrogel solution was cooled to 5 °C in a refrigerator. At this temperature, the hydrogel solution underwent gel-to-sol transition, affording a free-flowing liquid. cells were added from an overnight liquid culture, at a concentration of 10^7 cells per gram of hydrogel while the gel was in its solution state. The resulting solution was mixed thoroughly and allowed to equilibrate at 5 °C until all of the bubbles present

in the solution were removed. Finally, the hydrogel was warmed to 21 °C to undergo a sol to gel transition, resulting in a shear-responsive gel.

5.5.7 *3D-printing of microbial hydrogels*

A modified pneumatic direct-write 3D printer was assembled based on a Tronxy P802E 3D Printer kit, from Shenzen Tronxy Technology Co. The printer was controlled with an Arduino using the Marlin firmware. All computer aided design (CAD) models were designed in OpenSCAD. G-code commands for the printer were generated using Slic3r. The resulting G-code was modified using Python to introduce required commands for the dispensing of the hydrogel via pneumatic pressure. All printing was performed using a 30 wt % hydrogel ink with an extrusion air pressure of 20 psi, a print speed of 5 mm s-1, and a 0.41 mm inner diameter CML Supply conical nozzle attachment. Upon completion of the 3D printing, the structures were irradiated under 365 nm light (at 3.4 mW/cm2) for 3 min to cure and chemically fix the structures.

5.5.8 *Optical and Confocal Imaging*

Images of the 3D-printed hydrogels were captured using an iPhone XS. Confocal microscopy images were taken using a Leica TCS SP5 II laser scanning confocal microscope. All images were taken with a dry 20x objective. MCherry protein fluorescence was excited with a 561 nm laser at 5% laser power, and emission was scanned from 569 to 700 nm. GFP and Sytox green viability dye was excited with a 488 nm laser at 5% laser power, and emission was scanned from 500 to 550 nm. Samples were sequentially scanned and the output images were processed using ImageJ Java software.

5.5.9 *Live/dead imaging*

The microbe-laden hydrogels were prepared as described above. The microbial gels were then 3d-printed in culture pairs (algae and bacteria, algae and yeast, yeast and bacteria). These samples were irradiated with 365 nm UV light for 3 min to produce a single, rigid structure comprised of two hydrogel inks. These structures were then incubated in mixed growth media determined by the microbes present in the structures (LB for bacteria, SC for yeast, and COREs for algae). The samples were agitated at 30 °C, and the media was exchanged every 24 h to ensure fresh nutrient delivery to the embedded cells. At the imaging intervals described in this work, a small cross section of the structure was cut and removed for staining. Sytox Green stain stock solution was diluted to 5 μM, and 20 μL of the dye solution was exposed to the hydrogel sample for 5 min. The sample was then washed and imaged using a Leica SP5 confocal microscope.

5.5.10 *Cell segregation imaging*

Cell segregation studies were conducted by printing strands of yeast (*S. cerevisiae*)- and bacteria (*E. coli*)-laden hydrogel in contact with one another, by utilizing the two-material printing capabilities of the pneumatic-driven 3D printer. Bacteria and yeast were both seeded at concentrations of 10^7 cells/gram of hydrogel. Strands of the two hydrogel samples were printed in contact with one another and cured. The resulting structures were submerged incubated at 30 °C in 1:1 SC:LB media and imaged under confocal microscopy at 1, 3, and 7 days. The interface between the strands was imaged across 100 microns, with images taken at steps of approximately 3 microns. The resulting z-stacks were merged into one image to ensure the integrity of the interface through the thickness of the printed structure. E. coli used in this study are shown in the green channel, and yeast are shown in the red channel. All images were taken with a dry 10x objective. mCherry fluorescence was excited with a 561 nm laser at 5% laser power, and emission

was scanned from 569 to 700 nm. GFP fluorescence was excited with a 488 nm laser at 5% laser power, and emission was scanned from 500 to 550 nm.

5.5.11 *Cell invasion study*

To study the possible invasion of foreign cells from surrounding media into the printed hydrogels, overnight samples were prepared of the fluorescent yeast and bacteria. Samples of yeast and bacteria hydrogel were printed, and then submerged into diluted liquid culture in a LB-SC media mixture. These samples were incubated in a 30 °C shaker to promote microbial growth. The liquid culture was re-diluted in fresh media every two days to ensure cell survival both inside and outside the hydrogel. After a period of one week, the samples were removed from media and imaged with confocal microscopy.

5.5.12 *SEM imaging / Light microscopy imaging*

For scanning electron microscopy and optical microscopy, slightly different conditions were applied: Hydrogels were established in with phosphate buffered saline. The amount of photoinitiator was 1.5 µL per gram gel. The amount of cells used in the study was 10^6 cells per gram of gel. 3D printing was performed on a RepRap 3drag printer modified to be applicable for direct pressure dispensation. The computer-aided design model was designed with Solidworks and the G-code was generated using Slic3r. The model's measures were 10 x 3 x 3.5 mm (X, Y, Z) sliced with one perimeter. The nozzle print speed was 10 mm s^{-1}. The UV curing time was 60 s.

A minimal medium (MM) was used for cultivation. The composition of 1 L MM (pH = 6.9) was 10 g glucose, 2.5 g of $(NH_4)2SO_4$, 3 g of KH_2PO_4, 5.25 g of K_2HPO_4 and 0.25 g of $MgSO_4$ in Milli-Q water. 1mL trace element solution and vitamin solution each, as mentioned in Lahtvee *et al*. (2016), was added [43]. Batch cultivation of yeast-laden hydrogels was done in 5mL MM for 7 d

at 30°C and 200 rpm agitation. Medium was replaced every 24 h. The samples for SEM used in this study where pretreated as described in the literature.[44] Briefly, the samples were fixed with 3.7 % formaldehyde in 0.1 M phosphate buffer (Sörensen) for 48 h, dehydrated in an ascending ethanol series and critical point dried with CO_2 (Quorum Technologies). Dried samples where frozen in liquid N_2 and cut with cooled scalpel. Cross sections where sputter coated with a layer thickness of 7.5 nm of gold (Leica EM ACE600) and imaged with TM3000 Tabletop SEM (Hitachi) with 15 kV accelerating voltage. The samples for OM were fixed and dehydrated in the same way as the SEM samples. At the last step, they were transferred to 100% acetone and embedded in liquid paraffin. After cooling, the samples were cut with a microtome (Leica RM2255; 40 µm slices) and recovered on a glass slide, covered with 20 µL of dH_2O and a cover glass. Imaging was performed with a Leica DM750 microscope equipped with a Leica ICC50 HD camera system.

5.6 ACKNOWLEDGEMENTS

A.N. acknowledges the National Science Foundation (Grant No. 1752972), UW CoMotion Innovation Grant and UW Royalty Research Fund, 3M Non-Tenured Faculty Award for financial support. TB and PJL acknowledge funding from the European Union's Horizon 2020 research and innovation program under grant agreement No 668997, and the Estonian Research Council (grant PUT1488P).

5.7 REFERENCES

1. Saha, A.; Johnston, T. G.; Shafranek, R. T.; Goodman, C. J.; Zalatan, J. G.; Storti, D. W.; Ganter, M. A.; Nelson, A. Additive Manufacturing of Catalytically Active Living Materials. *ACS Appl. Mater. Interfaces* **2018**, *10* (16), 13373–13380.

2. Johnston, T. G.; Fellin, C. R.; Carignano, A.; Nelson, A. Poly(Alkyl Glycidyl Ether) Hydrogels for Harnessing the Bioactivity of Engineered Microbes. *Faraday Discuss.* **2019**.
3. Niwas, R.; Singh, V.; Singh, R.; Pant, G.; Mitra, K.; Tripathi, C. K. M. Cholesterol Oxidase Production from Entrapped Cells of Streptomyces Sp. *J. Basic Microbiol.* **2014**, *54* (11), 1233–1239.
4. Kumaravel, V.; Gopal, S. R. Immobilization of Bacillus Amyloliquefaciens MBL27 Cells for Enhanced Antimicrobial Protein Production Using Calcium Alginate Beads. *Biotechnol. Appl. Biochem.* **2010**, *57* (3), 97–103.
5. Connell, J. L.; Ritschdorff, E. T.; Whiteley, M.; Shear, J. B. 3D Printing of Microscopic Bacterial Communities. *Proc. Natl. Acad. Sci.* **2013**, *110* (46), 18380–18385.
6. Schaffner, M.; Rühs, P. A.; Coulter, F.; Kilcher, S.; Studart, A. R. 3D Printing of Bacteria into Functional Complex Materials. *Sci. Adv.* **2017**, *3* (12), eaao6804.
7. Liu, X.; Tang, T.-C.; Tham, E.; Yuk, H.; Lin, S.; Lu, T. K.; Zhao, X. Stretchable Living Materials and Devices with Hydrogel–Elastomer Hybrids Hosting Programmed Cells. *Proc. Natl. Acad. Sci.* **2017**, *114* (9), 2200–2205.
8. Lehner, B. A. E.; Schmieden, D. T.; Meyer, A. S. A Straightforward Approach for 3D Bacterial Printing. *ACS Synth. Biol.* **2017**, *6* (7), 1124–1130.
9. Higashi, K.; Ogawa, M.; Fujimoto, K.; Onoe, H.; Miki, N. Hollow Hydrogel Microfiber Encapsulating Microorganisms for Mass-Cultivation in Open Systems. *Micromachines* **2017**, *8* (6), 176.
10. Qian, F.; Zhu, C.; Knipe, J. M.; Ruelas, S.; Stolaroff, J. K.; DeOtte, J. R.; Duoss, E. B.; Spadaccini, C. M.; Henard, C. A.; Guarnieri, M. T.; Baker, S. E. Direct Writing of Tunable Living Inks for Bioprocess Intensification. *Nano Lett.* **2019**, *19* (9), 5829–5835.
11. Schmieden, D. T.; Basalo Vázquez, S. J.; Sangüesa, H.; van der Does, M.; Idema, T.; Meyer, A. S. Printing of Patterned, Engineered *E. Coli* Biofilms with a Low-Cost 3D Printer. *ACS Synth. Biol.* **2018**, *7* (5), 1328–1337.
12. Kadilak, A. L.; Rehaag, J. C.; Harrington, C. A.; Shor, L. M. A 3D-Printed Microbial Cell Culture Platform with *in Situ* PEGDA Hydrogel Barriers for Differential Substrate Delivery. *Biomicrofluidics* **2017**, *11* (5), 054109.
13. Desai, R. M.; Koshy, S. T.; Hilderbrand, S. A.; Mooney, D. J.; Joshi, N. S. Versatile Click Alginate Hydrogels Crosslinked via Tetrazine–Norbornene Chemistry. *Biomaterials* **2015**, *50*, 30–37.
14. Li, P.; Müller, M.; Chang, M. W.; Frettlöh, M.; Schönherr, H. Encapsulation of Autoinducer Sensing Reporter Bacteria in Reinforced Alginate-Based Microbeads. *ACS Appl. Mater. Interfaces* **2017**, *9* (27), 22321–22331.
15. Smith, M. J.; Francis, M. B. Improving Metabolite Production in Microbial Co-Cultures Using a Spatially Constrained Hydrogel: Improving Metabolite Production in Microbial Co-Cultures. *Biotechnol. Bioeng.* **2017**, *114* (6), 1195–1200.
16. Huang, J.; Liu, S.; Zhang, C.; Wang, X.; Pu, J.; Ba, F.; Xue, S.; Ye, H.; Zhao, T.; Li, K.; Wang, Y.; Zhang, J.; Wang, L.; Fan, C.; Lu, T. K.; Zhong, C. Programmable and Printable Bacillus Subtilis Biofilms as Engineered Living Materials. *Nat. Chem. Biol.* **2019**, *15* (1), 34–41.
17. Kandemir, N.; Vollmer, W.; Jakubovics, N. S.; Chen, J. Mechanical Interactions between Bacteria and Hydrogels. *Sci. Rep.* **2018**, *8* (1), 10893.
18. Millik, S. C.; Dostie, A. M.; Karis, D. G.; Smith, P. T.; McKenna, M.; Chan, N.; Curtis, C. D.; Nance, E.; Theberge, A. B.; Nelson, A. 3D Printed Coaxial Nozzles for the Extrusion of

Hydrogel Tubes toward Modeling Vascular Endothelium. *Biofabrication* **2019**, *11* (4), 045009.
19. Johnston, T. G.; Yuan, S.-F.; Wagner, J. M.; Yi, X.; Saha, A.; Smith, P.; Nelson, A.; Alper, H. S. Compartmentalized Microbes and Co-Cultures in Hydrogels for on-Demand Bioproduction and Preservation. *Nat. Commun.* **2020**, *11* (1), 563.
20. Arciola, C. R.; Campoccia, D.; Speziale, P.; Montanaro, L.; Costerton, J. W. Biofilm Formation in Staphylococcus Implant Infections. A Review of Molecular Mechanisms and Implications for Biofilm-Resistant Materials. *Biomaterials* **2012**, *33* (26), 5967–5982.
21. Simões, M.; Simões, L. C.; Vieira, M. J. A Review of Current and Emergent Biofilm Control Strategies. *LWT - Food Sci. Technol.* **2010**, *43* (4), 573–583.
22. Høiby, N.; Bjarnsholt, T.; Givskov, M.; Molin, S.; Ciofu, O. Antibiotic Resistance of Bacterial Biofilms. *Int. J. Antimicrob. Agents* **2010**, *35* (4), 322–332.
23. Stewart, P. S. Mechanisms of Antibiotic Resistance in Bacterial Biofilms. *Int. J. Med. Microbiol.* **2002**, *292* (2), 107–113.
24. Stewart, P. S.; William Costerton, J. Antibiotic Resistance of Bacteria in Biofilms. *The Lancet* **2001**, *358* (9276), 135–138.
25. Mah, T.-F.; Pitts, B.; Pellock, B.; Walker, G. C.; Stewart, P. S.; O'Toole, G. A. Biofilm Antibiotic Resistance. **2003**, *426*, 5.
26. Schiele, N. R.; Corr, D. T.; Huang, Y.; Raof, N. A.; Xie, Y.; Chrisey, D. B. Laser-Based Direct-Write Techniques for Cell Printing. *Biofabrication* **2010**, *2* (3), 032001.
27. Kokkinis, D.; Schaffner, M.; Studart, A. R. Multimaterial Magnetically Assisted 3D Printing of Composite Materials. *Nat. Commun.* **2015**, *6* (1), 8643.
28. Hardin, J. O.; Ober, T. J.; Valentine, A. D.; Lewis, J. A. Microfluidic Printheads for Multimaterial 3D Printing of Viscoelastic Inks. *Adv. Mater.* **2015**, *27* (21), 3279–3284.
29. Rutz, A. L.; Hyland, K. E.; Jakus, A. E.; Burghardt, W. R.; Shah, R. N. A Multimaterial Bioink Method for 3D Printing Tunable, Cell-Compatible Hydrogels. *Adv. Mater.* **2015**, *27* (9), 1607–1614.
30. Compton, B. G.; Lewis, J. A. 3D-Printing of Lightweight Cellular Composites. *Adv. Mater.* **2014**, *26* (34), 5930–5935.
31. Bandyopadhyay, A.; Heer, B. Additive Manufacturing of Multi-Material Structures. *Mater. Sci. Eng. R Rep.* **2018**, *129*, 1–16. https://doi.org/10.1016/j.mser.2018.04.001.
32. Roell, G. W.; Zha, J.; Carr, R. R.; Koffas, M. A.; Fong, S. S.; Tang, Y. J. Engineering Microbial Consortia by Division of Labor. *Microb. Cell Factories* **2019**, *18* (1), 35.
33. Zhang, H.; Wang, X. Modular Co-Culture Engineering, a New Approach for Metabolic Engineering. *Metab. Eng.* **2016**, *37*, 114–121. https://doi.org/10.1016/j.ymben.2016.05.007.
34. McCarty, N. S.; Ledesma-Amaro, R. Synthetic Biology Tools to Engineer Microbial Communities for Biotechnology. *Trends Biotechnol.* **2019**, *37* (2), 181–197.
35. Díaz, M. P.; Boyd, K. G.; Grigson, S. J. W.; Burgess, J. G. Biodegradation of Crude Oil across a Wide Range of Salinities by an Extremely Halotolerant Bacterial Consortium MPD-M, Immobilized onto Polypropylene Fibers: Biodegradation of Crude by Immobilised Bacteria. *Biotechnol. Bioeng.* **2002**, *79* (2), 145–153.
36. Dwyer, D. F.; Krumme, M. L.; Boyd, S. A.; Tiedje, J. M. Kinetics of Phenol Biodegradation by an Immobilized Methanogenic Consortium. *Appl. Environ. Microbiol.* **1986**, *52* (2), 345–351.
37. Fang, H.; Wenrong, H.; Yuezhong, L. Investigation of Isolation and Immobilization of a Microbial Consortium for Decoloring of Azo Dye 4BS. *Water Res.* **2004**, *38* (16), 3596–3604.

38. Patel, Y.; Gupte, A. Biological Treatment of Textile Dyes by Agar-Agar Immobilized Consortium in a Packed Bed Reactor. *Water Environ. Res.* **2015**, *87* (3), 242–251.
39. Pattanasupong, A.; Nagase, H.; Sugimoto, E.; Hori, Y.; Hirata, K.; Tani, K.; Nasu, M.; Miyamoto, K. Degradation of Carbendazim and 2,4-Dichlorophenoxyacetic Acid by Immobilized Consortium on Loofa Sponge. *J. Biosci. Bioeng.* **2004**, *98* (1), 28–33.
40. Su, Y.; Zhang, Y.; Wang, J.; Zhou, J.; Lu, X.; Lu, H. Enhanced Bio-Decolorization of Azo Dyes by Co-Immobilized Quinone-Reducing Consortium and Anthraquinone. *Bioresour. Technol.* **2009**, *100* (12), 2982–2987.
41. Wondraczek, L.; Pohnert, G.; Schacher, F. H.; Köhler, A.; Gottschaldt, M.; Schubert, U. S.; Küsel, K.; Brakhage, A. A. Artificial Microbial Arenas: Materials for Observing and Manipulating Microbial Consortia. *Adv. Mater.* **2019**, 1900284.
42. Yañez-Ocampo, G.; Sanchez-Salinas, E.; Jimenez-Tobon, G. A.; Penninckx, M.; Ortiz-Hernández, M. L. Removal of Two Organophosphate Pesticides by a Bacterial Consortium Immobilized in Alginate or Tezontle. *J. Hazard. Mater.* **2009**, *168* (2–3), 1554–1561.
43. Lahtvee, P.-J.; Kumar, R.; Hallström, B. M.; Nielsen, J. Adaptation to Different Types of Stress Converge on Mitochondrial Metabolism. *Mol. Biol. Cell* **2016**, *27* (15), 2505–2514.
44. Priks, H.; Butelmann, T.; Illarionov, A.; Johnston, T. G.; Fellin, C.; Tamm, T.; Nelson, A.; Kumar, R.; Lahtvee, P.-J. Physical Confinement Impacts Cellular Phenotype within Living Materials. *ACS Appl. Bio Mater.* **2020**. Preprint: https://doi.org/10.1021/acsabm.0c00335

5.8 FIGURES

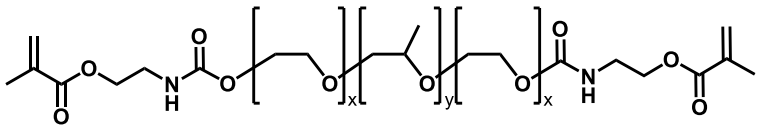

Figure 5.29. Chemical structure of F127-BUM.

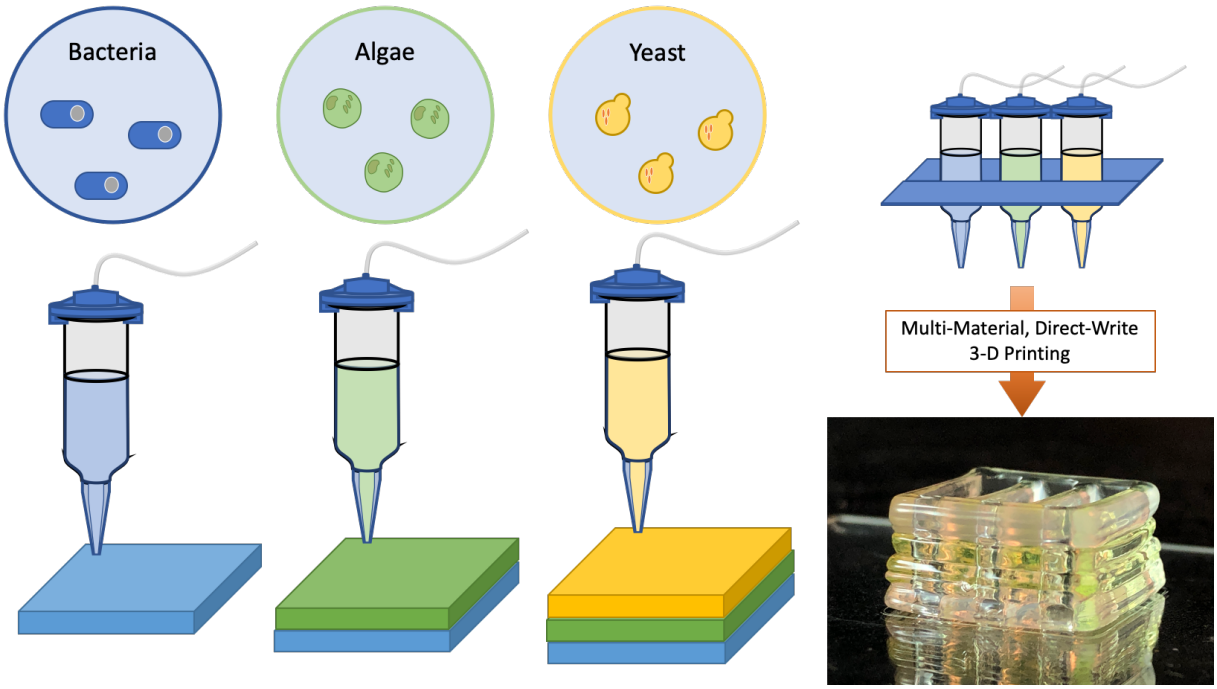

Figure 5.30. General multi-material additive manufacturing scheme.

General additive manufacturing scheme for the deposition of three different cell-laden hydrogel inks into a single printed construct. The three cell types are homogenously dispersed in separate F127-BUM hydrogels at low temperature and are warmed to ambient temperature (21 °C) to afford shear-thinning hydrogels. Using CAD design and 3D-printing, the different samples of cell-laden hydrogels can be precisely deposited to create a three-dimensional structure that houses all three species of microbes simultaneously. These structures can be cured post-printing to negate the shear- and temperature-responsive behaviors, allowing the structures to be handled and placed into aqueous environments without deformation.

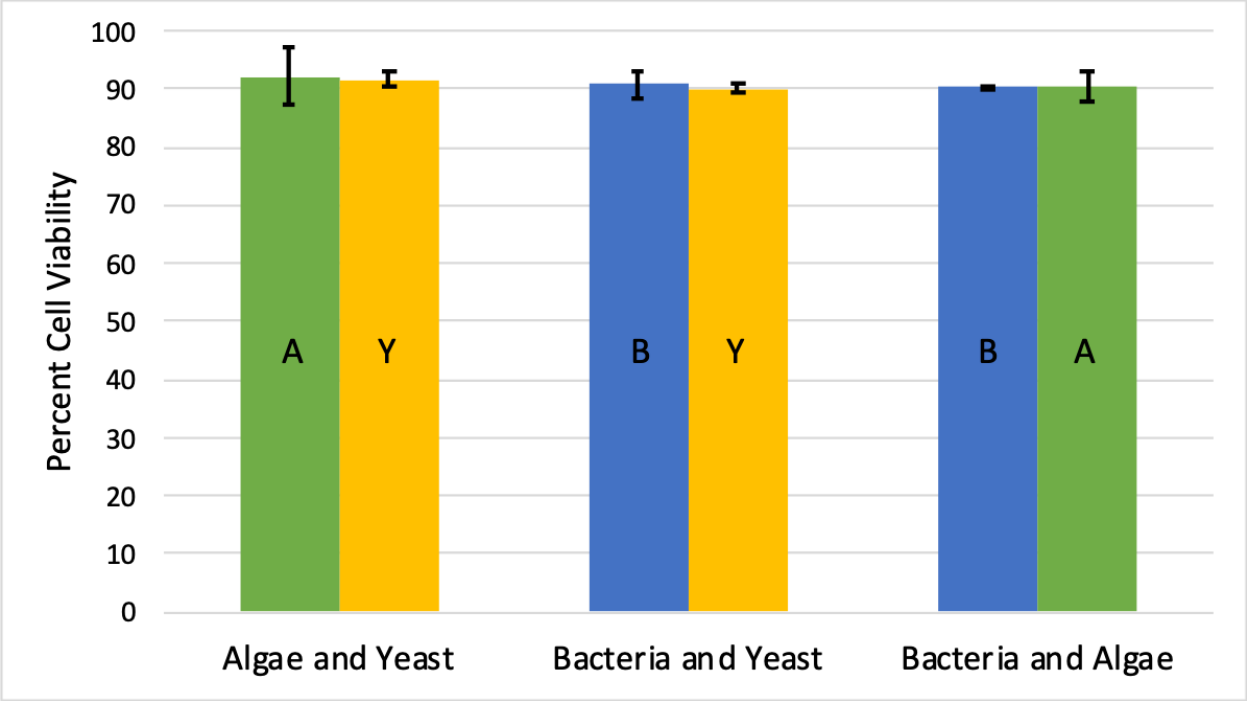

Figure 5.31. Cell viability results from 7 days of incubation in co-culture.

During a week of incubation in mixed cell culture medium, all cell types show high viability when encapsulated in the cured F127-BUM hydrogels. "A" represents algae, "B" represents bacteria, and "Y" represents yeast.

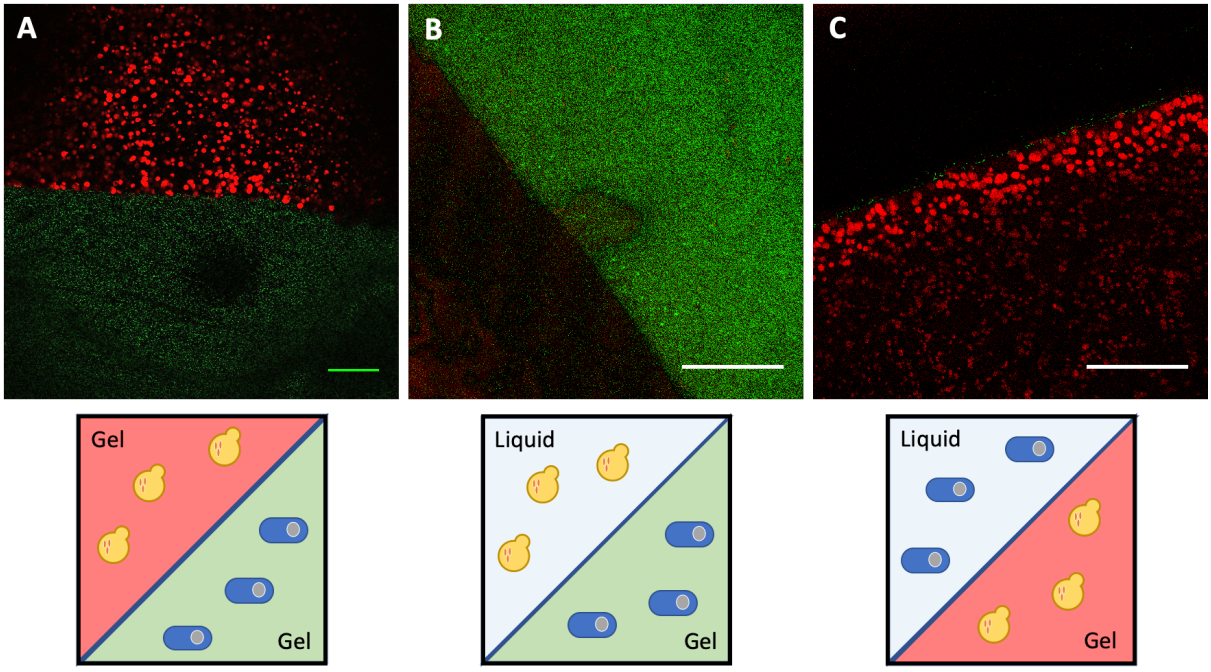

Figure 5.32. Cell invasion studies.

a) The interface of a hydrogels containing green fluorescent bacteria (green) and red fluorescent yeast (red), across 100 µm of sample depth. b) Sample of bacteria-laden hydrogel printed and incubated in yeast culture. c) Sample of yeast-laden hydrogel printed and incubated in bacterial liquid culture. Images shown after 7 d of co-culture. Scale bars are all 100 µm.

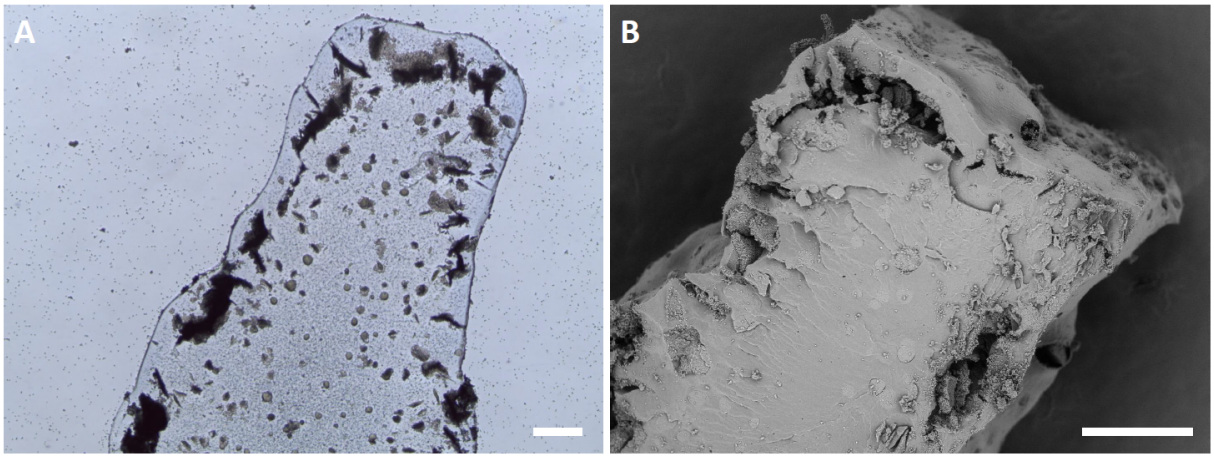

Figure 5.33. Optical and scanning electron microscopy.

a) Optical microscopy micrograph of a yeast-laden hydrogel slice. b) SEM micrograph of a yeast-laden hydrogel. Micrographs show larger colonies at the periphery (black cavities). Scale bars 250 µm.

Chapter 6. CONCLUSIONS AND FUTURE DIRECTIONS

We have demonstrated a novel platform for the application of living materials in a variety of sustainable, on-demand production processes. While this work represents a significant step forward in the immobilization of cells for whole-cell catalysis, there are still many areas of this research that call for continued exploration. Due to the amenability of this platform to a wide variety of cell types, continued collaborative efforts with experts in synthetic biology should allow for a continuously expanding toolbox of cell lines. This will facilitate immobilized consortia capable of producing an incredibly diverse collection of target molecules from the 3D printed bioreactors. While microbial species offer an enormous amount of flexibility in application, this platform should also be studied for the implementation of relevant mammalian cell lines as well. Similarly, the effective lifetimes of the reactors, both before and after various preservation treatments, should be explored for long-term studies, pushing beyond the one-year mark that is highlighted in this work.

With regards to the polymers employed in the hydrogels, further chain end modification chemistries could be explored to produce a material that could be triggered by either an external stimulus or a programmed behavior of the encapsulated cells to degrade the living materials at the end of their functional lifetimes. This would represent a further step in the direction of this technology towards a sustainable, circular economy of the material components. This would also allow for the recovery of the encapsulated cells, which would enable further understanding of how the cells behave and change due to prolonged enclosure within the living material.

Finally, the ability to 3D print these materials offers incredible flexibility in the deposition of the materials and the geometric complexity of the resulting constructs. However, the benefits of this complexity have not been explored. Pore size and diffusion rates of the hydrogels must be

better explored to fully leverage the printability. Once these characteristics of the living materials are better understood, spatial arrangement of cells within an immobilized consortia and overall geometries of a final printed construct can be modeled and optimized prior to printing, thus ensuring maximum efficiency of the living materials during the production phase. This will be of utmost importance when considering the implementation of this technology on an industrial scale or in alternative reactor designs, such as a flow reactor.

Through the use of these cell-friendly hydrogel materials, exciting applications in the study and harnessing of cellular consortia should continue to be made possible. While there is certainly still room for continued research in the space of living materials, the AMCALM platform detailed here has made significant strides in the study and implementation of a wide range of microbial species for the sustainable generation of industrially relevant, high-value compounds.

APPENDIX A

Appendix A accompanies Chapter 2.

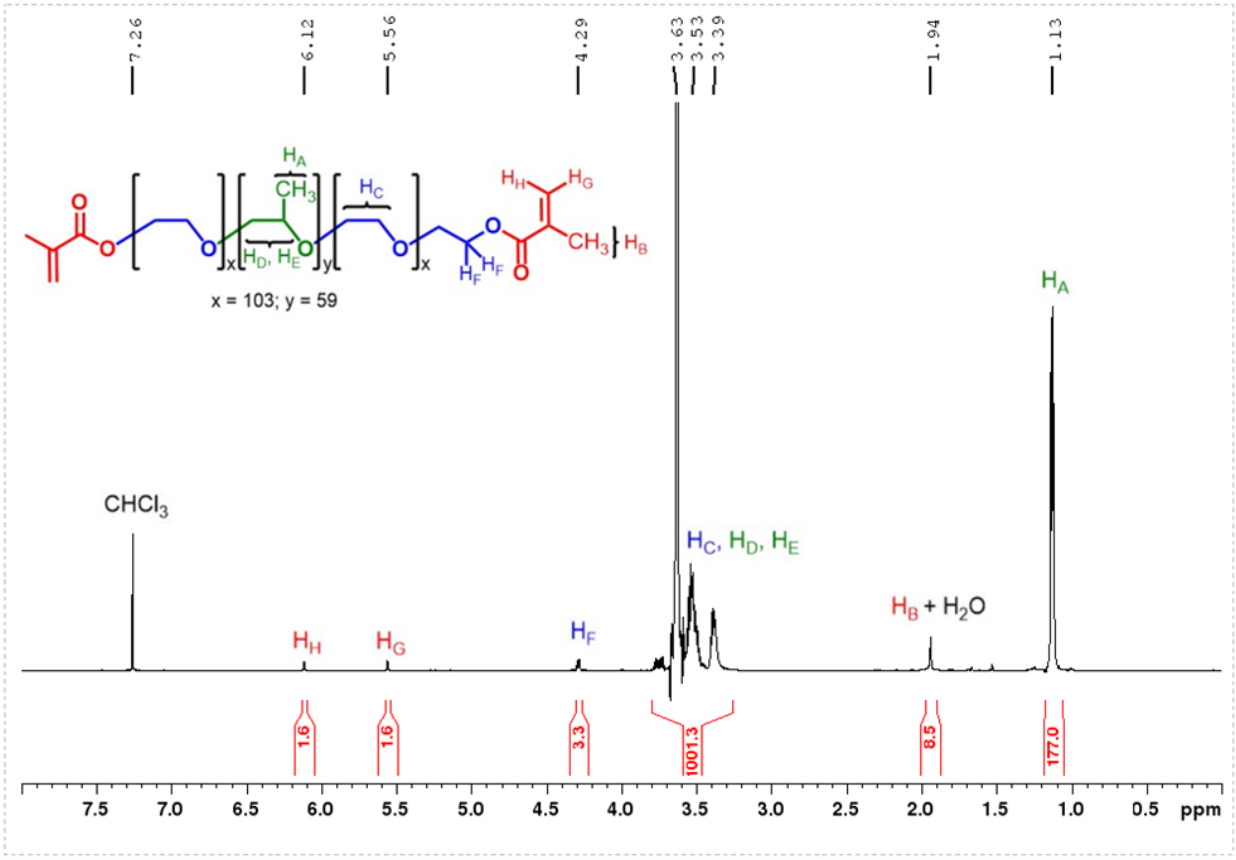

Figure A.34. ^{1}H NMR spectrum of F127-DMA in $CDCl_3$.

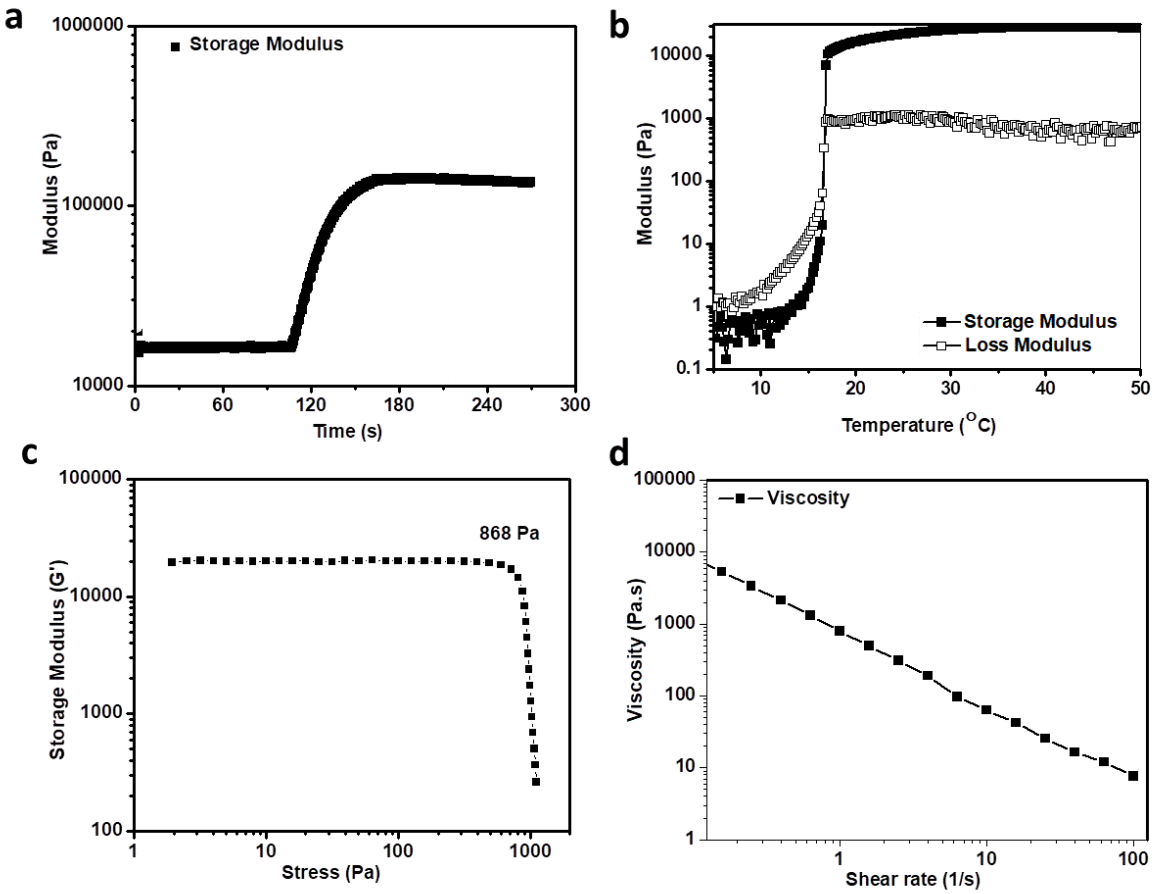

Figure A.35. Rheology for the yeast-embedded hydrogel ink.

(a) Storage modulus during photo crosslinking of the 25 wt% F127 DMA hydrogel in SC media at 25 °C. (b) Dyanamic oscillatory temperature ramp experiment for the hydrogel ink showing a T_{gel} at 16.7 °C . (c) Storage modulus vs shear stress showing yield stress at 868 Pa for the hydrogel ink. (d) Viscosity versus shear rate profile of the hydrogel ink. Rheological measurements in (b), (c), and (d) were performed with 10^6 yeast cells per g of hydrogel ink.

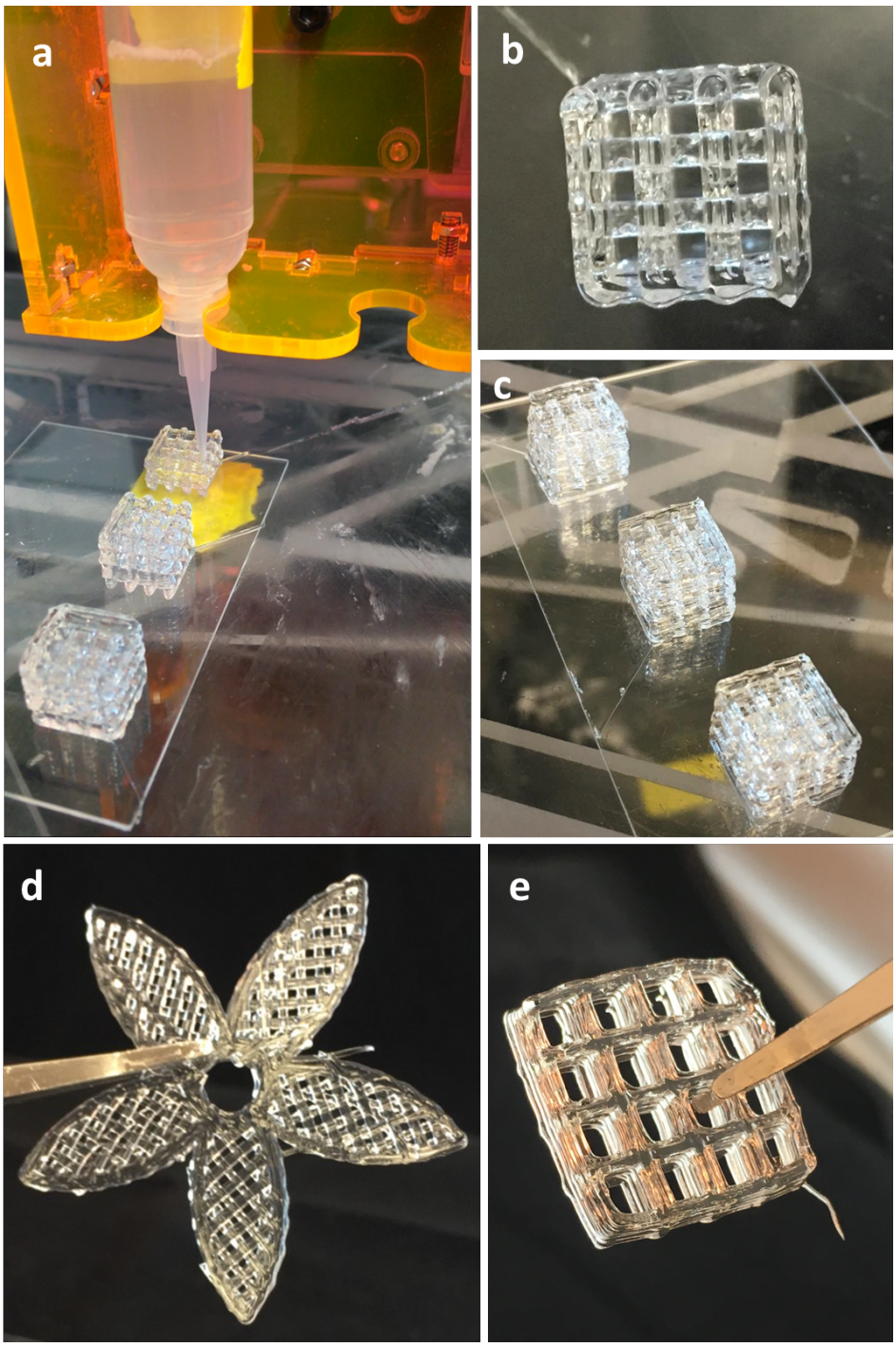

Figure A.36. Direct-write 3D printing examples

Direct-write 3D printing of cube lattices (a-c, 15 mm x 15 mm x 15 mm), flower (d, diameter 50 mm) and multi-layered grid (e, 20 mm x 20 mm x 5 mm) using 25 wt% F127-DMA in SC media containing 10^6 yeast cells per gram of hydrogel.

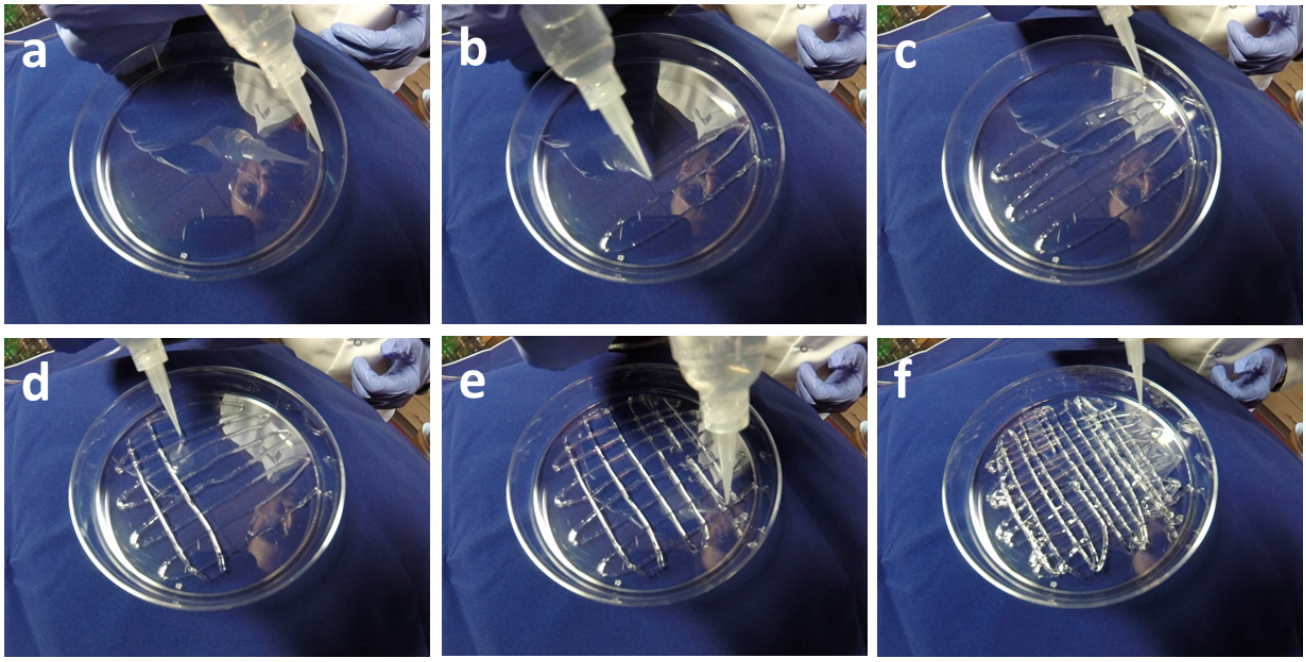

Figure A.37. Pictures for the extrusion of hydrogel ink

Direct write printing of the hydrogel ink for developing the high surface area 3D mesh

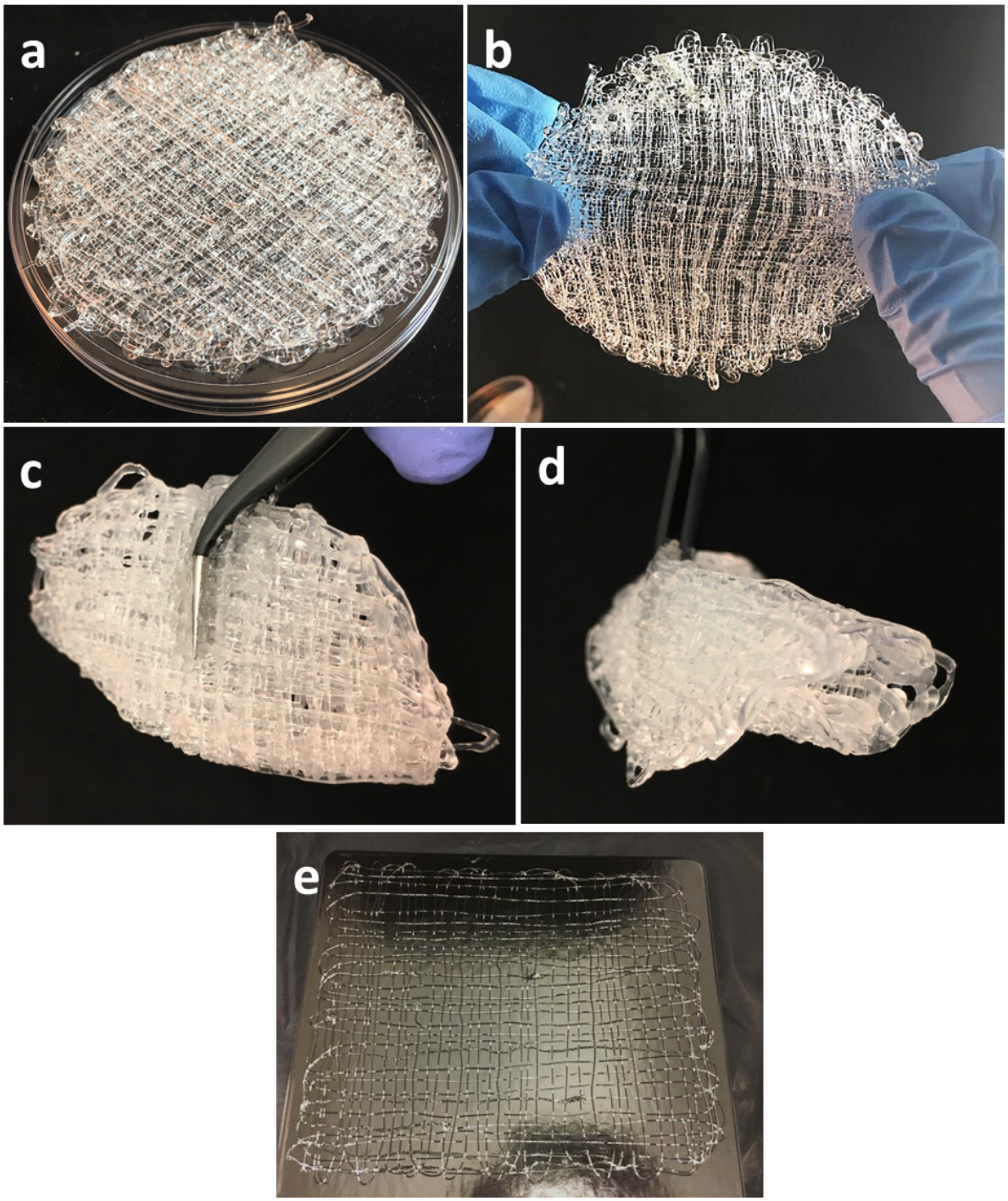

Figure A.38. Images of fabricated 3D meshes

Photographs of (a) the fabricated 3D mesh (diameter ~83 mm) and the (b) stretched, (c) folded and (d) rolled states of the 3D mesh. (e) Extrusion of hydrogel ink on a large surface (29 cm x 25 cm).

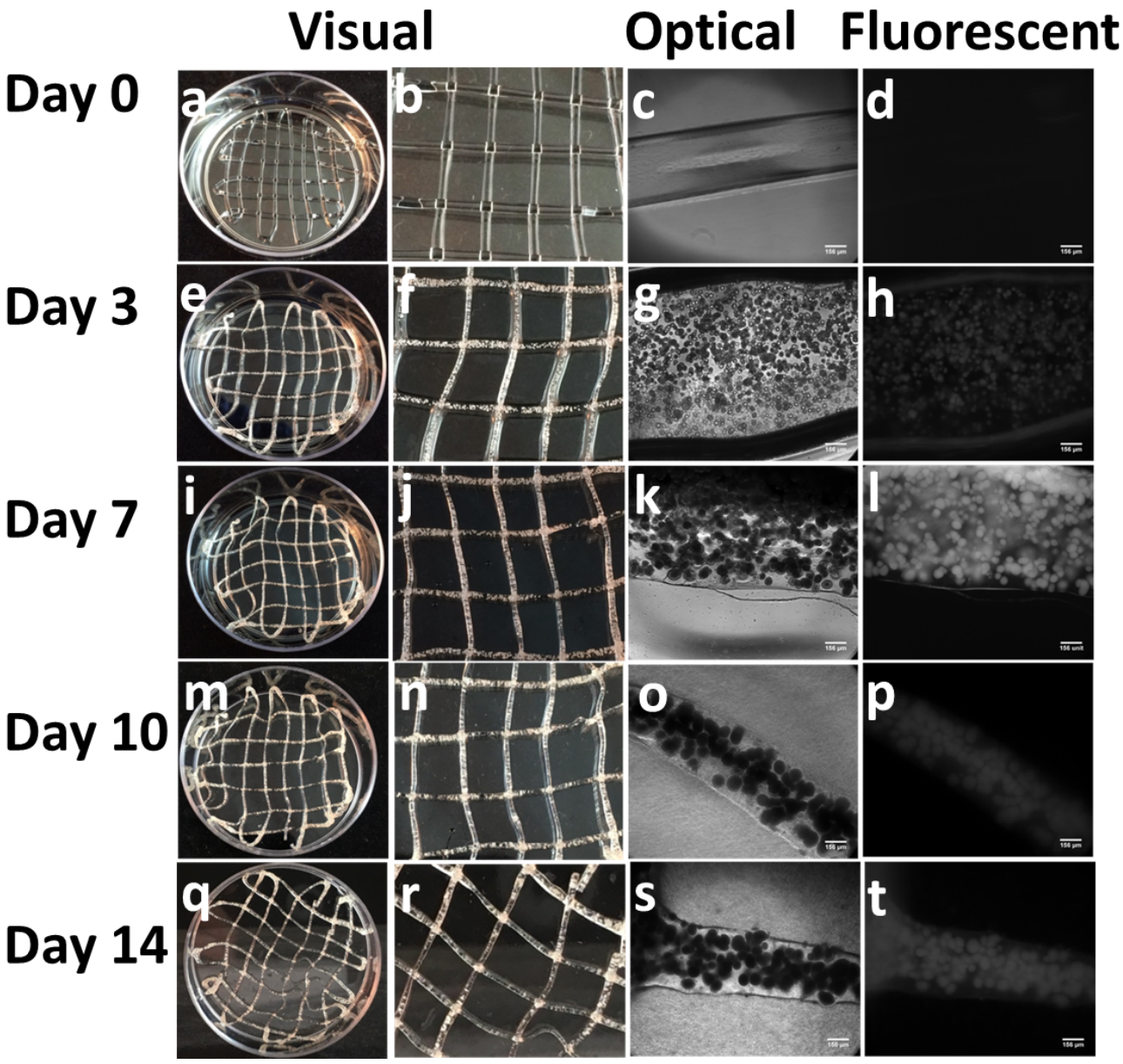

Figure A.39. Microscopy of AMCALMs

Visual and microscopy images of mCherry expressing cells embedded in the living materials. Mesh images in petri dish (60 mm diameter) (a), (e), (i), (m), and (q). Zoomed images of the meshes (b), (f), (j), (n), and (r). Optical microscopy images (c), (g), (k), (o), and (s). Fluorescent microscopy images (d), (h), (l), (p), and (t) (Scale bar in images corresponds to 156 µm).

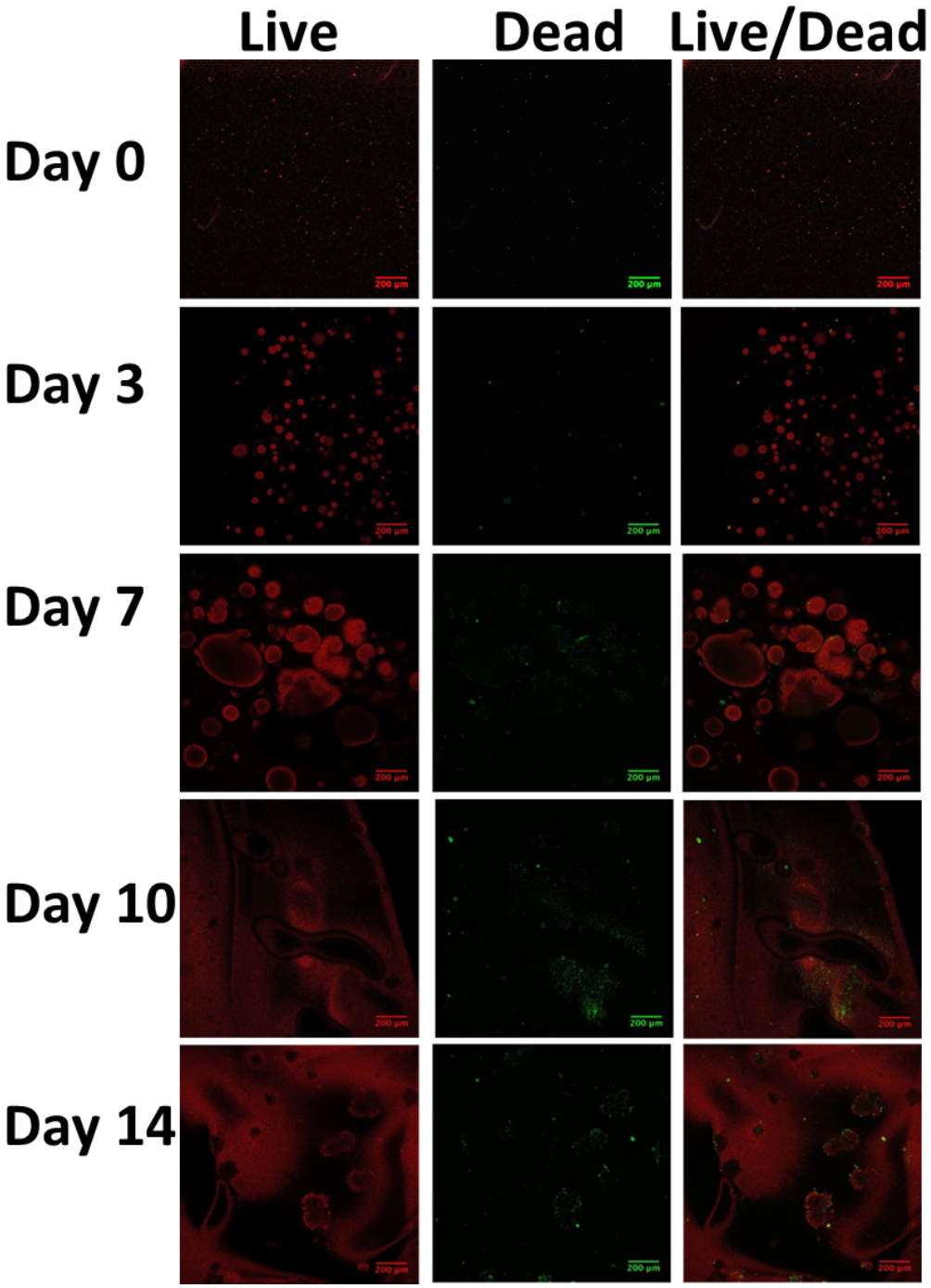

Figure A.40. Live/Dead results

Results for the live/dead assay from 0 to 14 days under confocal microscopy. The first column shows live (red) cells, while the second column shows the population of dead (green) cells in the hydrogel. The third column is an overlay of the first two to show the distribution of viable cells throughout the imaged material sample.

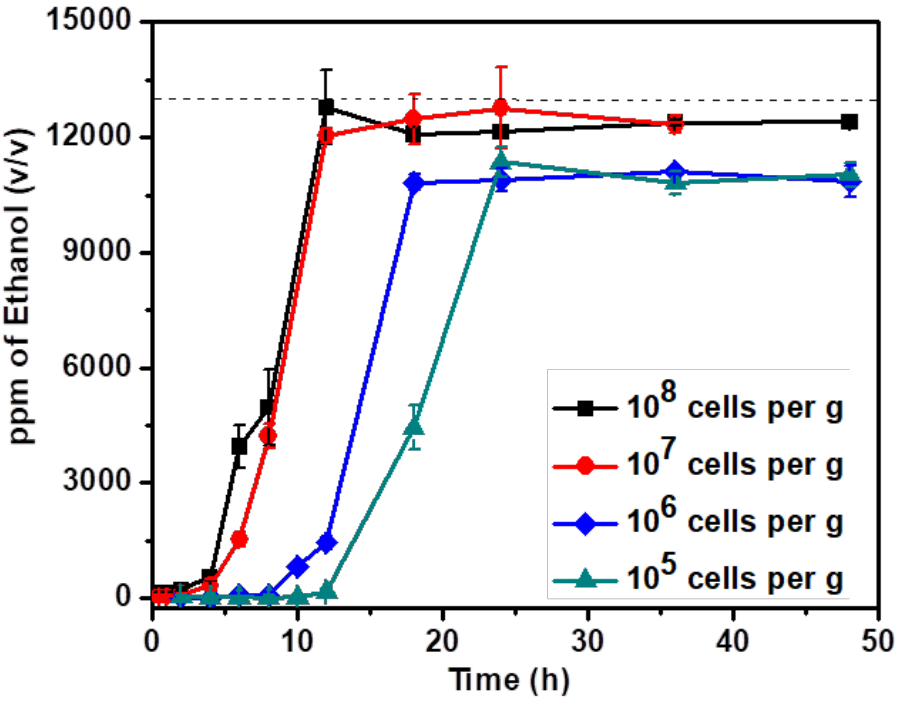

Figure A.41. AMCALM Kinetics study

Kinetics for the production of ethanol by 3D printed cubes with varying concentration of cells in the hydrogels in SC media containing 2 wt% of glucose (dotted line in the figure at 12693 ppm indicates 100% conversion of glucose into ethanol).

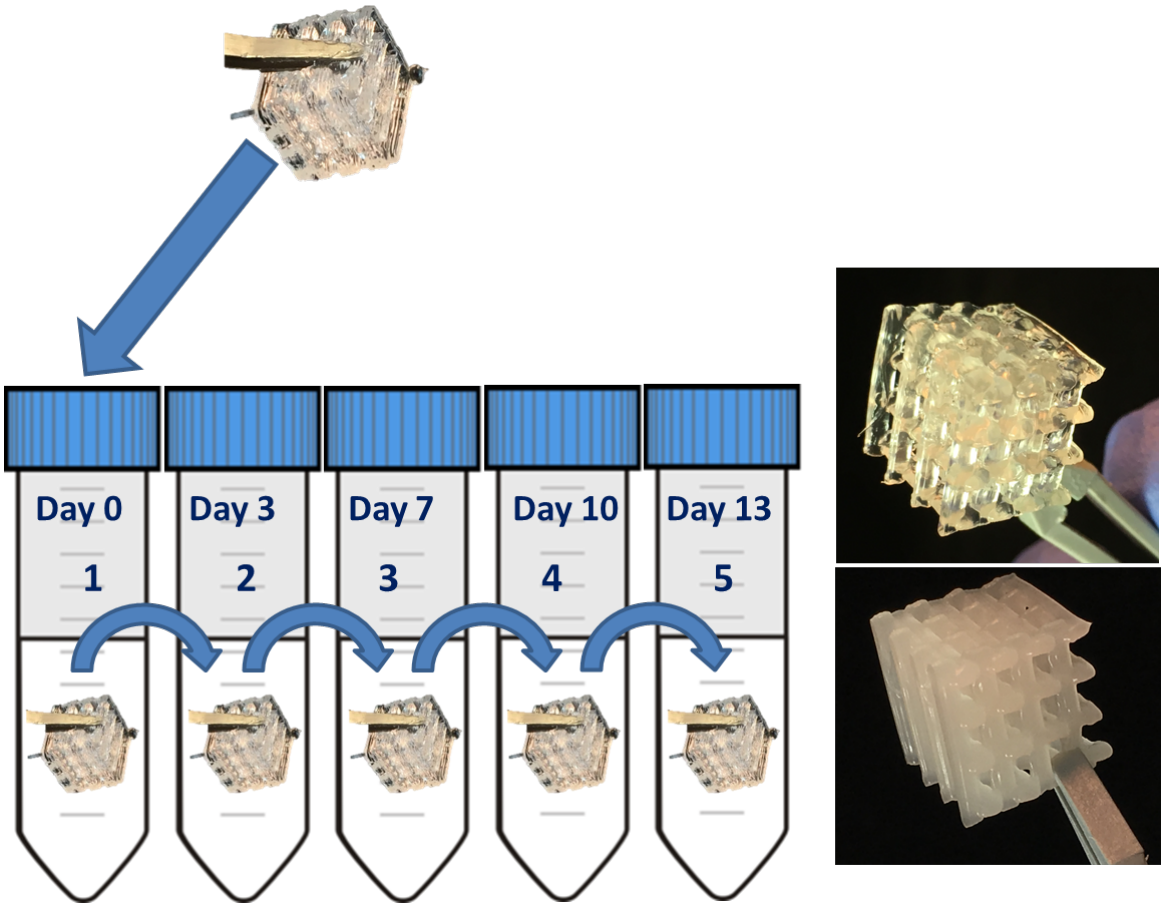

Figure A.42. Batch reaction scheme

Schematic for batch reactions for the biocatalysis using the living materials. Images of the 3D cubic lattices at day zero (top) before performing the fermentation batch reactions and after fourteen days (bottom) consisting of five consecutive batches of fermentation

.

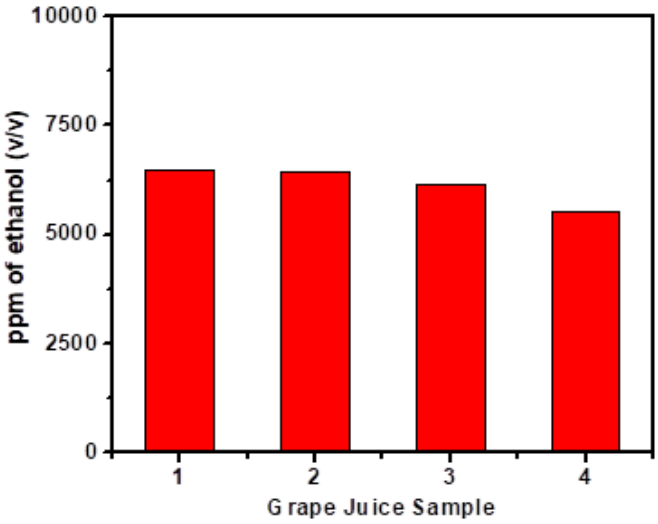

Figure A.43. Biocatalysis of natural sugars

Biocatalysis of natural sugars found in grape juice into ethanol by the yeast-embedded cubes. The quantity of ethanol produced was determined by GC after 48 h.

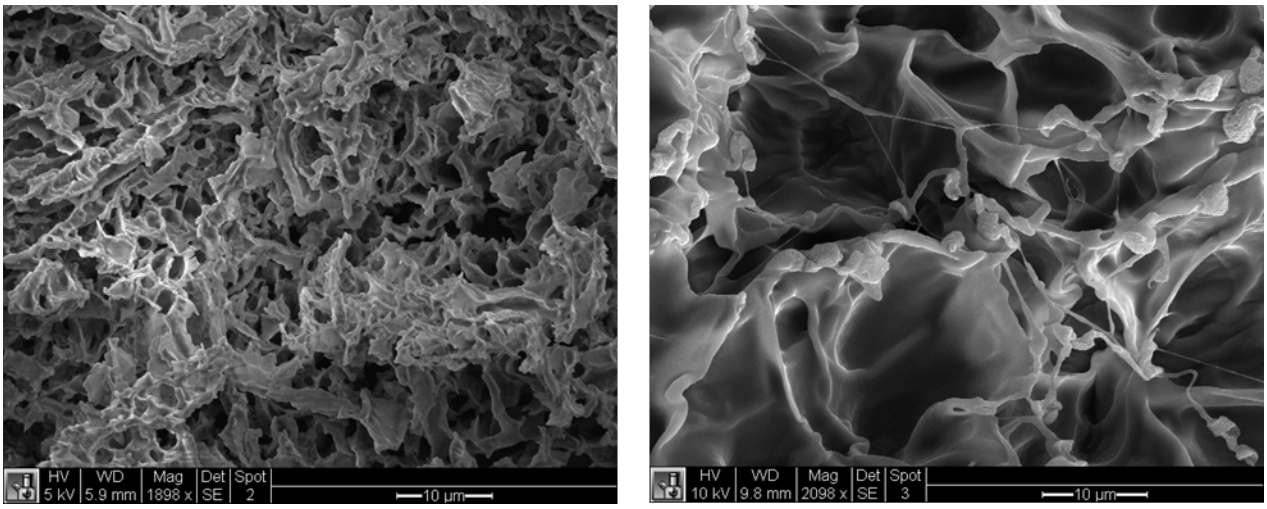

Figure A.44. SEM imaging

Scanning electron microscopy (SEM) images of the hydrogel for the lyophilized 25 wt% F127-DMA hydrogel in SC media showing of porous morphology.

Table A.1. Biocatalysis by the living materials with varying amounts of cells

Number of cells per g of living materials [a]	Amount of ethanol produced after 24 h (in ppm)	Efficiency for the conversion of ethanol from glucose (in %)
10^8	12141	93.7
10^7	12761	98.4
10^6	10895	84
10^5	11358	87.6

[a] Initial cell-count

Table A.2. Biocatalysis by the living materials with varying amounts of glucose

Amount of glucose in SC media (in g)	Amount of ethanol produced after 48 h (in ppm)	Efficiency for the conversion of ethanol from glucose (in %)
2	12405	95.7
5	28733	88.7
10	56036	86.4

APPENDIX B

Appendix B accompanies Chapter 3.

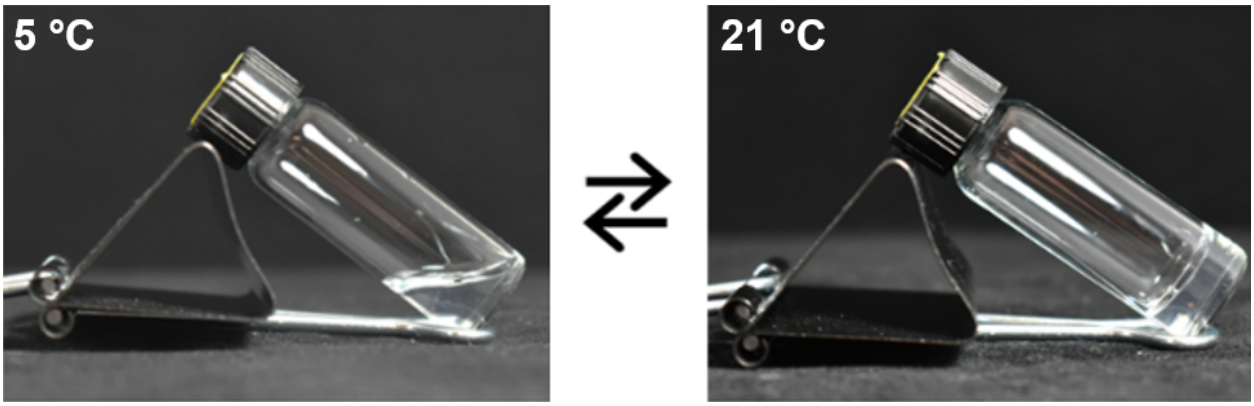

Figure B.1. Graphical representation of the temperature induced sol-gel transition of polymer 2.

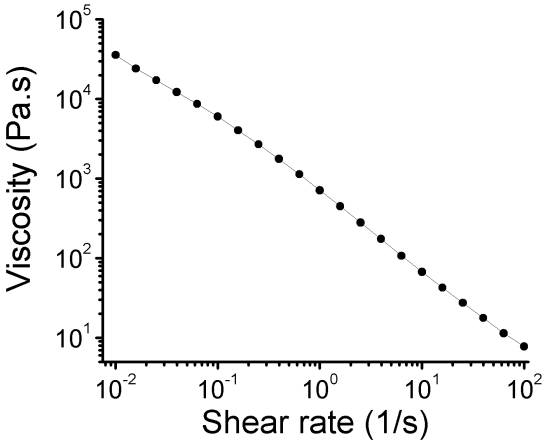

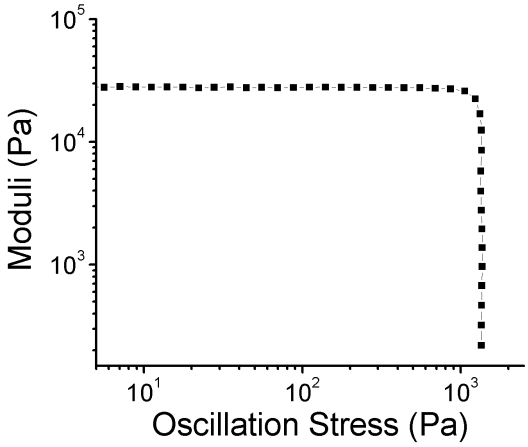

Figure B.2. Viscosity vs Shear Rate (left)

Figure B.3. Oscillatory Yield Stress (right)

Both experiments for a 20 wt % solution of Polymer 1

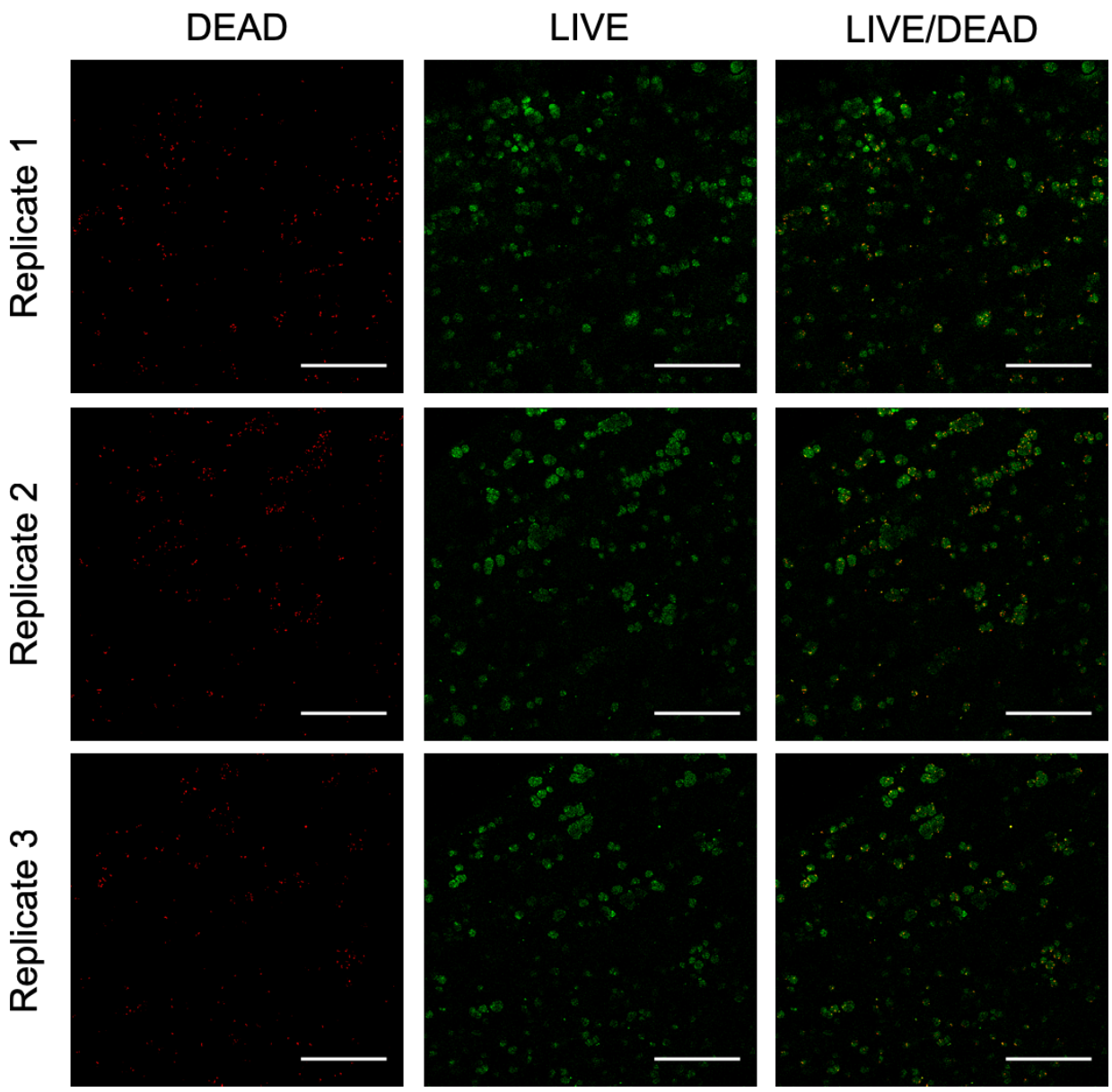

Figure B.4. Live/dead, day 1

Confocal microscopy images of live/dead assay results at day 1 of incubation in SC media. The first column shows the dead cells (red channel), while the second column shows the live cells (green channel). The third column is an overlay of the live and dead cell channels.

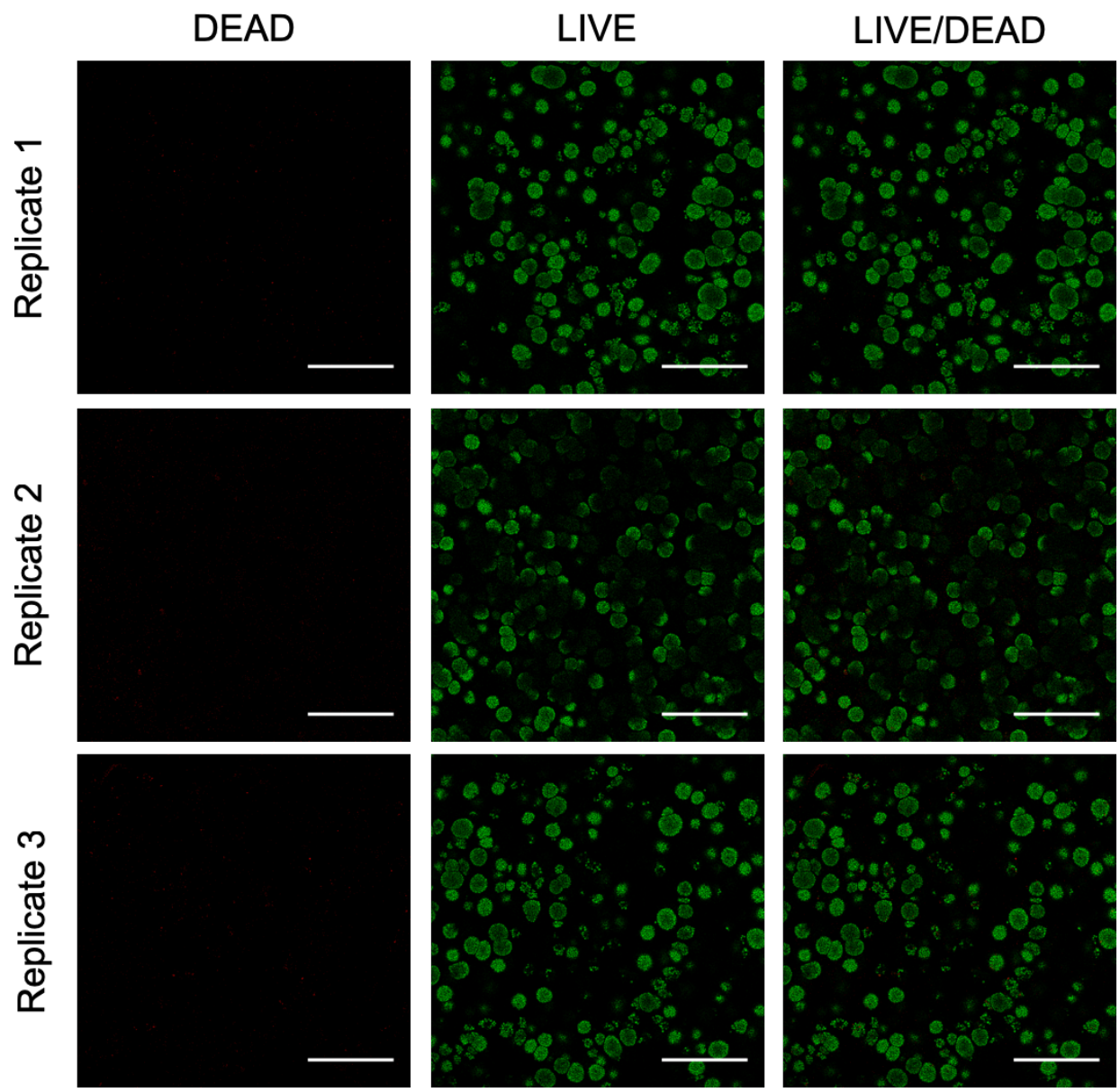

Figure B.5. Live/dead, day 3

Confocal microscopy images of live/dead assay results at day 3 of incubation in SC media. The first column shows the dead cells (red channel), while the second column shows the live cells (green channel). The third column is an overlay of the live and dead cell channels.

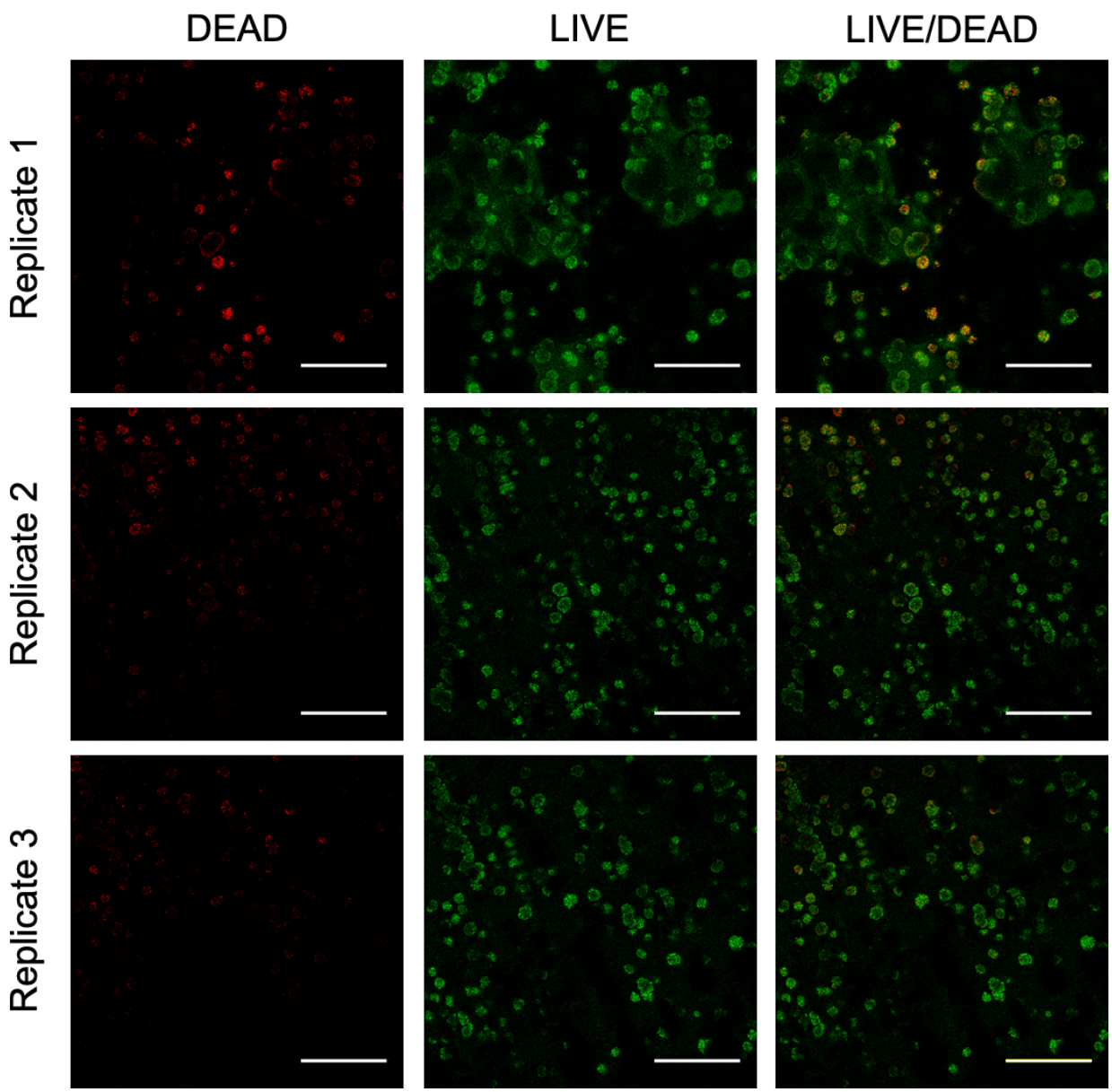

Figure B.6. Live/dead, day 7

Confocal microscopy images of live/dead assay results at day 7 of incubation in SC media. The first column shows the dead cells (red channel), while the second column shows the live cells (green channel). The third column is an overlay of the live and dead cell channels.

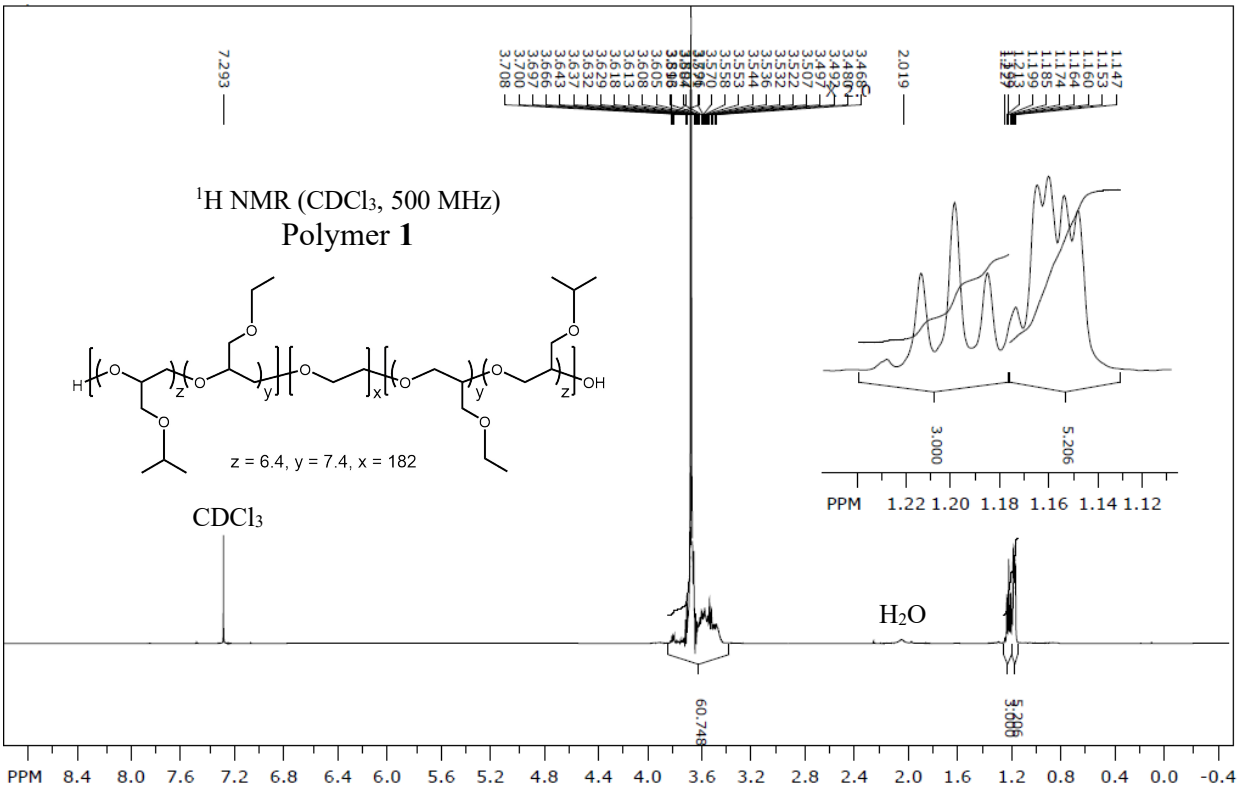

Figure B.7. ^{1}H NMR of Polymer **1**

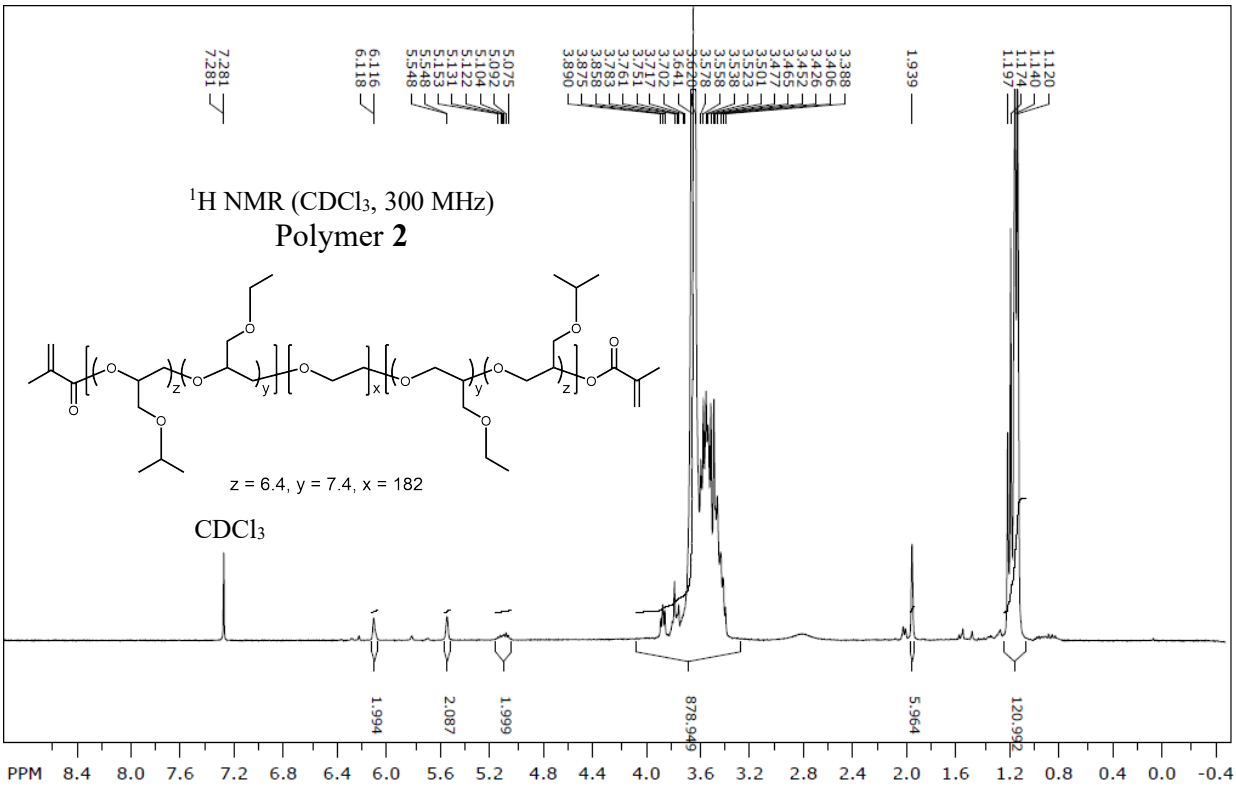

Figure B.8. ^{1}H NMR of Polymer **2**

APPENDIX C

Appendix C accompanies Chapter 4.

6.1 SUPPLEMENTARY EXPERIMENTAL RESULTS

6.1.1 *2,3-butanediol production in yeast with lyophilization and re-use*

2,3-Butanediol is a building block biochemical for a variety of downstream chemicals including methyl ethyl ketone, acetoin and 1,3-butadiene with applications in synthesizing plastics, food additives or industrial solvents [1]. 2,3-BDO has a global market demand of around 32 million tons per year with a value of $43 billion [2]. As a result, microbial 2,3-butanediol production has been extensively studied in the past few decades [1]. Previously, we have demonstrated that a multiplexed dCas9-based regulation system to simultaneously knock down the NADH sinks including *ADH1*/*3*/*5* and *GPD1* along with overexpression of endogenous NADH-dependent BDH1 enzyme can increase the production of 2,3-BDO by nearly 2-fold in a 2,3-BDO-producing *S. cerevisiae* CEN.PK2-a strain (harboring a heterologous pathway with overproducing NoxE, alsD and alsS enzymes) [3] (Figure 4.2a).

To evaluate the efficacy of the microbe-laden hydrogel system, two 2,3-BDO-producing yeast strains (BY4741 and CEN.PK2-a) were each encapsulated in the gel matrix and performance was compared pre- and post-preservation (Figure C.1). The 2,3-BDO productivity between the two engineered strains of BY4741 (0.035 g/L/h) and CEN.PK2-a (0.034 g/L/h) were comparable at 48 hours before lyophilization. After lyophilization, the 2,3-BDO productivity in preserved BY4741 gel (0.03 g/L/h) retained nearly 90% efficiency compared to the untreated sample, while the biological productivity in lyophilized CEN.PK2-a hydrogels decreased to 0.025 g/L/h (about 70% efficiency). Part of the decrease in efficiency seen with 2,3-BDO in the CEN.PK2-a strain was a

result of an increased acetoin byproduct titer seen in this condition that increased from 1.1 g/L (pre-lyophilization) to 1.8 g/L (post-preservation) at the 48-hour timepoint (Figure C.1b). Acetoin is formed from the bioconversion of 2,3-BDO into acetoin via reversible yeast butanediol dehydrogenase (BDH1) enzymatic reactions [4]. Regardless, the net metabolic activity (acetoin + 2,3-BDO) evaluated for both pre- and post-lyophylization is indicative of sustained metabolic activity by the yeast-laden gels.

6.1.2 *L-DOPA production in E. coli*

L-DOPA can be biosynthesized from tyrosine and is a precursor of the neurotransmitter dopamine in human [5] and has also been used as a drug for treating Parkinson's disease [6]. As a result, microbial production of L-DOPA [7-8] from low-cost lignocellulosic feedstocks [9-10] is an attractive process compared to direct extraction from plants restricted by the low yield and purity issues [11].

Previous studies have shown that introduction of feedback-inhibition-resistant 3-deoxy-d-arabinoheptulosonate-7-phosphate (DAHP) synthase (encoded by *aroG*^{fbr}) and chorismate mutase/prephenate dehydrogenase (encoded by *tyrA*^{fbr}) in a *tyrR* (encodes a transcriptional regulator of aromatic amino-acid biosynthesis) knockout *E. coli* can sufficiently overproduce tyrosine [12-13]. In order to redirect metabolic flow from the intracellular tyrosine pool to the L-DOPA biosynthesis pathway, 4-Hydroxyphenylacetate 3-hydroxylase (HpaBC) [8] was overexpressed in the tyrosine-producing strain eBL04 (Figure 4.2b). As expected, expression of *hpaBC* under the control of a constitutive promoter with a strong synthetic ribosomal binding site resulted in *E. coli* eBL0430D exhibiting a higher titer of L-DOPA (around 213 mg/L) than that of the eBL0432D strain that has a weaker overall expression (about 160 mg/L) (Figure C.2).

Additionally, a change in coloration of culture broth for both engineered strains was observed, indicative of the oxidation of L-DOPA to form brown melanin-like pigments [8, 14-15].

6.1.3 *Peptide antibiotic production in E. coli with lyophilization and re-use*

To expand beyond small molecules, we demonstrate that microbe-laden hydrogels are capable of producing small peptides—in this case, biosynthesis of peptide antibiotic colicin V (colV). ColV is secreted by *E. coli* and other members of *Enterobateriaceae* and previous studies have identified that four genes *cvaA*, *cvaB*, *cvaC* and *cvi* of the colicin V gene cluster are required for ColV synthesis, export, and native immunity [16-18] (Figure C.4a). The colicin V-producing strain expressing its cognate immunity protein Cvi alone is sufficient to protect itself from the killing activity of ColV [16]. The extracellular secretion of ColV, encoded by the *cvaC* gene, is mediated by an efflux system containing cytoplasmic proteins CvaA and CvaB as well as the host outer membrane protein TolC [17], then the CvaA-CvaB-TolC exporter recognizes the N-terminal 15-amino-acid leader sequence of primary translation polypeptide ColV and proteolytically processes it to render a mature 88-amino-acid ColV peptide. The secreted ColV is only active against sensitive cells when inserted into the inner membrane of a target cell resulting in membrane depolarization [16, 18].

In this study, ColV antibiotic-producing *E. coli* that was expressing *cvaA*, *cvaB*, *cvaC* and *cvi* genes was encapsulated in the F127-BUM hydrogel matrix. Using the printed gels, two bactericidal assays were conducted using the broth supernatant of the culture. These assays included a zone of inhibition test and bacterial suspension broth test to evaluate the antimicrobial activity of ColV. As shown in Figure 4.2d, the inhibition halo yielded by the gel system was consistently observed over four consecutive repeated uses after lyophilization, indicating the cell functionality in the gels was still retained and the diffusion of the peptide from the gel matrix was not inhibited. The

bactericidal activity was not affected by the preservation process for the first two repetitive uses and the efficiency was reduced to only around 80% for the last batch of re-use compared to the original (round 0). The average antimicrobial activity for four subsequent rounds of re-use after lyophilization was nearly 100% of the original gel based on the measurement of diameter of clear zones appeared on agar plates. In addition, the production of the secretory peptide antibiotic in gels was observed in the broth test (Figure C.4c) despite the slight reduction in antimicrobial functionality based on the inhibition zone test for the last two rounds of re-use (Figure C.4b). Thus, the overall production was maintained across the rounds of re-use using a mixture of bacteriastatic and bactericidal assays.

For benchmarking, the bactericidal activity of the liquid culture system was also compared to that in the hydrogel system (Figure C.4b and c). The zone of inhibition test (Figure C.4b) and broth test (Figure C.4c) clearly demonstrated that the antimicrobial peptide activity made in a free-cell system was inconsistent for iterative cell-re-use compared to the hydrogel system. In the 3rd re-culturing round, the inhibition zone in free-cell system was actually not observed and its bactericidal activity dramatically was reduced to 6.5%. Likewise, the larger error bars on the liquid culture demonstrates the extreme variability of samples from biological replicates indicative of the instability experienced in repeated liquid subculturings.

Overall, these results showcase the capability of the described hydrogel system in maintaining high cell density and supporting protection to lyophilization, thus resulting in a continuous operation of peptide antibiotic production. Moreover, it is expected that the printed gel can carry a higher next cell density/concentration than a microbial suspension system [19-20], thus leading to a stronger and more consistent production level.

6.1.4 *Betaxanthins production via a synthetic commensal consortium*

Betaxanthins are water-soluble natural yellow pigments that have been proposed as a substitute for artificial yellow dyes [21]. Previous studies have established a *de novo* plant betaxanthins biosynthesis pathway in *S. cerevisiae* for high-throughput screening of tyrosine hydroxylase mutant library and for the investigation of spectral and physical properties of various amine-betaxanthins [22-23]. Given these potential uses and interest, we decided to choose the compound as an example molecule that can be produced via a microbial consortium. In this study, we created a synthetic *E. coli*-yeast consortium (Figure 4.3b) whereby the L-DOPA secreted by engineered *E. coli* is consumed by the DOPA-4,5-dioxygenase (DOD)-overproducing yeast that converts L-DOPA into betalamic acid. The free betalamic acids then condense with primary or secondary amines to yield the fluorescent yellow betaxanthin pigments.

To evaluate the impact of medium components on fermentative performance, we evaluated free cell, suspension cultures using *E. coli* eBL0430D-*S. cerevisiae* sBY08 were tested at different temperatures (Figure C.7a). Betaxanthins titers gradually increased over time at 25 °C for both LBYSD and M9YSD conditions. Although the maximum titer of betaxanthins for each condition was nearly 2-fold higher when using LBYSD medium compared with using M9YSD, the production significantly declined over time for higher temperatures 33.5 to 40 °C, suggesting using M9YSD medium could provide a more stable condition for the product. Thus, M9YSD medium was chosen for the following studies. We found a consistent correspondence of betaxanthins titer between fermentation conducted in flask scale and tube scale (Figure C.7b); therefore, we chose to conduct experiments at the tube scale for operational convenience and condition multiplexing. Previous studies have demonstrated DOD reaction requires oxygen [22]. To verify the effect of aeration for test tube culture on betaxanthins production in the gel system, the DOD-yeast-laden

hydrogel was printed and cultured in a working volume of 3 mL or 5 mL medium supplemented with exogenous L-DOPA (Figure C.7c). Increasing the concentration of spiked L-DOPA or encapsulated cell biomass in gels enhanced betaxanthins production. Fermentation performed with 3 mL working volume led to a 1.2-fold increase in production compared to that with 5 mL medium, potentially due to the increased oxygenation; therefore, a 3 mL working volume was adopted for the subsequent experiments.

To further explore the impact of fermentation temperature and initial cells density on betaxanthins production, we evaluated varying temperatures and cell ratios for both liquid culture and gel systems (Figure 4.3c and Figure C.7d-l). To control gel ratios, various amount of gel was printed and cured. To control liquid culture ratios, different amounts of starting culture was re-suspended. In this study, each printed gel carried the same initial yeast or *E. coli* cell concentration of 1.5 x 10^8 cells per gram of polymer. In liquid culture, we altered the initial cell ratio ranging from 100:1 to 1:100 while keeping the initial net yeast and *E. coli* cell concentration constant at 3 x 10^6 cells per mL of culture. As shown in Figure 4.3c and Figure C.7d-l, the production using gel system surpassed the microbial suspension culture system for most conditions. The consortia productivity in gel system with a gel ratio of 1:6 outcompeted the liquid culture with cell number ratio 1:100 by nearly 2-fold, especially across a range of temperatures (25-33.5°C). For 1:1 ratio at 25 °C, the gel system produced more betaxanthins compared to liquid system. At this condition, despite the starting point containing equal amount of *E. coli* and yeast cells, the consortia composition in suspension culture could be biased towards having more yeast than bacteria since 25 °C is closest to the yeast optimal growth temperature. In contrast, the gel based system can better control the end-dynamics of the consortium which is important for improving production [19].

Next, we evaluated the reusability of the consortium-laden gels (Figure 4.3d and Figure C.8a-e). The activity throughout five consecutive rounds of re-use was determined by comparing the performance of gels with 6:1 ratio (as measured by the comparing the highest betaxanthins titer measured at 30 and 33.5 °C to that of the round 0 experiment) (Figure C.7l; top) to that using the liquids with 100:1 and 1:1 (10X) (the condition mimicking the same amount of initial cell number used in the 1:1 gel ratio condition) ratios (Figure C.7l; bottom). In this study, the gels retained their active metabolism and continuously produced betaxanthins and the titer substantially out-competed that of the free-cell fermentation system for both the 30 and 33.5 °C conditions (Figure C.8c-e). Importantly, the metabolic activity of the immobilized consortium was retained and exceeded 100% activity when compared with the original gel (round 0) for five continuous re-use at 30 °C (Figure C.8d). The consortia activity of gel at 33.5 °C was 100% and 95% of the original activity for the first three rounds and last two rounds of re-use, respectively (Figure C.8e). Although betaxanthins production for the round 0 took longer than that of a free-cell system (Figure C.7d-g), once the steady state of both embedded species was established, the gels rapidly produced their maximum biocatalytic rate, namely, a higher productivity was observed, for the next re-use rounds (Figure C.8a-c).

In contrast, the free-cell system at 30 °C performed a in a fluctuating manner and did not yield consistent betaxanthins titer for the five consecutive re-culturings (Figure C.8d). In fact, two of the biological triplicates could not make the betaxanthins after subculturing, suggesting that liquid culture system is unstable and subject to random consortia dynamics. Additionally, the free-cell system at 33.5 °C rapidly lost all ability to make betaxanthins (Figure C.8e). Moreover, the cell pellets of the 100:1 liquid samples at 96 hour fermentation timepoint at 33.5 °C for the first round of cell-re-use displayed brown pigments (Figure C.8b), likely due to the overabundance of *E. coli*

and the formation of melanin-like by-product yielded from oxidation of L-DOPA [8]. In addition, the pelleted cells showed no color change for 1:1 (10X) samples at the same condition. These results suggest the end consortia composition for continuous cell use experiment was varying through liquid culture. It should be noted that the titer obtained from the gel system may also be underestimated, due to some yellow pigmentation observed as being retained in the gel after fermentation.

Maintaining cell viability is paramount to industrial-scale bioprocesses [20]. Three different treatments for preservation of this consortia were conducted including lyophilization, refrigerated storage and liquid nitrogen freezing (Figure 4.3d and Figure C.9a and b). The lyophilization process resulted in no loss of consortia productivity over five subsequent repeated fermentations after the fifth round of initial re-use (Figure 4.3d). The biocatalytic efficiency at 30 °C was still retained at nearly 120% compared to the round 0 experiment. In addition, the gel after refrigerated storage treatment for one week still exhibited average consortia productivity at around 140% of the original for the last five rounds of re-use carried out at 30 °C (Figure 4.3d). The control of cooling rate as well as the use of cryoprotectants have been demonstrated to improve cell viability and long-term stability [20]. However, we demonstrate here that this hydrogel ink is capable of providing protection from these conditions. To further demonstrate this, we simply employed liquid nitrogen to freeze the gels that were selected from the round 5 experiment at 33.5 °C, and proceeded to store the frozen gels at -80 °C overnight. The consecutive re-use study even on these gels showed that the cell viability was not severely affected by these freezing conditions, a condition that usually causes mechanical damage of cell membranes due to the formation of large ice crystals or irreversible protein denaturation [20]. Specifically, the average metabolic activity of

entrapped consortia reduced to only nearly 85% of original for the last five repeated batches (Figure C.9b).

6.1.5 *Xylose/Glucose utilization via a yeast-yeast consortium with repeated gel-re-use*

Xylose is the most abundant components in hemicellulose of lignocellulosic feedstock 24, however, conventional wild-type yeast S. cerevisiae is not capable of assimilating xylose 25-26. Previous studies have demonstrated a number of methods to import this metabolism including heterologous overexpression of Scheffersomyces stipitis xylose reductase (XYL1), xylitol dehydrogenase (XYL2) and D-xylulokinase (XYL3) in S. cerevisiae resulting in a xylose-utilizing strain YSX3 improved cell growth and ethanol production from xylose 27.

We sought to use our hydrogel system to enable a yeast-yeast parallel consortium. Wild-type S. cerevisiae S288C along with an engineered xylose-utilizing yeast, YSX3, were each individually encapsulated in hydrogels and the glucose/xylose consumption efficiency was compared with the liquid culture system (Figure 4.3e and Figure C.11). The sugars utilization rate was not determined for the round 0 since the purpose of this round was to outgrow and establish the consortia population. Two separate experiments were performed in parallel for the round 0: one with the yeast-yeast co-culture in YPD medium containing only 20 g/L of glucose (Figure C.11a), and the other in YPDX medium comprising 15 g/L of xylose and 15 g/L of glucose (Figure 4.3e). In all cases of the re-use (for both gels and suspension systems), glucose was fully used within 24 hours and the systems exhibited a diauxic shift 26. As shown in Figure C.11a, the gels initially maintained in YPD medium for round 0 displayed nearly 3.5-fold improvement on the average of initial xylose consumption rate over the liquid cultures during three subsequent rounds of re-use. Additionally, a lag phase in xylose consumption rate for the first round of re-use in both systems was observed (Figure C.11c; left), due to the shift in metabolism 26.Furthermore, the

performance of liquid culture progressively declined over each round of the re-use (Figure 4.3e) and the xylose consumption rate for the round 3 (around 0.1 g/L/h) approached that seen in Figure C.11a (about 0.07 g/L/h), indicating the free-cell system could not properly maintain the dynamics of the consortium. In contrast, our consortia-laden hydrogels exhibited a higher xylose consumption rate (0.3 g/L/h on average) compared to the liquid culture system over each round of repetitive use with the increasing improvement on xylose utilization (1.5-fold increase in round 1, 1.8-fold increase in round 2, and 2.7-fold improvement in round 3) (Figure 4.3e).

6.2 FIGURES

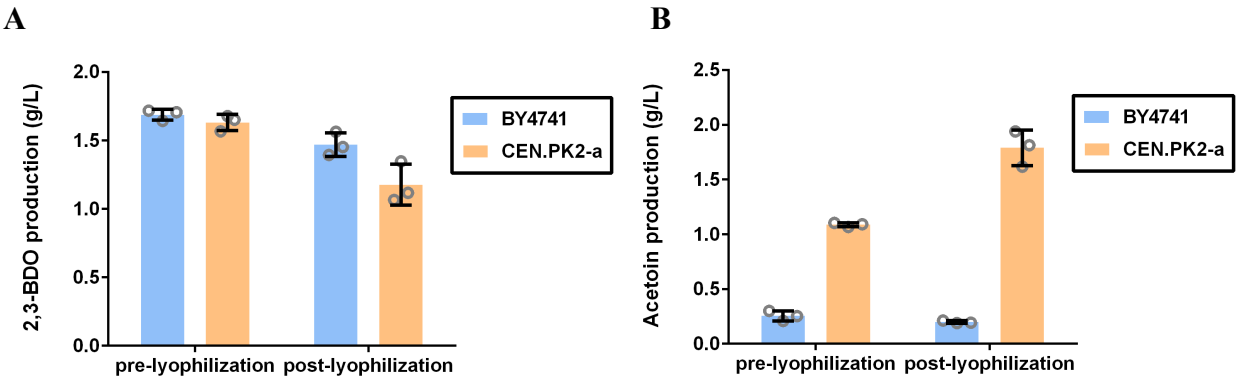

Figure C.1. Gel-re-run for 2,3-butanediol (BDO) production.

A) The comparison of 2,3-BDO production between S. cerevisiae BY4741 and CEN.PK2-a strains before and after lyophilization. B) The comparison of by-product acetoin formation between BY4741 and CEN.PK2-a strains before and after lyophilization. Each data point and error bar represent means and standard deviations from biological triplicates, respectively.

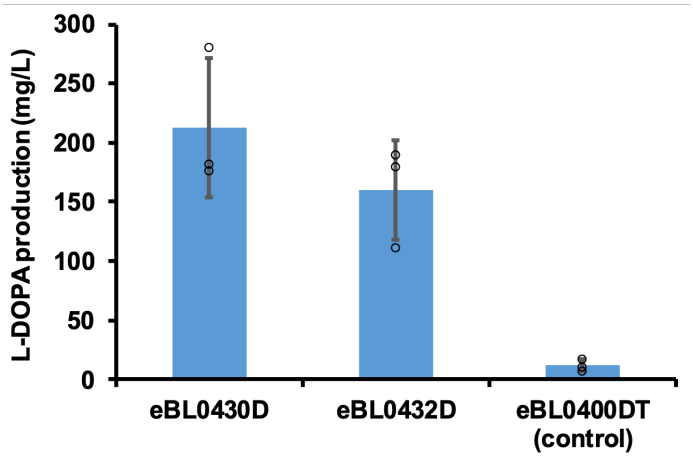

Figure C.2. L-DOPA production in E. coli.

The comparison of L-DOPA production between engineered E. coli strains and control strain eBL0400DT. The highest L-DOPA producer eBL0430D strain was used for DOPA and betaxanthins experiments. Each data point and error bar represent means and standard deviations from biological triplicates, respectively.

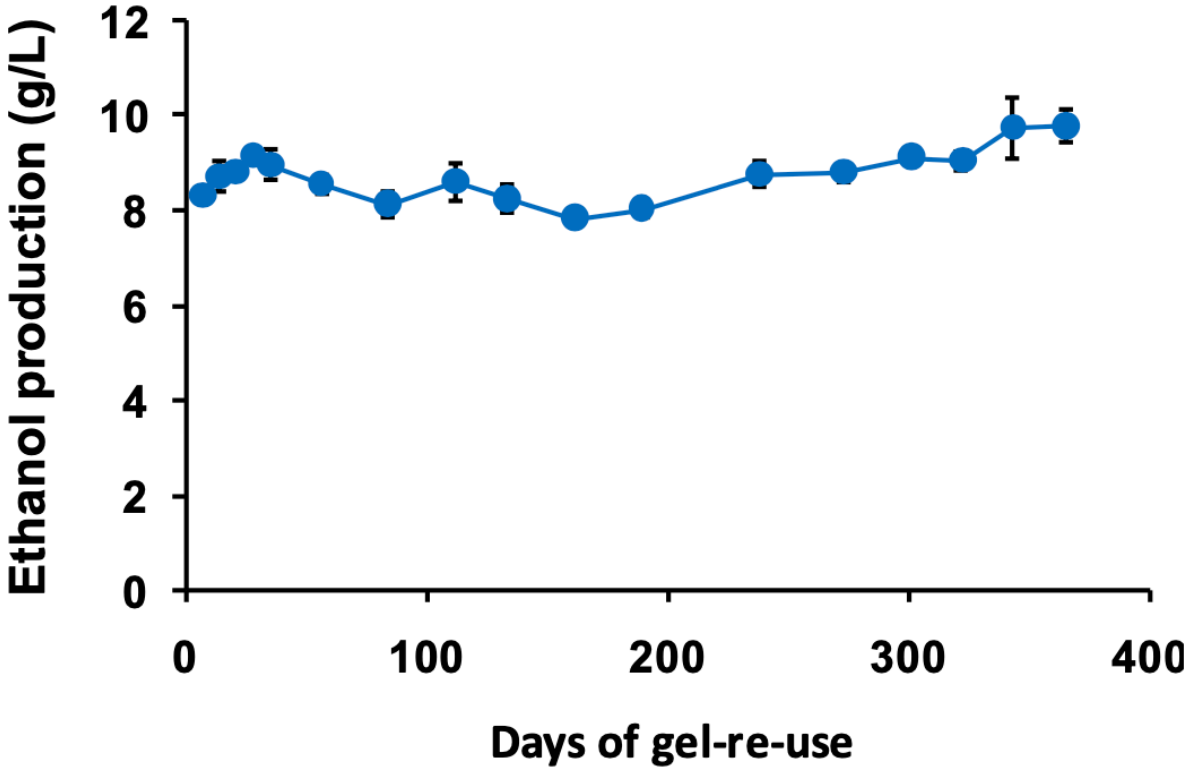

Figure C.3. The reusability of yeast-laden hydrogels for a year-long ethanol fermentation. Ethanol titer (g/L) in yeast-embedded polymers are measured for each round of reuse. Each data point and error bar represent means and standard deviations from four biological replicates.

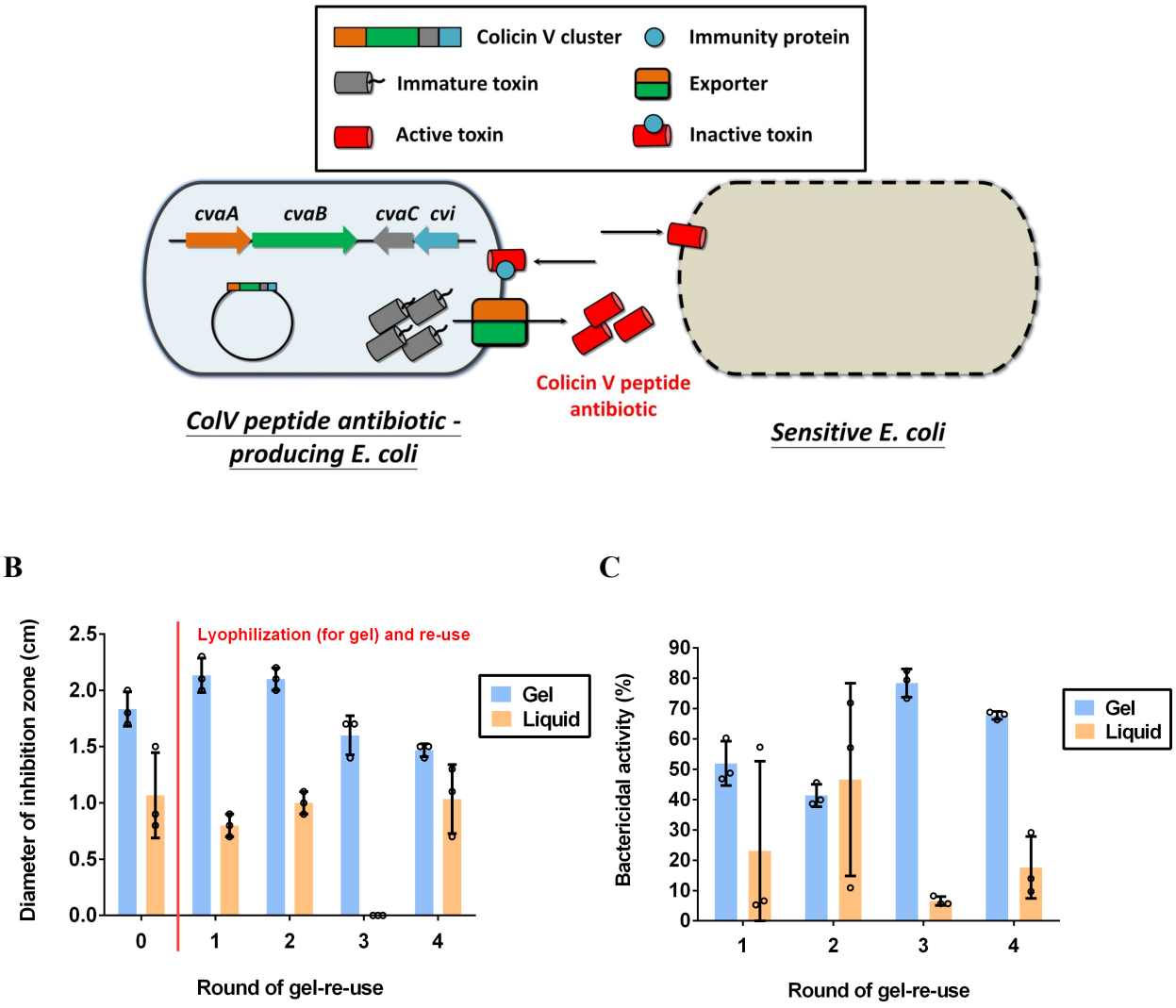

Figure C.4. Gel-re-run for colicin V (ColV) peptide antibiotic production.

A) The bactericidal mechanism of ColV. Zone of inhibition test (B) and broth test (C) are used for evaluating antimicrobial activity of ColV in gel system and liquid culture before and after lyophilization. The inconsistency in toxin production by liquid culture suggested that liquid culture might be unstable and subject to random dynamics. Each data point and error bar represent means and standard deviations from biological triplicates, respectively.

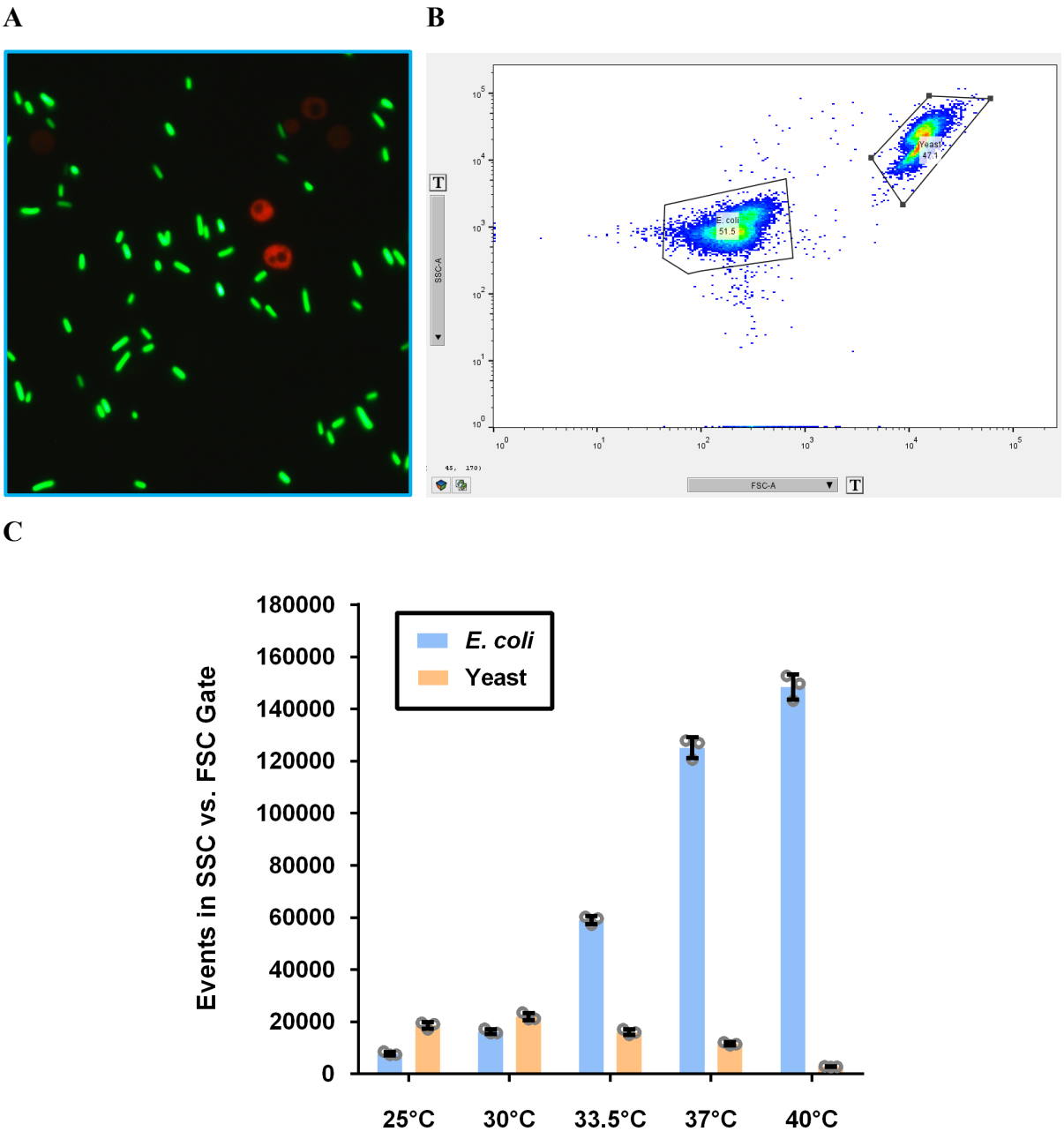

Figure C.5. Co-culture flow cytometry.

A) Visual confirmation of fluorescence and mixed culture under fluorescence microscope. B) SSC versus FSC plot for distinguishing and counting E. coli and yeast using BD Fortessa flow cytometry. C) Impact on consortia dynamics for bulk culture with different temperatures. Each data point and error bar represent means and standard deviations from biological triplicates, respectively.

A

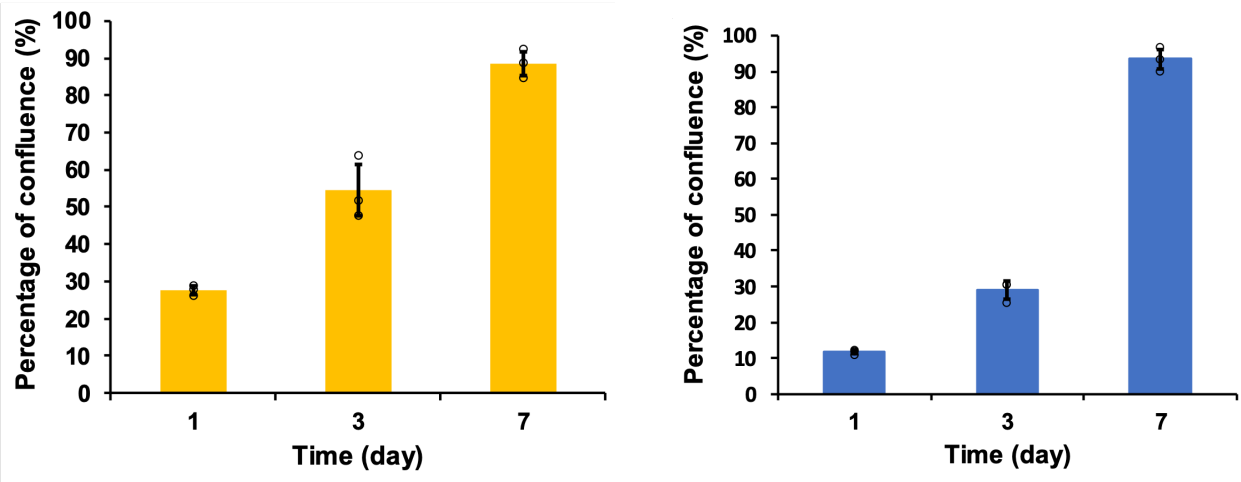
Percentage of confluence (%)
100
90
80
70
60
50
40
30
20
10
0
1
3
7
Time (day)
Percentage of confluence (%)
100
90
80
70
60
50
40
30
20
10
0
1
3
7
Time (day)

B

Day 7 Standards

30 °C – Yeast in SC

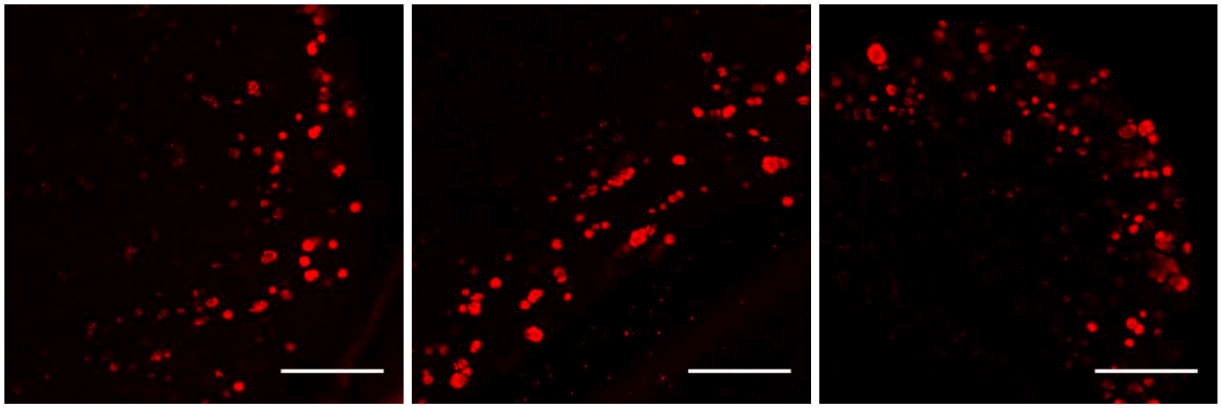

37 °C – *E. coli* in LB

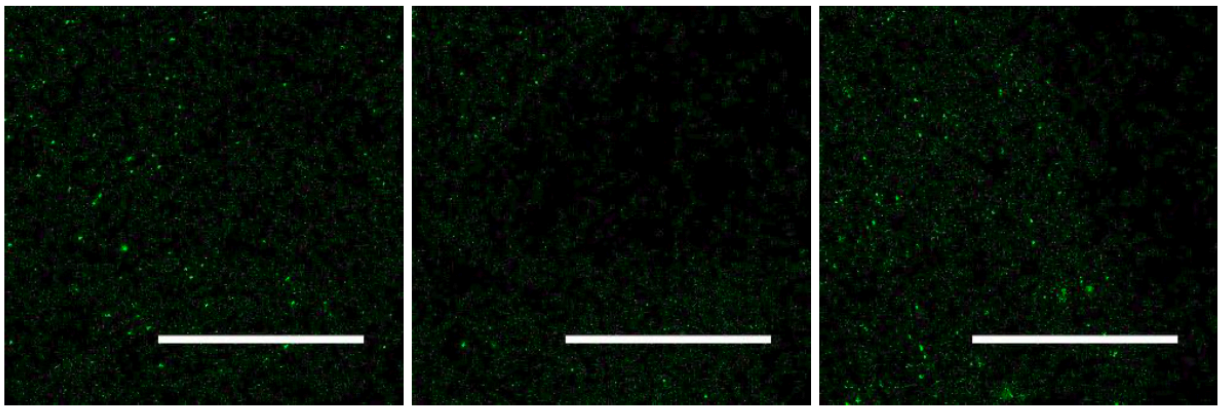

C

Day 1

25 °C – Yeast

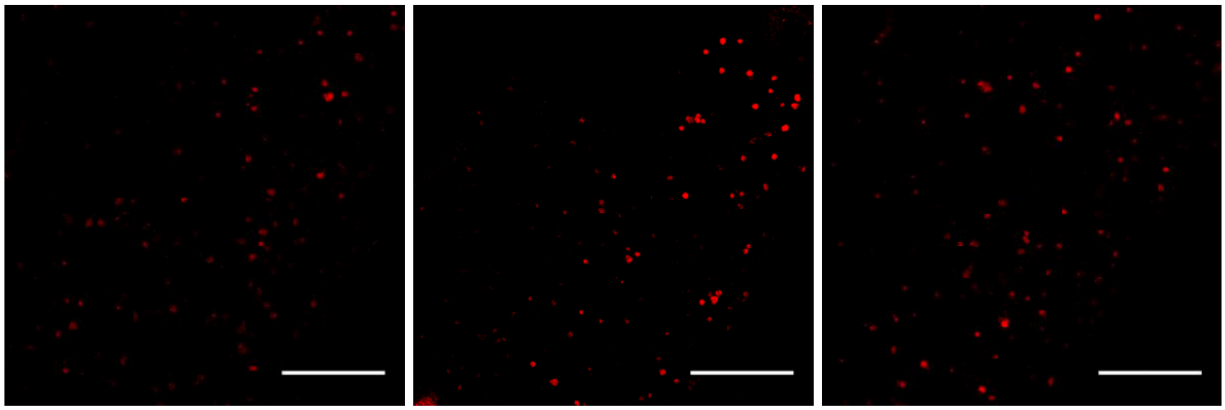

25 °C – *E. coli*

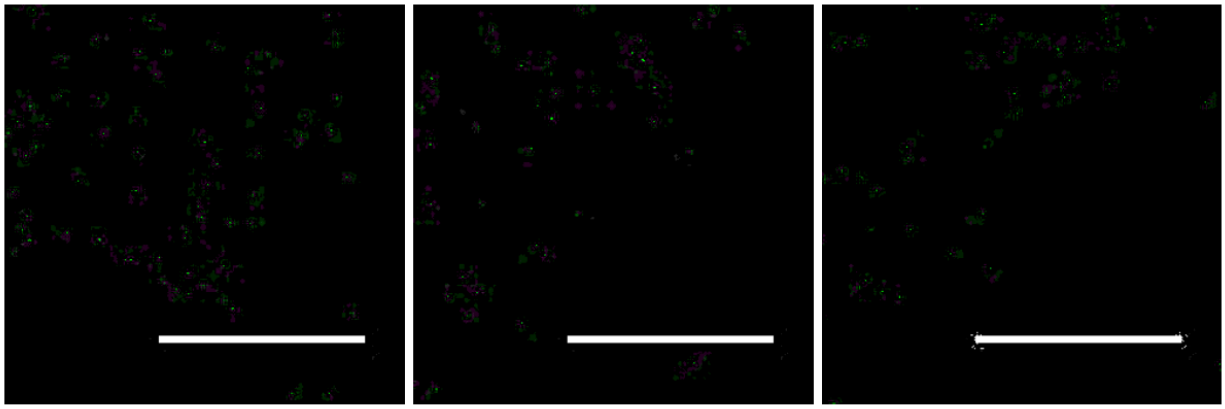

Day 3

25 °C – Yeast

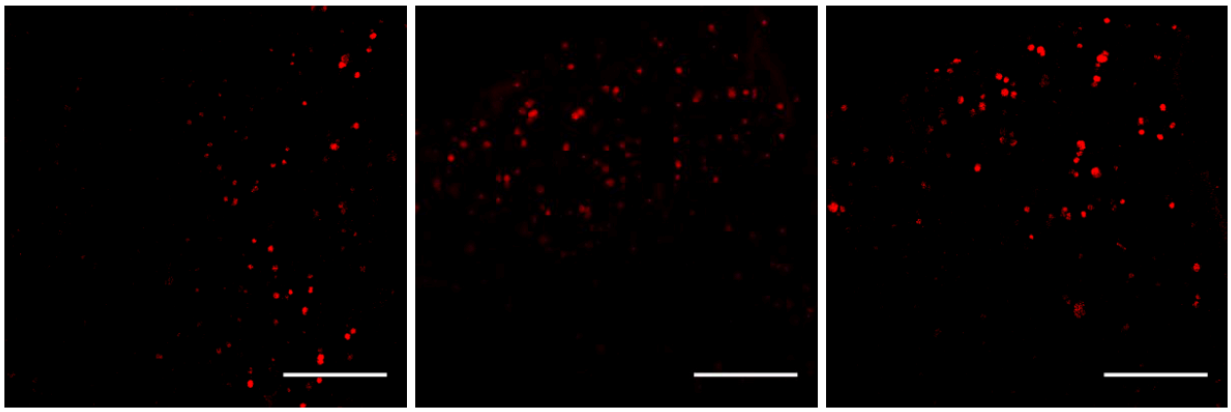

25 °C – *E. coli*

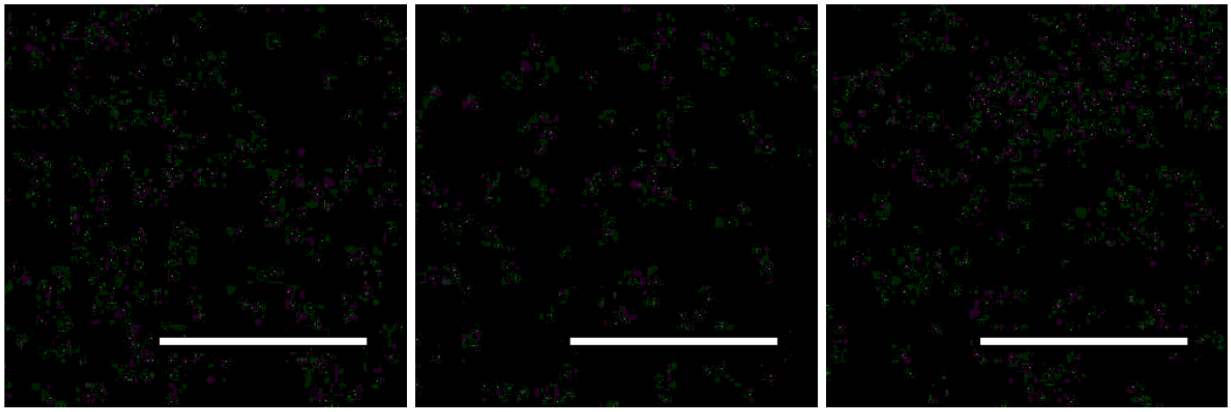

Day 7

25 °C – Yeast

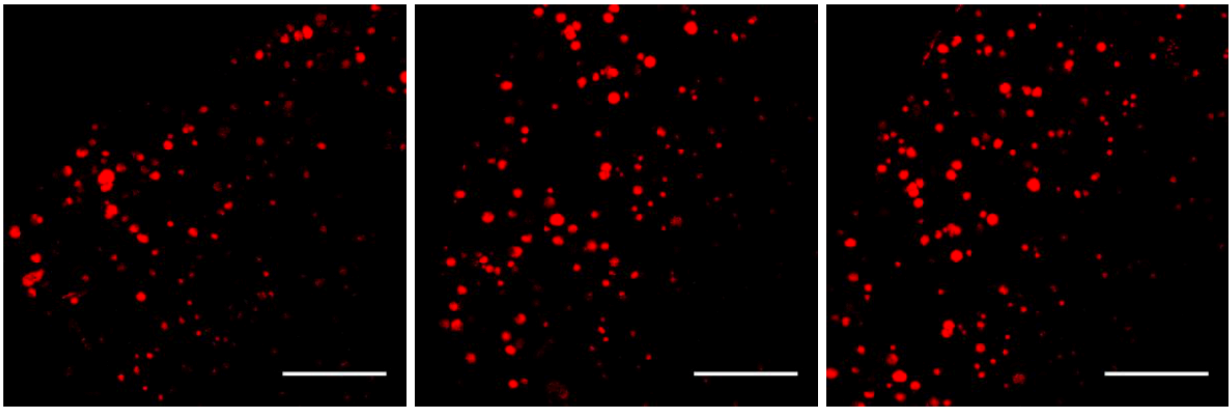

25 °C – *E. coli*

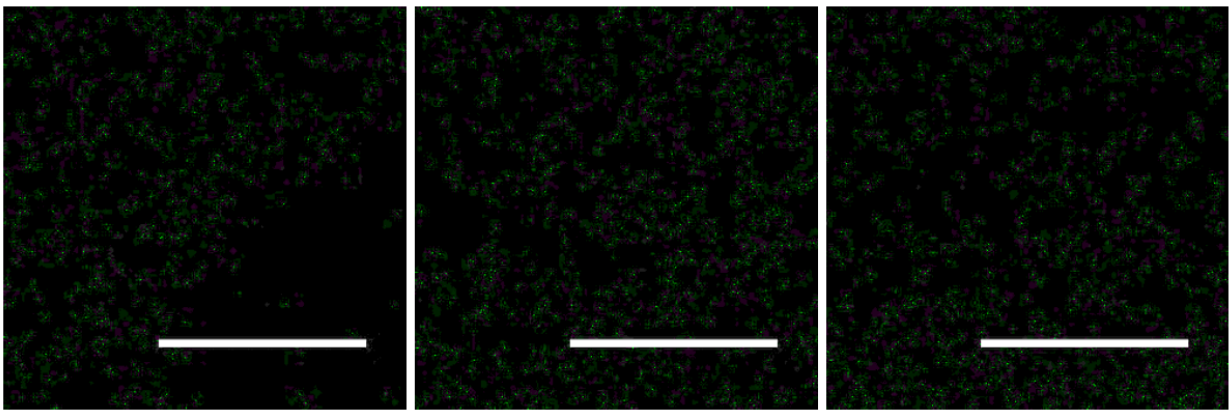

Day 1

30 °C – Yeast

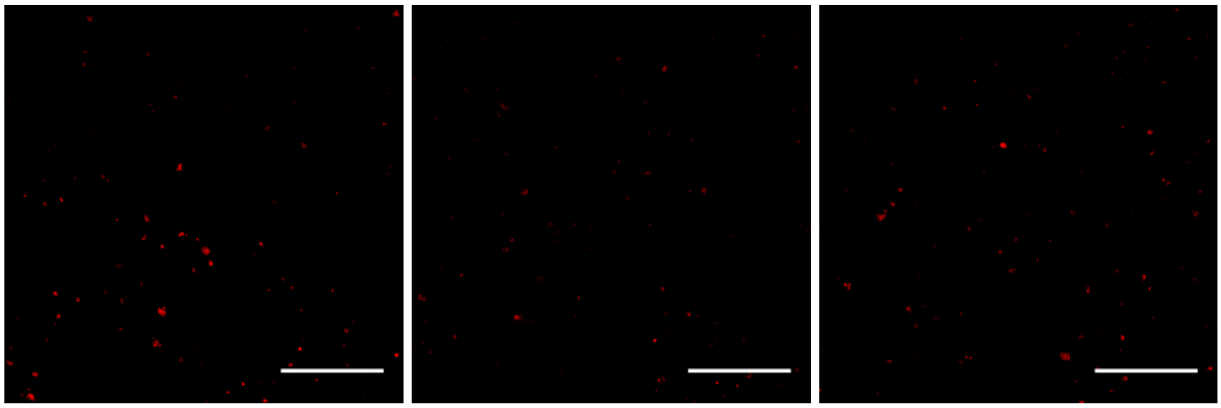

30 °C – *E. coli*

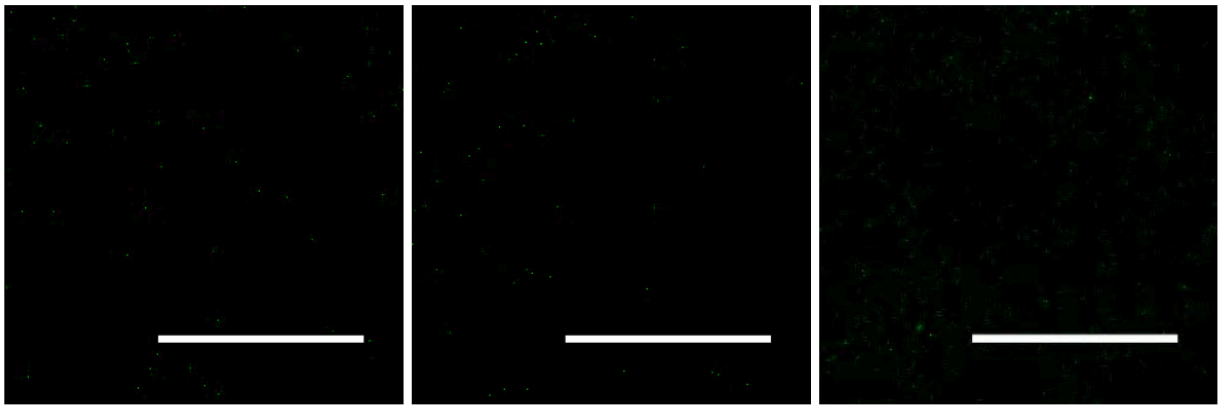

Day 3

30 °C – Yeast

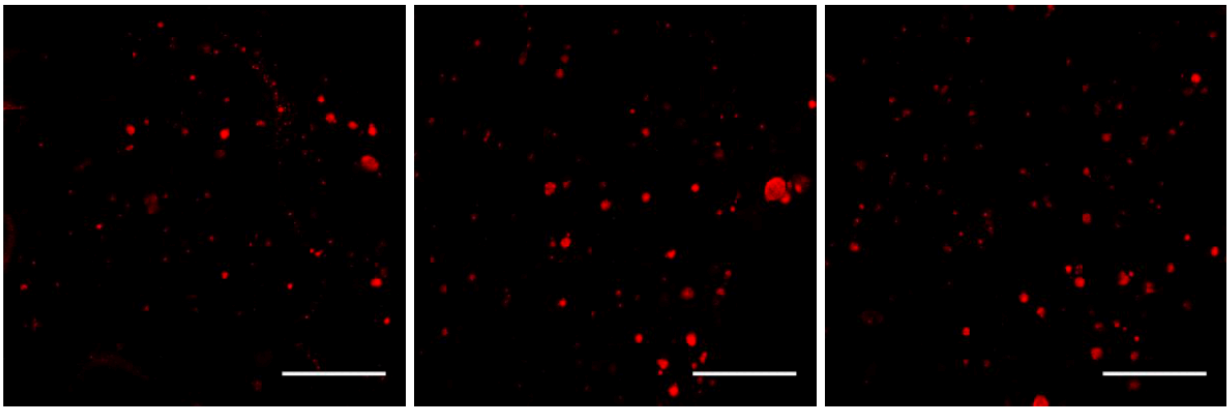

30 °C – *E. coli*

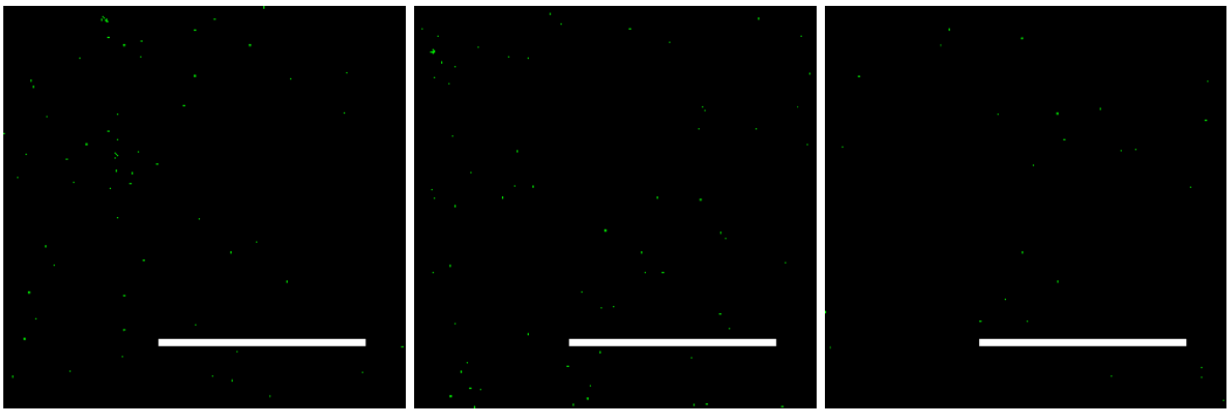

Day 7

30 °C – Yeast

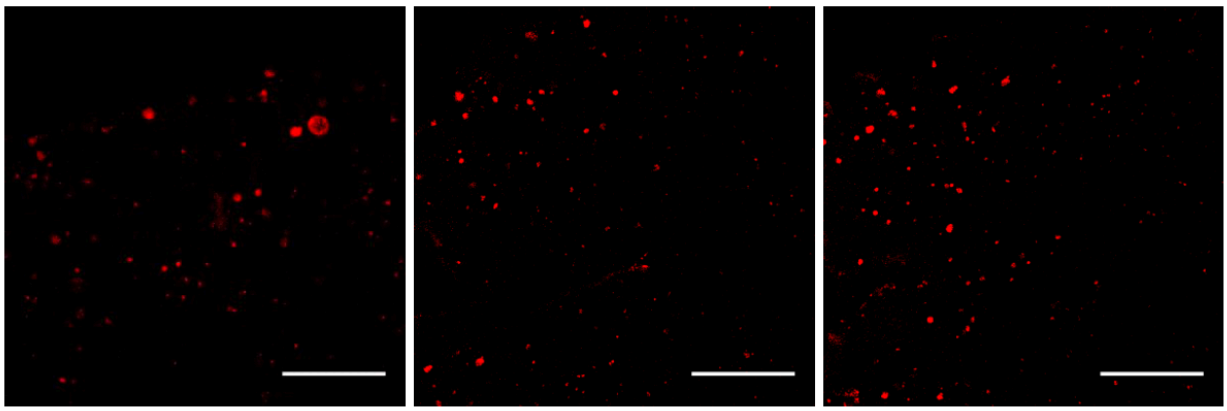

30 °C – *E. coli*

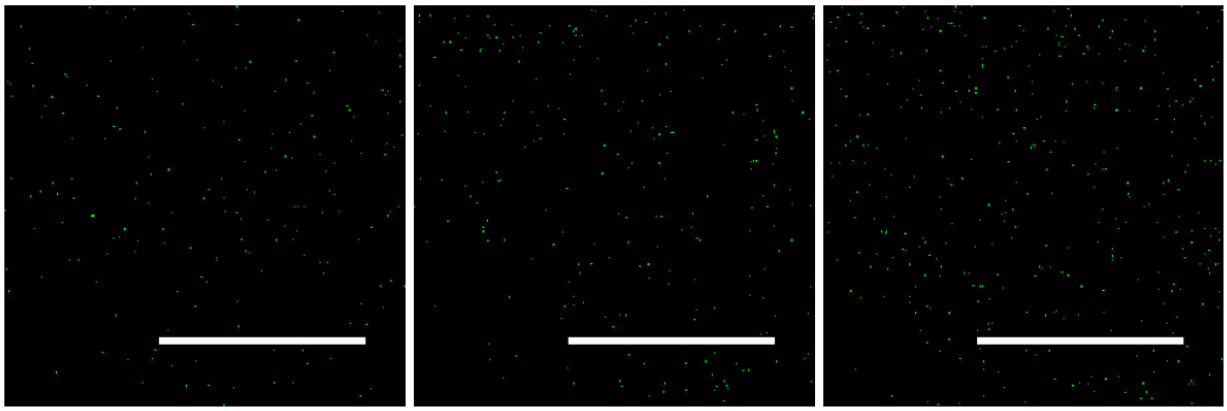

Day 1

33.5 °C – Yeast

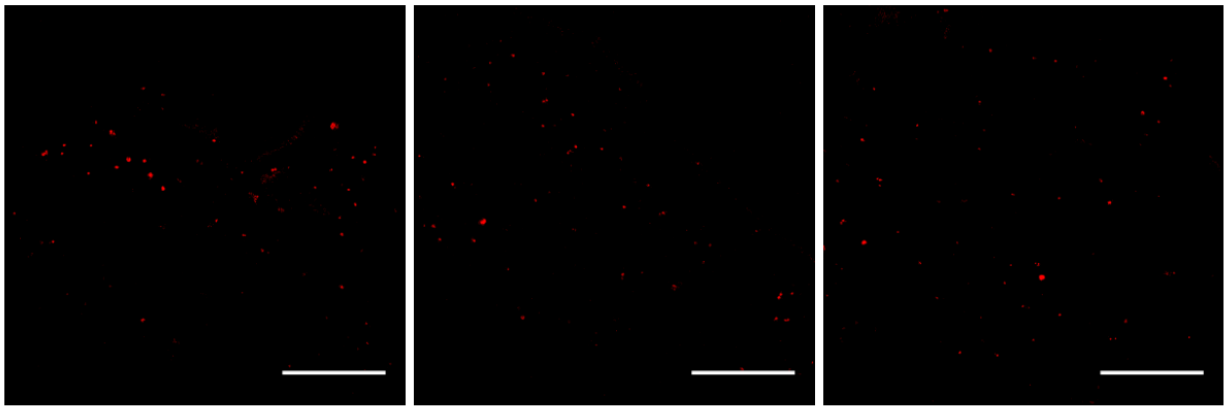

33.5 °C – *E. coli*

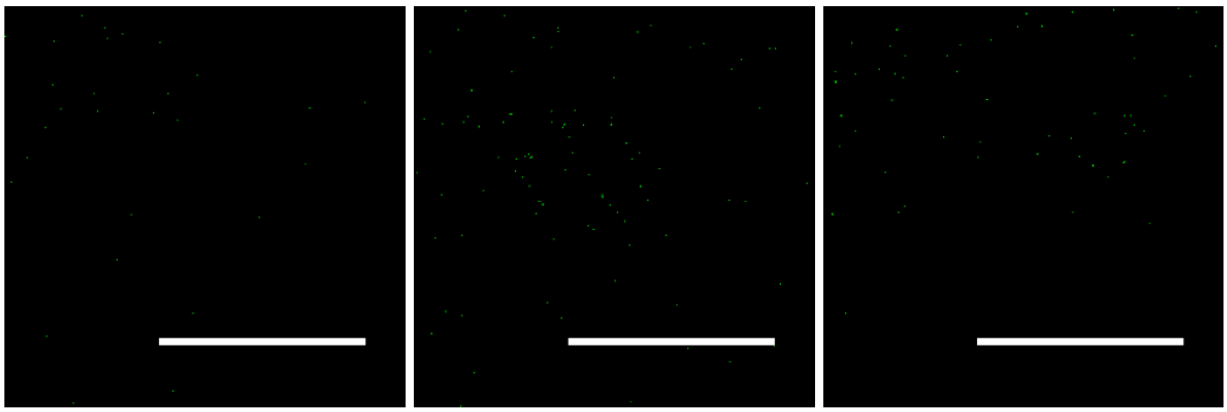

Day 3

33.5 °C – Yeast

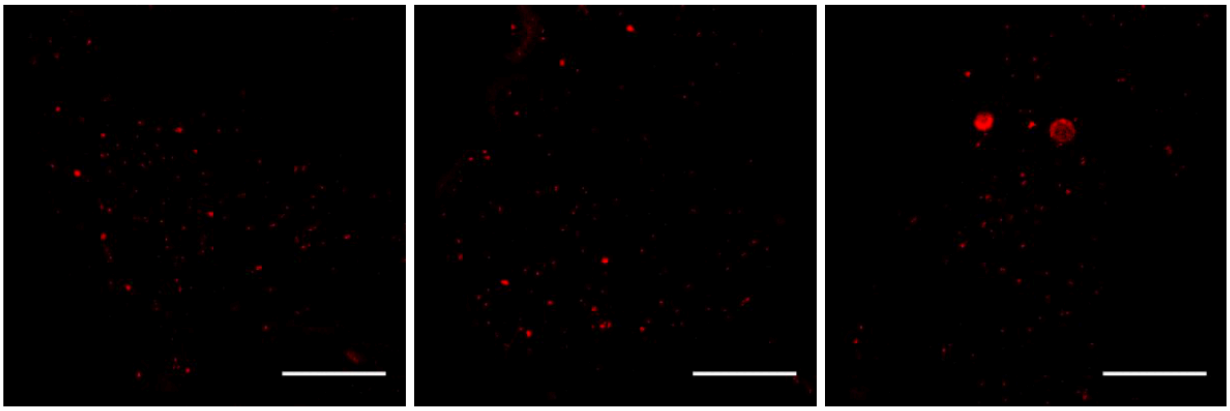

33.5 °C – *E. coli*

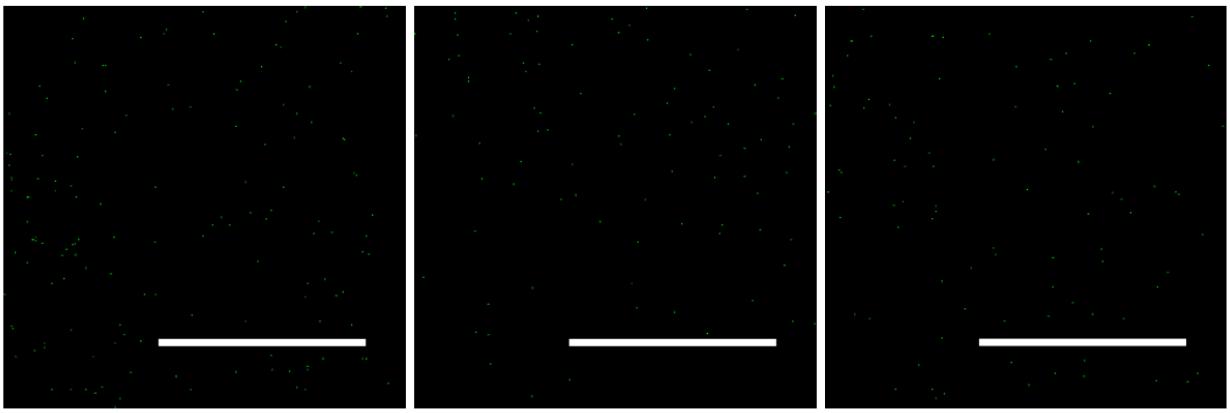

Day 7

33.5 °C – Yeast

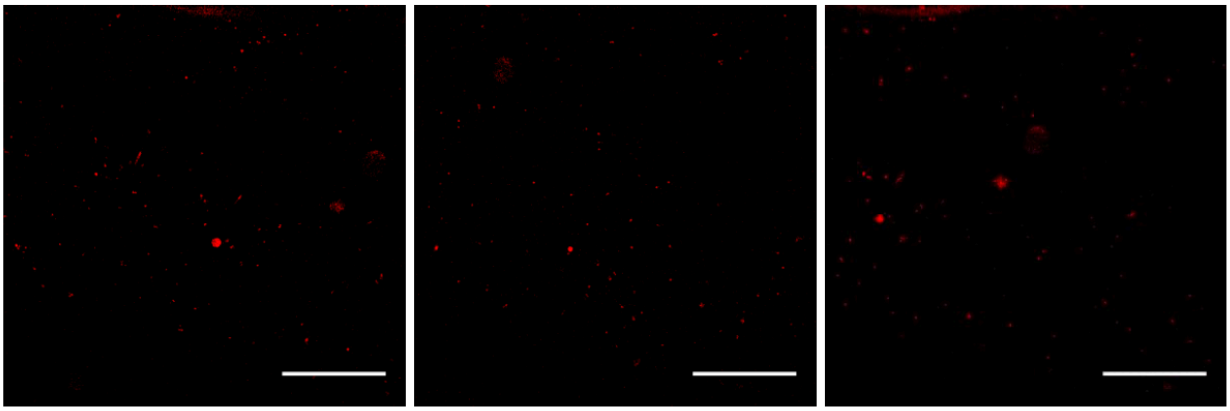

33.5 °C – *E. coli*

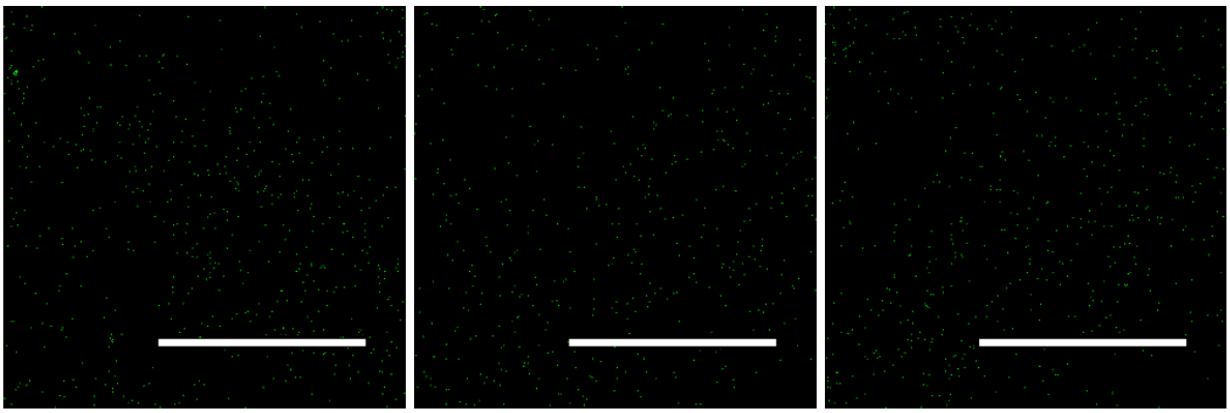

Day 1

37 °C – Yeast

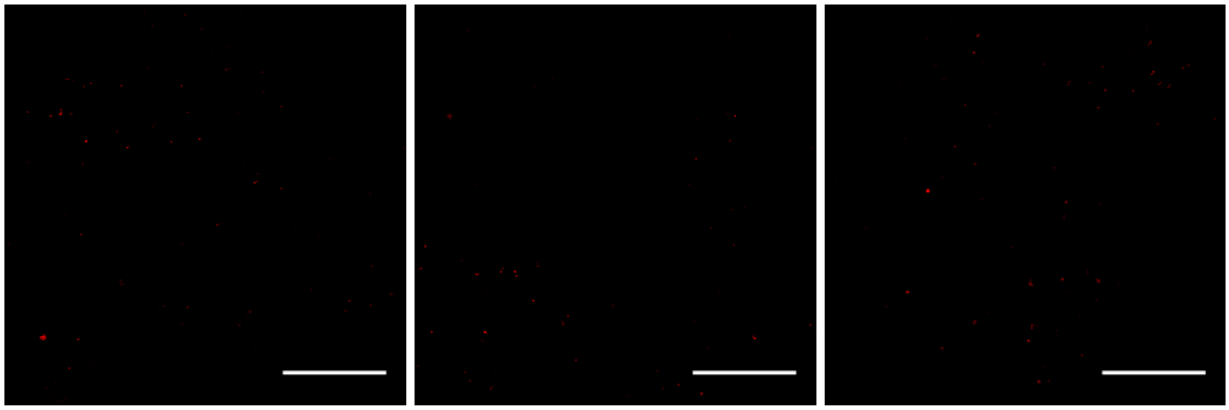

37 °C – *E. coli*

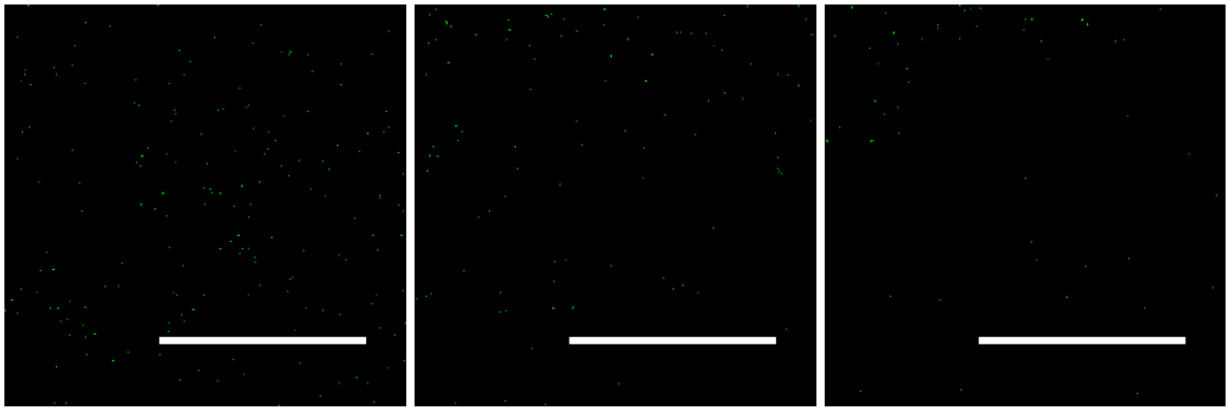

Day 3

37 °C – Yeast

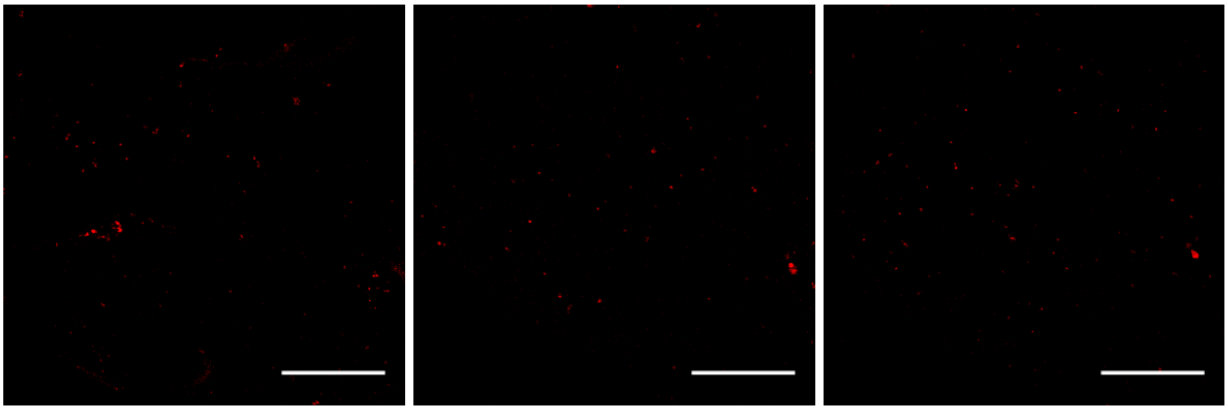

37 °C – *E. coli*

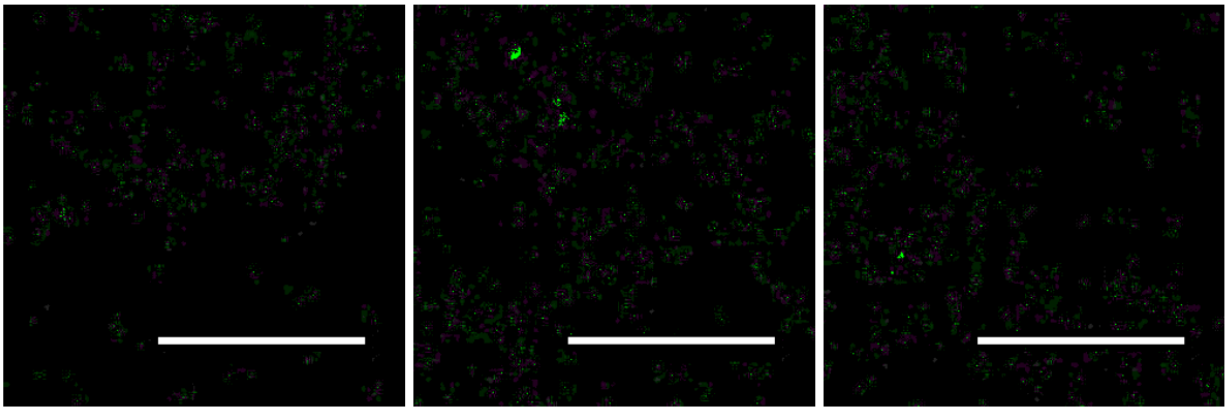

Day 7

37 °C – Yeast

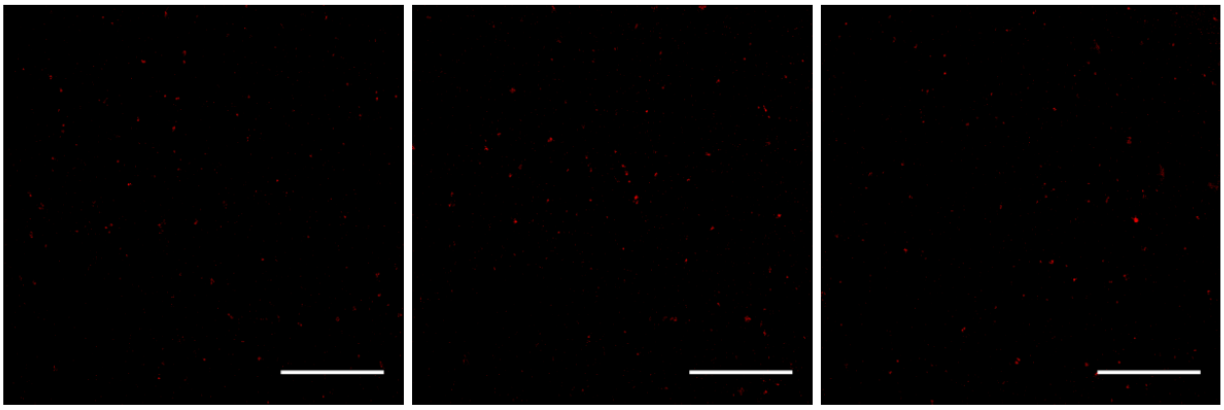

37 °C – *E. coli*

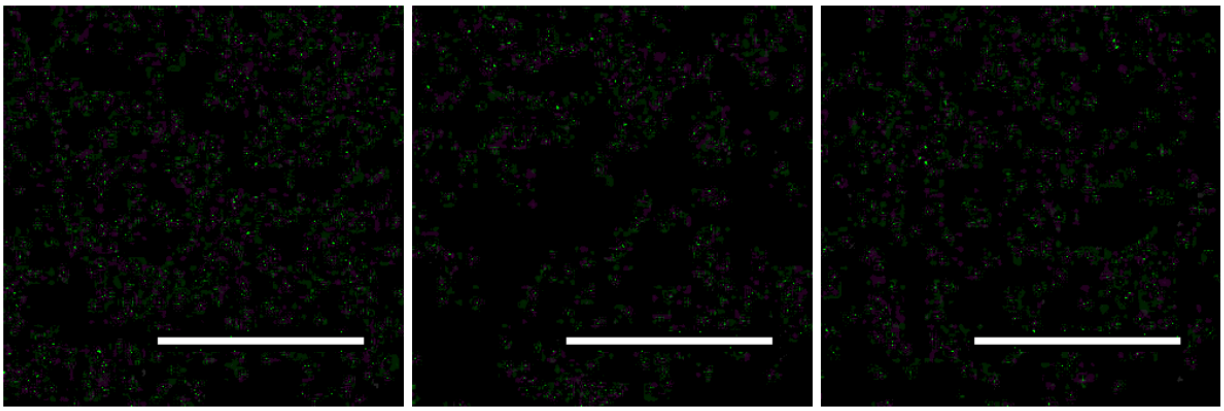

Day 1

40 °C – Yeast

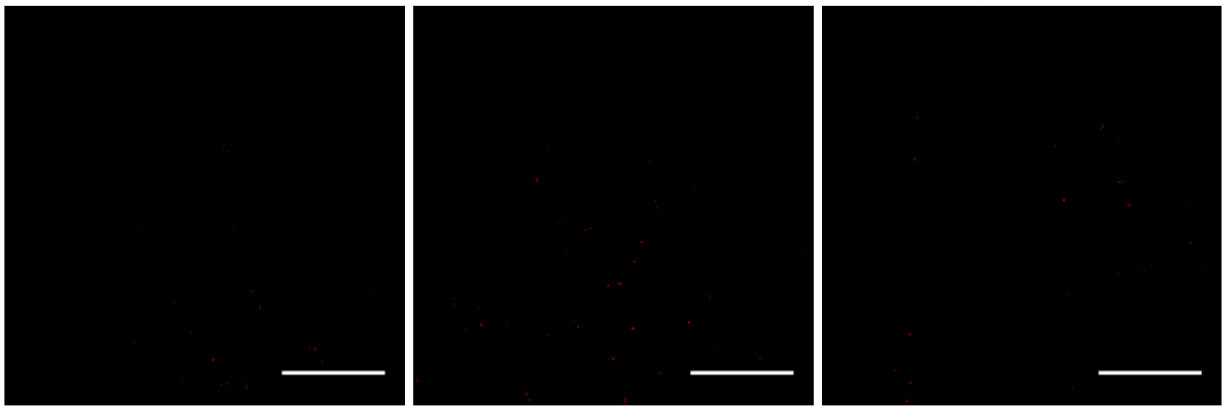

40 °C – *E. coli*

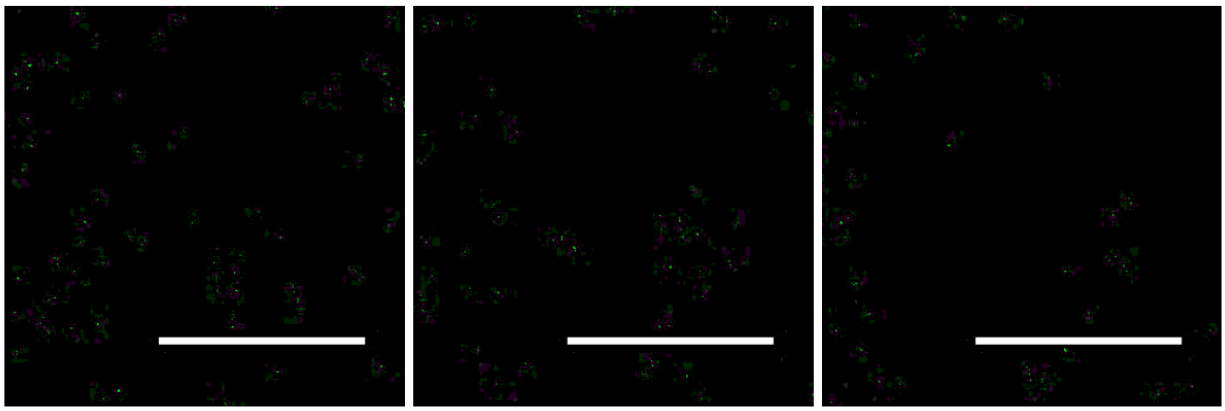

Day 3

40 °C – Yeast

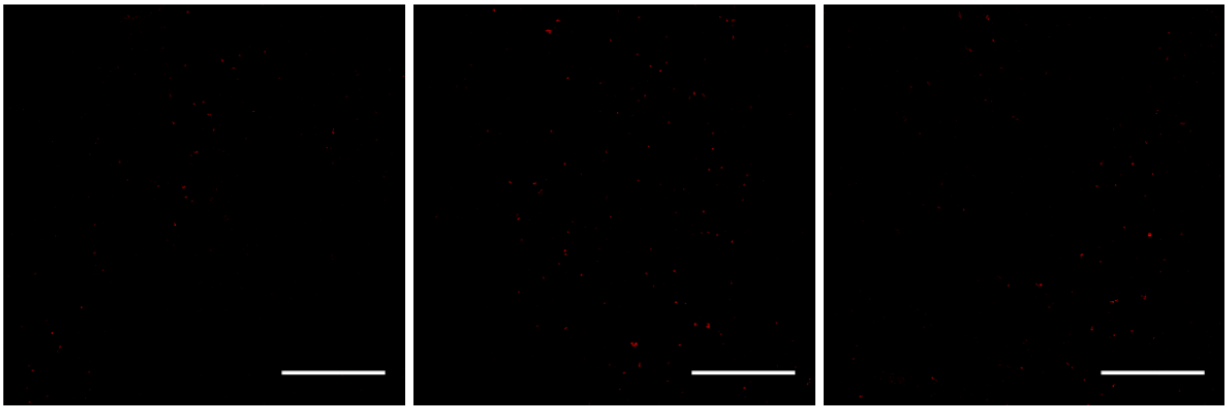

40 °C – *E. coli*

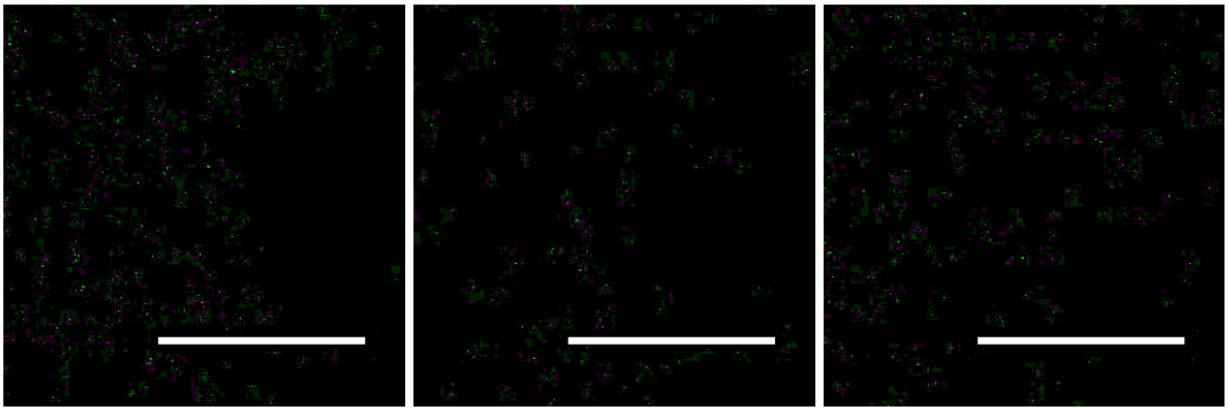

Day 7

40 °C – Yeast

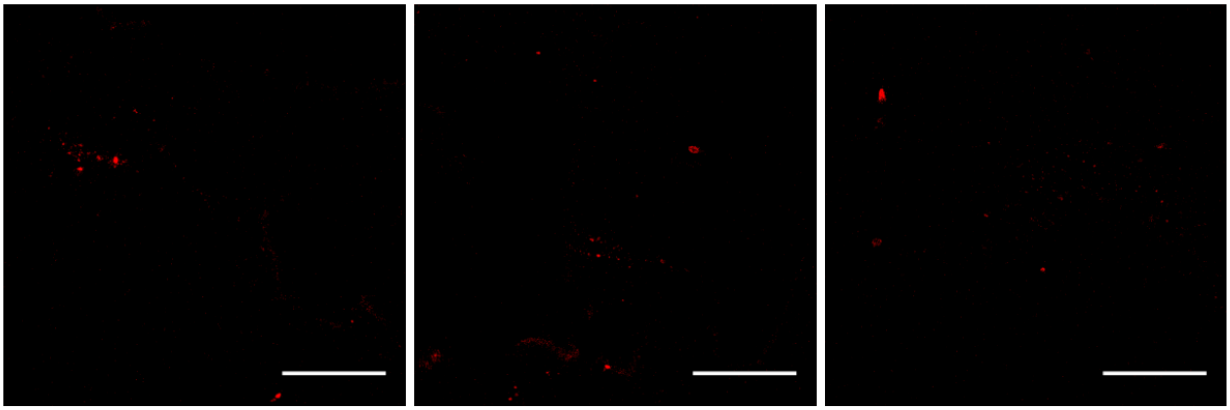

40 °C – *E. coli*

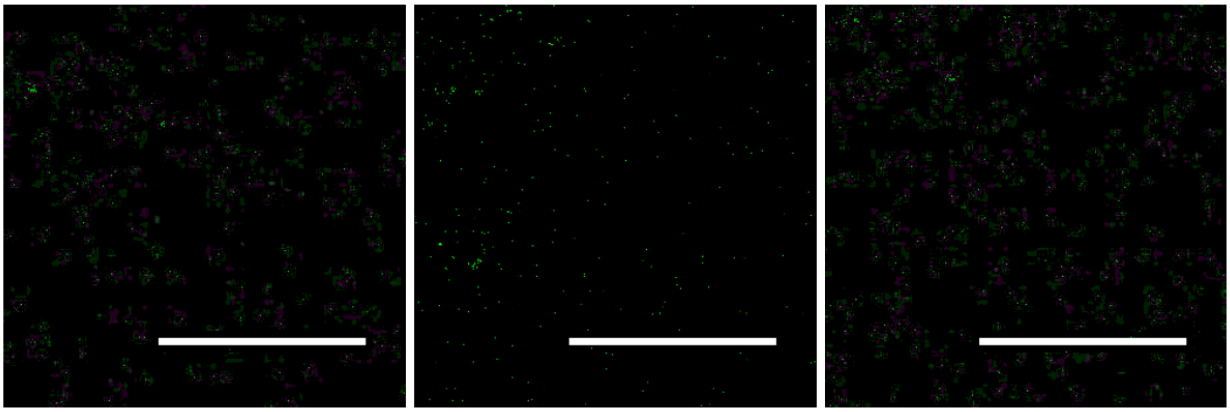

D

Day 1

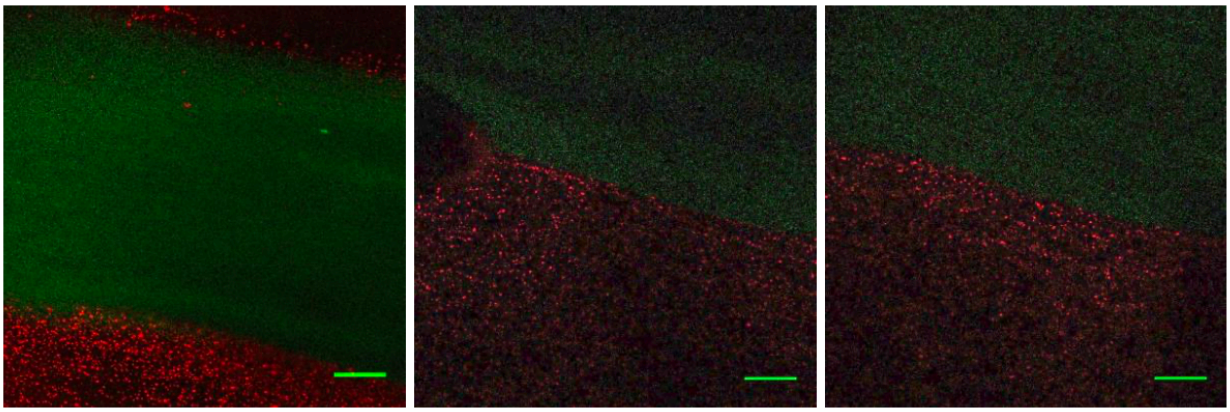

Day 3

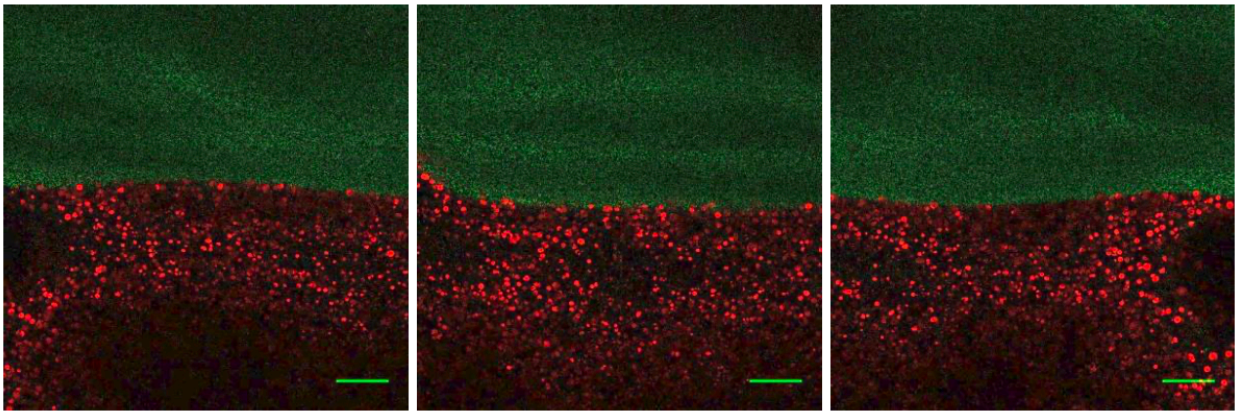

Day 7

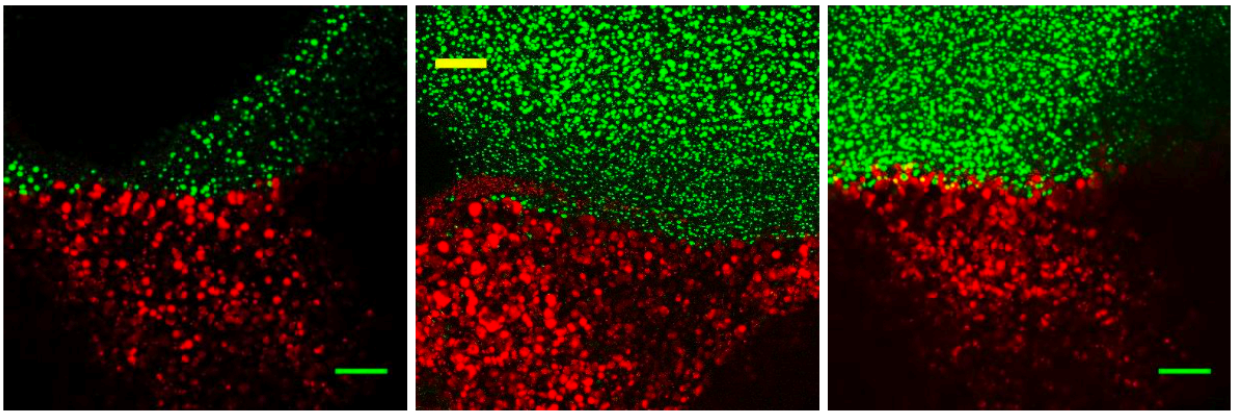

Figure C.6. Cell segregation and confluence in extrusion printed co-culture gels.

A) Confluence analysis results for the optimal E. coli growth condition (37 °C) in consortia hydrogels (left) and optimal yeast growth condition (25 °C) in consortia hydrogels (right). The E. coli and yeast samples achieved a confluence of 88.6% and 93.5% on day 7, respectively, in the

hydrogel-based consortia relative to the optimal mono-culture gels. B) Standard images used in the confluence analysis of cell growth in consortia hydrogels, representing the ideal growth conditions for yeast and E. coli monocultures (30 °C in SC media, and 37 °C in LB media, respectively). C) Images used for calculation of percent confluence of the microbial consortia hydrogels, at listed temperatures and days of incubation. D) Images depicting the cell segregation of bacteria and yeast in their respective hydrogel samples, with little to no movement or mixing of colonies between the hydrogels. The images were captured using confocal microscopy, showing a z-stack of 100 microns of depth at the interface between gel samples printed with RFP yeast and GFP bacteria. All images have 200-micron scale bars.

A

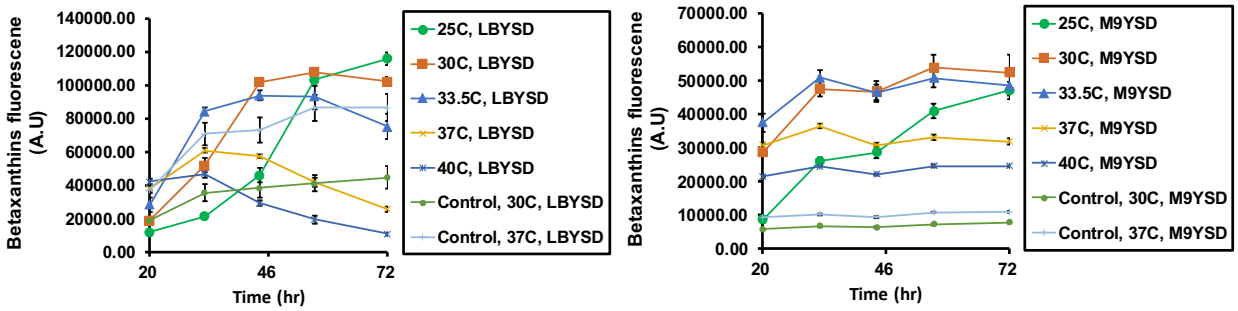
Betaxanthins fluorescene (A.U)
140000.00
120000.00
100000.00
80000.00
60000.00
40000.00
20000.00
0.00
20
46
72
Time (hr)
25C, LBYSD
30C, LBYSD
33.5C, LBYSD
37C, LBYSD
40C, LBYSD
Control, 30C, LBYSD
Control, 37C, LBYSD
Betaxanthins fluorescene (A.U)
70000.00
60000.00
50000.00
40000.00
30000.00
20000.00
10000.00
0.00
20
46
72
Time (hr)
25C, M9YSD
30C, M9YSD
33.5C, M9YSD
37C, M9YSD
40C, M9YSD
Control, 30C, M9YSD
Control, 37C, M9YSD

B

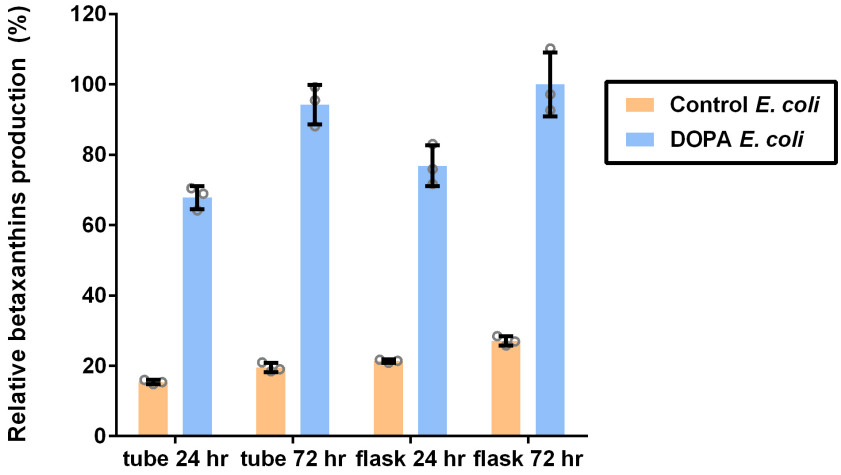
Relative betaxanthins production (%)
120
100
80
60
40
20
0
tube 24 hr
tube 72 hr
flask 24 hr
flask 72 hr
Control E. coli
DOPA E. coli

C

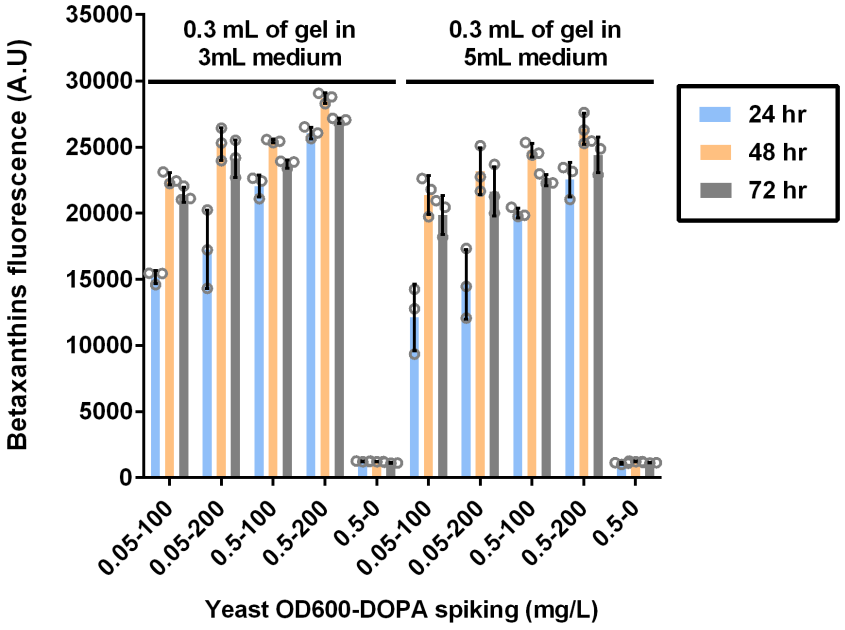
Betaxanthins fluorescence (A.U)
35000
30000
25000
20000
15000
10000
5000
0
0.3 mL of gel in 3mL medium
0.3 mL of gel in 5mL medium
24 hr
48 hr
72 hr
0.05-100
0.05-200
0.5-100
0.5-200
0.5-0
0.05-100
0.05-200
0.5-100
0.5-200
0.5-0
Yeast OD600-DOPA spiking (mg/L)

D

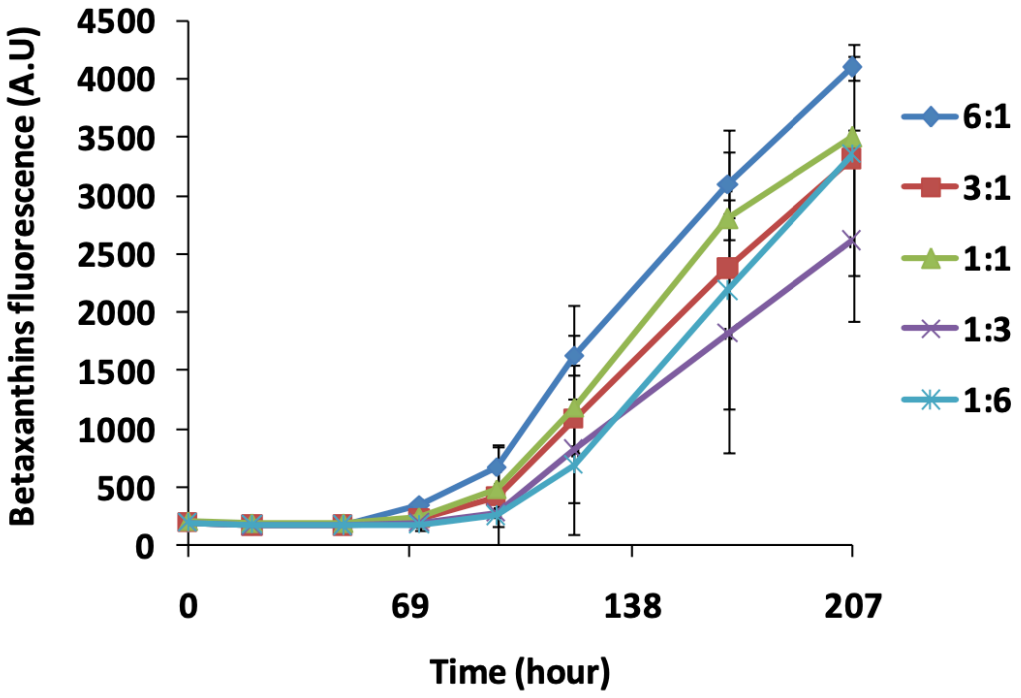
Betaxanthins fluorescence (A.U)
4500
4000
3500
3000
2500
2000
1500
1000
500
0
0
69
138
207
Time (hour)
6:1
3:1
1:1
1:3
1:6

E

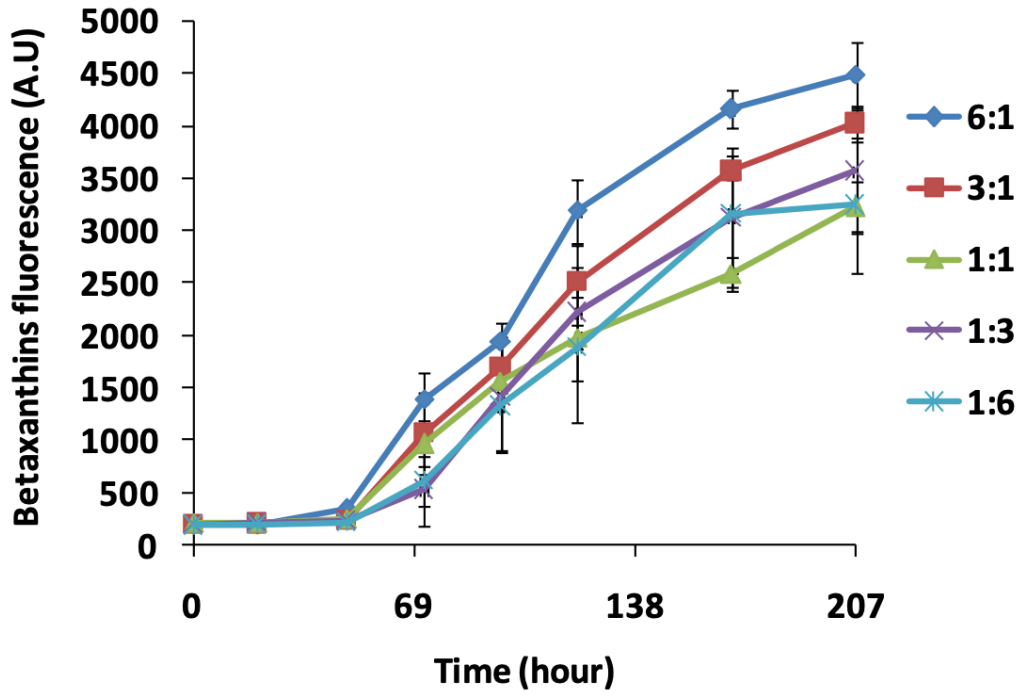
Betaxanthins fluorescence (A.U)
5000
4500
4000
3500
3000
2500
2000
1500
1000
500
0
0
69
138
207
Time (hour)
6:1
3:1
1:1
1:3
1:6

F

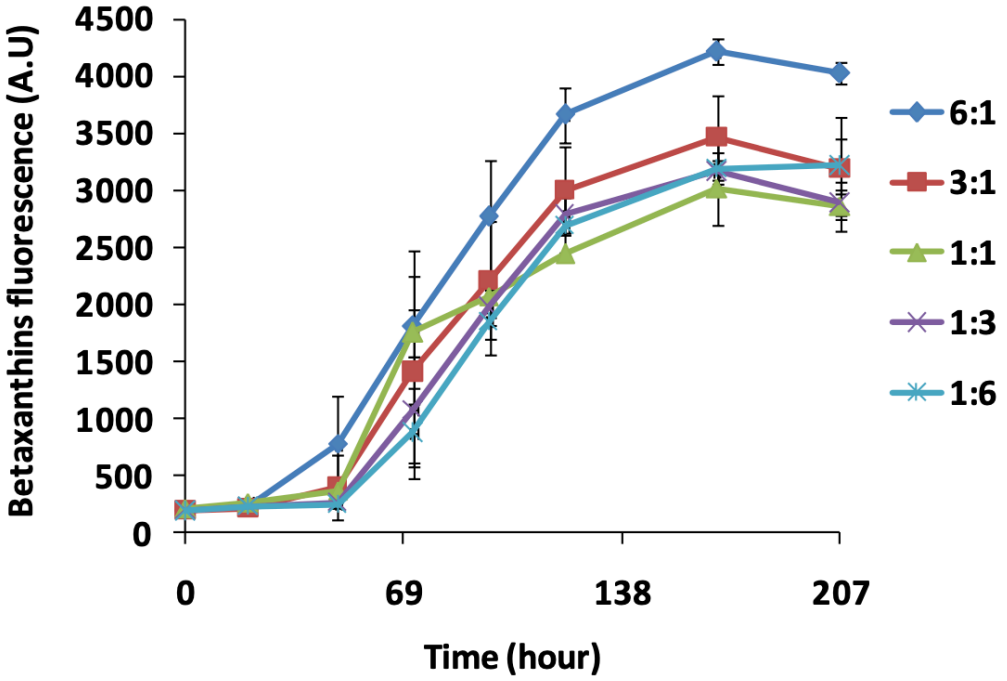
Betaxanthins fluorescence (A.U)
4500
4000
3500
3000
2500
2000
1500
1000
500
0
0
69
138
207
Time (hour)
6:1
3:1
1:1
1:3
1:6

G

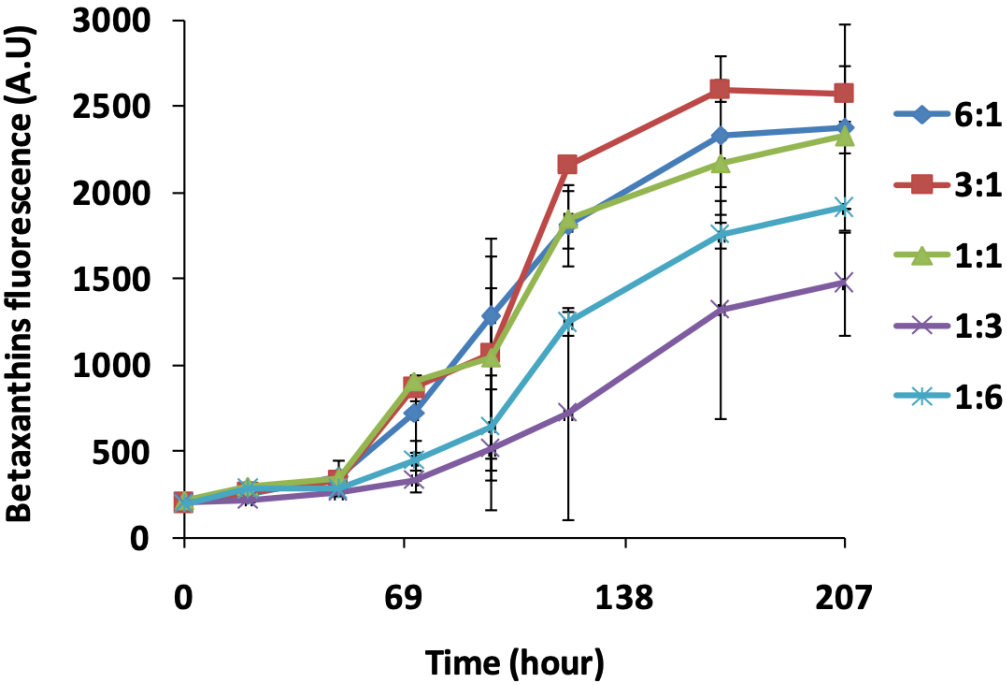
Betaxanthins fluorescence (A.U)
3000
2500
2000
1500
1000
500
0
0
69
138
207
Time (hour)
6:1
3:1
1:1
1:3
1:6

H

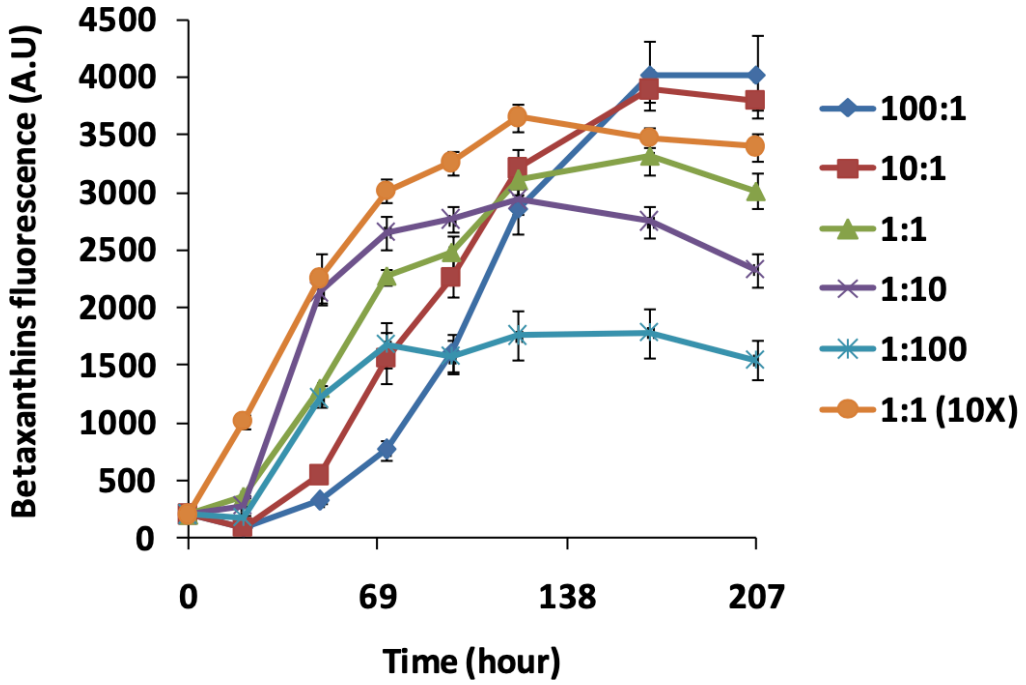
Betaxanthins fluorescence (A.U)
4500
4000
3500
3000
2500
2000
1500
1000
500
0
0
69
138
207
Time (hour)
100:1
10:1
1:1
1:10
1:100
1:1 (10X)

I

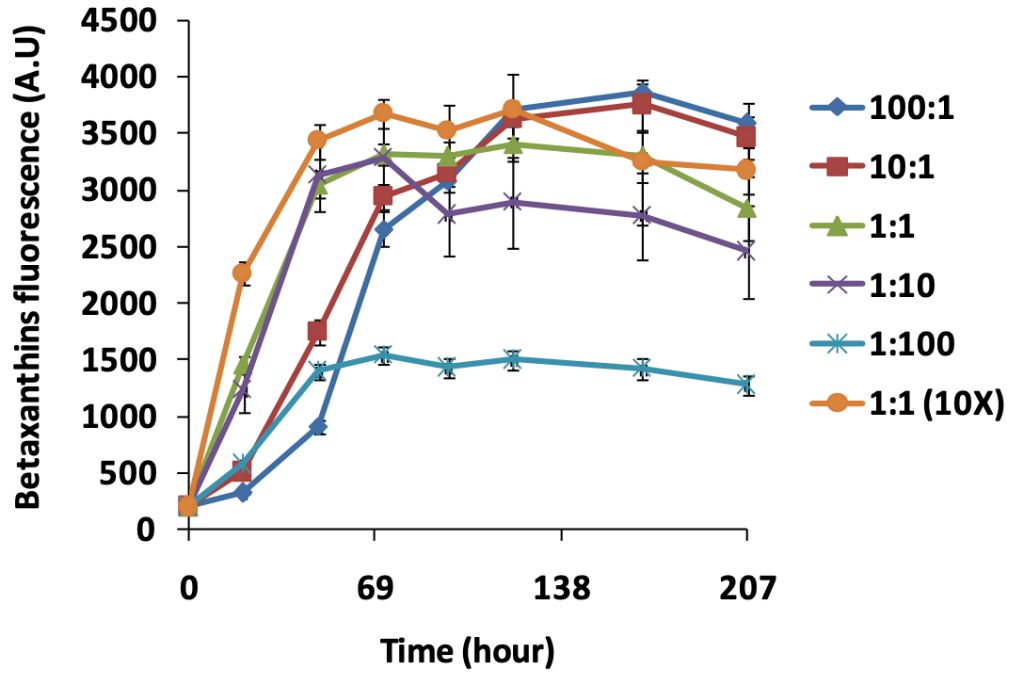
Betaxanthins fluorescence (A.U)
4500
4000
3500
3000
2500
2000
1500
1000
500
0
0
69
138
207
Time (hour)
100:1
10:1
1:1
1:10
1:100
1:1 (10X)

J

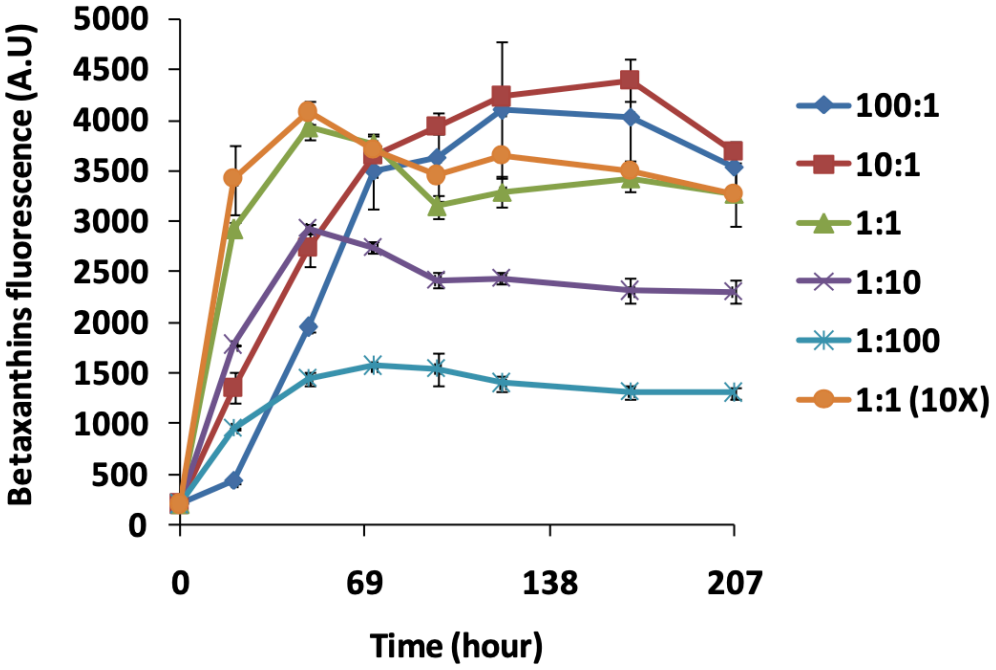
Betaxanthins fluorescence (A.U)
5000
4500
4000
3500
3000
2500
2000
1500
1000
500
0
0
69
138
207
Time (hour)
100:1
10:1
1:1
1:10
1:100
1:1 (10X)

K

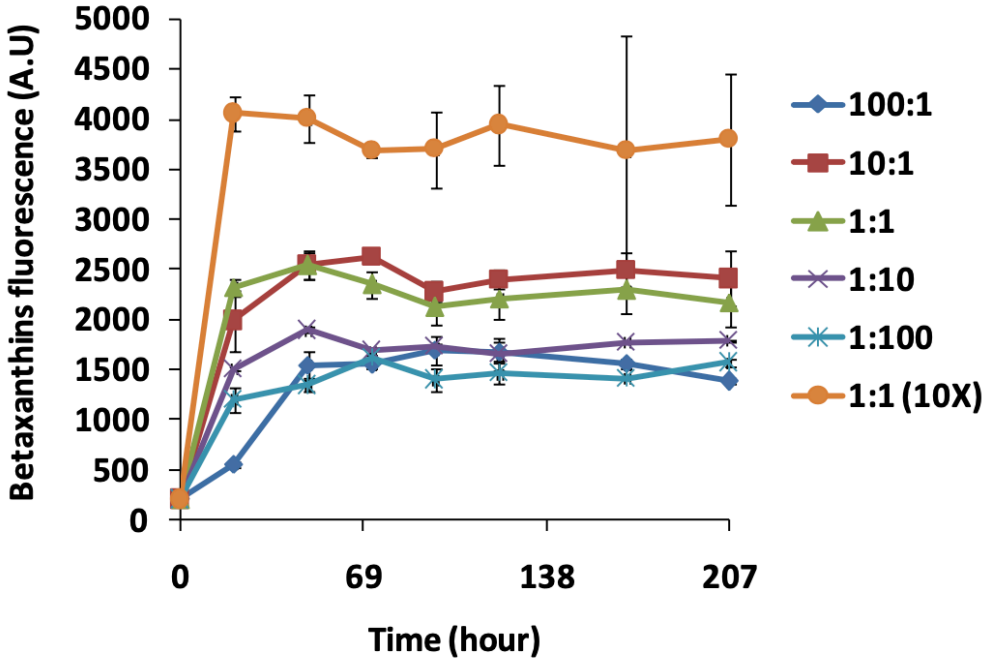
Betaxanthins fluorescence (A.U)
5000
4500
4000
3500
3000
2500
2000
1500
1000
500
0
0
69
138
207
Time (hour)
100:1
10:1
1:1
1:10
1:100
1:1 (10X)

L

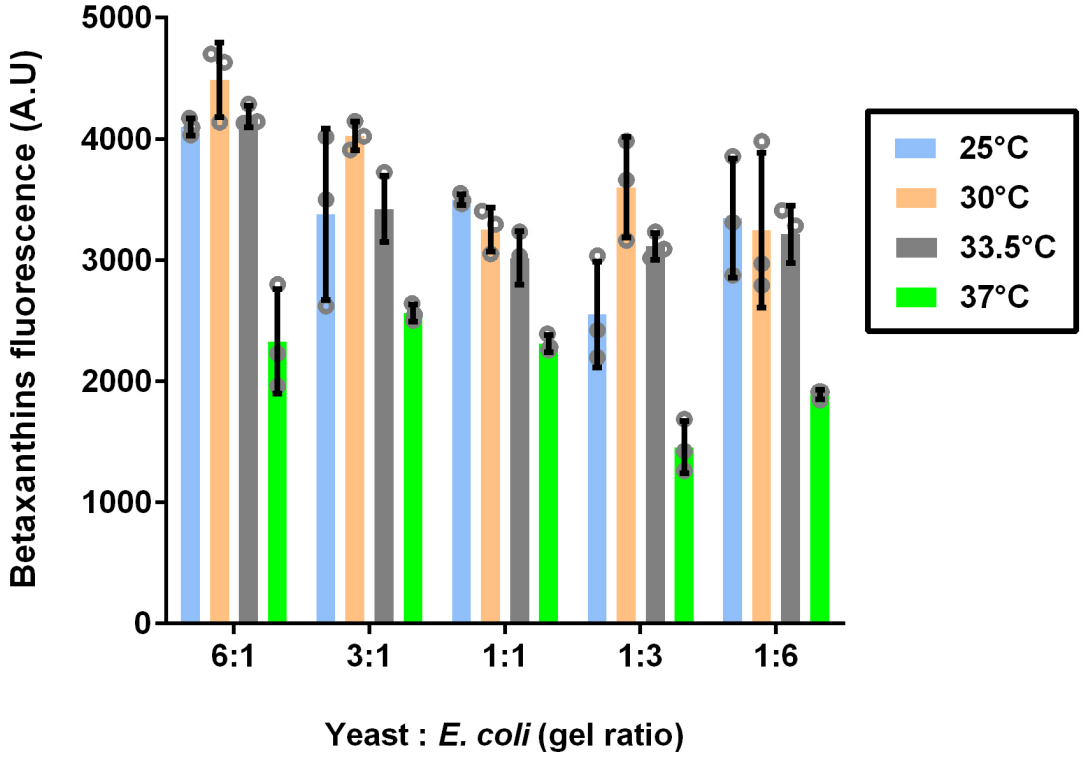
Betaxanthins fluorescence (A.U)
5000
4000
3000
2000
1000
0
6:1
3:1
1:1
1:3
1:6
Yeast : E. coli (gel ratio)
25°C
30°C
33.5°C
37°C

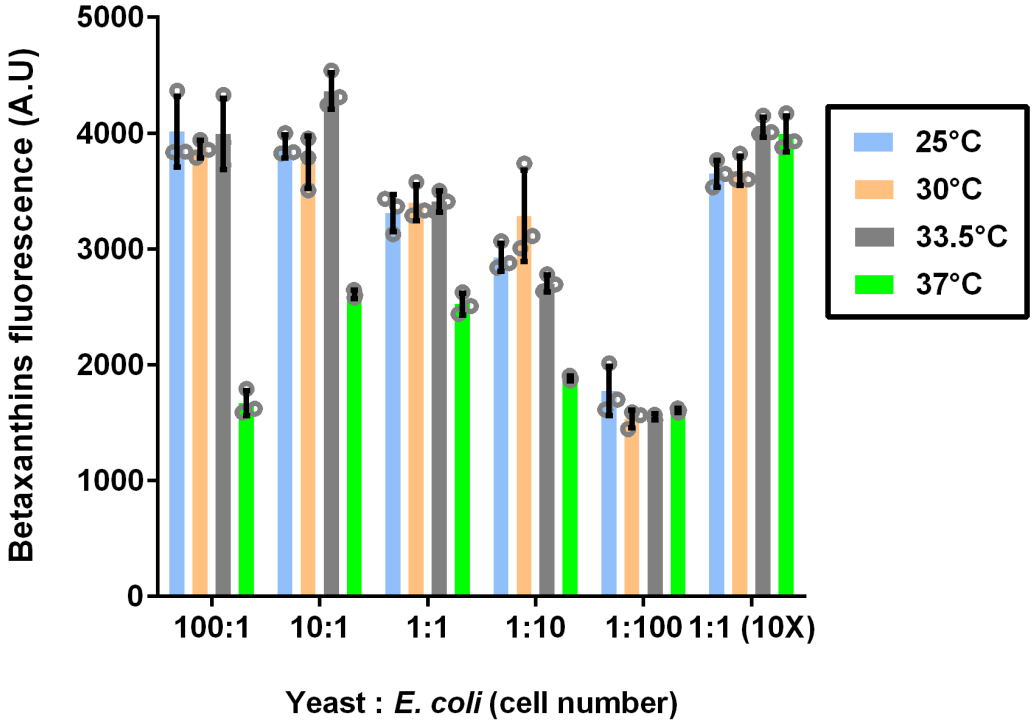
Betaxanthins fluorescence (A.U)
5000
4000
3000
2000
1000
0
100:1
10:1
1:1
1:10
1:100
1:1 (10X)
Yeast : E. coli (cell number)
25°C
30°C
33.5°C
37°C

Figure C.7. Betaxanthins production.

A) Medium optimization for betaxanthins production with different temperatures. Yeast sBY08 and E. coli eBL0430D strains were used for this study. Production was evaluated using LBYSD (left) or M9YSD medium (right) supplemented with 20 g/L glucose and appropriate amount of antibiotics. B) The comparison of betaxanthins production for bulk culture between tube and flask scales. Betaxanthins fluorescence was measured at 24 and 72-hour time points. While production at flask scale works better than that at tube scale, probably because flask provides more oxygen transfer (DOD reaction requires oxygen), tube scale was chosen for the following experiments for operational convenience. C) Betaxanthins production via DOD yeast-laden hydrogel. The comparison of betaxanthins production for yeast-laden gel between 3 mL and 5mL gel culture volume. 3 mL culture volume was selected for the following experiments due to higher betaxanthins production possibly resulted from better oxygenation compared to that using 5 mL culture condition. D-G) Betaxanthins production via E. coli-yeast consortia gels in round 0. The productions are evaluated through altering gel ratios and fermentation temperatures. Time course of betaxanthins production for hydrogel system at 25 (D), 30 (E), 33.5 (F) and 37 (G) °C. H-K) Betaxanthins production via E. coli-yeast bulk culture in round 0. The productions are evaluated through altering cell number and fermentation temperatures. Time course of betaxanthins production for bulk culture at 25 (H), 30 (I), 33.5 (J) and 37 (K) °C. L) The comparison of maximum production of betaxanthins in the round 0 between hydrogel system (top) and liquid culture (bottom).

A

➢ 30 °C

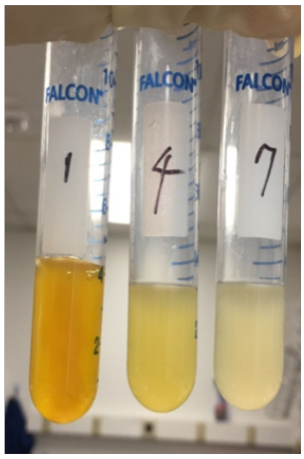

gel culture | liquid culture | liquid culture (10X)

➢ 33.5 °C

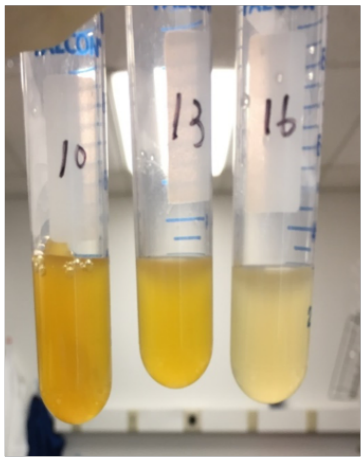

gel culture | liquid culture | liquid culture (10X)

B

➢ 30 °C

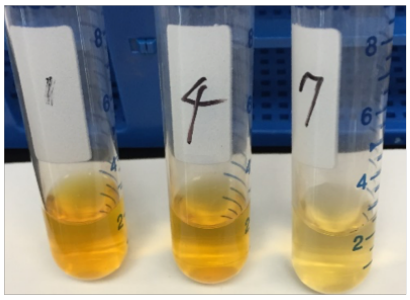

gel culture | liquid culture | liquid culture (10X)

Pellet displayed dark brown instead of yellow for liquid culture.

➢ 33.5 °C

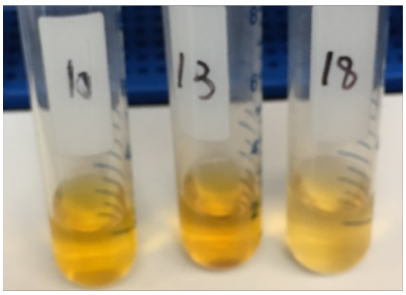

gel culture | liquid culture | liquid culture (10X)

C

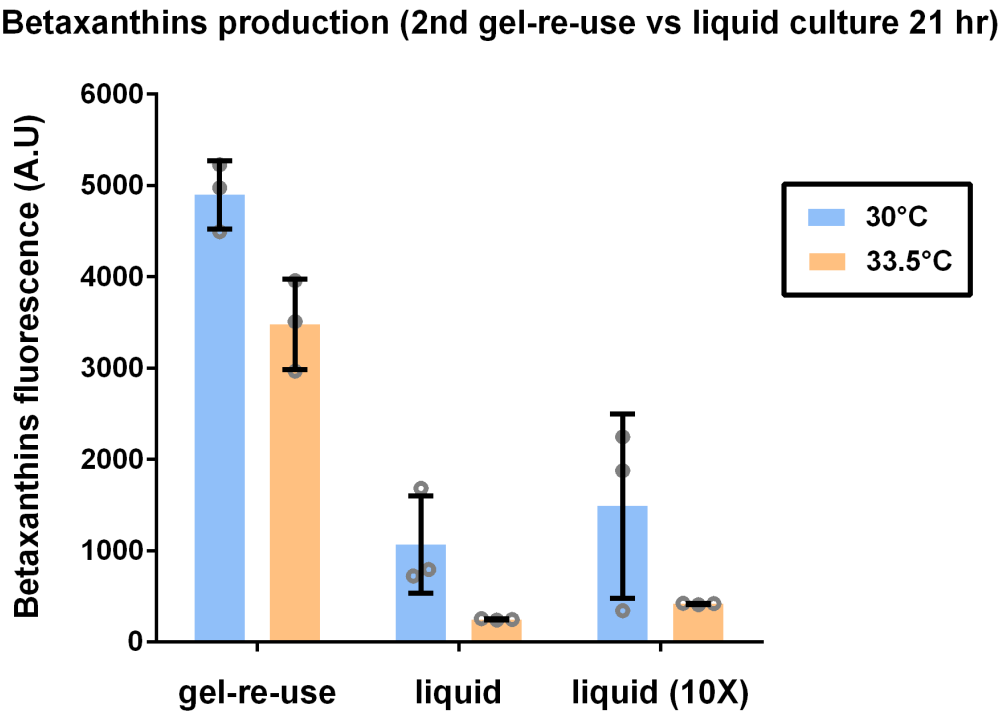
Betaxanthins production (2nd gel-re-use vs liquid culture 21 hr)
Betaxanthins fluorescence (A.U)
6000
5000
4000
3000
2000
1000
0
gel-re-use
liquid
liquid (10X)
30°C
33.5°C

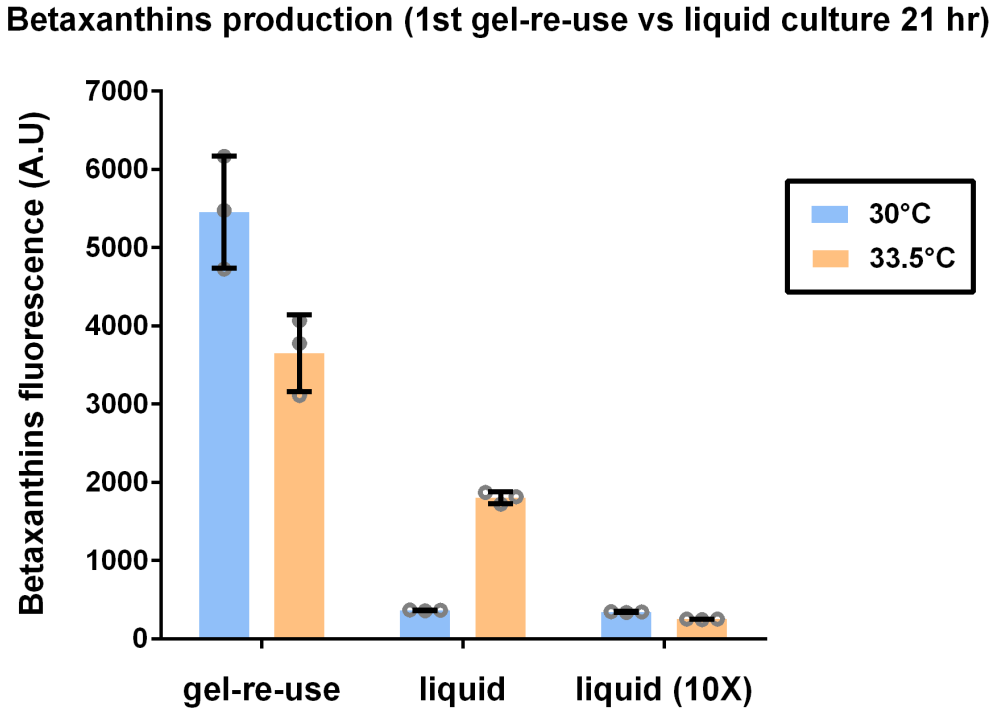
Betaxanthins production (1st gel-re-use vs liquid culture 21 hr)
Betaxanthins fluorescence (A.U)
7000
6000
5000
4000
3000
2000
1000
0
gel-re-use
liquid
liquid (10X)
30°C
33.5°C

D

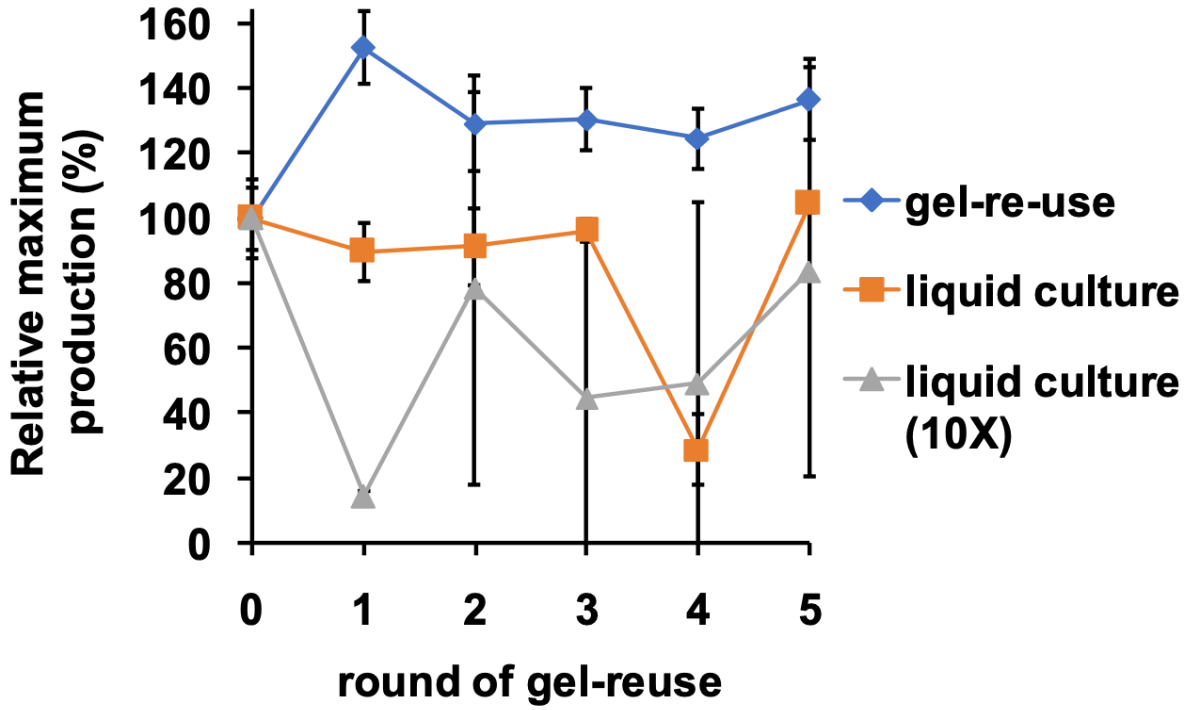
Relative maximum production (%)
160
140
120
100
80
60
40
20
0
0
1
2
3
4
5
round of gel-reuse
gel-re-use
liquid culture
liquid culture (10X)

E

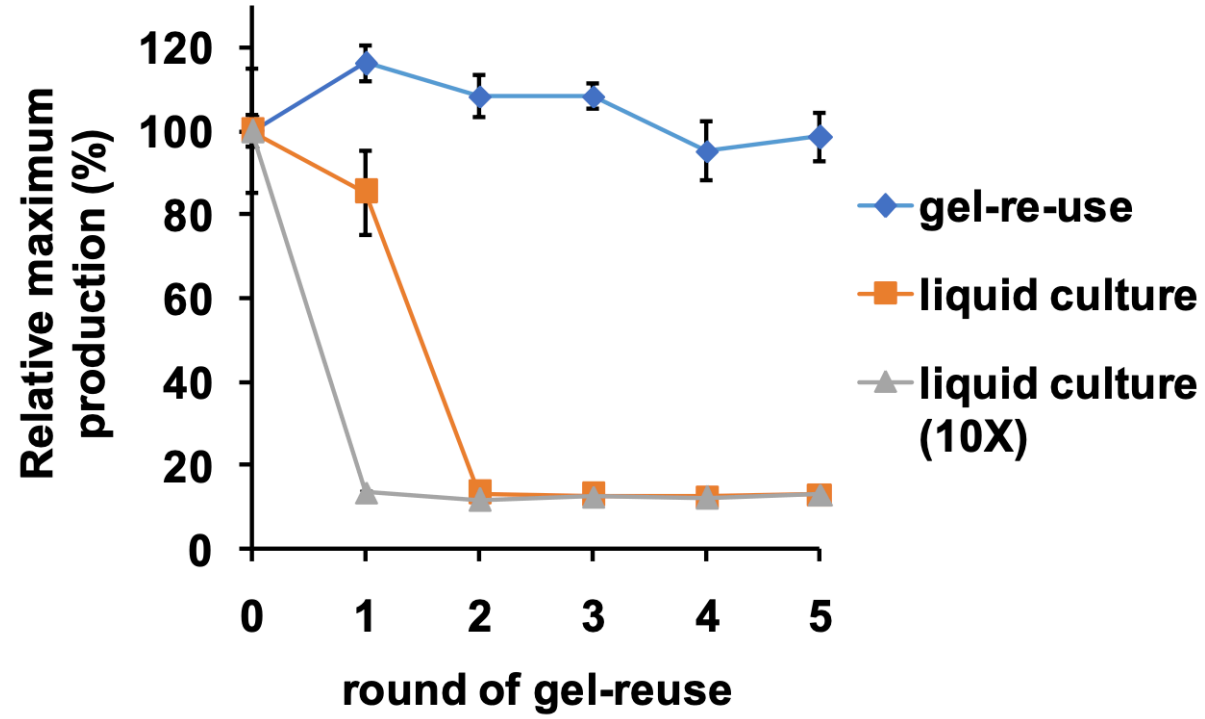
Relative maximum production (%)
120
100
80
60
40
20
0
0
1
2
3
4
5
round of gel-reuse
gel-re-use
liquid culture
liquid culture (10X)

Figure C.8. Gel-re-run for betaxanthins production via E. coli-yeast consortia.

Cell-laden gels were removed from round 0. The performances between each sample were compared at 21 (A) and 96 hr (B) fermentation for the 1st round of gel-re-use. C) The consortia activity between the 1st and 2nd round of gel-re-use were compared. Liquid culture in the 2nd round incubated at 30 °C for 21 hr (bottom) produced more betaxanthins than that in the 1st round (top). These results show that liquid culture can't easily control the consortia dynamics for the cell recycle batch fermentation purpose. The comparison of maximum betaxanthins production at 30 (D) and 33.5 °C (E) between gel and liquid culture for 5 consecutive cell-reuse cycles.

A

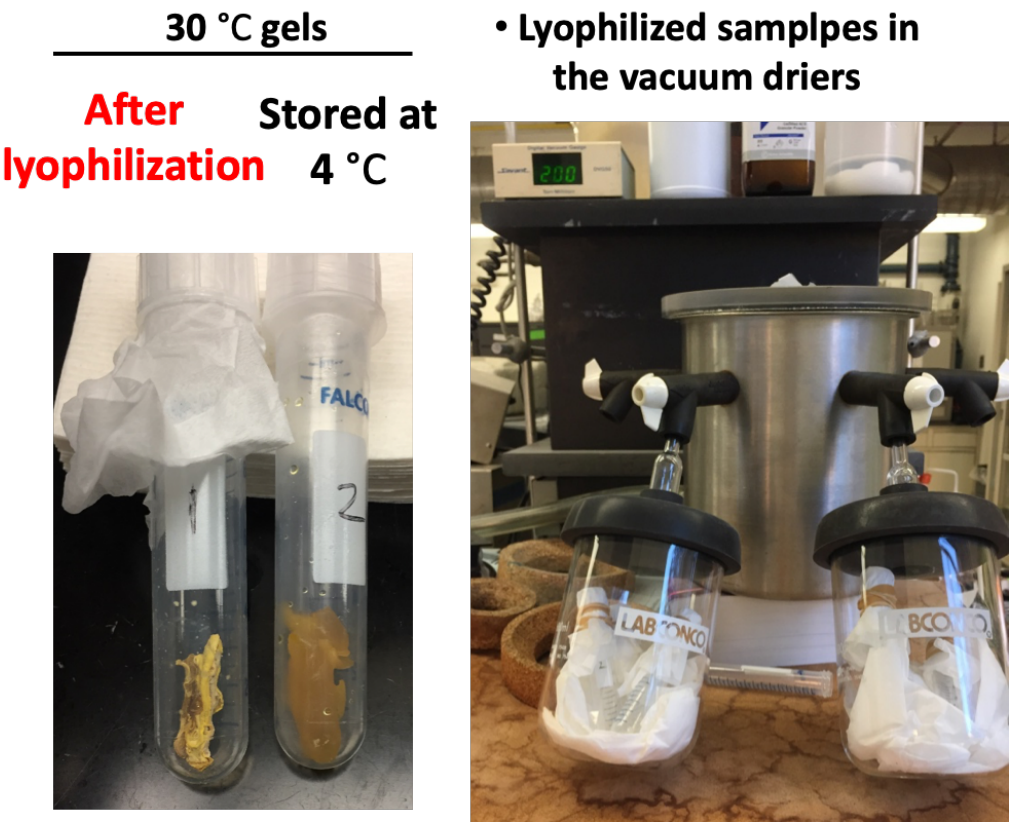
30 °C gels
After lyophilization
Stored at 4 °C
• Lyophilized samplpes in the vacuum driers

B

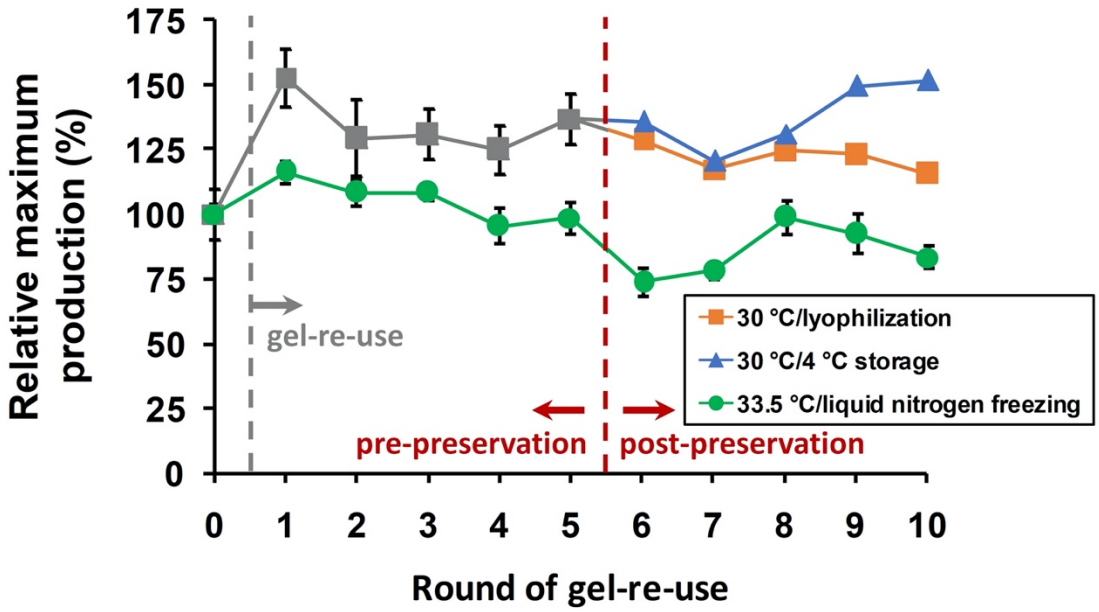
Relative maximum production (%)
175
150
125
100
75
50
25
0
0 1 2 3 4 5 6 7 8 9 10
Round of gel-re-use
gel-re-use
pre-preservation
post-preservation
30 °C/lyophilization
30 °C/4 °C storage
33.5 °C/liquid nitrogen freezing

C

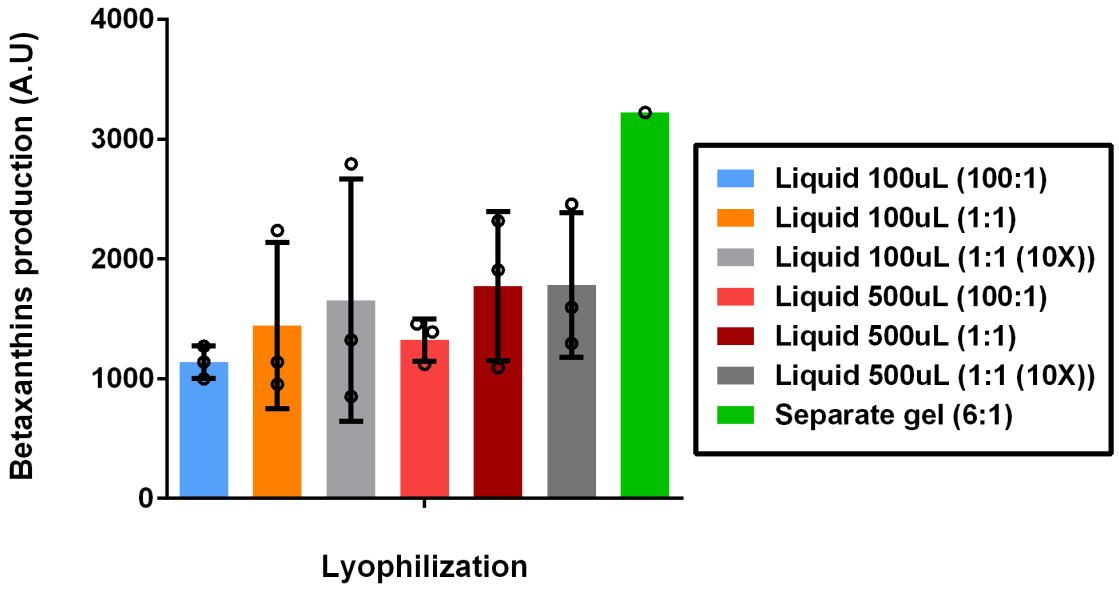
Betaxanthins production (A.U)
4000
3000
2000
1000
0
Lyophilization
Liquid 100uL (100:1)
Liquid 100uL (1:1)
Liquid 100uL (1:1 (10X))
Liquid 500uL (100:1)
Liquid 500uL (1:1)
Liquid 500uL (1:1 (10X))
Separate gel (6:1)

D

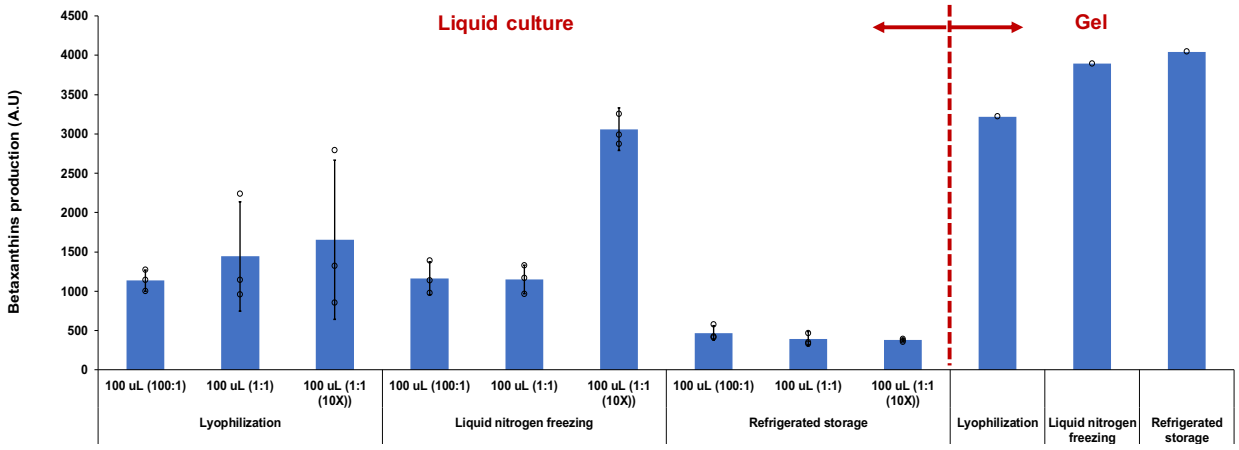
Betaxanthins production (A.U)
4500
4000
3500
3000
2500
2000
1500
1000
500
0
Liquid culture
Gel
100 uL (100:1)
100 uL (1:1)
100 uL (1:1 (10X))
Lyophilization
Liquid nitrogen freezing
Refrigerated storage

E

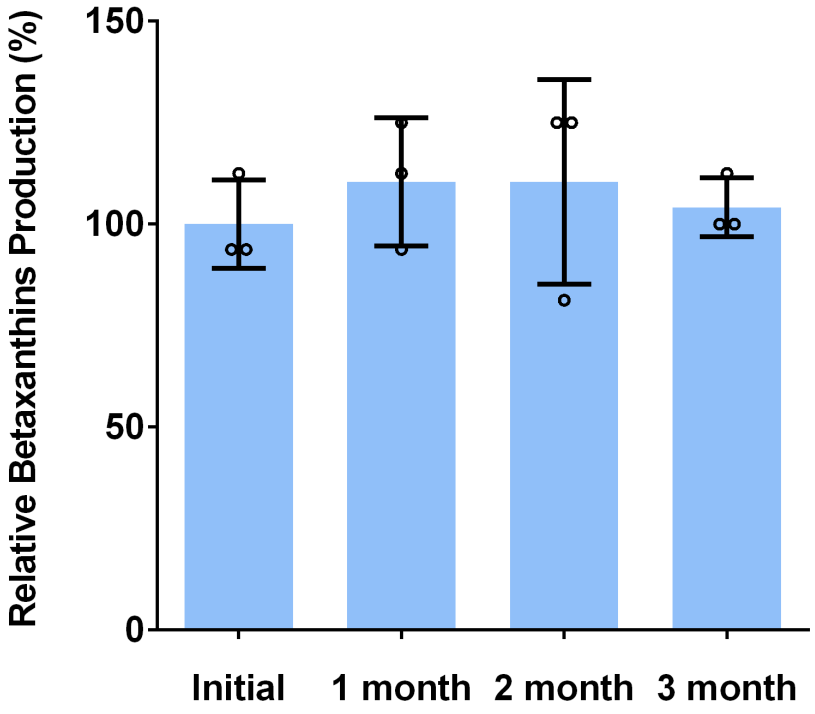
Relative Betaxanthins Production (%)
150
100
50
0
Initial
1 month
2 month
3 month

F

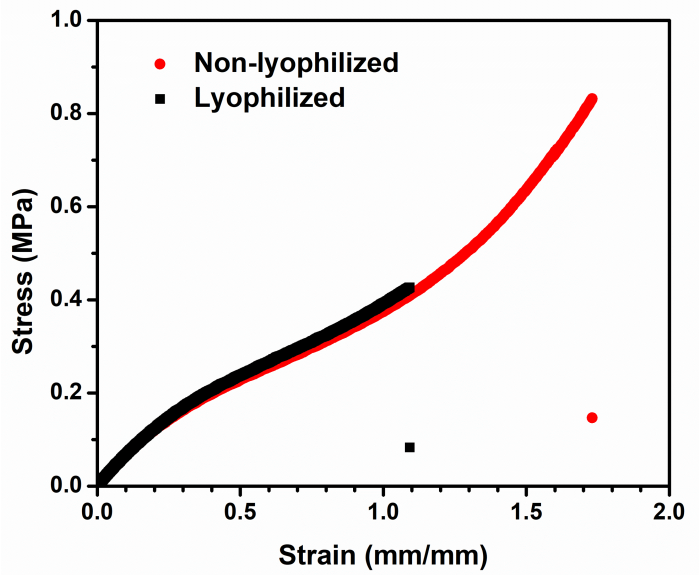

	E (MPa)	σ (MPa)	ε
Non-lyophilized	0.67 ± 0.03	0.83 ± 0.11	1.73 ± 0.21
Lyophilized	0.67 ± 0.02	0.43 ± 0.07	1.09 ± 0.17

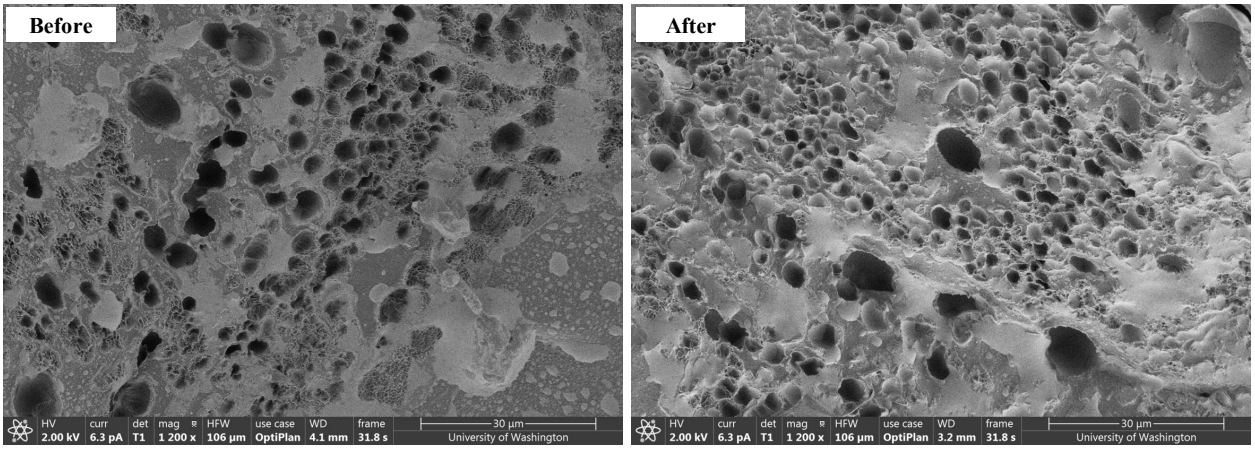

G

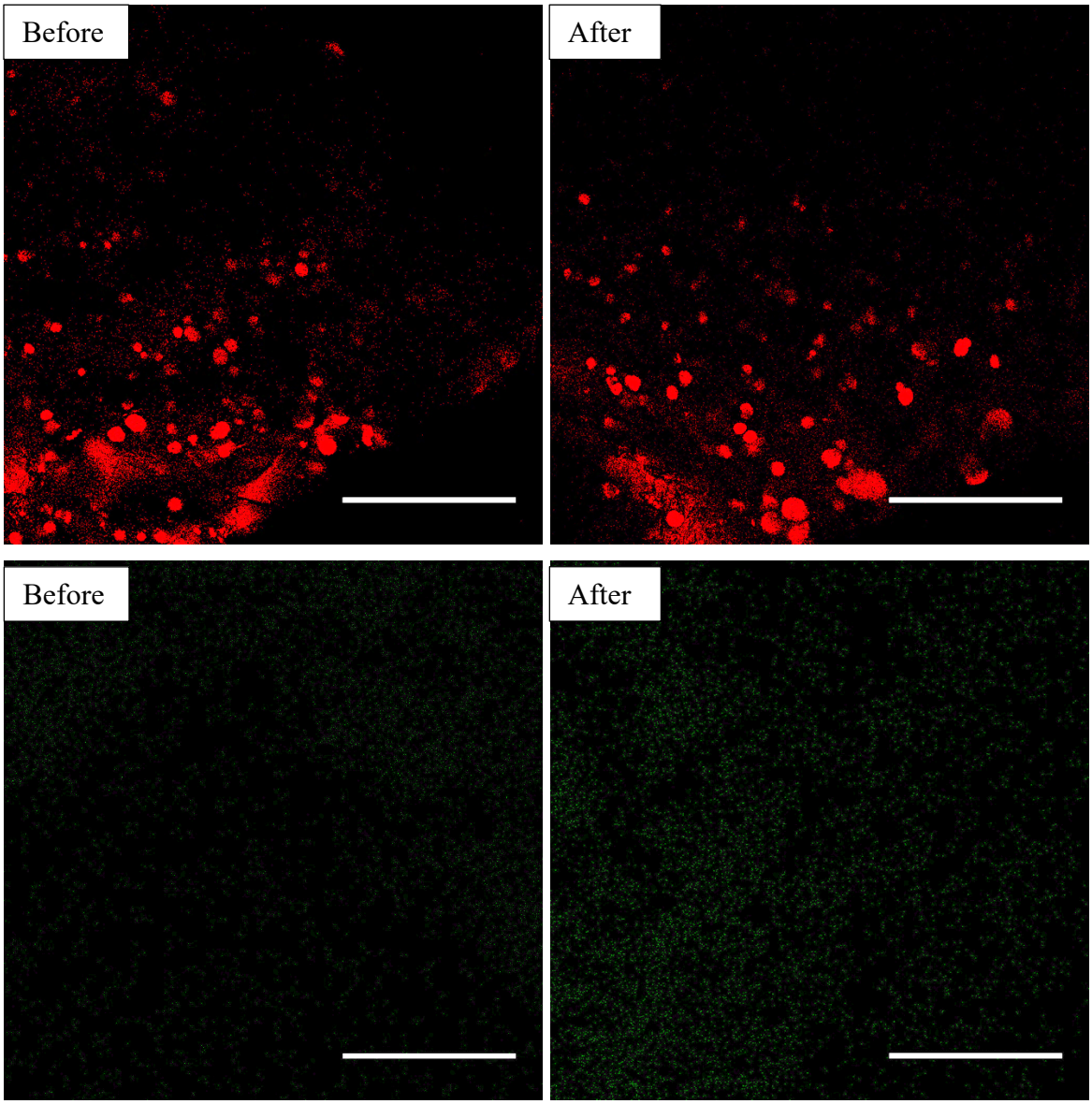

H

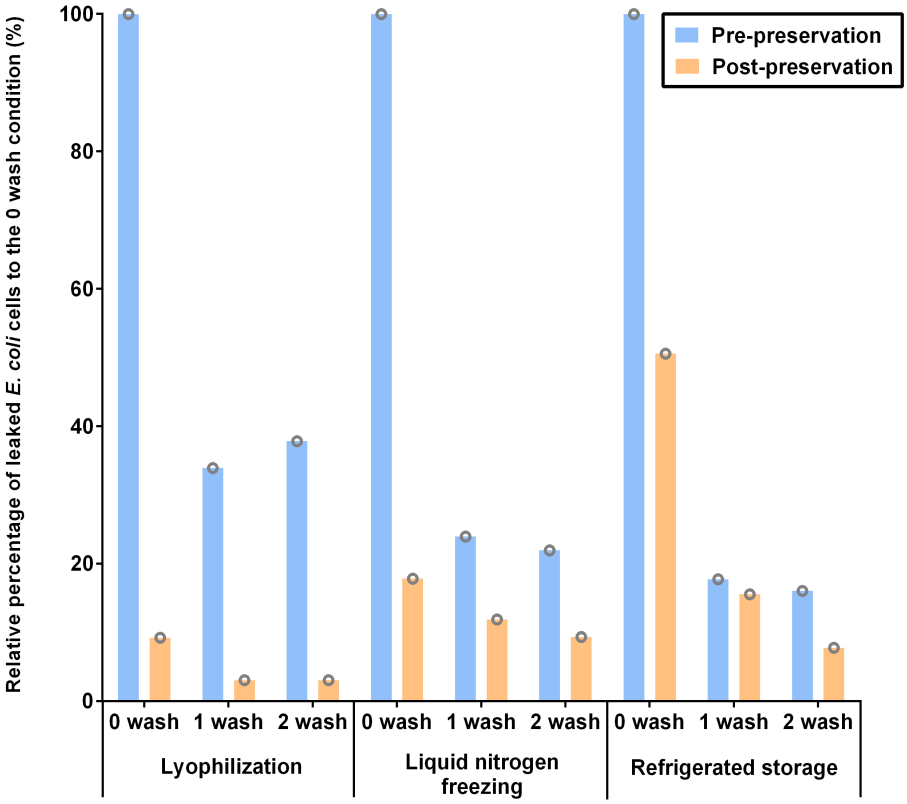
Relative percentage of leaked E. coli cells to the 0 wash condition (%)
100
80
60
40
20
0
Pre-preservation
Post-preservation
0 wash
1 wash
2 wash
Lyophilization
Liquid nitrogen freezing
Refrigerated storage

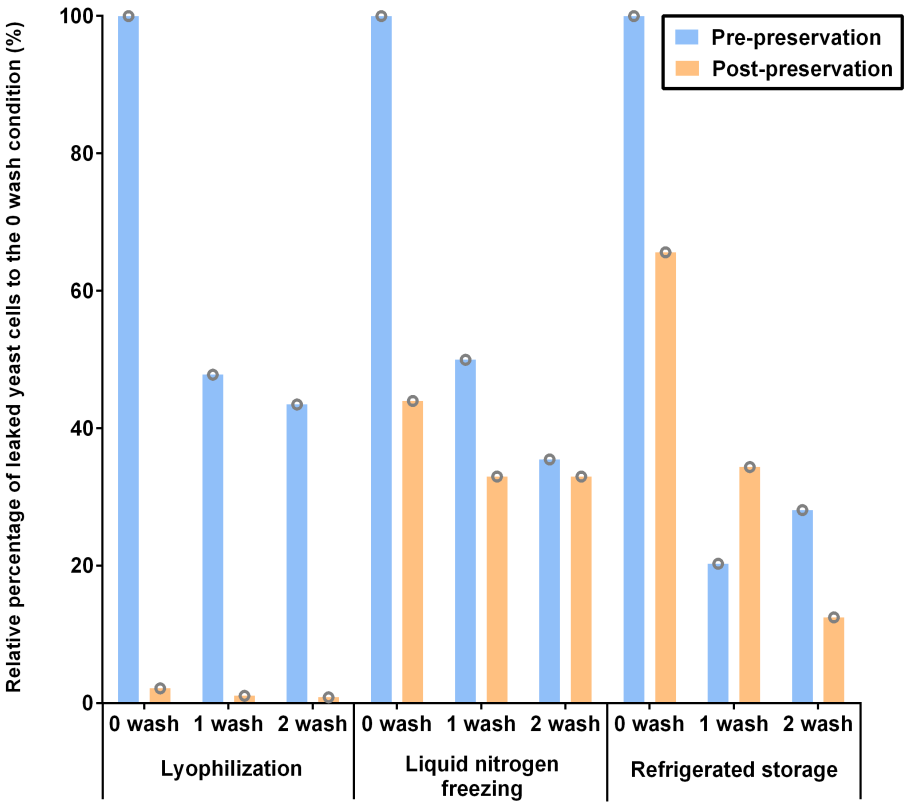
Relative percentage of leaked yeast cells to the 0 wash condition (%)
100
80
60
40
20
0
Pre-preservation
Post-preservation
0 wash
1 wash
2 wash
Lyophilization
Liquid nitrogen freezing
Refrigerated storage

Figure C.9. Investigation of consortia activity for betaxanthins production after preservation process.

Lyophilization method is mostly used in this study (A). Three different preservation methods including lyophilization, refrigerated storage and liquid nitrogen freezing were applied to preservation of consortia-laden polymers. Additional five consecutive uses after preservation process were performed. 30 °C gels after round 5 were split (n=1) for examining the impact of lyophilization and refrigerated storage on betaxanthins production (B). C-D) The comparison of preservation capacity between liquid culture (n=3) and hydrogel (n=1) for betaxanthins production. Liquid 100 uL or 500 uL condition represent 100 or 500 μL of pre-preserved bulk culture sample was taken and proceeded to different preservation treatments. Fermentation was performed at 30 °C for all conditions. E) Production of betaxanthins pre-lyophilization, and post-lyophilization, with an extended period of storage (1 month, n=3). F) Comparison of tensile testing and SEM analysis of 30 wt% F127-BUM hydrogels before and after lyophilization. The values for Young's modulus, and stress and strain at the point of material failure under tensile stress (the top figure and table, n=3). The bottom figure is the SEM images of the betaxanthins production gels before (left image) and after (right image) two consecutive rounds of on-demand fermentation. The similarities in morphology and pore size of the hydrogel in both conditions implies that multiple rounds of fermentation does not affect the integrity of the hydrogel material. All images have 30-micron scale bars. G) Confocal microscopy of red fluorescing yeast and green fluorescing bacteria pre- and post-lyophilization, showing cell distribution within the hydrogel material unaffected by preservation. All images have 200-micron scale bars. H) The impact of washing process for consortia hydrogels on the percentage of leaked E. coli (top) and yeast (bottom) cells between pre- and post-preservation was compared (n=1 for each condition).

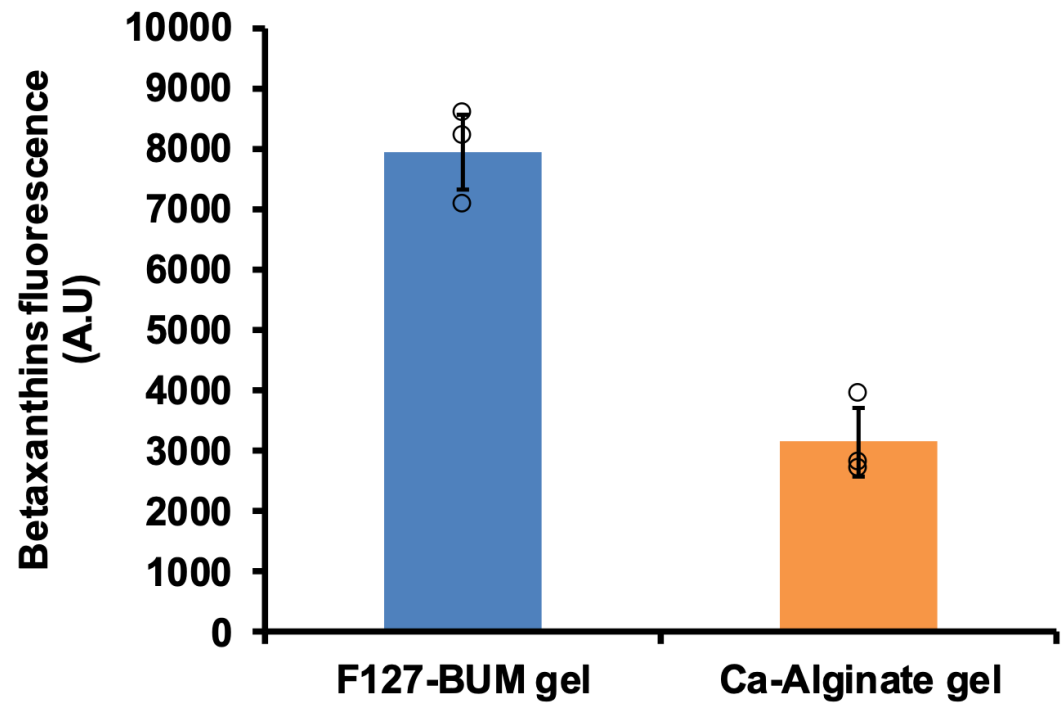

Figure C.10. The comparison of maximum betaxanthins production between F127-BUM and calcium alginate hydrogels.

Results from the comparison between our F127-BUM hydrogels, and commonly employed calcium alginate hydrogels show that the F127-BUM system is much more effective in the production and release of betaxanthins (2.53-fold increase in efficiency) over a period of 72 hours. Each data point and error bar represent means and standard deviations from biological triplicates, respectively, unless stated otherwise in the Methods section.

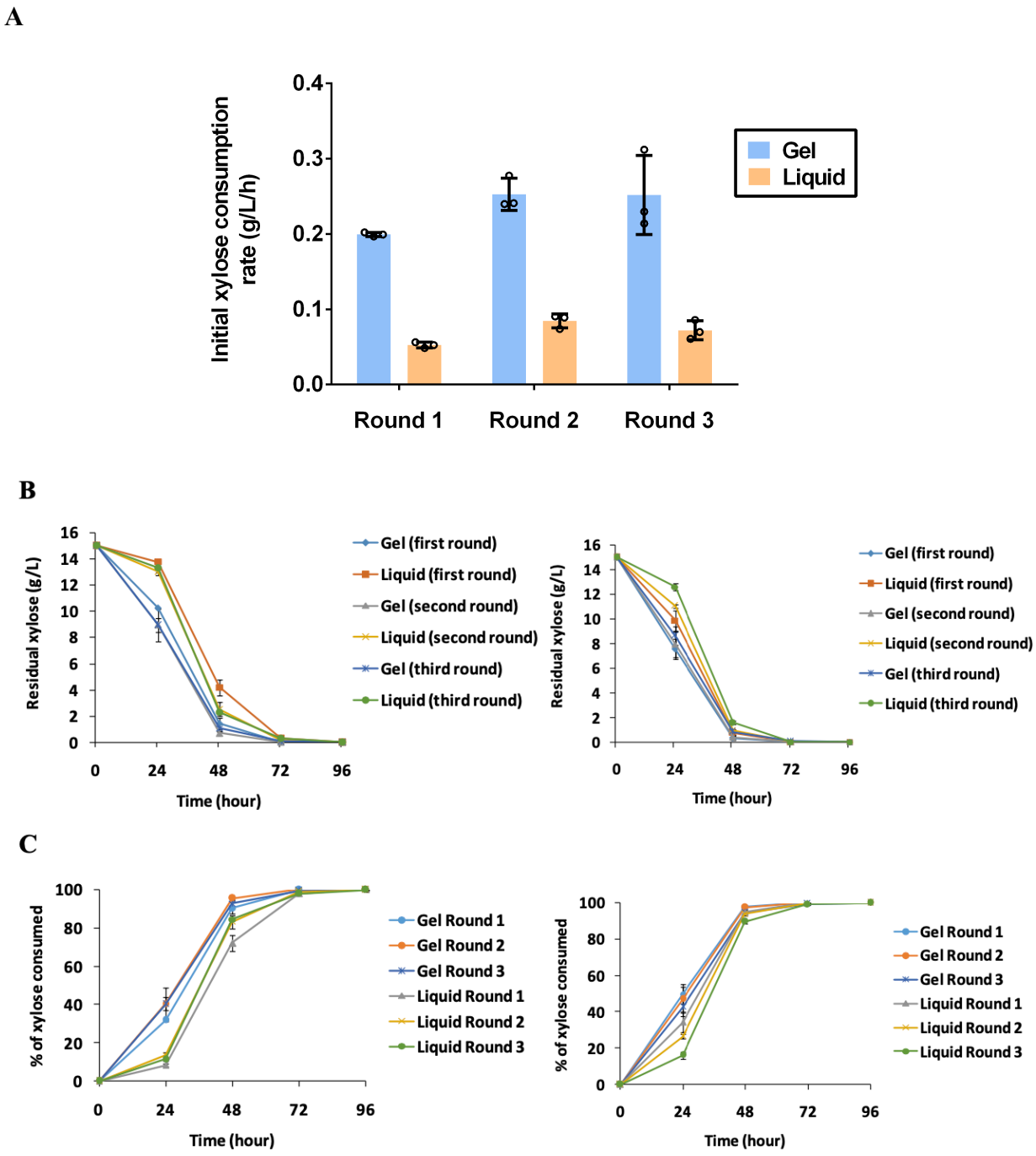

Figure C.11. Gel-re-run for xylose/glucose utilization via a parallel yeast-yeast consortium.

A) Investigation of consortia activity on glucose/xylose utilization in hydrogel system and liquid culture with re-use. Round 0 was grown in YPD containing 20 g/L glucose to outgrow consortia population. Then all samples were cultivated in YPDX media for three consecutive uses. Xylose consumption rate for each round of re-use was compared. B) Time profile of residual xylose concentration for each round of re-use (round 0 was grown in YPD (left) or YPDX (right)).

C) Time profile of xylose consumption for each round of re-use (round 0 was grown in YPD (left) or YPDX (right)). Each data point and error bar represent means and standard deviations from biological triplicates, respectively.

6.3 TABLES

Table C.1. List of strains and plasmids used in this study

Strain/plasmid	Description	Source
E. coli strain		
NEB10β	Δ*(ara-leu) 7697 araD139 fhuA* Δ*lacX74 galK16 galE15 e14- ϕ80dlacZΔM15 recA1 relA1 endA1 nupG rpsL (Str^R) rph spoT1* Δ*(mrr-hsdRMS-mcrBC)*	New England Biolabs
MG1655	K-12 F– λ– *ilvG– rfb-50 rph-1*	ATCC
BL21(DE3)	*E. coli* str. B F$^-$ *ompT gal dcm lon hsdS$_B$*($r_B^- m_B^-$) *λ(DE3 [lacI lacUV5-T7p07 ind1 sam7 nin5]*) [*malB*$^+$]$_{K\text{-}12}$(λ^S)	New England Biolabs
CD02	[MG1655] *nfsA*::*BBa J23119-sfGFP*; Kan^R	Dr. Jesse G. Zalatan's lab
MC4100_pHK11	*E. coli* MC4100 carries pHK11containing colicin V gene cluster *cvaAB-cvaC-cvi*; Amp^R	16
DH5α_pET28b	*E. coli* DH5α (ATCC) was transformed with pET28b empty vector; Kan^R	This study
eBL01	*E. coli* BL21(DE3) Δt*yrR*	This study
eBL04	[eBL01] pET28-pYIBN-*aroG*$^{(fbr)}$-B30rbs-*tyrA*$^{(fbr)}$-tRRNC; Kan^R	This study
eBL0400DT	[eBL04] pCDFDuet-1; Kan^R; Spc^R	This study
eBL0430D	[eBL04] pCDF-pLPP-B30rbs-*hpaB-hpaC*-T7t; Kan^R; Spc^R	This study
eBL0432D	[eBL04] pCDF-pLPP-B32rbs-*hpaB-hpaC*-T7t; Kan^R; Spc^R	This study
S. cerevisiae strain		
BY4741	*MATα SUC2 gal2 mal2 mel flo1 flo8-1 hap1 ho bio1 bio6 his3*Δ1 *leu2*Δ0 *met15*Δ0 *ura3*Δ0	ATCC

CEN.PK2-a	*MAT*a/α; *ura3-52/ura3-52; trp1-289/trp1-289; leu2-3_112/leu2-3_112; his3 Δ1/his3 Δ1; MAL2-8C/MAL2-8C; SUC2/SUC2*	28
S288C	*MATα SUC2 gal2 mal2 mel flo1 flo8-1 hap1 ho bio1 bio6*	ATCC
SO992	*MATa ura3 leu2 trp1 his3, can1R, ADE+*	29
yJS001	[SO992] *mfa2::*pTEF1-*mCherry*	29
JMW001	[BY4741] *trp1::*TDH3p-*mKate2*	3
BY4741_BDO	[BY4741] p416-pFBA1-*NoxE*-tIDP1-pTPI1-*alsD*-tSPG5-pPGK1-*alsS*-tPRM9	3
CEN.PK2-a_BDO	[CEN.PK2-a] p416-pFBA1-NoxE-tIDP1-pTPI1-alsD-tSPG5-pPGK1-alsS-tPRM9	3
sBY08	[BY4741] *leu2::*pGPD-*MjDOD*-tPRM9 (LEU2 integration with URA3 marker)	This study
YSX3	*MATα trp1-112 leu2::LEU2-PsXYL1 ura3::URA3-PsXYL2 Ty3::NEO-PsXYL3*	27
Plasmids		
pET28b-Duet-1	DNA fragment containing two T7 promoters on pRSFDuet-1 was cloned into pET28b empty vector	This study
pCDF-Duet-1	For construction L-DOPA producing plasmids	This study
pCDF-pT7-*tyrA*$^{(fbr)}$-pT7-*aroG*$^{(fbr)}$	FRT flanked kanamycin resistance gene was removed from pCDF-Kan^{FRT}-tyrA$^{(fbr)}$-aroG$^{(fbr)}$	This study
pET28-pT7-*aroG*$^{(fbr)}$-tT7	For construction of pET28-pYIBN-*aroG*$^{(fbr)}$	This study
pET28-pYIBN-*aroG*$^{(fbr)}$	For construction of pET28-pYIBN-*aroG*$^{(fbr)}$-B30rbs-*tyrA*$^{(fbr)}$-tRRNC	This study
pET28-pYIBN-*aroG*$^{(fbr)}$-B30rbs-*tyrA*$^{(fbr)}$-tRRNC	For tyrosine production	This study

pCDF-pLPP-B30rbs-*hpaB*-*hpaC*-T7t	For L-DOPA production testing	This study
pCDF-pLPP-B32rbs-*hpaB*-*hpaC*-T7t	For L-DOPA production testing	This study
pCMC0759	For amplification of *MjDOD* gene	22
P416-pGPD-tPRM9	For construction of p416-pGPD-*MjDOD*-tPRM9	30
p416-pGPD-*MjDOD*-tPRM9	For generating a URA3 integrative cassette employed for betaxanthins production	This study

Table C.2. List of primers used in this study

Primer ID	**Primer description**	**Sequence (5'->3')**
P1	tyrR_delFwd	TTACGCCGAAGTGCCCGTTTTTCCGTCTTTGTGTCAATGATTGTTGACAGATTCCGGGGATCCGTCGACC
P2	tyrR_delRvs	CATCAGGCATATTCGCGCTTACTCTTCGTTCTTCTTCTGACTCAGACCATGTGTAGGCTGGAGCTGCTTCG
P3	tyrR_delFwd1	CAAAACGCCCAGCGAAAAATAATGCAATATCGGGTGCTGACCGGATATCTTTACGCCGAAGTGCCCG
P4	tyrR_delRvs1	AGCTCTGGCTGTACTGAAAGCATAATTTAATATGCCTGATGGTGTTGCACCATCAGGCATATTCGCGCTTACTC
P5	SeqtyrRf	GATTTCCGTCGTCAGCTTATC
P6	SeqtyrRr	CAGCTGGTGGATGAAATCAC
P7	TyrAroCDFf	TGGTGTCCGACAGCCTGCATTAGGAAAT
P8	TyrAroCDFr	CGCTTATAGTAACGTTTGATTAACG
P9	CDFTyrAroF	CTGGCGTTAATCAAACGTTACTATAAGCGTTTC

P10	CDFTyrAroR	ATTTCCTAATGCAGGCTGTCGGACACCATCGAATGGCGCAAAA
P11	ACYCDuetUP1_F	GGATCTCGACGCTCTCCCT
P12	T7 terminatorR	GCTAGTTATTGCTCAGCGGTG
P13	p28Duet1F	CTGCTGCCACCGCTGAGCA
P14	p28Duet1R	AGTCGCATAAGGGAGAGCGTC
P25	AroGfbrp21F	TGTTTAACTTTAAGAAGGAGATATACATATGAATTATCAGAACGACGATTTACGCATC
P26	AroGfbrp21R	CGCAAGCTTGTCGACGGAGCTCGAATTCTTACCCGCGACGCGCTTTTA
P27	p28AroGF	GAATTCGAGCTCCGTCGA
P28	p28AroGR	ATGTATATCTCCTTCTTAAAGTTAAACAAAATTATTTC
P33	yibNf	AAATTGCATTCCAGTTAACGCG
P34	yibNAroGr	TGCGTAAATCGTCGTTCTGATAATTCATGGGGGGTAACAACTCCC
P35	yibNAroG1f	GTTACCCCCCATGAATTATCAGAACGACGATTTACGCATC
P36	yibNAroG1r	GGAAGAGAGTCAATTCAGGGTGGTGAATTTACCCGCGACGCGCTTTTA
P37	p28yibNAroGf	CGCGGGTAAATTCACCACCCTGAATTGACTC
P38	p28yibNAroGr	AGCCAGCGCGTTAACTGGAATGCAATTTTGAGCGCAACGCAATTAATGTAAG
P39	p28ATf	ATCCTTAGCGAAAGCTAAGGATTTTTTTTACCATCTTAGTATATTAGTTAAGTATAAG
P40	p28ATB30r	CTAGTATTTCTCCTCTTTAATCTCTAGAGGAAGAGAGTCAATTCAG

P41	yibNtyrAr2	TTTCCTAATGCAGGAGTCGCATATTACTGGCGATTGTCATTCGC
P42	B30tyrAF	TCTAGAGATTAAAGAGGAGAAATACTAGATGGTTGCTGAATTGACCGC
P43	rrncterm	CCAGTAATATGCGACTCCTGCATTAGGAAAATCCTTAGCGAAAGCTAAGGATTTTTTTTA
P67	lppB30	CCCATCAAAAAAATATTCTCAACATAAAAAACTTTGTGTAATACTTGTAACGCTTCTAGAGATTAAAGAGGAGAAATACTAG
P68	lppB32	CCCATCAAAAAAATATTCTCAACATAAAAAACTTTGTGTAATACTTGTAACGCTTCTAGAGTCACACAGGAAAGTACTAG
P69	lppHpaBCB30f	TCTAGAGATTAAAGAGGAGAAATACTAGATGAAACCAGAAGATTTCCGC
P70	lppHpaBCB30r	CAGGCGCGCCGAGCTCGAATTCGGATCCTTAAATCGCAGCTTCCATTTCC
P71	lppHpaBCB32f	CTTCTAGAGTCACACAGGAAAGTACTAGATGAAACCAGAAGATTTCCGC
P72	pCDFlppTcXALf	GGATCCGAATTCGAGCTCG
P73	pCDFlppTcXALr	AGTTTTTTATGTTGAGAATATTTTTTTGATGGGTGAGCGCAACGCAATTAATGTAAG
P74	SpeIMjDODf	GGACTAGTATGAAGGGAACCTACTACATCAAC
P75	EcoRIMjDODr	CGGAATTCTTAGGATCCGTCGGTCTTTTG
P78	NJM675	TCAAAAAGATCCATGTATAATCTTCATTATTACAGCCCTCTTGACCTCTAATCATGAATGTTCTCGGGTGTCGGGGCTGGCTTAACTATG

P79	NJM676	TATGTAGATTGCGTATATAGTTTCGTCTACCCTATGAACA TATTCCATTTTGTAATTTCGTGTCGGTCAGTGAGCGAGG AAGCGGAAGAG

The underlined sequence indicates that the nucleotides used to be annealed to the template for PCR amplification.

6.4 REFERENCES

1. Ji, X.-J.; Huang, H.; Ouyang, P.-K., Microbial 2,3-butanediol production: A state-of-the-art review. *Biotechnol. Adv.* **2011,** *29* (3), 351-364.
2. Köpke, M.; Mihalcea, C.; Liew, F.; Tizard, J. H.; Ali, M. S.; Conolly, J. J.; Al-Sinawi, B.; Simpson, S. D., 2,3-Butanediol Production by Acetogenic Bacteria, an Alternative Route to Chemical Synthesis, Using Industrial Waste Gas. *Appl. Environ. Microbiol.* **2011,** *77* (15), 5467.
3. Deaner, M.; Holzman, A.; Alper, H. S., Modular Ligation Extension of Guide RNA Operons (LEGO) for Multiplexed dCas9 Regulation of Metabolic Pathways in Saccharomyces cerevisiae. *Biotechnology Journal* **2018,** *13* (9), 1700582.
4. González, E.; Fernández, M. R.; Marco, D.; Calam, E.; Sumoy, L.; Parés, X.; Dequin, S.; Biosca, J. A., Role of Saccharomyces cerevisiae Oxidoreductases Bdh1p and Ara1p in the Metabolism of Acetoin and 2,3-Butanediol. *Appl. Environ. Microbiol.* **2010,** *76* (3), 670-679.
5. Broadley, K. J., The vascular effects of trace amines and amphetamines. *Pharmacol. Ther.* **2010,** *125* (3), 363-375.
6. Miguelez, C.; Benazzouz, A.; Ugedo, L.; De Deurwaerdère, P., Impairment of Serotonergic Transmission by the Antiparkinsonian Drug L-DOPA: Mechanisms and Clinical Implications. *Front. Cell. Neurosci.* **2017,** *11* (274).
7. Surwase, S. N.; Jadhav, J. P., Bioconversion of l-tyrosine to l-DOPA by a novel bacterium Bacillus sp. JPJ. *Amino Acids* **2011,** *41* (2), 495-506.
8. Muñoz, A. J.; Hernández-Chávez, G.; de Anda, R.; Martínez, A.; Bolívar, F.; Gosset, G., Metabolic engineering of Escherichia coli for improving l-3,4-dihydroxyphenylalanine (l-DOPA) synthesis from glucose. *J. Ind. Microbiol. Biotechnol.* **2011,** *38* (11), 1845.
9. Yuan, S.-F.; Hsu, T.-C.; Wang, C.-A.; Jang, M.-F.; Kuo, Y.-C.; Alper, H. S.; Guo, G.-L.; Hwang, W.-S., Production of optically pure l(+)-lactic acid from waste plywood chips using an isolated thermotolerant Enterococcus faecalis SI at a pilot scale. *J. Ind. Microbiol. Biotechnol.* **2018,** *45* (11), 961-970.
10. Yuan, S.-F.; Guo, G.-L.; Hwang, W.-S., Ethanol production from dilute-acid steam exploded lignocellulosic feedstocks using an isolated multistress-tolerant Pichia kudriavzevii strain. *Microbial Biotechnology* **2017,** *10* (6), 1581-1590.
11. Yuan, S.-F.; Alper, H. S., Metabolic engineering of microbial cell factories for production of nutraceuticals. *Microbial Cell Factories* **2019,** *18* (1), 46.
12. Nakagawa, A.; Minami, H.; Kim, J.-S.; Koyanagi, T.; Katayama, T.; Sato, F.; Kumagai, H., A bacterial platform for fermentative production of plant alkaloids. *Nature Communications* **2011,** *2*, 326.

13. Kim, S. C.; Min, B. E.; Hwang, H. G.; Seo, S. W.; Jung, G. Y., Pathway optimization by re-design of untranslated regions for L-tyrosine production in Escherichia coli. *Sci. Rep.* **2015,** *5*, 13853-13853.
14. Huang, Q.; Lin, Y.; Yan, Y., Caffeic acid production enhancement by engineering a phenylalanine over-producing Escherichia coli strain. *Biotechnol. Bioeng.* **2013,** *110* (12), 3188-3196.
15. Santos, C. N. S.; Stephanopoulos, G., Melanin-Based High-Throughput Screen for L-Tyrosine Production in Escherichia coli. *Appl. Environ. Microbiol.* **2008,** *74* (4), 1190.
16. Gilson, L.; Mahanty, H. K.; Kolter, R., Four plasmid genes are required for colicin V synthesis, export, and immunity. *J. Bacteriol.* **1987,** *169* (6), 2466.
17. Cascales, E.; Buchanan, S. K.; Duché, D.; Kleanthous, C.; Lloubès, R.; Postle, K.; Riley, M.; Slatin, S.; Cavard, D., Colicin Biology. *Microbiol. Mol. Biol. Rev.* **2007,** *71* (1), 158.
18. Gérard, F.; Pradel, N.; Wu, L.-F., Bactericidal Activity of Colicin V Is Mediated by an Inner Membrane Protein, SdaC, of <em>Escherichia coli</em&gt. *J. Bacteriol.* **2005,** *187* (6), 1945.
19. Eş, I.; Vieira, J. D. G.; Amaral, A. C., Principles, techniques, and applications of biocatalyst immobilization for industrial application. *Appl. Microbiol. Biotechnol.* **2015,** *99* (5), 2065-2082.
20. Alonso, S., Novel Preservation Techniques for Microbial Cultures. In *Novel Food Fermentation Technologies*, Ojha, K. S.; Tiwari, B. K., Eds. Springer International Publishing: Cham, 2016; pp 7-33.
21. Martins, N.; Roriz, C. L.; Morales, P.; Barros, L.; Ferreira, I. C. F. R., Coloring attributes of betalains: a key emphasis on stability and future applications. *Food Funct.* **2017,** *8* (4), 1357-1372.
22. Grewal, P. S.; Modavi, C.; Russ, Z. N.; Harris, N. C.; Dueber, J. E., Bioproduction of a betalain color palette in Saccharomyces cerevisiae. *Metab. Eng.* **2018,** *45*, 180-188.
23. DeLoache, W. C.; Russ, Z. N.; Narcross, L.; Gonzales, A. M.; Martin, V. J. J.; Dueber, J. E., An enzyme-coupled biosensor enables (S)-reticuline production in yeast from glucose. *Nat. Chem. Biol.* **2015,** *11*, 465.
24. Gírio, F. M.; Fonseca, C.; Carvalheiro, F.; Duarte, L. C.; Marques, S.; Bogel-Łukasik, R., Hemicelluloses for fuel ethanol: A review. *Bioresour. Technol.* **2010,** *101* (13), 4775-4800.
25. Kwak, S.; Jin, Y.-S., Production of fuels and chemicals from xylose by engineered Saccharomyces cerevisiae: a review and perspective. *Microbial Cell Factories* **2017,** *16* (1), 82.
26. Moysés, D. N.; Reis, V. C. B.; de Almeida, J. R. M.; de Moraes, L. M. P.; Torres, F. A. G., Xylose Fermentation by Saccharomyces cerevisiae: Challenges and Prospects. *Int. J. Mol. Sci.* **2016,** *17* (3), 207-207.
27. Jin, Y.-S.; Ni, H.; Laplaza, J. M.; Jeffries, T. W., Optimal Growth and Ethanol Production from Xylose by Recombinant Saccharomyces cerevisiae Require Moderate D-Xylulokinase Activity. *Appl. Environ. Microbiol.* **2003,** *69* (1), 495.

APPENDIX D

Appendix D is a continued study into the behavior of the living materials and the encapsulated microbes, performed concurrently with the content of Chapter 5.

6.5 ABSTRACT

Additive manufacturing allows three-dimensional printing of polymeric materials together with cells, creating living materials for applications in biomedical research and biotechnology. However, understanding the cellular phenotype within living materials is lacking and a key limitation for their wider application. Herein, we present an approach to characterize the cellular phenotype within living materials. We immobilized the budding yeast *Saccharomyces cerevisiae* in three different photo-cross-linkable triblock polymeric hydrogels containing F127-bis-urethane methacrylate, F127-dimethacrylate, or poly(alkyl glycidyl ether)-dimethacrylate. Using optical and scanning electron microscopy, we showed that hydrogels based on these polymers were stable under physiological conditions, but yeast colonies showed differences in the interaction within the living materials. We found that the physical confinement, imparted by compositional and structural properties of the hydrogels, impacted the cellular phenotype by reducing the size of cells in living materials compared with suspension cells. These properties also contributed to the differences in immobilization patterns, growth of colonies, and colony coatings. We observed that a composition-dependent degradation of polymers was likely possible by cells residing in the living materials. In conclusion, our investigation highlights the need for a holistic understanding of the cellular response within hydrogels to facilitate the synthesis of application-specific polymers and the design of advanced living materials in the future.

6.6 INTRODUCTION

Three-dimensional (3D) printing of natural and synthetic materials for biomedical and biotechnology applications is a promising research field with applications that include screening tools and production platforms in a sustainable economy.[1] Self-assembling block copolymer hydrogels have been demonstrated for extrusion-based 3D printing, and offer exciting opportunities to create synthetic polymer hydrogel networks that can immobilize microbial cells and recapitulate the environment of a biofilm.[2,3] These microbe-laden hydrogels form living materials (LMs) that are permissive for metabolic activity and can provide significant improvement with respect to robustness, reproducibility, and scale-up over traditional immobilization methods using natural biopolymers.[4] The multiscale properties of hydrogels of such polymers allow their applications in diverse fields, such as drug delivery[5], tissue engineering[6], and biotechnology[4,7]. Precise material deposition, together with a high degree of spatial control, allows the manufacturing of pre-designed and custom-made structures.[8,9] One prominent triblock copolymer hydrogel for extrusion-based printing is based on Pluronic F127, which embodies dual-responsive properties towards temperature (sol at 4 °C, gel at 25 °C) and the applied shear forces.[10] This ABA triblock copolymer, wherein the 'A' blocks are hydrophilic poly(ethylene oxide) and the 'B' block is a hydrophobic poly(propylene oxide), can self-assemble to form micelles in aqueous solution. As the concentration of the F127 in solution increases, the polymer reaches a critical gel concentration. The Nelson group recently developed BAB triblock copolymer hydrogels for direct-write extrusion printing with hydrophobic poly(alkyl glycidyl ether) 'B' blocks that flank a central poly(ethylene oxide) 'A' block that exhibits similar stimuli-responsive behaviors as F127.[11] In contrast to F127, the BAB triblock copolymers form reverse flower micelles in solution.[11–13] Furthermore, the chain-end modification of BAB and ABA triblock

copolymers allows for cross-linking by means of photo-initiated polymerization while or after completion of the 3D printing process to afford robust hydrogel structures.[14–16] Polymer hydrogels based on F127-dimethacrylate (F127-DMA), F127-bisurethane methacrylate (F127-BUM), and poly(isopropyl glycidyl ether-*stat*-ethyl glycidyl ether)-*block*-poly(ethylene oxide)-*block*-poly(isopropyl glycidyl ether-*stat*-ethyl glycidyl ether) dimethacrylate (PGE-DMA) have previously been reported for encapsulation and direct-write extrusion printing of microbes.[4,17–19] In all of these cases, the hydrogels maintained the viability and metabolic activity of yeast or bacteria to afford immobilized bioreactors with long-term metabolic activity.[4,17,18]

Methods for the characterization of the physico-chemical properties of such hydrogels, particularly their stiffness, swelling ratio, and rheology, are well established.[20,21] However, similar robust analysis methodologies for understanding cellular phenotypes of microbial cells confined within hydrogels are lacking, but necessary, before LM-based technologies could be used in specific, reproducible, and efficient processes. Previously, optical microscopy (OM) and scanning electron microscopy (SEM) have been used to investigate cell-gel-morphology[22–24] and hydrogels themselves[24–26], but only to an illustrative extent. For this reason, we focused on these reliable and accessible microscopy tools and techniques for the characterization of LMs and for the investigation of cellular phenotypes in a physiological environment. In all instances, we used the budding yeast *Saccharomyces cerevisiae*, which has been previously reported to be viable in these materials and assigned the generally recognized as safe (GRAS)[27] status making it applicable in food and pharma industries.[4,17,18] In our study, we selected three different functionalized triblock copolymers: F127-DMA[4], F127-BUM[17,19], and PGE-DMA[18]. These polymers are advantageous over calcium alginate for microbial encapsulation because the materials are covalently cross-linked and charge-neutral. The carboxylate groups of alginate have previously been shown to inhibit the

transport of charged molecules through these hydrogel matrices.[17] We investigated the stability and degradation of the hydrogels of these polymers after cultivation in a physiological environment, the polymer-cell interface, the localization of cells, the proliferation of colonies, the effect of cellular growth on the polymers, and the effect of physical confinement on cellular phenotype using both OM and SEM methods. Further, we used a computational approach for SEM image analysis to determine cell size changes in living materials and suspension cell cultures. This allowed us to assess the effects of different polymers on the cellular phenotype. The detailed workflow of our study is illustrated in Figure D.1.

6.7 Results and Discussion

6.7.1 *Stability of cell-free hydrogels under physiological conditions*

F127-DMA and F127-BUM hydrogels were prepared as 30 wt% in PBS buffer, while PGE-DMA was prepared as 20 wt%, and all formulations included 0.15 wt% 2-hydroxy-2-methylpropiophenone as a photoinitiator. These hydrogels have previously been shown to be printable using a direct-write extrusion printer.[4,17,18] Despite the fact that F127-DMA and F127-BUM were present at the same concentration in their respective hydrogels, the latter polymer resulted in hydrogels that had a larger storage modulus (247 kPa versus 203 kPa).[4,19] The data were acquired in milli-Q water, but the storage modulus pattern should remain relatively similar in PBS.[28] The difference in stiffness of F127-based gels is attributed to the presence of carbamate linkage at the polymer chain ends in F127-BUM (Figure D.S1), which can form intermolecular hydrogen bonds. The PGE-DMA hydrogel had a lower storage modulus (96 kPa) largely due to the lower concentration of polymer present.[18] Concentrations of PGE-DMA beyond 20 wt% were not possible as the hydrogel became too stiff for processing. The lower feasible concentration for PGE-DMA gel formation is attributed to the difference in the self-assembled networks. In

particular, the presence of bridging chains in BAB triblock copolymer assemblies could facilitate the gelation (Figure D.1a).

We first sought to understand how cells proliferate and affect the surrounding hydrogel matrix, which was observed using optical microscopy (OM) and scanning electron microscopy (SEM). The stability of the cross-linked hydrogels in the absence of any cells was observed for 14 d in a minimal medium (MM). The images presented here serve as a control (Figure D.2) to appreciate the differences with yeast-laden hydrogels, where the structures might transform due to proliferation of cells. At both macroscopic and microscopic levels, the control samples appeared stable throughout the cultivation period under physiological conditions. Moreover, we did not observe any changes in the physiological environment as determined by glucose and pH measurements (Figure D.S2a, b). The mass of the control structures remained unchanged.

6.7.2 *Stability of yeast-laden hydrogels*

After ascertaining the stability of all hydrogels printed without cells, we focused on understanding the impact of long-term proliferation of immobilized cells on the hydrogels and whether different proliferation patterns were adopted by cells in the distinct LMs. Here, we printed the same formulations as mentioned before with a cell inoculum of 10^6 cells g^{-1} hydrogel using a direct-write extrusion printer. After ultraviolet (UV) curing, we washed each LM for 60 s in 70 % ethanol to ensure sterility of printed structures and to avoid potential contamination of the culture medium from peripheral cells. We cultivated the LMs in 5 mL MM for 14 d in at least triplicates with a change of medium every 24 h. Representative samples were collected for processing either for OM or SEM on days 0, 7, and 14. During sample fixation and dehydration for microscopy analysis, some cells detached from the cross-section surface.

Starting on day 0 (after equilibration for 24 h at room temperature), small colonies were observed inside the 3D printed structures (Figure D.S4a, c, e, g, i, k). After one-week, clear differences were observed in how cells grew inside each of the hydrogels; those distinct proliferation patterns remained largely consistent during the second week. Peripheral colonies in F127-based LMs tended to merge and formulate a separate film around LMs (Figure D.3a, b, d, e). These materials cracked open beyond a particular cell number (Figure D.S4d, j). For some samples in F127-DMA, the cell-free layer and cell-laden layer tended to separate completely (Figure D.S4b, h; Figure D.S6). The growth of colonies in PGE-DMA was directed towards the periphery (Figure D.3c, f; Figure D.S4f). A separated layer as in F127-based LMs was not observed. We observed that there was a colony diameter size gradient in all LMs, with smaller colonies in the middle and larger ones toward the periphery (Figure D.S5). Colony diameters in the middle of the structure for all three hydrogel compositions stayed in the range of 26-38 μm, with similar observations for day 7 and 14 samples (Figure D.3; Figure D.S4). Cell-retaining structures became swollen due to cellular proliferation (Figure D.3g), and colonies in the middle region started to show an altered morphology indicating phenotypic differences in cells (Figure D.3i). Potentially, there was a limitation of nutrients for inner cells that contributed towards a clear colony size gradient (Figure D.S5); the cells in the smaller, nutrient-limited inner colonies were also likely more prone to cell death (Figure D.3i, D.S5). A similar pattern has been reported in a recent study by Qian and colleagues.[7]

Two days after the start of the experiment, glucose was always depleted within every 24 h batch cultivation (Figure D.S2c), and the pH did not drop substantially (Figure D.S2d). The cells started to escape into the culture medium at different time points. F127-DMA retained cells the longest (5.13 ± 1.55 d), whereas F127-BUM, although structurally almost identical, retained them

for 3 d, and PGE-DMA for 2 d (Figure D.S2e). Due to growth, swelling, and retention time differences in F127-DMA and F127-BUM, the living materials were 136.80 (± 27.78) %, 53.39 (± 4.15) % respectively, heavier after one week, (Figure D.S2f). The observed mass increase was only 41.28 (± 9.93) % for PGE-DMA (Figure D.S2f). After the cells started escaping from hydrogels, they continuously washed out from the cavity between the inner and outer layer of F127-based materials and resulted in an increase of about 40 % (relative to the start) after two weeks of cultivation (Figure D.S2f). However, since PGE-DMA did not form such cavities, its weight stayed the same during the second week (Figure D.S2f). Interestingly, the increase in mass was the same (roughly 40 %) for all LMs after two weeks of incubation. This appears to be the carrying capacity of all tested living materials under our experimental conditions after two weeks and suggests that modifications to hydrogels would be necessary to increase the capacity in the future.

6.7.3 *Growth patterns of yeast colonies in living materials*

To understand cellular growth within the hydrogels, we 3D printed these materials with a lower number of cells (~10^5 g^{-1} hydrogel), allowing us to observe single colonies after 48 h of cultivation. Batch cultivation in 5 mL MM was carried out with a medium change every 24 h. As observed before, cells were retained in both F127-DMA and F127-BUM hydrogels on day two, whereas cells started to escape from PGE-DMA (Figure D.S7a). Therefore, the comparison of glucose consumption in PGE-DMA hydrogels with F127-based hydrogels was not possible from the second day onwards. Within 24 h, glucose was consumed slightly faster in PGE-DMA and F127-DMA hydrogels compared to F127-BUM hydrogels, where the difference in starting/finishing glucose was only minimal (Figure D.S7b). After 48 h, glucose was consumed significantly more in the medium of F127-DMA than F127-BUM, supporting the aforementioned

observation (Figure D.S7b). The ABA block architecture of F127-DMA and F127-BUM, and the BAB block architecture of PGE-DMA afford different physically and chemically cross-linked networks and storage moduli. Those differences, among others, further support differences in glucose diffusion through the hydrogel (Figure D.S7b). Further studies are required to assess the diffusion of molecules through these hydrogel matrices, wherein the polymer composition, architecture, and concentration are altered in order to design or select other LMs based on these diffusion parameters.[29,30]

Interestingly, the morphology of colonies differed between F127-based LMs and PGE-DMA hydrogels. While the colonies in F127-based materials were spherical in shape (Figure D.4a, b, d, e), PGE-embedded colonies showed a more irregular spindle-like or elliptic shape (Figure D.4c, f, h). For this reason, it was impossible to properly measure and compare the colony size and growth rate inside PGE-DMA relative to the F127-based hydrogels. Additionally, lesions appeared on the surface of PGE-DMA hydrogels, confirming the escape of cells into the medium (Figure D.4i), which were not observed in F127-based hydrogels. After 72 h, the F127-based hydrogels had single colonies in the range of 90-250 μm, and the proliferation of the colonies toward the center of the hydrogel did not exhibit a significant change in size to the ones after 48 h (Figure D.S8).

6.7.4 *Cellular phenotyping in living materials*

Further investigations of the cell-laden hydrogels revealed a thin organic coating around the cell colonies in the F127-DMA and F127-BUM hydrogels (Figure D.5a, b), which was not present in the PGE-DMA hydrogels (Figure D.5c). This difference became evident within 24 h after 3D printing and incubation at room temperature. A supercritical CO_2 extraction protocol was used with rapid release of CO_2 to separate and measure the thin polymer coating (100 – 160 nm) around yeast colonies (Figure D.S3.2). As colonies increased in size, the thin surrounding coating

ruptured, and only remnants of the coating were observed on a colony surface (Figure D.S9). Based on SEM images, we determined that the film ruptured when the colony diameter had reached a size of about 60 – 80 µm within the LMs (Figure D.S9).

The different cell-polymer interactions, as well as retention times, consequently led to the question of impact of physical confinement on the cell phenotype. To address this question, we performed a computational analysis on the acquired SEM images as described in the materials and methods section. During this analysis, cell size (in μm^3) parameter was utilized to investigate the effects of physical confinement on the cells in hydrogels in comparison to suspension cells. We evaluated cell size differences after 48 h in the aforementioned samples (used in Figure D.4). Suspension cells were cultivated, fixed and dehydrated in the same way as the immobilized cells (Figure D.S10). Interestingly, cells encapsulated in hydrogels were significantly ($p < 0.05$) smaller than the suspension cells (Figure D.5d). Cell size differences were even evident among the LMs (Figure D.5d). The cause of cell size differences was likely multifarious instead of an individual attributable factor, as a cellular phenotype is an integrated readout of manifold cellular processes and naturally, physical confinement in hydrogels is an additional factor for immobilized cells compared to suspension cells (Figure D.5). The previous studies on effects of physical confinement in a calcium alginate matrix indicate changes in cellular physiology of yeast.[31,32] Though, a molecular investigation of cells was not in the scope of the present study, it would be very valuable to understand underlying molecular mechanisms responsible for phenotypic differences in LMs for their development as a technology of the future.

6.7.5 *Polymer integrity analysis in living materials*

In certain applications polymer integrity could be of essence in the LMs but in other instances a controlled polymer degradation might be preferred, making the study of polymer degradation an

important component for development of the LM based technologies. F127-BUM contains carbamate bonds on the periphery of micelles making it susceptible to enzymatic degradation by cells, which can secrete proteases[32], and thus provides an excellent model for studying polymer degradation (Figure D.1; Figure D.6). To validate this idea, we conducted a 14-day experiment with and without a protease inhibitor cocktail for all the LMs in the study (Figure D.6). The concentration of inhibitors used in these experiments did not have an influence on control structures nor on the cell proliferation. We used the fast release of gas in the supercritical CO_2 extraction protocol to identify differences between degraded and intact polymers in LMs (Figure D.6, Figure D.S3.2).

The addition of inhibitors, as expected, did not have any effect on the outcome with F127-DMA and PGE-DMA compared to the control condition - shown by similar images (Figure D.6a, b, e, f). It should also be noted that in the case of PGE-DMA, the effect of the fast gas release appeared less pronounced compared to F127-based materials. This result could be attributed to the lower polymer concentration used in the formation of PGE-DMA hydrogels. During fast CO_2 extraction, less dense (or degraded) materials allow the gas to escape more easily (Figure D.6c, e, f), whereas denser materials withhold the gas resulting in cavities (Figure D.6a, b, d). A clear difference was observed in the F127-BUM samples, where the sample appeared altered in the absence of the inhibitor indicating a polymer degradation (Figure D.6c, d). To ensure the reproducibility of these observations, we repeated the experiment for F127-BUM with a culture medium change every 48 h allowing secreted proteases more reaction time to potentially cleave the bonds. Following this approach, we found an even more pronounced difference, indicating a possible effect of enzymes on the integrity of F127-BUM (Figure D.S3.2e, f). This was also supported by a higher cell retention time in F127-DMA compared with F127-BUM (Figure

D.S2e). Using different proteases to study the enzyme degradation of F127-BUM might be worth an investigation in the future, and can potentially make it an attractive candidate for use in biomedical applications, such as angiogenesis research, where enzyme-driven matrix degradation is vital.[33]

6.8 CONCLUSIONS

Our ability to develop new polymeric materials and their hydrogels for 3D printing LMs is outpacing our understanding of LMs due to the lack of investigations into how the mutual interactions of incorporated cells in the living materials impact both the cells and the polymers. Understanding such cellular-polymeric interactions is crucial to draw conclusions about the effects of physical confinement on cells within these materials.

We investigated three triblock polymeric hydrogels together with yeast-laden LMs with scanning electron and optical microscopy techniques and revealed several previously unreported features, *e.g.* proliferation patterns of colonies, alteration of cell sizes, colony encapsulations, and potential polymer degradation. The distinct compositional and structural features of the living materials make them suitable for different applications, *e.g.* in biomedical research, where degradable polymers are needed, or biotechnology, where cell retention is desirable. Factors, such as the printing thickness and diffusion, should also be considered to ensure a sufficient nutrient supply to all cells within the LMs. Here, we have demonstrated changes in cellular phenotypes due to physical confinement within three hydrogels. However, our current study precludes understanding underlying molecular mechanisms of phenotypic changes, but it would constitute an important area of exploration in the future.

6.9 ACKNOWLEDGEMENTS

This project has received funding from the European Union's Horizon 2020 research and innovation program under grant agreement No. 668997, and the Estonian Research Council (grant PUT1488P). TB and HP would additionally like to acknowledge mobility grants MB-2018-1/25 by *Bayerisches Hochschulzentrum für Mittel-, Ost- und Südosteuropa* (BAYHOST) and the European Regional Development Fund, respectively. AN acknowledges the National Science Foundation (Grant No. 1752972), UW CoMotion Innovation Grant and UW Royalty Research Fund for financial support of this work. We thank Külli Jaako and Monika Jürgenson, at the Institute of Biomedicine and Translational Medicine, Faculty of Medicine, University of Tartu, for access to microscopy resources.

6.10 REFERENCES

1. Dasgupta, Q.; Black, L. D. A FRESH SLATE for 3D Bioprinting. *Science*. American Association for the Advancement of Science August 2, 2019, pp 446–447.
2. Smith, P. T.; Basu, A.; Saha, A.; Nelson, A. Chemical Modification and Printability of Shear-Thinning Hydrogel Inks for Direct-Write 3D Printing. *Polymer (Guildf).* **2018**, *152*, 42–50.
3. Huang, J.; Liu, S.; Zhang, C.; Wang, X.; Pu, J.; Ba, F.; Xue, S.; Ye, H.; Zhao, T.; Li, K.; Wang, Y.; Zhang, J.; Wang, L.; Fan, C.; Lu, T. K.; Zhong, C. Programmable and Printable *Bacillus subtilis* Biofilms as Engineered Living Materials. *Nat. Chem. Biol.* **2019**, *15* (1), 34–41.
4. Saha, A.; Johnston, T. G.; Shafranek, R. T.; Goodman, C. J.; Zalatan, J. G.; Storti, D. W.; Ganter, M. A.; Nelson, A. Additive Manufacturing of Catalytically Active Living Materials. *ACS Appl. Mater. Interfaces* **2018**, acsami.8b02719.
5. Li, J.; Mooney, D. J. Designing Hydrogels for Controlled Drug Delivery. *Nat. Rev. Mater.* **2016**, *1* (12), 16071.
6. Zhu, J.; Marchant, R. E. Design Properties of Hydrogel Tissue-Engineering Scaffolds. *Expert Review of Medical Devices*. Taylor & Francis September 2011, pp 607–626.
7. Qian, F.; Zhu, C.; Knipe, J. M.; Ruelas, S.; Stolaroff, J. K.; DeOtte, J. R.; Duoss, E. B.; Spadaccini, C. M.; Henard, C. A.; Guarnieri, M. T.; Baker, S. E. Direct Writing of Tunable Living Inks for Bioprocess Intensification. *Nano Lett.* **2019**, *19* (9), 5829–5835.
8. Gopinathan, J.; Noh, I. Recent Trends in Bioinks for 3D Printing. *Biomater. Res.* **2018**, *22* (1), 11.
9. Hölzl, K.; Lin, S.; Tytgat, L.; Van Vlierberghe, S.; Gu, L.; Ovsianikov, A. Bioink Properties before, during and after 3D Bioprinting. *Biofabrication* **2016**, *8* (3), 032002.

10. Wu, W.; DeConinck, A.; Lewis, J. A. Omnidirectional Printing of 3D Microvascular Networks. *Adv. Mater.* **2011**, *23* (24), H178–H183.
11. Fellin, C. R.; Adelmund, S. M.; Karis, D. G.; Shafranek, R. T.; Ono, R. J.; Martin, C. G.; Johnston, T. G.; DeForest, C. A.; Nelson, A. Tunable Temperature- and Shear-Responsive Hydrogels Based on Poly(Alkyl Glycidyl Ether)S. *Polym. Int.* **2018**, No. August.
12. Adams, M. L.; Lavasanifar, A.; Kwon, G. S. Amphiphilic Block Copolymers for Drug Delivery. *J. Pharm. Sci.* **2003**, *92* (7), 1343–1355.
13. Chu, B.; Liu, T.; Wu, C.; Zhou, Z.; Mark Nace, V. Structures and Properties of Block Copolymers in Solution. *Macromol. Symp.* **1997**, *118* (1), 221–227.
14. Malda, J.; Visser, J.; Melchels, F. P.; Jüngst, T.; Hennink, W. E.; Dhert, W. J. A.; Groll, J.; Hutmacher, D. W. 25th Anniversary Article: Engineering Hydrogels for Biofabrication. *Adv. Mater.* **2013**, *25* (36), 5011–5028.
15. Pereira, R. F.; Bártolo, P. J. 3D Bioprinting of Photocrosslinkable Hydrogel Constructs. *J. Appl. Polym. Sci.* **2015**, *132* (48).
16. Wang, Z.; Kumar, H.; Tian, Z.; Jin, X.; Holzman, J. F.; Menard, F.; Kim, K. Visible Light Photoinitiation of Cell-Adhesive Gelatin Methacryloyl Hydrogels for Stereolithography 3D Bioprinting. *ACS Appl. Mater. Interfaces* **2018**, *10* (32), 26859–26869.
17. Johnston, T. G.; Yuan, S.-F.; Wagner, J. M.; Yi, X.; Saha, A.; Smith, P.; Nelson, A.; Alper, H. S. Compartmentalized Microbes and Co-Cultures in Hydrogels for on-Demand Bioproduction and Preservation. *Nat. Commun.* **2020**, *11* (1), 563.
18. Johnston, T. G.; Fellin, C. R.; Carignano, A.; Nelson, A. Poly(Alkyl Glycidyl Ether) Hydrogels for Harnessing the Bioactivity of Engineered Microbes. *Faraday Discuss.* **2019**, *219* (0), 58–72.
19. Millik, S. C.; Dostie, A. M.; Karis, D. G.; Smith, P. T.; McKenna, M.; Chan, N.; Curtis, C. D.; Nance, E.; Theberge, A. B.; Nelson, A. 3D Printed Coaxial Nozzles for the Extrusion of Hydrogel Tubes toward Modeling Vascular Endothelium. *Biofabrication* **2019**, *11* (4), 045009.
20. Drira, Z.; Yadavalli, V. K. Nanomechanical Measurements of Polyethylene Glycol Hydrogels Using Atomic Force Microscopy. *J. Mech. Behav. Biomed. Mater.* **2013**, *18*, 20–28.
21. Shachaf, Y.; Gonen-Wadmany, M.; Seliktar, D. The Biocompatibility of Pluronic®F127 Fibrinogen-Based Hydrogels. *Biomaterials* **2010**, *31* (10), 2836–2847.
22. Iurciuc (Tincu), C.-E.; Savin, A.; Atanase, L. I.; Martin, P.; Popa, M. Physico-Chemical Characteristics and Fermentative Activity of the Hydrogel Particles Based on Polysaccharides Mixture with Yeast Cells Immobilized, Obtained by Ionotropic Gelation. *Food Bioprod. Process.* **2017**, *104*, 104–123.
23. Iurciuc (Tincu), C.-E.; Savin, A.; Atanase, L. I.; Danu, M.; Martin, P.; Popa, M. Encapsulation of *Saccharomyces cerevisia*e in Hydrogel Particles Based Gellan Ionically Cross-Linked with Zinc Acetate. *Powder Technol.* **2018**, *325*, 476–489.
24. Bryant, S. J.; Cuy, J. L.; Hauch, K. D.; Ratner, B. D. Photo-Patterning of Porous Hydrogels for Tissue Engineering. *Biomaterials* **2007**, *28* (19), 2978–2986.
25. Kim, S.-H.; Chu, C.-C. Synthesis and Characterization of Dextran-Methacrylate Hydrogels and Structural Study by SEM. *J. Biomed. Mater. Res.* **2000**, *49* (4), 517–527.
26. Kim, S.; Chu, C.-C. Pore Structure Analysis of Swollen Dextran-Methacrylate Hydrogels by SEM and Mercury Intrusion Porosimetry. *J. Biomed. Mater. Res.* **2000**, *53* (3), 258–266.
27. U.S. Food & Drug Administration (FDA). *Code of Federal Regulations Title 21*; US Federal Government: Washington, 2019.

28. Jiang, J.; Li, C.; Lombardi, J.; Colby, R. H.; Rigas, B.; Rafailovich, M. H.; Sokolov, J. C. The Effect of Physiologically Relevant Additives on the Rheological Properties of Concentrated Pluronic Copolymer Gels. *Polymer (Guildf).* **2008**, *49* (16), 3561–3567.
29. Figueiredo, L.; Pace, R.; D'Arros, C.; Réthoré, G.; Guicheux, J.; Le Visage, C.; Weiss, P. Assessing Glucose and Oxygen Diffusion in Hydrogels for the Rational Design of 3D Stem Cell Scaffolds in Regenerative Medicine. *J. Tissue Eng. Regen. Med.* **2018**, *12* (5), 1238–1246.
30. Sandrin, D.; Wagner, D.; Sitta, C. E.; Thoma, R.; Felekyan, S.; Hermes, H. E.; Janiak, C.; de Sousa Amadeu, N.; Kühnemuth, R.; Löwen, H.; Egelhaaf, S. U.; Seidel, C. A. M. Diffusion of Macromolecules in a Polymer Hydrogel: From Microscopic to Macroscopic Scales. *Phys. Chem. Chem. Phys.* **2016**, *18* (18), 12860–12876.
31. Nagarajan, S.; Kruckeberg, A. L.; Schmidt, K. H.; Kroll, E.; Hamilton, M.; McInnerney, K.; Summers, R.; Taylor, T.; Rosenzweig, F. Uncoupling Reproduction from Metabolism Extends Chronological Lifespan in Yeast. *Proc. Natl. Acad. Sci. U. S. A.* **2014**, *111* (15), E1538-47.
32. Moreno-García, J.; García-Martínez, T.; Mauricio, J. C.; Moreno, J. Yeast Immobilization Systems for Alcoholic Wine Fermentations: Actual Trends and Future Perspectives. *Frontiers in Microbiology*. Frontiers Media S.A. February 15, 2018.
33. Song, K. H.; Highley, C. B.; Rouff, A.; Burdick, J. A. Complex 3D-Printed Microchannels within Cell-Degradable Hydrogels. *Adv. Funct. Mater.* **2018**, *28* (31), 1801331.

6.11 Main Figures

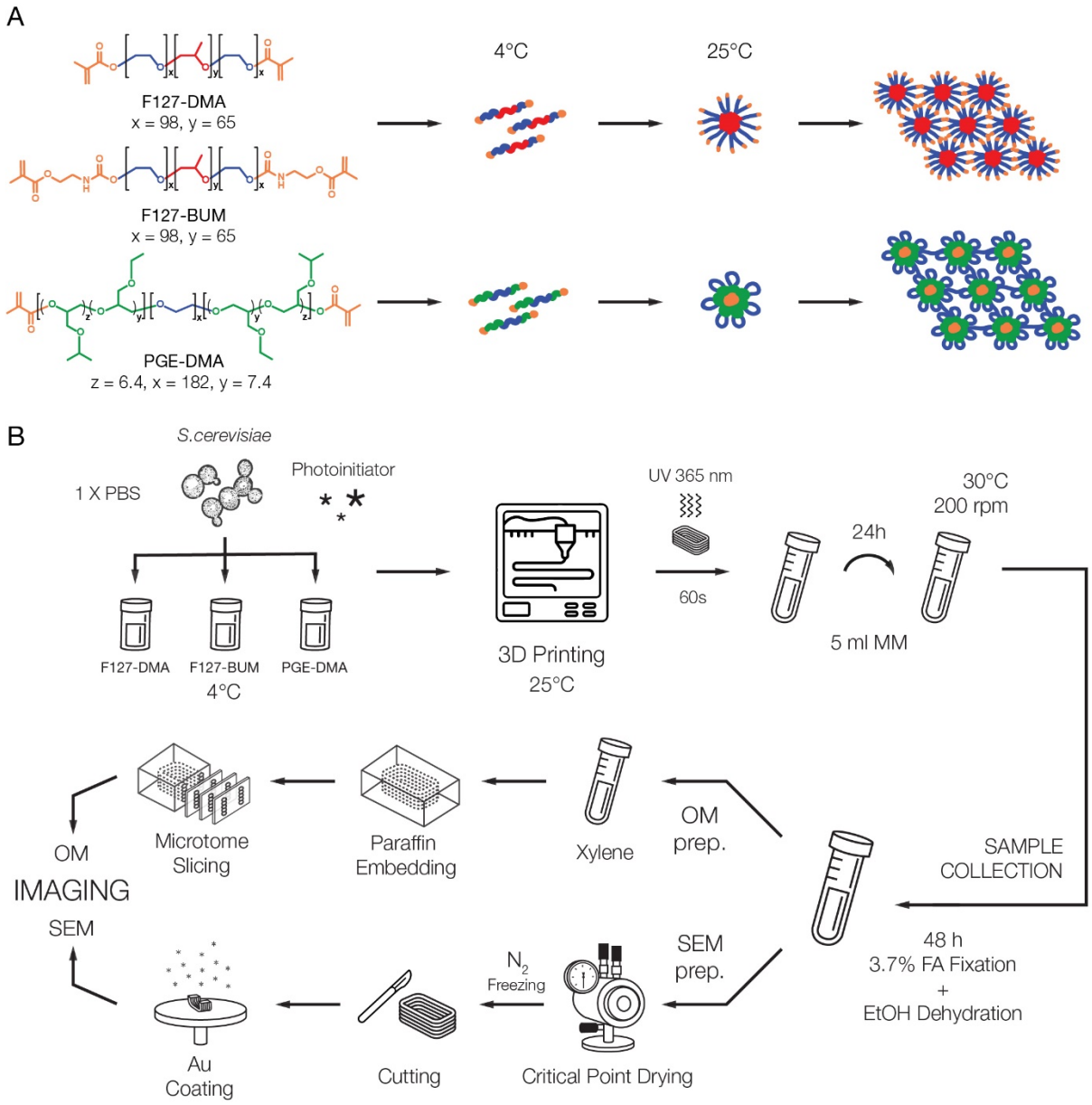

Figure D.1. Schematic diagram showing polymer chemistry (A) and experiment workflow (B). The polymers were mixed with PBS, cells, and photoinitiator at 4 °C and printed at 25 °C to be cured after printing. Batch cultivation time was 24 h for varying days. Samples were collected, fixed, and dehydrated. Specific preparation protocols were applied for SEM or OM imaging.

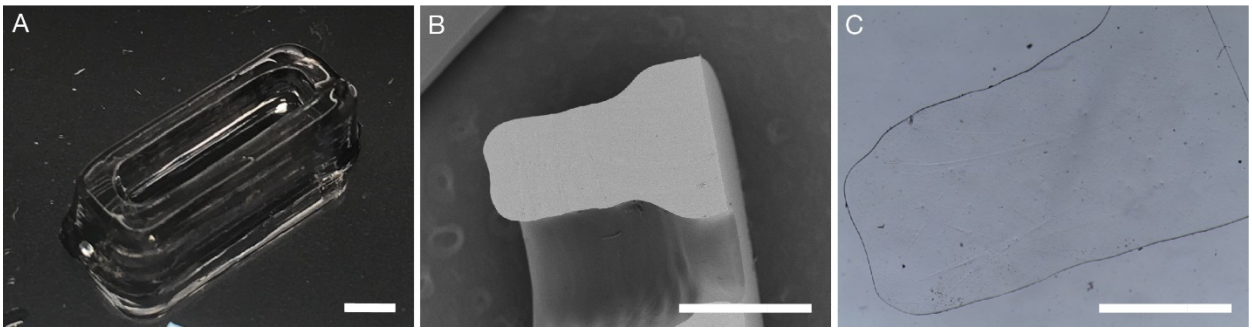

Figure D.2. Illustrative images of control structures (hydrogels printed without cells).

Photograph after 24 h equilibration (A). Cross-sectional SEM micrograph (B). OM micrograph, slice thickness 40 μm (C). Scale bar 1 mm.

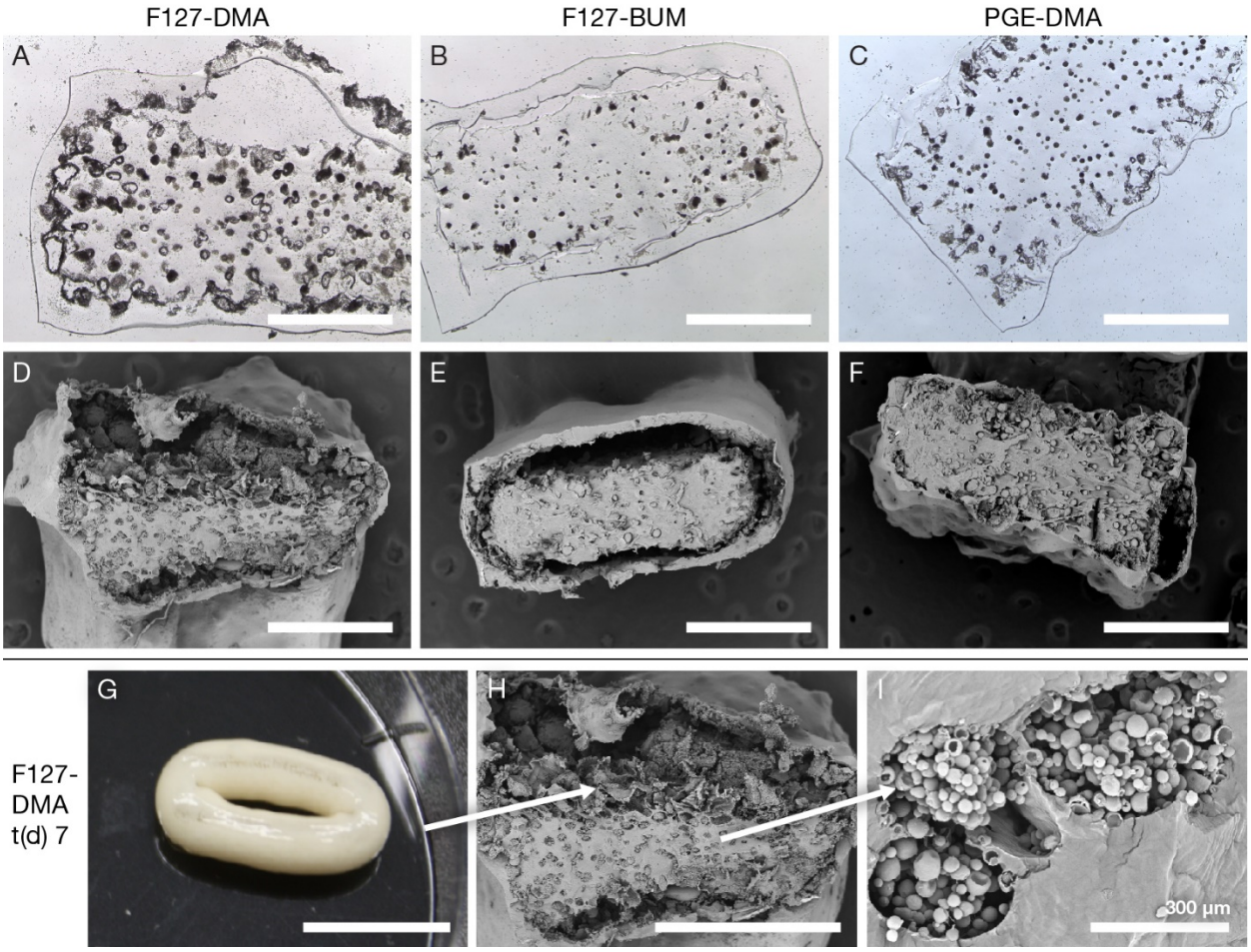

Figure D.3. OM (A - C) and SEM (D - F, H, I) micrographs of LMs after 7 days of incubation. Cells escaped from PGE-DMA without major disruption of the material, F127-DMA and F127-BUM formed separated layers (center vs. shell). Most cell proliferation occurred at the interface. The LMs swelled up and retained cells up to a particular cell number (G). As peripheral colonies joined into one major colony (G, H) the colonies residing in the middle of the hydrogel were deprived of access to nutrients causing cell death in colonies (I). Scale bar 1 mm unless marked differently.

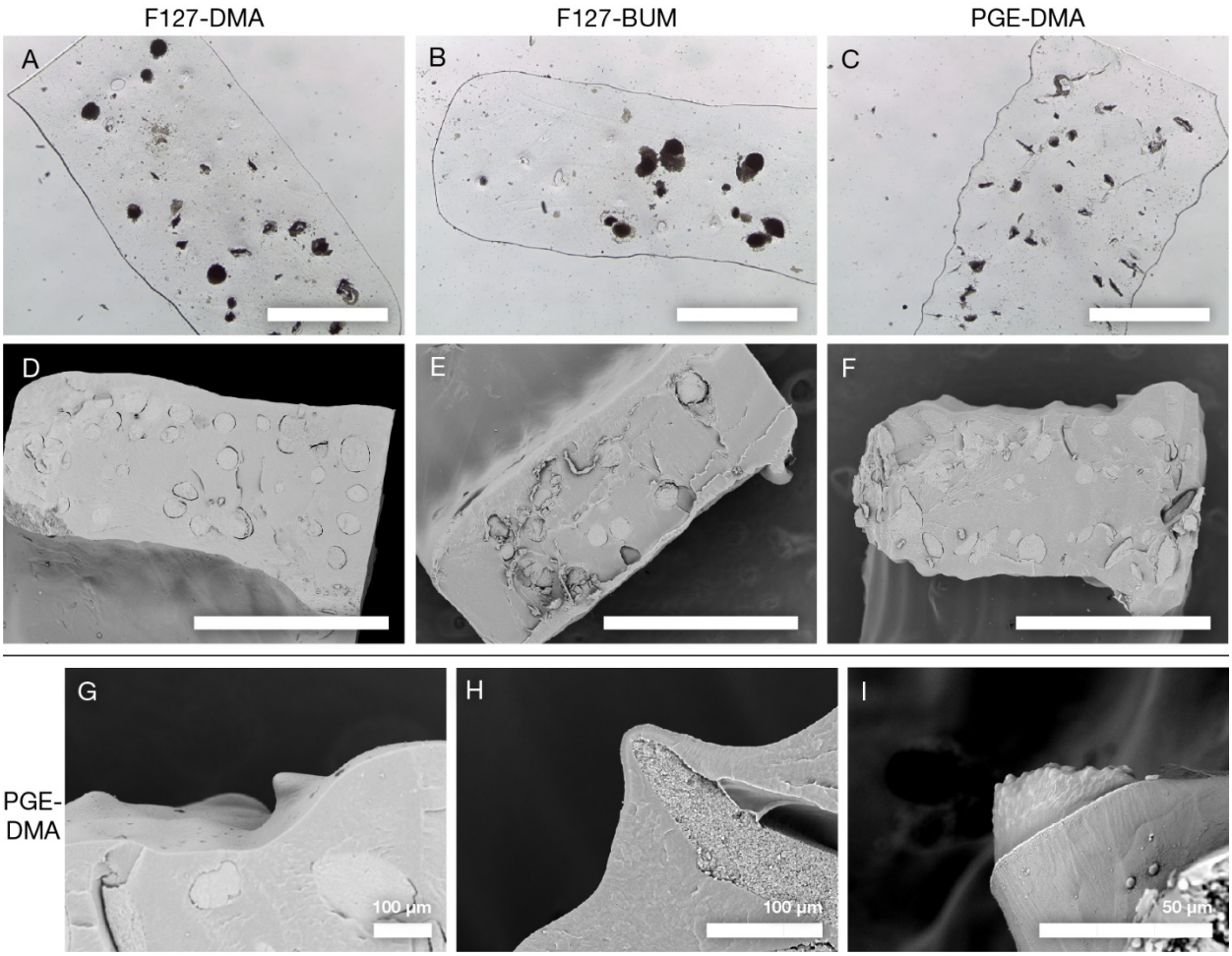

Figure D.4. SEM and OM micrographs of LMs after 48 h of incubation (A - F) and the escape mode of cells from PGE-DMA (G - I).

Peripheral colonies in PGE-DMA formed spindle-like structures (C, F, H), while F127-DMA and F127-BUM formed spherical colonies (A, B, D, E). When the material broke, cells started escaping into the medium (I). Scale bar 1 mm unless marked differently.

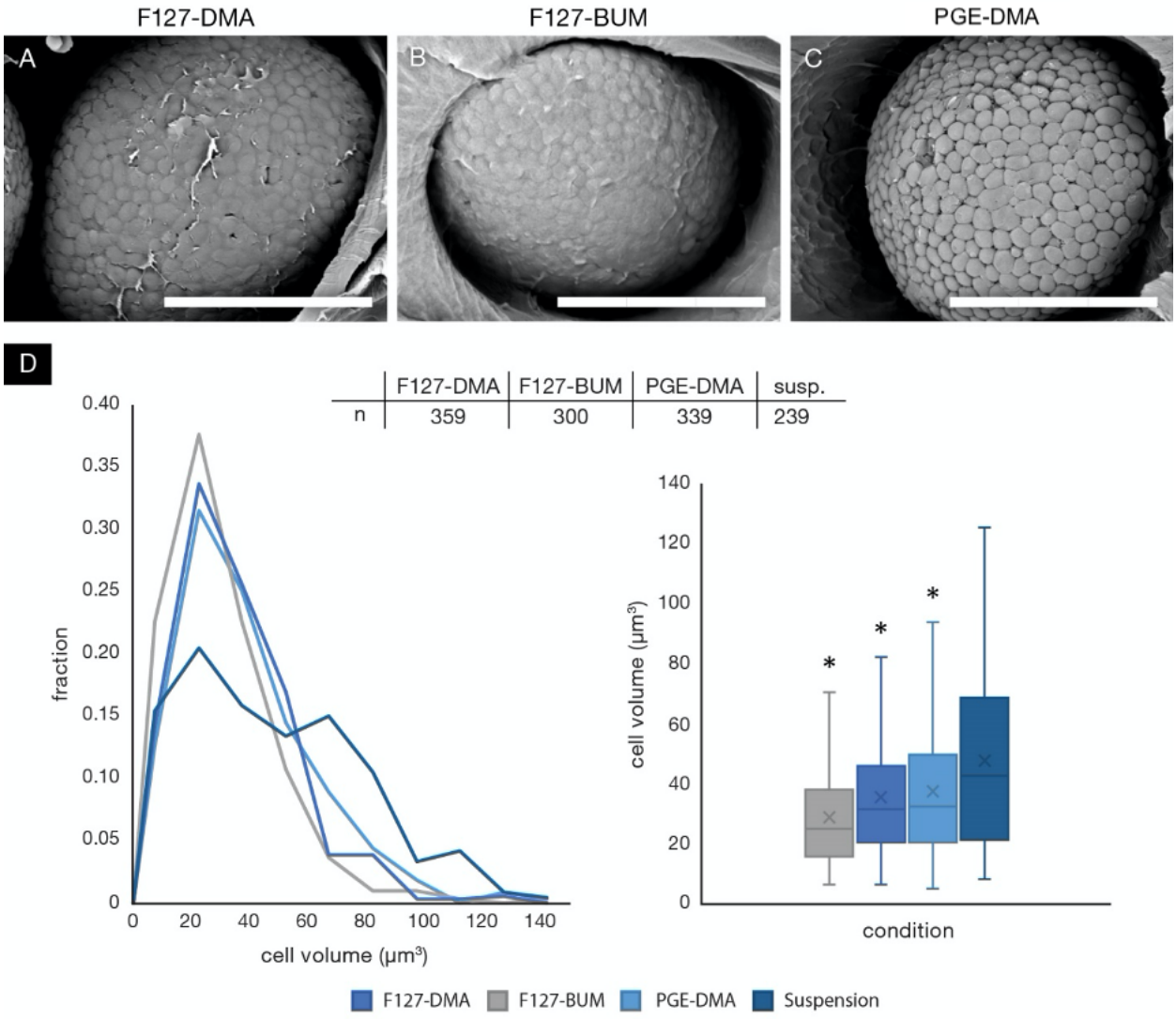

Figure D.5. Organic film covers yeast cell colonies in LMs and cell size (µm3).

F127-DMA (A) and F127-BUM (B) both had a thin organic coating around colonies, while PGE-DMA (C) lacked a similar polymer coating. Scale bar 20 µm. Size (in µm3) distribution of cells in LMs and suspension cell culture (D). A total of ≥ 239 cells per condition were analyzed. LMs were incubated for 48 h before processing and the measurement. * $p < 0.05$, significant difference from suspension cells, x: mean.

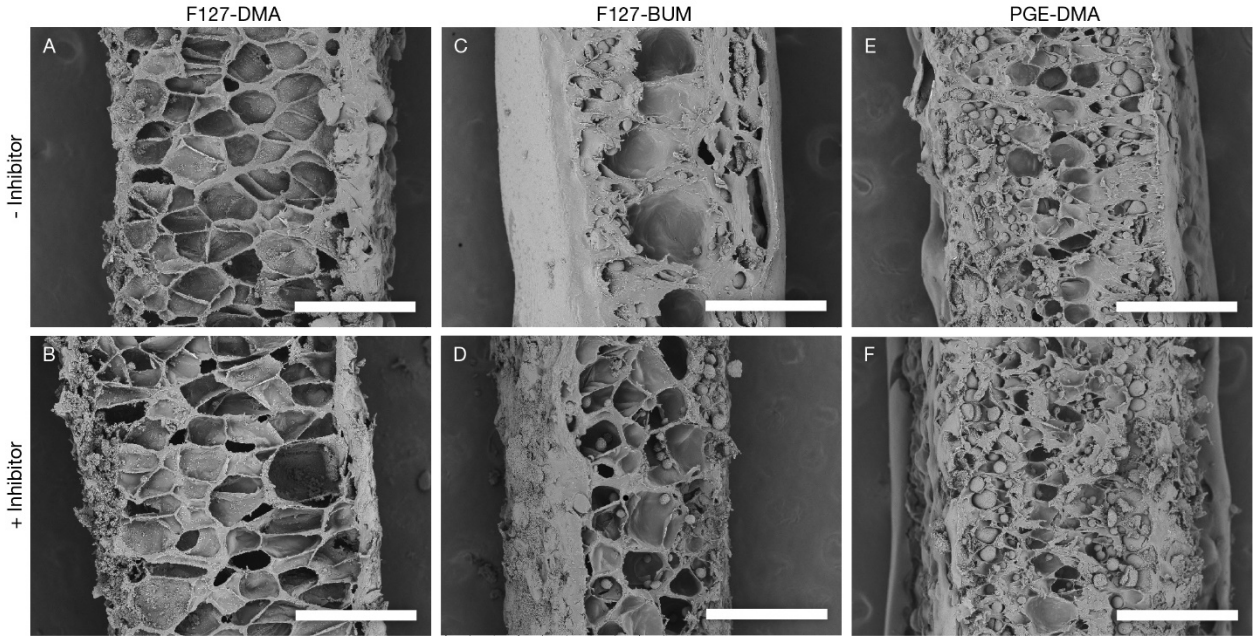

Figure D.6. SEM micrographs showing cavities after pressure release of CO2 inside LMs.

Upper panel: normal cultivation; lower panel: enzyme inhibitors added into the MM. No visual differences were detected in DMA-functionalized polymers (A – B, E - F). Differences were observed in F127-BUM (C, D): when the enzyme inhibitors were missing, the material was degraded allowing the gas to escape more easily during sample preparation (C), whereas gas got trapped in intact material and formed more cavities (D). 24 h 5 mL batches over 14 days. Scale bar 500 μm. All samples prepared in the single critical CO2 extraction experiments to avoid technical variations.

6.12 SUPPLEMENTARY FIGURES

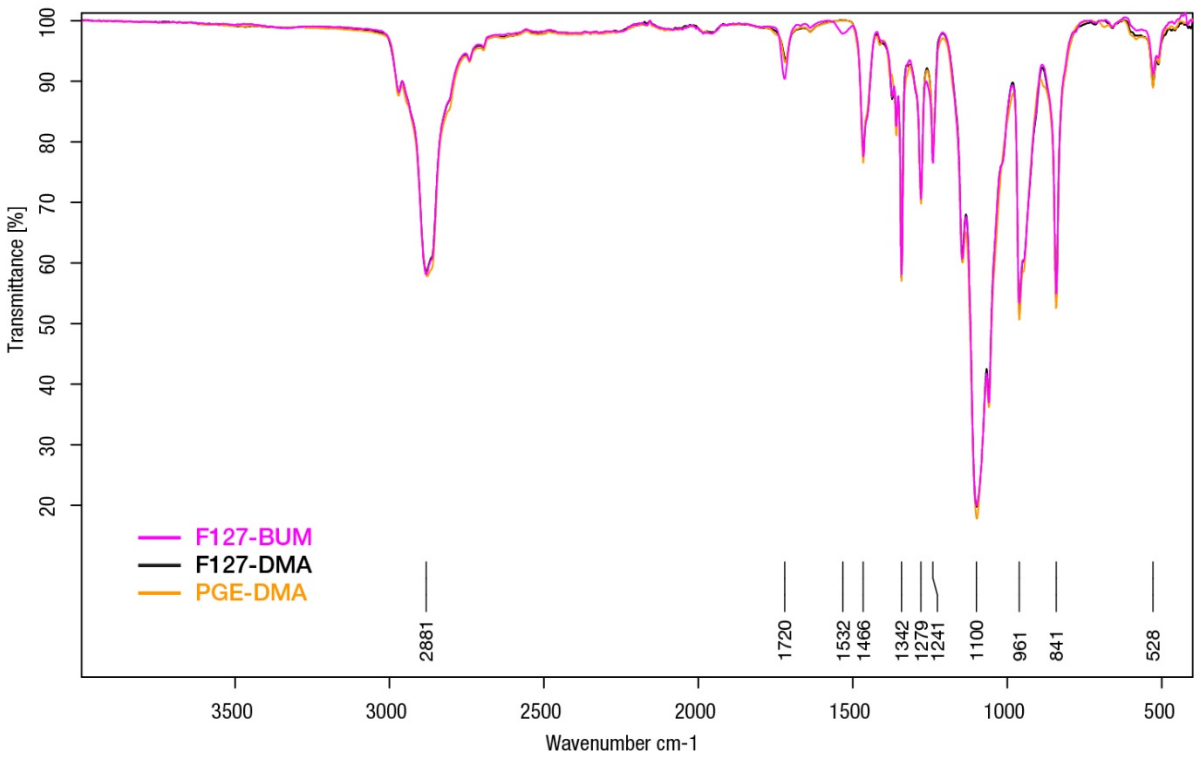

Figure D.S1. FTIR spectra of the three polymers.

The FTIR spectra of all 3 polymers appeared largely similar but F127-BUM clearly showed carbamate functional groups (–CON–) at 1532 cm-1. The spectrum also had less transmittance at 1720 cm-1, which validates one extra carbonyl (C=O) bond per repeating unit as compared to F127-DMA and PGE-DMA. Spectral lines of PGE-DMA and F127-DMA overlap.

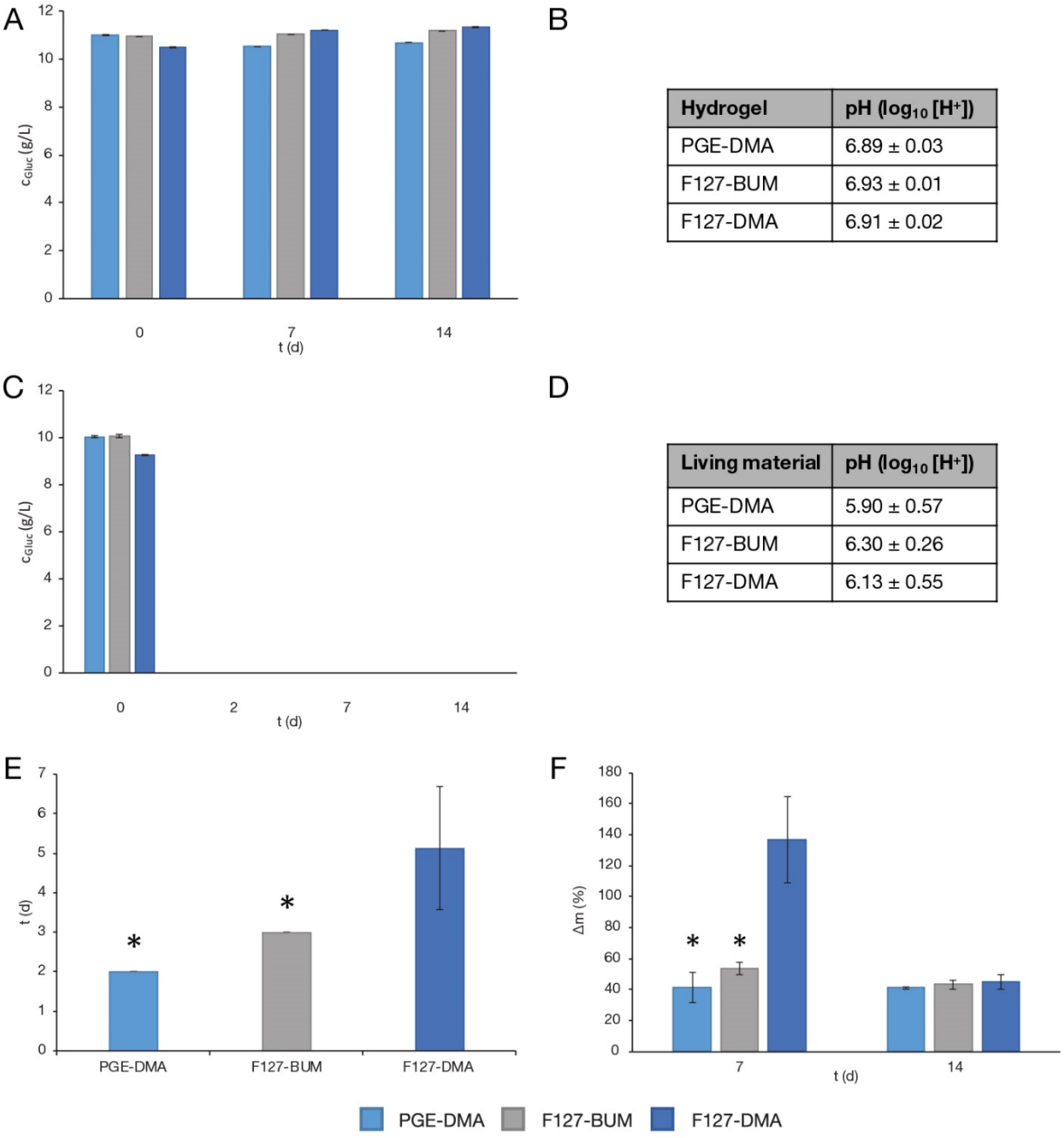

Hydrogel	pH (log_{10} [H^+])
PGE-DMA	6.89 ± 0.03
F127-BUM	6.93 ± 0.01
F127-DMA	6.91 ± 0.02

Living material	pH (log_{10} [H^+])
PGE-DMA	5.90 ± 0.57
F127-BUM	6.30 ± 0.26
F127-DMA	6.13 ± 0.55

Figure D.S2. Medium/LM analysis upon cultivation over different times.

Control structures (A, B). LMs or their respective medium (C - F). MM glucose concentration over time (A, C). Average pH after each batch (B, D). Cell retention time (E). LM mass differences from starting day to day 7 or 14 (F). Gluc: glucose. * $p < 0.05$, significant difference from F127-DMA.

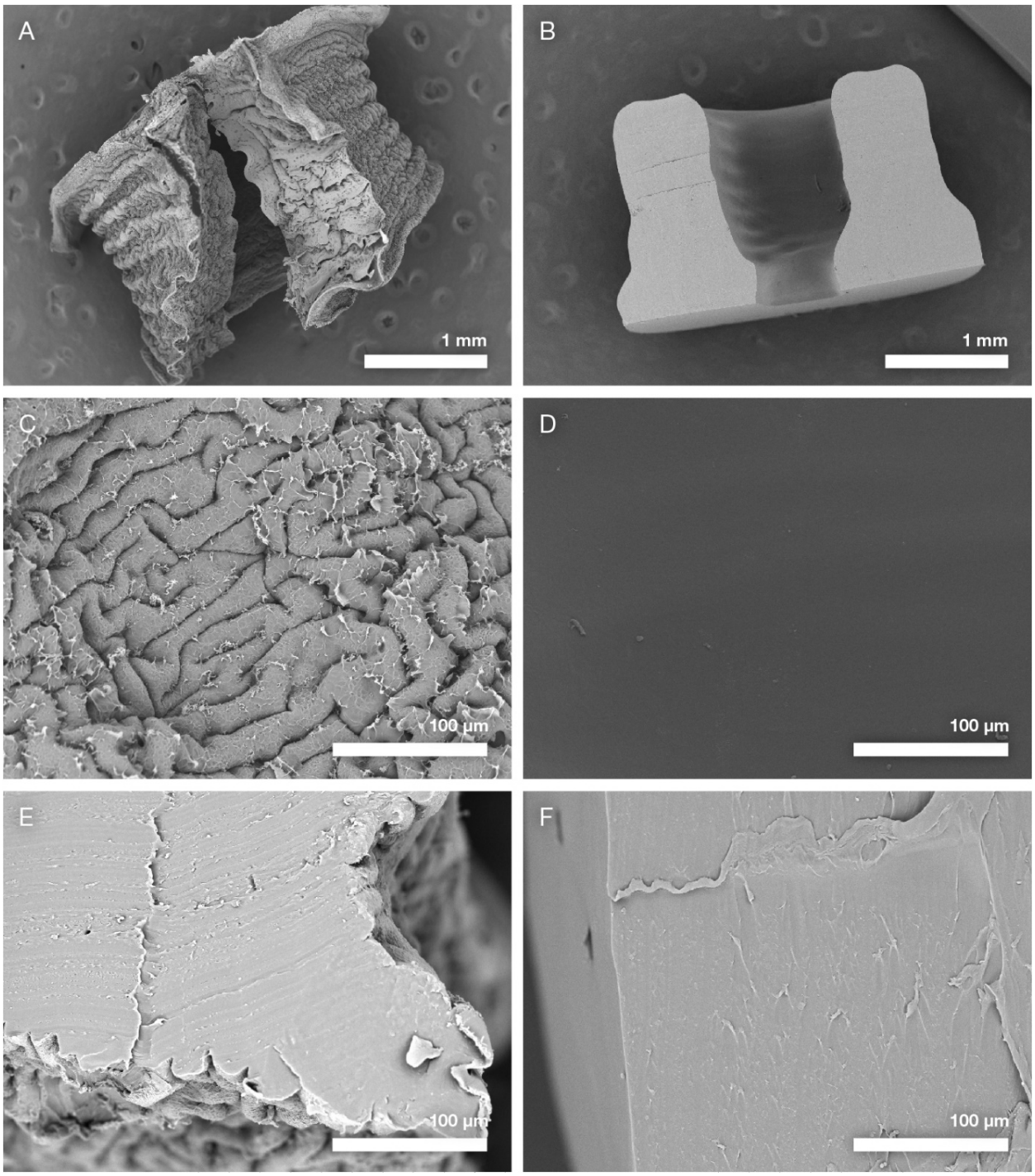

Figure D.S3.1. Freeze-drying vs supercritical CO2 extraction.

A (simpler) alternative to the process of supercritical CO2 extraction is freeze-drying; their performance is compared by presenting an F127-BUM freeze-dried sample (A) as compared to a supercritical CO2 extracted one (B). A closer look at surface topology of the freeze-dried sample (C) shows a “brain”-like surface finish caused by uneven drying, in sharp contrast to the

supercritical CO2 extracted sample (D). Freeze-drying can be used as an alternative for studying cross-sections of these materials, but with the caveat that the samples need to be sectioned after the drying process, because of ~20 μm deformations in the outer perimeter (E) as opposed to the supercritical CO2 extracted sample (F). Here is an overview of a freeze-dried sample (A) compared to a supercritical CO2 extracted sample (B). The surface topology of the freeze-dried sample (C) and the supercritical CO2 extracted sample (D). Cross-section and perimeter comparison of freeze-dried (E) and supercritical CO2 extracted (F) sample. F127-BUM samples displayed.

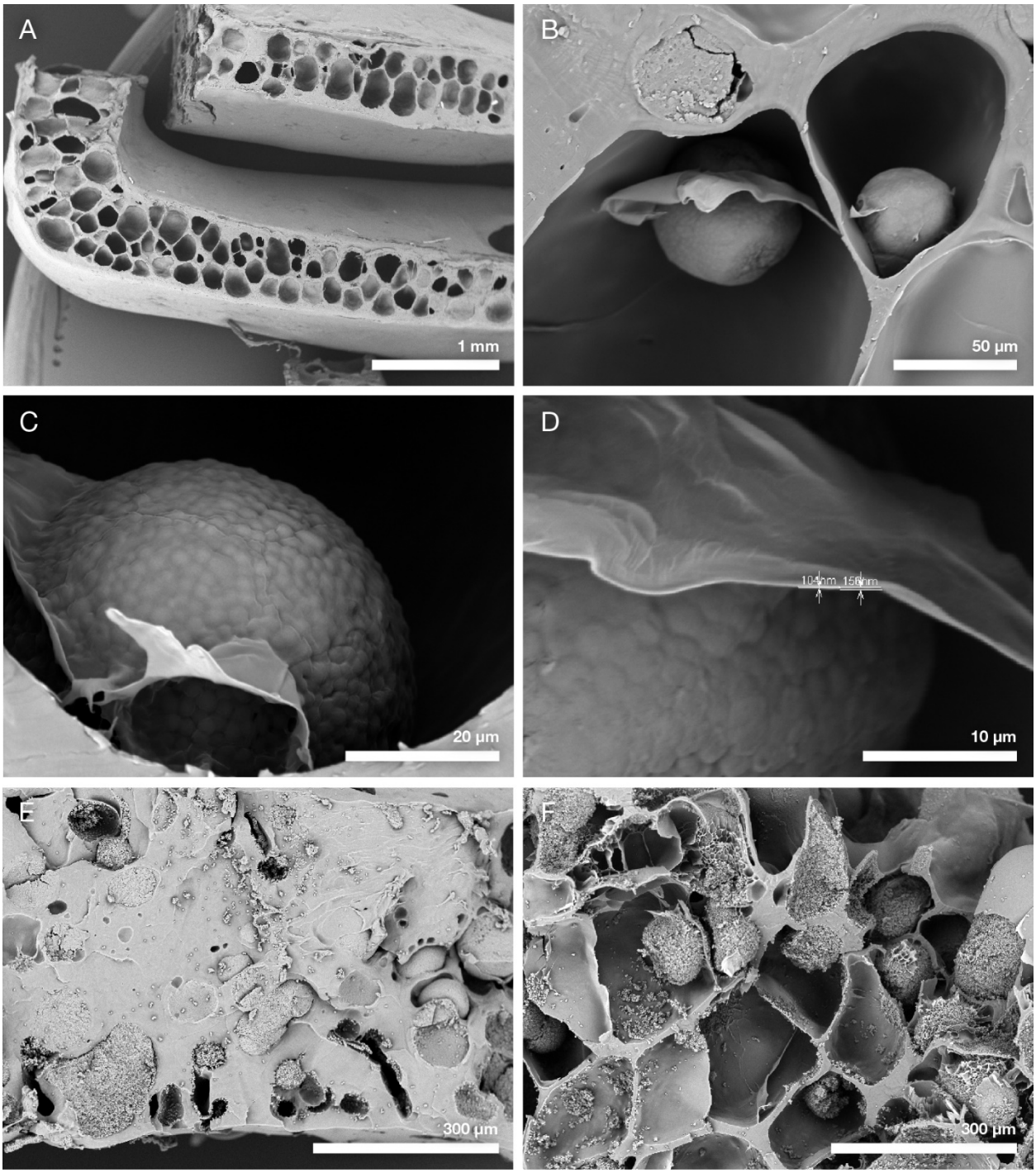

Figure D.S3.2. Special features of fast pressure release during CO_2 extraction.

Fast CO_2 release at the end of supercritical CO_2 extraction process generates local stresses in the gel that lead to mechanical changes resulting in a foam-like structure (A) and the separation of regions in the material (B, C) based on the local structural and mechanical properties. The amount and size of the generated pores depends on the speed of gas release. This method is a valuable tool

for studying gas retention in the material, the thickness of thin film coatings around colonies (D) and possible degradation of the matrix (E, F). Foam-like structure generated due to fast CO_2 release at the end of supercritical CO_2 extraction (A). Separation (B, C) and measurement (D) of the thin polymer coating around yeast colonies in F127-BUM after 48 h of incubation. F127-BUM samples with (F) and without (E) protease inhibitor showing that when inhibitor was missing, the gas did not get trapped with fast CO_2 release (pictures taken after 14 d with 48 h media change).

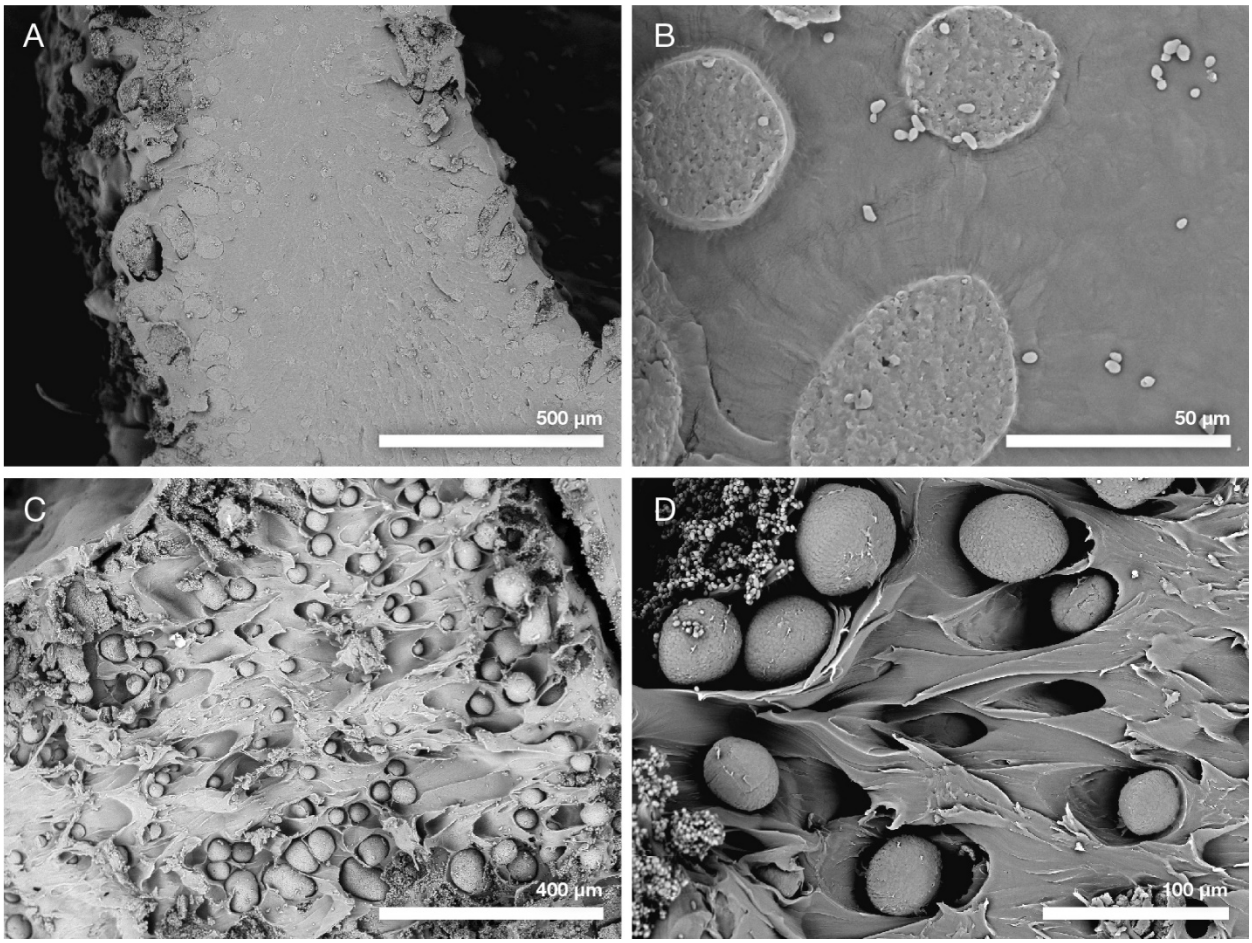

Figure D.S3.3. Sample cutting - exposing cell-material interactions in hydrogels.

Varying the sample and the blade temperature together with the speed of cutting can be used to demonstrate various aspects of LMs. A combination of sample and scalpel cooling (~20 s) together with fast incisions results in the most accurate SEM images in terms of polymeric material and colony localization (A, B), but with this technique it is impossible to evaluate the colony size and shape because of the unknown location of the obtained cross-section in respect to the colony. A shorter duration of sample and scalpel cooling (~10 s) together with slow incision highlights biologically relevant information such as cell-polymer encapsulations (Figure 5a-c) and colony size and shape (C, D) but results in cutting marks across the polymer (D). Different sample cuttings and resulting images: samples prepared with longer cooling of sample and scalpel showing relatively smooth cuts (A, B). Samples prepared with short sample and scalpel cooling showing clear colonies (C, D).

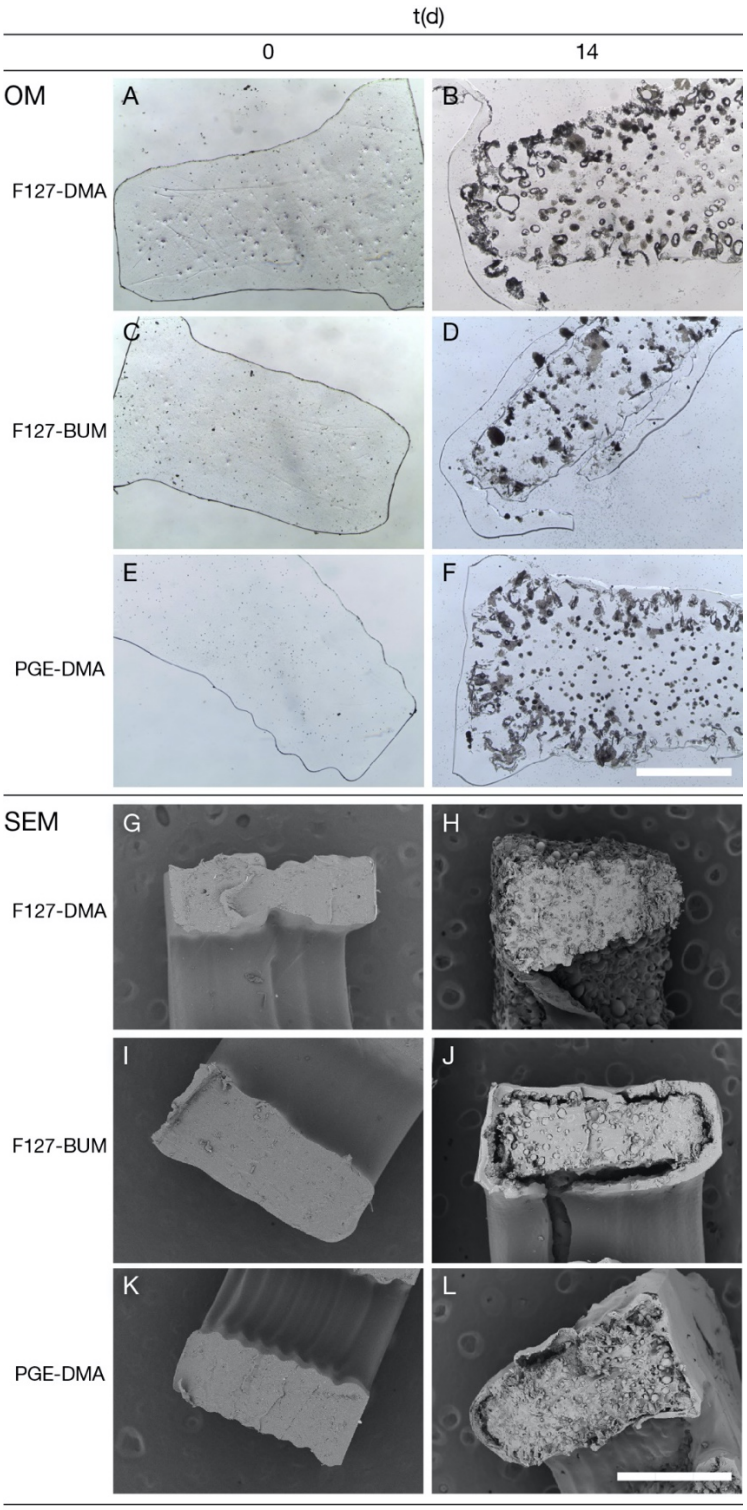

Figure D.S4. OM and SEM Micrographs of LMs after 14-day cultivation.

OM (A-F) and SEM (G-L) micrographs of LMs after 0 (A, C, E, G, I, K) and 14 (B, D, F, H, J, L) d of incubation. Small colonies can already be observed on day 0. Disrupted LMs on day 14 with full separation of layers in F127-DMA (B, H). Scale bar 1 mm.

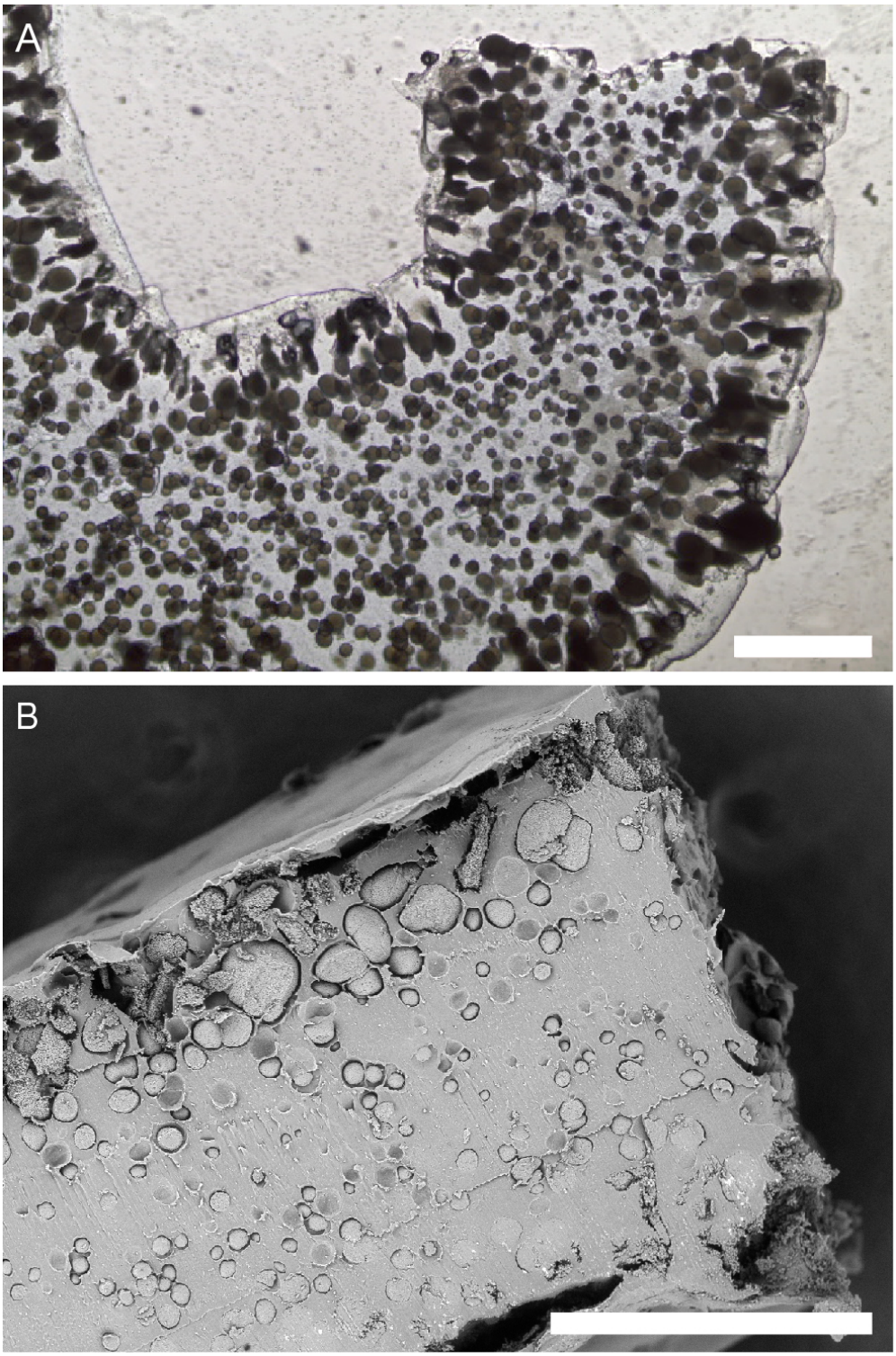

Figure D.S5. Cell colony size gradient.

OM micrograph of PGE-DMA, day 14, slice thickness 150 µm (A). SEM micrograph of PGE-DMA, day 14 (B). Scale bar 500 µm. PGE-DMA illustrative for all LMs.

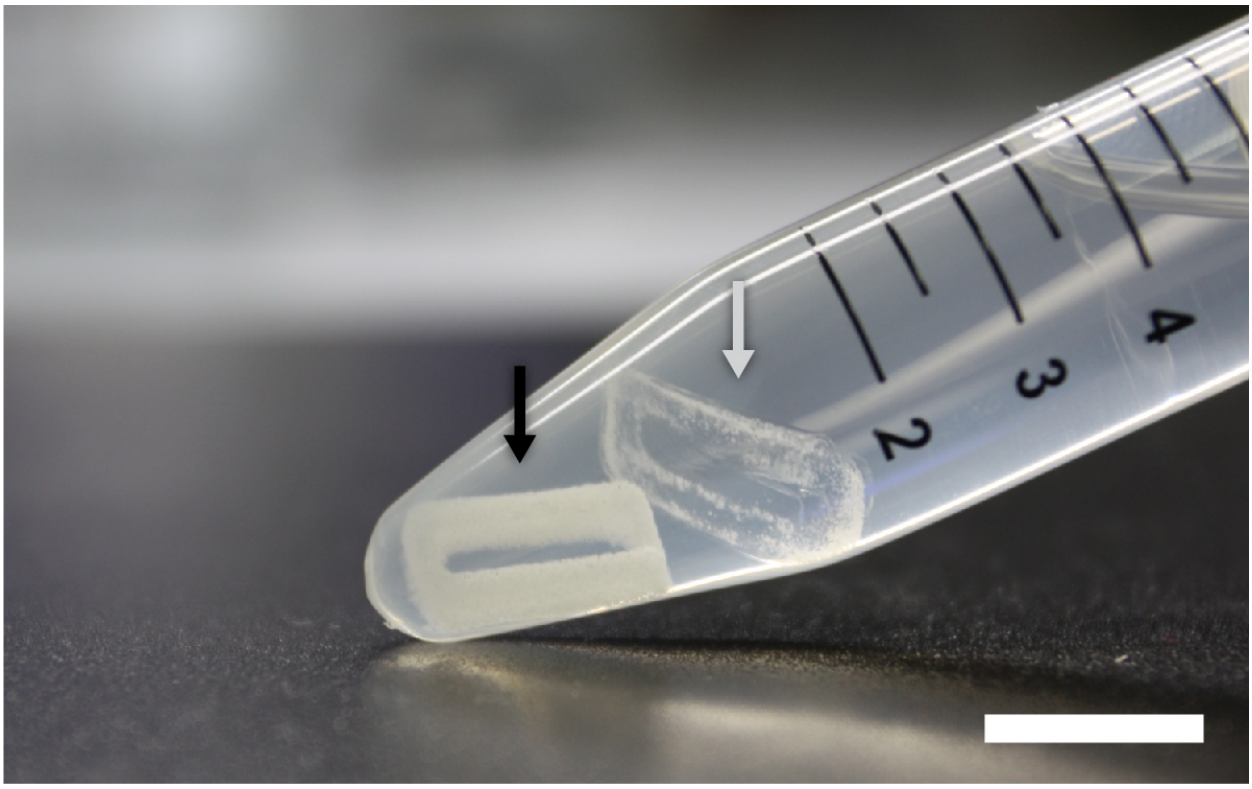

Figure D.S6. Separation of outer hydrogel layer.

Photo of F127-DMA after 14 d of incubation. Full separation of inner (black arrow) and outer (grey arrow) layer. Scale bar: 10 mm.

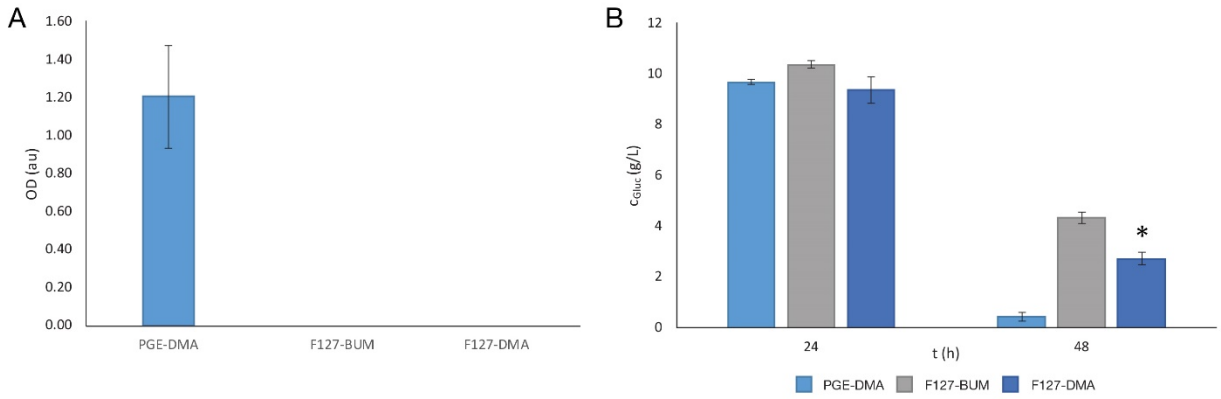

Figure D.S7. OD and glucose consumption after 48h.

OD of MM after 48 h (A). Glucose concentration of MM with different LMs (B). * $p < 0.05$, significant difference from F127-DMA.

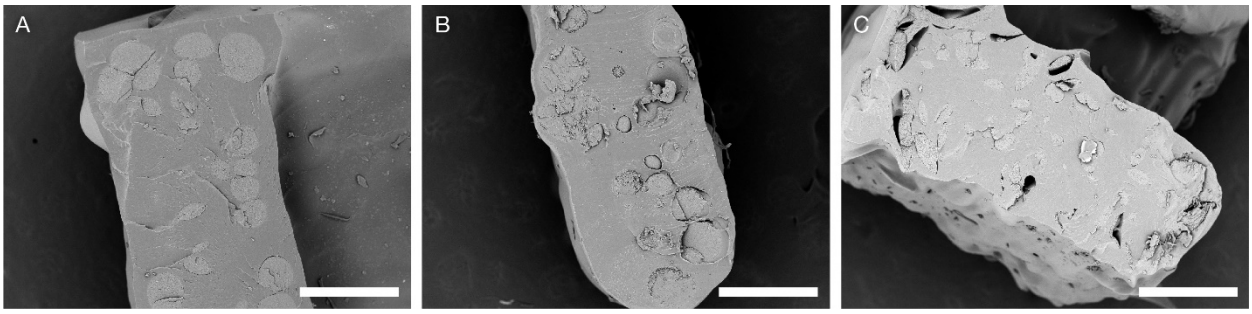

Figure D.S8. SEM micrographs of LMs after 72 h incubation.
F127-DMA (A), F127-BUM (B), PGE-DMA (C).

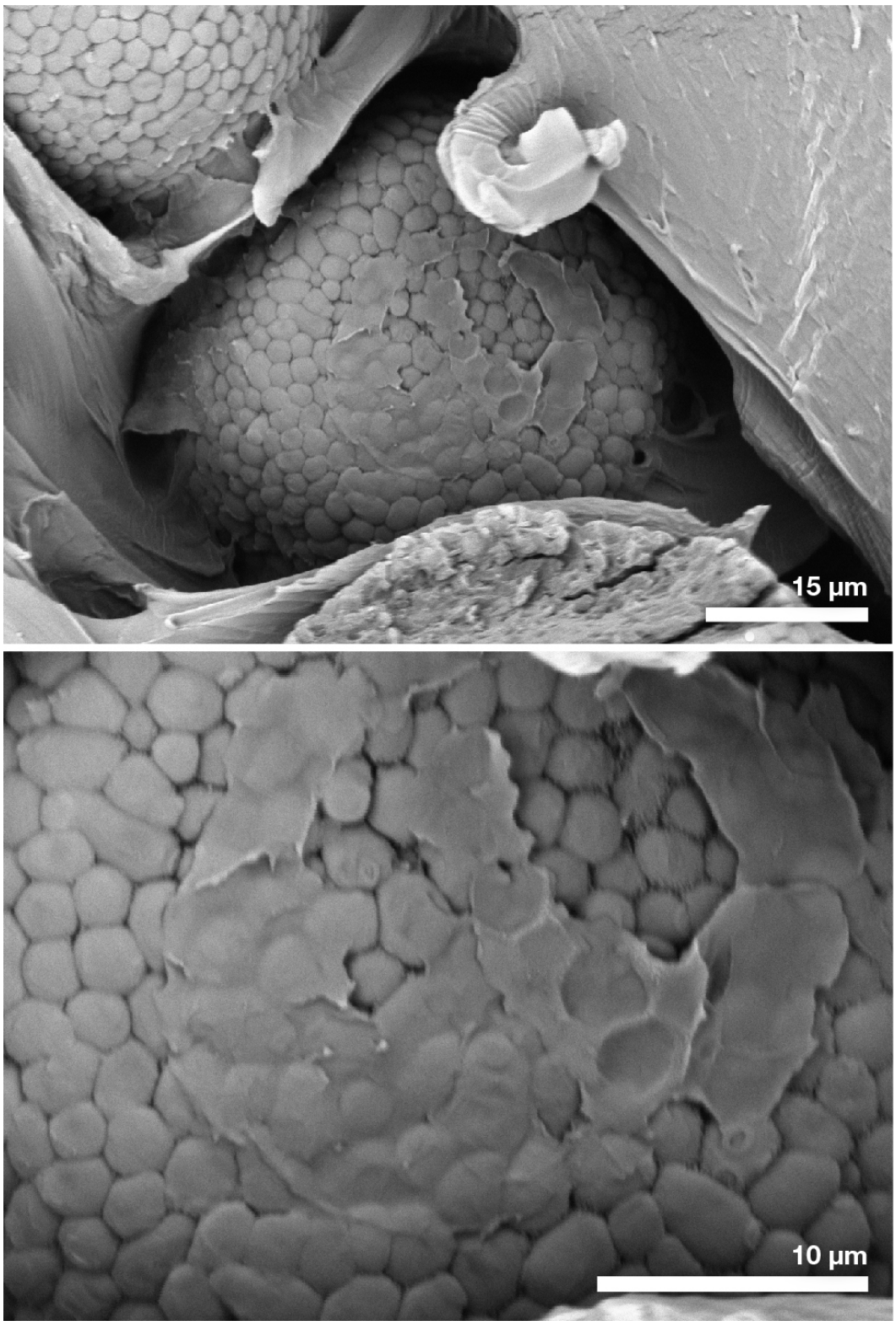

Figure D.S9. Polymer coating remnants on colony surfaces.

Remnants started appearing after the colony reached a certain size (60-80µm) in F127-based materials.

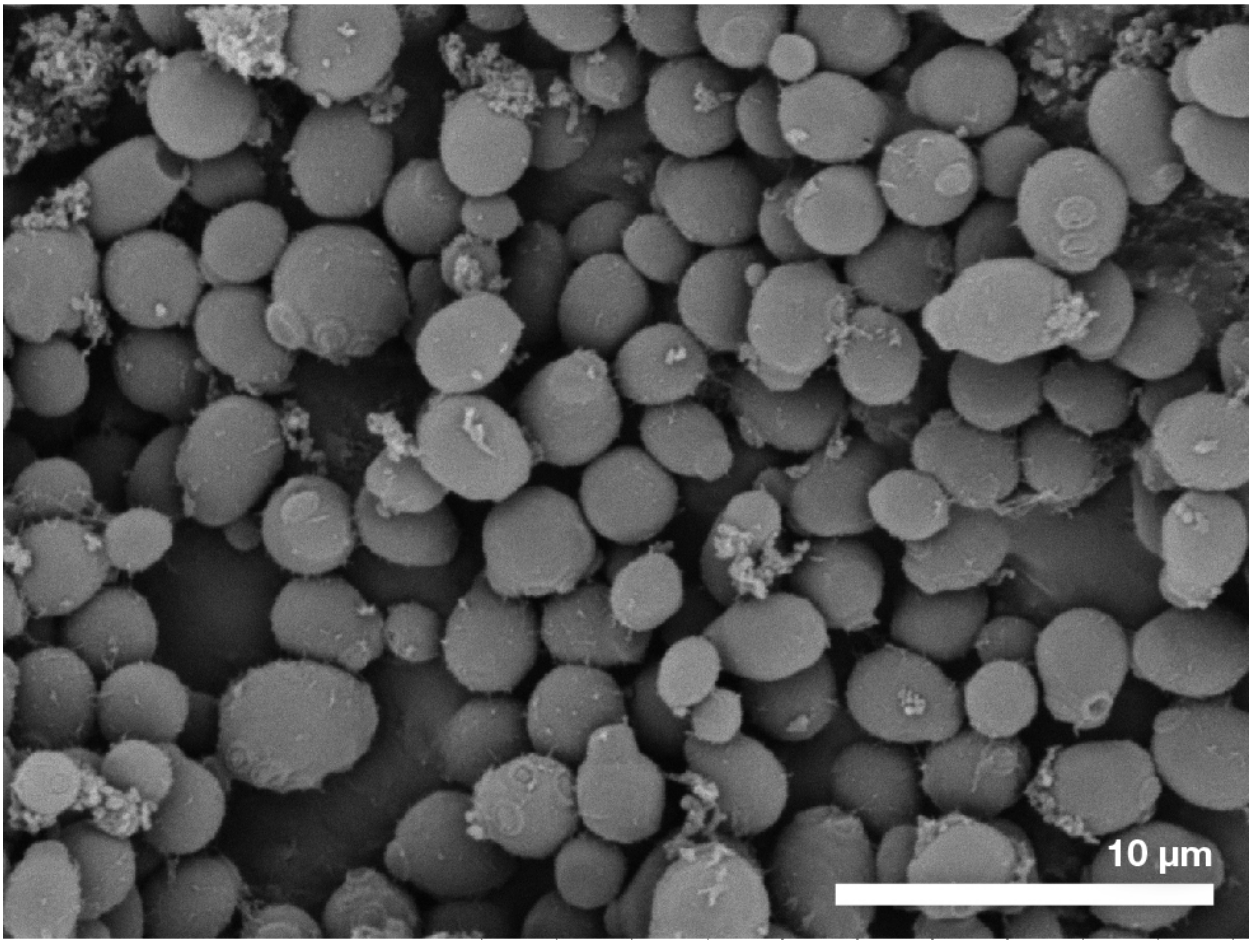

Figure D.S10. SEM micrograph of yeast suspension cells.

VITA

EDUCATION

2020	PhD in Chemistry – University of Washington Graduate Research Advisor – Alshakim Nelson
2012	BS with Honors in Biochemistry, Minor in Chemistry – University of Washington Undergraduate Research Advisor – Charles Campbell

PUBLICATIONS

1. Li, S.; Yang, M.; Zhou, W.; **Johnston, T. G.**; Wang, R.; Zhu, J. Dextran Hydrogel Coated Surface Plasmon Resonance Imaging (SPRi) Sensor for Sensitive and Label-Free Detection of Small Molecule Drugs. *Applied Surface Science* **2015**, *355*, 570–576. https://doi.org/10.1016/j.apsusc.2015.05.020.

2. Saha, A.; **Johnston, T. G.***; Shafranek, R. T.; Goodman, C. J.; Zalatan, J. G.; Storti, D. W.; Ganter, M. A.; Nelson, A. Additive Manufacturing of Catalytically Active Living Materials. *ACS Applied Materials & Interfaces* **2018**, *10* (16), 13373–13380. https://doi.org/10.1021/acsami.8b02719.

3. Fellin, C. R.; Adelmund, S. M.; Karis, D. G.; Shafranek, R. T.; Ono, R. J.; Martin, C. G.; **Johnston, T. G.**; DeForest, C. A.; Nelson, A. Tunable Temperature- and Shear-responsive Hydrogels Based on Poly(Alkyl Glycidyl Ether)s. *Polym. Int.* **2019**, *68* (7), 1238–1246. https://doi.org/10.1002/pi.5716.

4. **Johnston, T. G.**; Fellin, C. R.; Carignano, A.; Nelson, A. Poly(Alkyl Glycidyl Ether) Hydrogels for Harnessing the Bioactivity of Engineered Microbes. *Faraday Discuss.* **2019**, *219*, 58–72. https://doi.org/10.1039/C9FD00019D.

5. **Johnston, T. G.**; Yuan, S.-F.; Wagner, J. M.; Yi, X.; Saha, A.; Smith, P.; Nelson, A.; Alper, H. S. Compartmentalized Microbes and Co-Cultures in Hydrogels for on-Demand Bioproduction and Preservation. *Nat Commun* **2020**, *11* (1), 563. https://doi.org/10.1038/s41467-020-14371-4.

6. **Johnston, T. G.**; Fillman, J. P.; Priks, H.; Butelmann, T.; Tamm, T.; Kumar, R.; Lahtvee, P.-J.; Nelson, A. Cell-Laden Hydrogels for Multi-Kingdom 3D Printing. Accepted, *Macromol. Biosci.* **2020**.

7. Sanchez-Rexach, E.; **Johnston, T. G.**; Jehanno, C.; Sardon, H.; Nelson, A. Sustainable Materials and Chemical Processes for Additive Manufacturing. Submitted, **2020**.

8. Priks, H.; Butelmann, T.; Illarionov, A.; **Johnston, T. G.**; Fellin, C.; Tamm, T.; Nelson, A.; Kumar, R.; Lahtvee, P.-J. Physical Confinement Impacts Cellular Phenotype within

Living Materials. Accepted, *ACS Appl. Bio Mater.* **2020**. Preprint: https://doi.org/10.1101/2020.03.25.004887.

9. Yuan, S.-F.; Yi, X.; **Johnston, T. G.**; Nelson, A.; Alper, H. S. *De novo* resveratrol production through modular engineering of an *Escherichia coli–Saccharomyces cerevisiae* co-culture. Submitted, **2020**.

*Denotes co-first authorship